H. S. ELBESHTI

DESIGN, SYNTHESIS AND BIOLOGICAL ACTIVITY OF NOVEL ANTITUMOR ACTIVE PLATINUM AND COPPER BASED COMPLEXES CONTAINING QUINOXALINE LIGANDS

THE GRADUATE SCHOOL OF NATURAL AND APPLIED SCIENCES
OF
ATILIM UNIVERSITY

HAGER SADEK ELBESHTI

DOCTOR OF PHILOSOPHY THESIS
IN
THE DEPARTMENT OF CHEMISTRY

January 2022

ATILIM UNIVERSITY 2022

DESIGN, SYNTHESIS AND BIOLOGICAL ACTIVITY OF NOVEL ANTITUMOR ACTIVE PLATINUM AND COPPER BASED COMPLEXES CONTAINING QUINOXALINE LIGANDS

A THESIS SUBMITTED TO
THE GRADUATE SCHOOL OF NATURAL AND APPLIED SCIENCES
OF
ATILIM UNIVERSITY

BY

HAGER SADEK ELBESHTI

IN PARTIAL FULFILLMENT OF THE REQUIREMENTS
FOR
DOCTOR OF PHILOSOPHY
IN
THE DEPARTMENT OF CHEMISTRY

January 2022

Approval of the Graduate School of Natural and Applied Sciences, Atılım University.

_____

Prof. Dr. Ender Keskinkılıç
Director

I certify that this thesis satisfies all the requirements as a thesis for the degree of **Doctor of Philosophy in Chemistry, Atılım University**.

_____

Prof. Dr. Şeniz Özalp Yaman
Head of Department

This is to certify that we have read the thesis "DESIGN, SYNTHESIS AND BIOLOGICAL ACTIVITY OF NOVEL ANTITUMOR ACTIVE PLATINUM AND COPPER BASED COMPLEXES CONTAINING QUINOXALINE LIGANDS" submitted by HAGER SADEK ELBESHTI and that in our opinion it is fully adequate, in scope and quality, as a thesis for the degree of Doctor of Philosophy.

_____

Prof.Dr. Şeniz Özalp Yaman
Supervisor

Examining Committee Members

Prof. Dr. Ceyhan Kayran
Chemistry Department, METU _____

Prof. Dr. Şeniz Özalp Yaman
Chemical Eng. Department, Atılım University _____

Prof. Dr. Nezire Saygılı
Basic Pharma. Sci. Department, Hacettepe University _____

Prof. Dr. Nesrin E. Machin
Chemical Eng. Department, Atılım University _____

Assoc.Prof. Dr. Hakan Kayı
Chemical Eng. Department, Ankara University _____

Date: 24.01.2022

I declare and guarantee that all data, knowledge and information in this document has been obtained, processed and presented in accordance with academic rules and ethical conduct. Based on these rules and conduct, I have fully cited and referenced all material and results that are not original to this work.

Name, Last name: Hager Sadek Elbeshti

Signature:

ABSTRACT

DESIGN, SYNTHESIS AND BIOLOGICAL ACTIVITY OF NOVEL ANTITUMOR ACTIVE PLATINUM AND COPPER BASED COMPLEXES CONTAINING QUINOXALINE LIGANDS

Hager Sadek El- Beshti

Supervisor: Prof. Dr. Şeniz ÖZALP YAMAN

January 2022, 193 pages

Across the globe, today, cancer accounts for many fatalities, thus calling for better and updated antineoplastic agents within biomedicine and health sciences. In this regard, inorganic chemistry for pharmaceutic purposes is essential in creating drugs based in metal to fight cancer as such medicine has been shown to be potentially effective to fight cancer in humans. In light of this background, this research focuses on synthesis and anticancer activity of (2,3-di-pyridin-2-yl-quinoxaline), (2,3-di-thenyl-2-yl-quinoxaline), (2,3,2',3'-tetra-pyridin-2-yl-[6,6']biquinoxaline) and (2,3,2',3'-tetra-thenyl-2-yl-[6,6']biquinoxaline) containing copper(II) and platinum(II) compounds as prodrug candidates.

The binding interaction of these compounds with calf thymus DNA (CT-DNA) and human serum albumin (HSA) of the complexes were assessed with UV titration, thermal decomposition, viscometric, and fluorometric measurements. The nature of the binding of the complexes on DNA were revealed as electrostatic interaction between the cationic metal complex ions and the negative phosphate groups of CT-DNA upon removal of one or two labile chloride ion(s), except $Pt(tpbq)Cl_2$, $Pt(ttbq)Cl_2$, and $Cu(tpbq)Cl_2$; van der Waals and hydrogen bonds interaction were proposed for these complexes. In addition, our complexes induced a surface contact through the hygroscopic region of serum albumin.

Antitumor activity of the complexes against human glioblastoma A172, LN229, and U87 cell lines and human lung A549, human breast MDA-231, human cervix HeLa, and human prostate PC-3 cell lines were investigated by examining cell viability

(MTT), oxidative stress, apoptosis-TUNEL, *in vitro* migration an invasion, in vitro-Comet DNA demage, and plasmid DNA interaction assays. The U87 and HeLa cells were investigated as the cancer cells most sensitive to our complexes. The exerted cytotoxic effect of complexes was attributed to the formation of the reactive oxygen species in vitro. It is clearly demonstrated that $Cu(dtq)_2Cl_2$, $Cu(ttbq)Cl_2$, $Pt(ttbq)Cl_2$ and $Pt(tpbq)Cl_2$ have the highest DNA degradation potential and anticancer effect among the tested complexes by leading apoptosis. Wound healing and invasion analysis results also supported the higher anticancer activity of those complexes.

Keywords: Pt(II); Cu(II); Quinoxaline; DNA binding; HSA binding; DNA cleavage; MTT cell viability; ROS generation; Apoptosis; Invasion/Migration assay.

ÖZ

KİNOKSALİN LİGANTLARI İÇEREN YENİ ANTITUMOR AKTİF BAKIR VE PLATİN TEMELLİ KOMPLEKSLERİN TASARIMI, SENTEZİ VE BİYOLOJİK AKTİVİTELERİ

Hager Sadek El- Beshti

Tez Danışmanı: Prof. Dr. Şeniz ÖZALP YAMAN

Ocak 2022, 193 sayfa

Bugün dünya genelinde kanser en önde gelen ölüm sebebidir. Bu nedenle biyotıp ve sağlık bilimlerinde daha iyi ve güncel antineoplastik ajanlar geliştirilmesi büyük bir önem taşımaktadır. Metal temelli ilaçların kanserle savaşmak için yüksek bir potansiyele sahip olduğu bilinmektedir. Elde edilen verilerin ışığında yapılan bu araştırma ön ilaç adayı olarak (2,3-di-piridin-2-il-kinoksalin) (dpq), (2,3-di-tiyenyl-2-il-kinoksalin) (dtq), (2,3,2',3'-tetra-piridin-2-il-[6,6']bikinoksalin) (tpbq) ve (2,3,2',3'-tetra-tiyenyl-2-il-[6,6']bikinoksalin) içeren bakır(II)/platin(II) bileşiklerinin sentezi ve antikanser aktivitelerini hedeflemektedir.

Sentezlenen bileşiklerin buzağı timus DNA'sı (CT-DNA) ve insan serum albümini (HSA) ile bağlanma etkileşimleri UV titrasyonu, termal bozunma, viskometrik ve florometrik ölçümlerle değerlendirilmiştir. Yapılan çalışmalar sonucunda $Pt(tpbq)Cl_2$, $Pt(ttbq)Cl_2$ ve $Cu(tpbq)Cl_2$ dışında sentezlenen tüm komplekslerin CT-DNA'ya elektrostatik etkileşim ile bağlandığı, bu etkileşimin komplekslerde yer alan oynak klor iyonlarının yapıdan uzaklaşması ile oluşan kompleks katyon ile CT-DNA'nın negatif fosfat grupları arasındaki elektrostatik çekimden kaynaklanabileceği öngörülmüştür. $Pt(tpbq)Cl_2$, Pt(ttbq)Cl, ve $Cu(tpbq)Cl_2$ komplekslerinin ise CT-DNA ile van der Waals ve hydrogen bağı oluşturduğu sonucuna varılmıştır. Ayrıca, komplekslerin HSA'nın higroskopik bölgesine tutunduğu gözlenmiştir.

Komplekslerin antitümör aktiviteleri, insan glioblastoma A172, LN229 ve U87 hücre hatları, insan akciğer A549, insan meme MDA-231, insan serviks HeLa ve insan prostat PC-3 hücre hatlarında çalışılmıştır. Hücre canlılığı (MTT), oksidatif stres, apoptoz –TUNAL, *in vitro*-hücre göç ve istila, *in vitro*-Komet DNA hasar ve plazmit DNA etkileşim testleri gerçekleştirilmiştir. Sürdürülen çalışmalar sonucunda U87 ve HeLa hücreleri, komplekslerimize en duyarlı kanser hücreleri olarak belirlenmiştir. Komplekslerin sitotoksik etkilerinin bu hücre hatlarında meydana getirdikleri reaktif oksijen türlerinin oluşumudan kaynaklandığı ve $Cu(dtq)_2Cl_2$, $Cu(ttbq)Cl_2$, $Pt(ttbq)Cl_2$ ve $Pt(tpbq)Cl_2$'nin test edilen kompleksler arasında apoptoz yoluyla en yüksek DNA degradasyonu potansiyeline ve antikanser etkisine sahip olduğu gösterilmiştir. Yara iyileşmesi ve istila analizi sonuçları da bu kompleklserin yüksek antikanser aktivitesini destekler niteliktedir.

Anahtar Kelimeler: Pt(II); Cu(II); Kinoksalin; DNA'ya bağlanma; HSA'ya bağlama; DNA kırılması; MTT hücre canlılığı; ROS üretimi; apoptoz; İstila/Göç tahlili.

DEDICATION

I dedicate this thesis to

The memory my father Sadek
My great mother Fatema
My wonderful husband Salem
My brother and sisters
My lovely children Ahmed and Malek

ACKNOWLEDGMENTS

First and foremost, I am grateful to Allah almighty for giving me strength, knowledge, health and wisdom to undertake this study.

I would like to express my appreciation and thanks to my supervisor Prof. Dr. Şeniz Özalp Yaman for her support, guidance and patience during my study.

I owe much thanks and appreciation to Prof. Dr. Zuhal Gerçek at the Bulent Ecevit University for her support in designing (tpbq and ttbq) ligands and synthesis of all the ligands for the present work.

I would like to express my thanks and appreciation to Assoc. Prof. Dr. Hakan KAYI for his support and help, the DFT-calculation in our study could not have been made possible without his the precious input and contribution.

I am grateful to Prof. Dr. Nezire Saygılı for her kindest help during NMR discussions.

I would like to express my appreciation and thanks to Dr. Zelal Adigüzel, Dr. Yüksel Çetin and Dr. Yasemin Yildizhan in Tübitak MAM to carry out the cytotoxicity experiments.

I would like to express my appreciation to my best friend V. Selen Yaman for her support and help during my research.

I am grateful to my family and my friends for thier support, trust, and encouragement for me during my research.

In addition, I wish to express my thanks to all staffs in the Department of Chemical Engineering at Atilim University for their efforts and help.

TABLE OF CONTENTS

LIST OF TABLES

LIST OF FIGURES

LIST OF ABBREVIATIONS

AN	-	Acetonitrile
DMF	-	Dimethylformamide
Carboplatin	-	[$Pt(NH_3)_2$(*O*,*O*-cyclobutane-1,1-dicarboxylate)]
cis-DDP	-	cis-diamminedichloroplatinum(II)
Cisplatin	-	[*cis*-$Pt(NH_3)_2Cl_2$]
CT-DNA	-	Calf-Thymus DNA
DNA	-	Deoxyribonucleic acid
HSA	-	Human serum albumin
MS	-	Mass Spectrometry
NMR	-	Nuclear Magnetic Resonance
Oxaliplatin	-	[Pt(1,2-*trans*-*R*,*R*-diaminocyclohexane)(O-O-oxalato)]
Carbopin	-	[$Pt(NH_3)_2$(*O*,*O*-cyclobutane-1,1-dicarboxylate)]
Picoplan	-	[*cis*-$Pt(NH_3)$(2-picoline)Cl_2]
RNA	-	Ribonucleic acid
UV–vis	-	Ultraviolet–visible Spectroscopy
ΔG^o	-	Standard Gibbs Free Energy
ΔH^o	-	Standard Enthalpy Change

CHAPTER 1

1 INTRODUCTION

As a cure for cancer patients, chemotherapy relies on search for substances that can annihilate such quickly multiplying growth to prevent their spread on larger scales. In this relation, an important point is doing so while not inflicting any damage to other cells [1]. A related field in chemotherapy incorporates the use of metal ion and compounds for this purpose - hence the term Medicinal Inorganic Chemistry [2]. The discipline is vital in making drugs to fight cancer based in metal with the high likelihood of curing it [2]. It is understood that a major success in this field has been the application of cisplatin to hard tumor cases, kill harmful cells, and free the body from oncogenes. Known otherwise as cancer penicillin because of its high potential to cure various forms of this illness [3], the substance is in particular effective in cases of testicular cancer. Very quickly, cisplatin can change deadly prognosis in these cases to cured ones in 80% of incidents upon early application [4]. Yet, not all has gone so well and cisplatin had to confront some difficulties that resulted in restricted application. To begin with, there are major dose-restricting reactions, causing inefficient massing of cisplatin in tumors; next comes the harder issue of its low effect on other cancer forms as certain tumors are simply immune toward this drug. Added to this fact is that those that react can in time create their own immunity as well [5]. Consequently, additional studies have been in progress on cytotoxic platinum coordinates, leading to a global application of two additional platinum-based treatments; these are carboplatin and oxaliplatin. Though the advancement has been slow, there have been strides made with improved toxicity profile in case of carboplatin and a wider range of operation for oxaliplatin and platinum(IV). Up to present, platinum-based treatments have been applied in over half of all chemotherapy cases [6]. Copper compounds are another case of such drugs with various nitrogen donor ligands like purine and amino acids [7, 8]. Certain

combinations of chelating drugs based in copper have shown more antineoplasticity compared to cisplatin in vitro and in vivo cases [9]. Copper-based drugs seem to operate quite differently compared to cisplatin [10]. Sigman et al. state that the bis -(1,10-phenanthroline) copper(I) mixture with H_2O_2 can significantly separate DNA [11]. In this work, quinoxaline ligands are applied due to their major popularity in the field over the past decade [12-14]. Quinoxaline is otherwise known as 1,4-benzodiazine, benzoparadiazine, phenpiazine and benzopyrazine, and it is a heterocyclic material with circular formation of benzene and pyrazine [15]. Together with its other offshoots, it establishes a major group of nitrogen-based heterocycles, in which hetero atoms have somehow less antibonding orbitals, thus being satisfactorily receiving metal d-orbital density [16]. For this reason, this group of agents are commonly applied as bridging in homobimetallic as well as heterobimetallic compounds [17]. Quinoxalines (QXs) or benzopyrazines and their offshoots have many drug-related and biological characteristics mainly to fight viruses, bacteria, fungi, cancerous growth, and malaria [18, 19]. Numerous works show us pyridine platinum(II) compounds similar to cisplatin can be useful as well, with one applying peridyl-quinoxaline ligands as an agent in metal-based drugs [20]. The platinum(II) compounds and quinoxaline bonding ligands operations are crucial in terms of biology, biochemistry, and mass produced pharmaceutics nowadays [21].

The present research is synthesizing a novel Pt(II)/Cu(II) compound with quinoxaline ligands [2,3-di-pyridin-2-yl-quinoxaline] (dpq), [2,3-di-thenyl-2-yl-quinoxaline] (dtq), [2,3,2',3'-tetra-pyridin-2-yl-[6,6']biquinoxaline] (tpbq) and [2,3,2',3'-tetra-thenyl-2-yl-[6,6']biquinoxaline] (ttbq) are examined using spectroscopy (FTIR, NMR, UV–visible (UV–Vis)) as well as mass spectrometry. Here, we determine the binding mode of action in between the compounds and CT- DNA and as well as blood protein (HSA) with the help of UV-Vis, fluorescence spectroscopy, thermal denaturation and viscometric measurements. Antitumor activity of the complexes against cancer cell lines were investigated by examining cell viability, oxidative stress, apoptosis, and migration/invasion. Cytotoxicity of the complexes was evaluated by MTT test.

1.1 Aim of the Study

The present work attempts to meet the following objectives:

1- Develop novel of mono-nuclear copper and platinum compounds.

2- Identify the interaction and binding behavior taking place between these compounds and DNA and blood protein (HSA).

3- Study the antitumor activity and cytotoxic processes in these compounds as opposed to cisplatin given the many complexities associated with this kind of treatment – thus, the motivation behind creating platinum and copper-based compounds for better and more effective cancer treatment.

1.2 Thesis Structure

This work intends to contain in itself enough history as to the theories involved, highlight the outcomes of the tests, and explain these outcomes in detail to form a vivid image of the subject at issue. To this end, the following describes each chapter breakdown:

Chapter One offers a common introduction related to the issue and objectives.

Chapter Two contains the main chemotherapy agents considered for cancer therapy, along with a short background as to how cisplatin compounds were made while pointing to the objectives and scope of research. Included here will be a literature review on the topic of platinum/copper and quinoxaline as antitumor agents.

Chapter Three proposes a new Pt(II) / Cu(II) complex using quinoxaline ligands, together with a testing methodology to see their binding behavior with DNA and HSA in different ways, and antitumor activity of the complexes against cancer cell lines were investigated by examining cell viability, oxidative stress, apoptosis, migration/invasion and cytotoxicity.

Lastly, Chapter Four concludes with a discussion related to the outcomes of the tests to be contrasted with former attempts so as to validate and further develop the approach.

In the end, the chapter offers a series of conclusions in accordance to the theory and experiments employed herein.

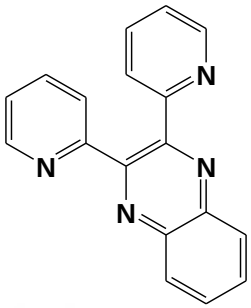

2,3-Di-pyridin-2-yl-quinoxaline

(**dpq**)

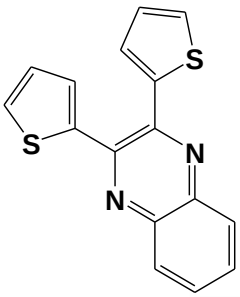

2,3-Di-thenyl-2-yl-quinoxaline

(**dtq**)

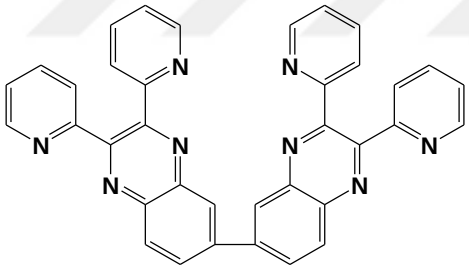

2,3,2',3'-Tetra-pyridin-2-yl-[6,6']biquinoxalinyl

(**tpbq**)

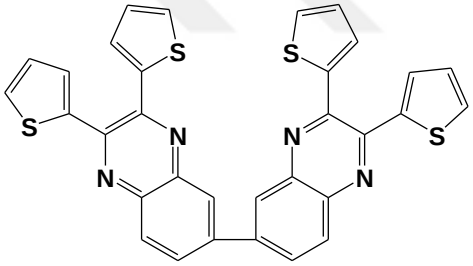

2,3,2',3'-Tetra-thenyl-2-yl-[6,6']biquinoxalinyl

(**ttbq**)

Figure 1.1 List of ligands used in this thesis.

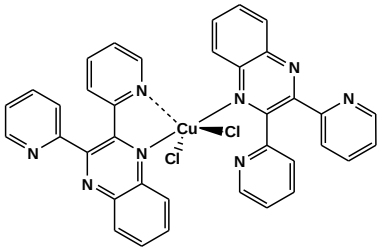

Cu(dpq)$_2$Cl$_2$

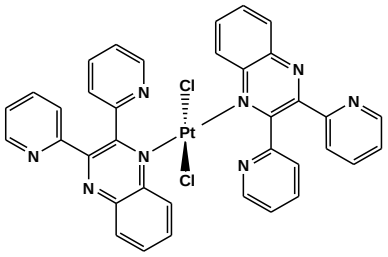

Pt(dpq)$_2$Cl$_2$

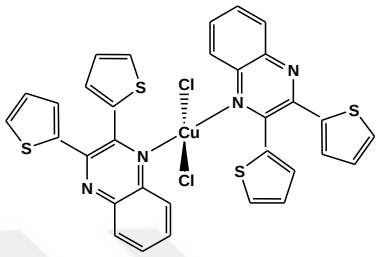

Cu(dtq)$_2$Cl$_2$

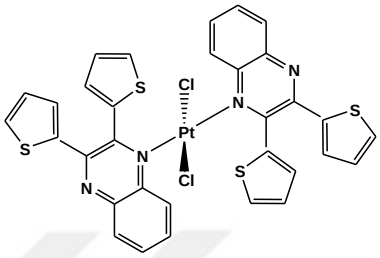

Pt(dtq)$_2$Cl$_2$

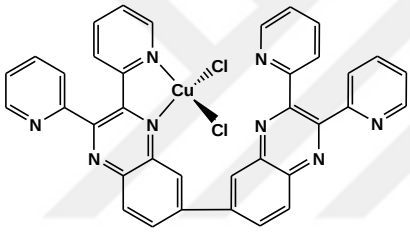

Cu(tpbq)$_2$Cl$_2$

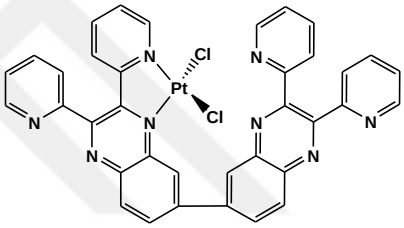

Pt(tpbq)$_2$Cl$_2$

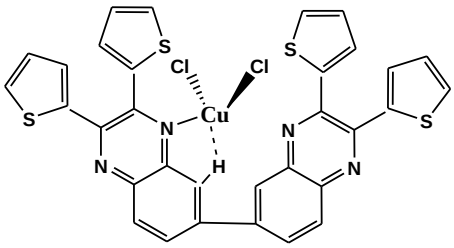

Cu(ttbq)$_2$Cl$_2$

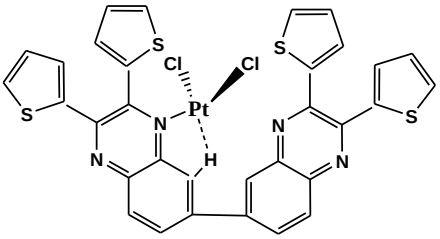

Pt(ttbq)$_2$Cl$_2$

Figure 1.2 List of DFT calculated complexes used in this thesis.

CHAPTER 2

2 LITERATURE REVIEW

2.1 Cancer and Causes

Cancer ranks among the top highly important topics facing the world today, both in health and economic terms, with the highest death rate following heart failures. It may be triggered in any cell within our body, which comprises billions and billions of them. In general terms, these cells tend to develop and break up to generate new ones in time; once aged or impaired, they cease to live and others come in their place [22]. Though, upon cancer, this cycle is interrupted, and with a growing number of unusual cells the old or impaired ones mutate to begin anew whereas they have to be replaced by other healthy ones which, conversely, might develop in places where there is no need for such new life – hence, leading to a frenzy of cell division that eventually appears as a tumor [23].

Cancer is not being a unique kind of illness, but it has a considerable variety; that is, over 100 of them. The naming of these forms is based on where they start; for instance, breast cancer and lung cancer [24].

In this respect, metastasis is the advancement of this illness from where it started to spread other regions in the body, calling for therapy that relies on a number of elements as the nature of cancer and the way it spreads. Therapy, in general, can be either operations, radiation and/or chemical treatment, with other alternatives as hormone treatments, immunotherapy, biotherapy, or stem cell replacement.

Cancer can be triggered by many ways and it can be prevented; in the United States alone, some 480,000 individuals lose their lives annually due to smoking based on 2014 survey. Other elements that can bring about cancer are excessive drinking, overweight, lack of bodily action, and unhealthy eating habits.

Apart from these, no other cause can be avoided – among them, for now, the major one being the process of getting old. Based on reports by the American Cancer Society, 87% of cancers are found in those aged 50 or more [25].

2.2 Medicinal inorganic chemistry

Inorganic chemistry for therapeutic purposes is the process of exposing the body to metal ions by choice or by accident; in the former case, the goal can be for treatment or for identification of an illness. Metal ions can freely release their electrons from their common elemental or metallic status and generate ions with a positive charge and easy solution in any fluid – and that is where they can start doing what they can in biological terms. While they lack electrons, many biological cells like proteins and DNA have plenty of them, leading to a swapping of these opposite charges, which results in bind formed between ions and molecules. The first structure-activity relationship, which was created by Paul Ehrlich early in the 1900s and gave rise to the inorganic complex known as arsphenamine – also regarded as Salvarsan or Ehrlich 606 – which proved to be effective against syphilis. In this way, he became known as the father of chemotherapy – a topic that he described as applying medicine to damage harmful cell while protecting its host [25].

2.2.1 Platinum Antitumor Complexes

In this regard, platinum plays a major part in pharmacological initiatives, having been use by medical experts as cis-diamminedichloroplatinum(II) or cis-platin and offering significant advantages in the form of combination therapy against metastatic testicular, ovarian and bladder cancers [26]. The material was known as Peyrone´s Chloride as well in the past [27], with its cytotoxic properties finally unfolded in the late 60s by Barnett Rosenberg et al. [28]. Presently, cisplatin is one of the important for many anti-cancer drugs and the start of more advanced chemotherapy approaches that involve metal compounds to counteract cancerous cell multiplication within the nuclear DNA [29, 30].

Put differently, this compound is known to develop a very spontaneous species when it is within the cell membrane [31, 32] able to interact with the DNA by creating intra-

strand bonds [33, 34]. These bonds, in turn, modify the DNA's second form and prevent further copying and multiplication, eventually killing the cell [31]. Yet, owing to such impacts as toxicity of cisplatin [35], there have been attempts to come up with other alternatives to employ platinum(II) (Figure 2.1) [36-40] As a 2nd generation and similar to cisplatin, carboplatin somehow possesses fewer such effects while being equally effective because of reduced levels of interaction; yet, this substance does not have a wider scope of application as regards tumors and it requires intravenous use. The 3rd generation comprises those combinations with various chiral amines. To illustrate, oxaliplatin first appeared in the French market in 1996 and, later, authorized for use across Europe in 1999 followed by in the US in 2002 [41]; this compound was efficient against cholorectal tumors, proved to be promising at the pre-clinical level in cases where cisplatin proved ineffective, and was taken orally [42 - 48]. A different form, nedaplatin, is also based on platinum from cis-diamine or glycolate, authorized for use in Japan in 1995, well reputed for improved safety standards compared to cisplatin [49], and serving in combination to treat urological cancer [49]. Another compound, lobaplatin, is based on platinum as well and introduced as 1,2-diammino-l-methyl-cyclobutane-platinum(II)-lactate, with efficiency ranging from the lungs, to ovarian and gastric cancer xenografts [41]. With non-cross-resistance to cisplatin, specifically in case of highly subtle cancer cells, lobaplatin became initially authorized to treat prolonged cases of myelogenous leukemia, small-cell lung cancer (SCLC) and metastatic cancer [50]. Picoplatin, similar to cisplatin with 2-methylpyridines and previously named ZD0473, became available for steric coverage engulfing the platinum center and protecting the drug against nucleophiles and DNA-repair tracks to improve resistance [51]. Another one, satraplatin, bis-(acetato)(ammine)dichloro-(cyclohexylamine)platinum(IV), is a pioneer in as an oral platinum-based product with both different pharmacodynamics and pharmacokinetics as opposed to alternative platinum-based products. For this reason, the range of its application varies as well [41]. The compound Lipoplatin is liposomal and based on cisplatin intended for improved pharmacokinetics and better safety standards, which make room for changing the amount to be administered depending on the intended cancer cells [52]. The liposomes comprise dipalmitoyl phosphotidylglycerol, soyphosphatidyl choline,

cholesterol and methoxy-polyethylene glycol-distreatoyl phosphatidyl-ethanolamine [52]. A different drug, ProLindac, an oxaliplatin with a hydrophilic (hydroxypropylmethacrylamide) polymer joined with the active moiety, attacks the tumor and holds onto it at the cell level [53].

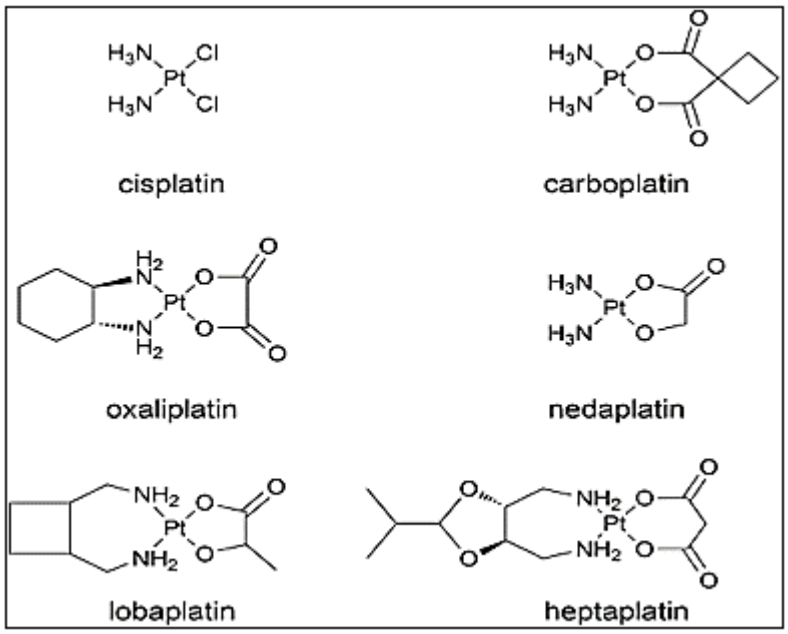

Figure 2.1 Some of the anticancer derivatives of platinum analogues [54].

2.2.1.1 Platinum(II) Complexes with Nitrogen and Sulfur-Donor Ligands

There have been many other platinum-based drugs created lately pending further studies into how effective they can be for use against different kinds of tumor cells. Such studies require constituent compound simulations – in this case, platinum – through coordination with other ligands for optimum efficiency. The pharmacokinetics, range of application, and the degree of toxicity in many scenarios can be enhanced to overcome such difficulties arising from the original constituents or parent compounds, while the technology continues to witness further developments in formulating new platinum(II)–S compounds. [36] These formulations are inspired

mainly by reference to detoxifying sulfur ligands and Pt–Sulfur bonds alongside alternative nucleophiles [55].

The kinetics in this respect are evidence that the N-donor ligands can move toward the Pt(II) compounds easily which represents an important opportunity considering that Pt(II)-DNA exchanges are the main driving force in combatting tumors by platinum-based treatments [56, 57]. In fact, many platinum(II) and bidentate N, S ligand complexes have so far proved to be effective as anti-cancer substances [35], and they have set the agenda for making other metal-based treatments using nitrogen and sulfur as complements [58].

Lots of studies refer to the benefits of pyridine platinum(II) complexes and their similarity with cisplatin [59], pointing to planar ligands being substituted with pyridines and reducing deactivation and, at the same time, attaching to DNA in the same manner as cisplatin [60]. What's more, platinum complexes made using aniline and 2-pyridinecarboxaldehyde have shown promising outcomes in case of contact with hormone independent human mammary carcinoma cell line MDA-MB 231 [61], namely [dichloro-N-(pyridine-2-yl)methylenebenzamine] platinum(II) [62]. Those similar to Cisplatin and having an aliphatic amine group have very elevated levels of cytotoxicity concerning cell lines irresponsive against cisplatin [63, 64]. To find out how platinum-based treatment having N-donor atoms can be utilized most efficiently, the main point is to see the way the material bonds the DNA to generate adducts [65]. DNA is still at the heart of many drugs used in advanced experiments; to mention one, there are metal-based compounds [66], and as regards platinum(II), the drug starts the activities by interacting with the DNA [67] based on an intercalative pattern; for example, in planar forms like [Pt^{II}(5,5-diethylbarbiturate)] and [Pt^{II}(5,5-diethylbarbiturate)(terpyridine)NO_3.0.5H_2O] [68]. In other events, groove binding or electrostatic operations exist; to illustrate, [Pt(6-phenyl-2,2′-bipyridine)(2,4-diamino-6-(4-pyridyl)-1,3,5-triazine)] and dichloro-N-(pyridine-2-yl methylene)benzamine platinum(II) [69]. Also platinum(II) dithiocarbamate complexes, [Pt(S_2CNR_2)Cl(PAr_3)], [Pd_2(tpbd)Cl_2]Cl_2 (PP1), [Pt_2(tpbd)Cl_2]Cl_2 (PP2) and

[PdPt(tpbd)Cl_2]Cl_2 (PP3) (tpbd = *N*,*N*,*N*′,*N*′-tetrakis(2-pyridylmethyl)benzene-1,4-diamine) and their activity against some cancer cell lines [70, 71].

2.2.1.2 Cisplatin-DNA Coordinations

Genetic DNA, which is located in the nucleus. Any form of exchange involving mitochondrial DNA can be regarded as inefficient so far as the antitumor properties of platinum compounds are concerned [72]. Once the compound arrives at the DNA, the possibilities for coordination are different, as the process mainly takes place through the N7 atoms of guanine, whereas binds between N7 and N1 of adenine and N3 of cytosine take place rather minimally [73, 74]. Because DNA bears a different variety of purine and pyrimidine bases, it accounts for 60% of the bindings of the type 1,2-(GPG).

In other words, the process occurs by means of two molecules of guanosine-5'-n monophosphate (5'-GMP) positioned on opposite strands of DNA. Another 25% appears as coordination by 1,2-(APG), that is, bindings with adenosine-5'-monophosphate (5'-AMP) and 5'-GMP again on opposite strands of DNA. The remaining forms of binding only occasionally take place among them, monofunctional with 1,3-(GPG), and by means of guanosine positioned on the same strand. In this sense, (Figure 2.2) illustrates the cisplatin-DNA binding forms [75, 76].

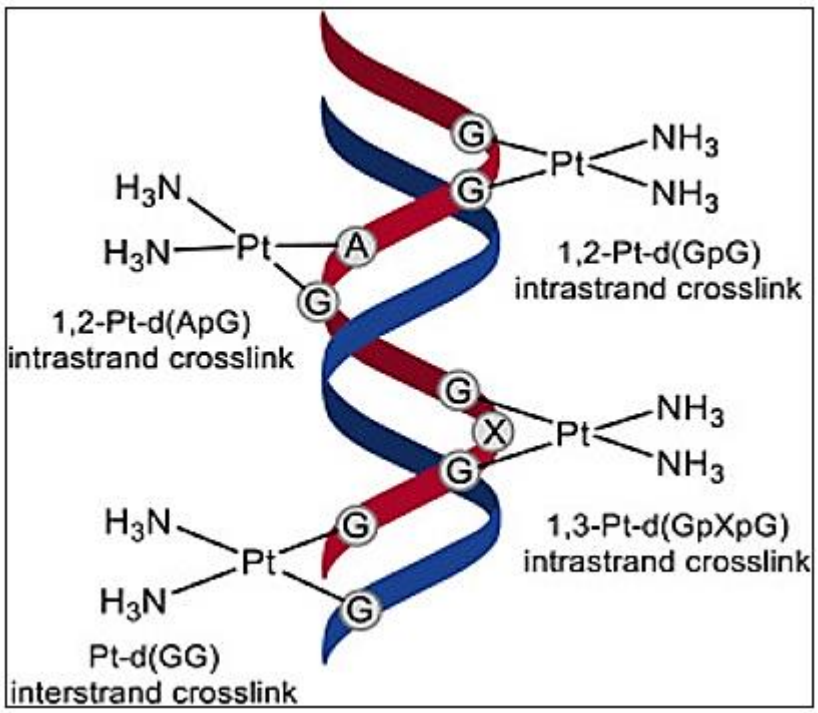

Figure 2.2 The different ways of coordinations of cisplatin to DNA [75].

2.2.1.3 The mechanism of action of platinum drugs.

The action mechanism of platinum drugs, approved by the US Food and Drug Administration (FDA) and the European Medicines Agency (EMA), can be divided into four mechanisms: (i) cellular uptake, (ii) aquation/activation, (iii) DNA binding; and (iv) cellular processes ending up in apoptosis (Figure 2.3).

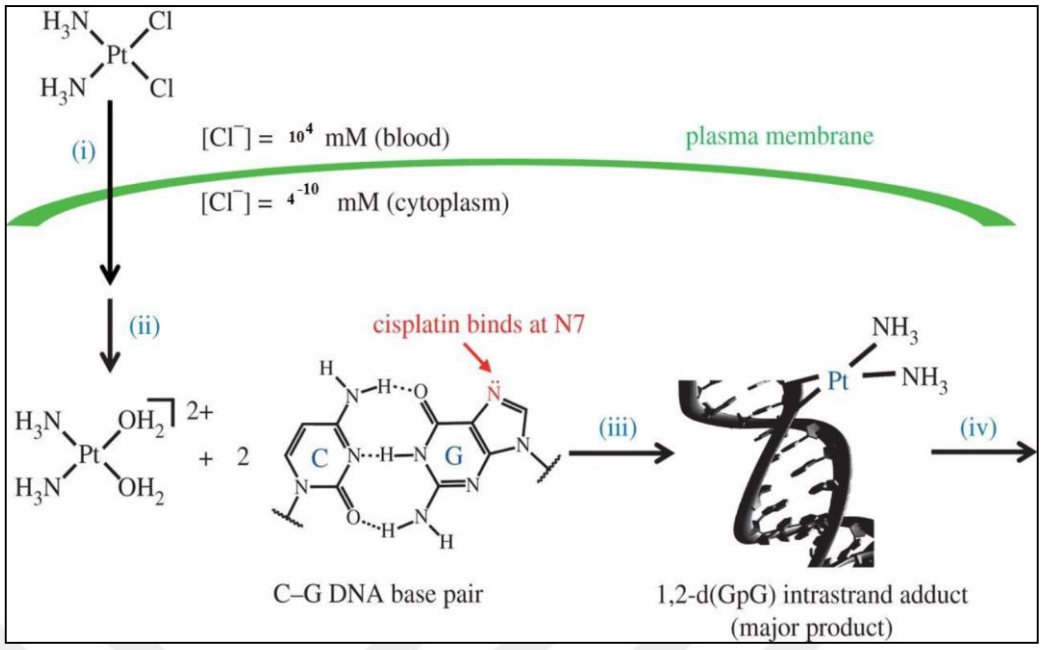

Figure 2.3 Mechanism of action of platinum complexes; (i) cellular uptake, (ii) aquation-activation, (iii) DNA binding and (iv) apoptosis cell [50].

Chemotherapy with cisplatinum administered intravenously involves its supplement within a saline fluid dilute it. Next, it has to travel through the cell membrane to interact with DNA. Its perception has been under question as far as initial studies show, depending on passive or active transmission. However, today both these possibilities have been acknowledged [77]. In particular, now a lot of research is going into the significance of copper carriers like CTR1 to facilitate intake of cisplatin by yeast [78]. Still, there is enough information to support the idea that human cells accept CTR1 cisplatin in some way capable of binding DNA and causing apoptosis [79]. Alternative membrane proteins can as well prove beneficial in platinum-based drug intake. In addition, over-expressing membranes of OCT1 and OCT2 organic cation carriers have been shown to react more to oxaliplatin compared to cisplatin [80].

Within the cell, platinum compounds are replaced with ligands. For cisplatin, cytosolic chloride ion concentration that lowers (approx. 4 mM), compared with the the extracellular matrix (approx. 100 mM).

Within the cell, the charge-free cisplatin molecule also experiences hydrolysis, by means of which a chlorine ligand takes the place of one H_2O molecule, thus creating a type with positive charge. Such hydrolysis inside the cell takes place because of significantly reduced values of chloride ion (~3-20 mM) and high amounts of H_2O [81,82].

Within the cell, cisplatin can aim for a series of destinations, such as DNA, RNA, and sulfur containing enzymes like metallothionein and glutathione and mitochondria [83]. As a common trend, the nucleophilic place on DNA is the N7 atoms of the purine, and that is open in the main groove. These locations are ideally platinated [83]. It is possible for a variety of cisplatin–DNA compounds or adducts to generate – of which, the primary ones include two chlorine ligands of cisplatin substituted with purine nitrogen atoms on the neighboring bases within one string of the DNA [84]. When damage occurs to DNA in cells, the common response is to stop the evolution of the cell cycle so that it can repair the damage the DNA prior to transferring to the daughter's cells, thereby avoiding the movement of harmful mutagenic lesions [85].

2.2.1.4 Adverse effects of cisplatin

After decreasing impacts on kidneys by means of water consumption and those effects related to the digestive system by means of antiemetics, neurotoxicity is the next crucial side effect that cisplatin chemotherapy can have on the body, and it accounts for about ~47% of the cases. The sings associated with this side effect are numbness, tingling, paresthesiae in the extremities, walking uneasily, feeling numb in the toes, deep tendon reactions, reduced reflex in ankles, and reduced dexterity. Regrettably, these effects are likely to remain and continue to deteriorate within the initial four months, even likely to last up to 52 months once treatment is terminated. Added amounts of platinum inside the cells from the neighboring nervous system, as opposed to tissues within the central nervous system, have been shown by research to be among the other clinical signs associated with peripheral neuropathy [86, 87]. Cisplatin, in combination with alternative cytotoxic materials proves to be effective in increasing the survival ratio according to tests on a sizeable group of individuals with various malignancies. The overall dose administered, however, remains a major concern in

terms of forming nephrotoxicity in subjects taking increased volumes ifosfamide, cisplatin and etoposide together [88, 89].

2.2.2 Copper Complexes as Antitumor Agents

There have also been attempts to examine the tumor-fighting properties of many basic copper compounds containing nitrogen donor ligands, for instance purine, thiosemicarbazone, imidazole, benzohydroxamic acid and amino acid [90–92]. Among these, combined chelate copper-based compounds show better antineoplastic properties compared to cisplatin as far as laboratory and clinical attempts are concerned [93, 94]. Copper compounds display another set processes that differ from cisplatin used in patients. To begin with, [Cu(malonate)$(phen)_2$] has proved to trigger apoptosis in cultured mammalian cells, apart from its reputation for intervening in cellular oxidative stress, improving membrane lipid peroxidation, and disrupting mitochondriac breathing processes in fungi [95, 96].

Copper(II) compounds with ethyl-2-[bis(2-pyridylmethyl)amino]propionate ligand (ETDPA), as [Cu(ETDPA)]Cl_2 and [Cu(ETDPA)(phen)]$(ClO_4)_2$. The DNA-binding attributes of these copper compounds vary. In detail, [Cu(ETDPA)]Cl_2 connects in a way that differs from classical intercalation binding; whereas [Cu(ETDPA)(phen)]$(ClO_4)_2$ does so in the intercalation style. The cytotoxicity properties reveal that [Cu(ETDPA)(phen)]$(ClO_4)_2$ can act more efficiently against cancer cell multiplication compared to [Cu(ETDPA)]Cl_2 [10].

The chemistry of copper, especially phenanthroline compounds, are mainly sugar-based and often do not involve in nucleobase oxidation; yet, they can cut up strand straight away upon removing the hydrogen atom from the deoxyribose moiety. Sigman et al. proved that the bis-(1,10-phenanthroline)copper(I) compound, mixed with H_2O_2, can effectively split DNA [11]. In this respect, Cu$(Phen)_2$ have been shown to be much more efficient compared to Cu(Phen), though there is a far lower association constant as regards the second phenanthroline ligand - almost 105.5 M^{-1}, which is far below applicability levels in biological terms [97]. As a result, there have been two other alternatives, 2- and 3-Clip-Phen, formulated in (Figure 2.4) which accommodate two

phenanthroline ligands connected by the 2 or 3 positions with a serinol bridge to better account for the two phenanthroline units' coordination in the surroundings of the same copper ion. The oxidative nuclease processes pertaining to these compounds and molecules have been seen much more active compared to phenanthroline. The Clip-Phen compounds are of advanced DNA cleavage activity [98]. After the synthesis of the active Cu(3-Clip-Phen) compound, various structural platin compounds were also generated to include this ingredient, with just a single Clip-Phen unit to examine the nuclease activity. Accordingly, cis-[Pt(Cu-3-Clip-Phen)$_2$Cl$_2$] in geometries with Cis-, trans- and irregular forms is shown to disintegrate; still, though, cis-[Pt(Cu-3-Clip-Phen)$_2$Cl$_2$] appears to have far more antiproliferative effect as opposed to the rest of the platinum compounds [99]. Also, CuC Top inhibitors are efficient anticancer compounds used alone or in combination with other drugs. Copper complexes exerts an effective inhibitory action on topoisomerases, which participate in the regulation of DNA topology [100].

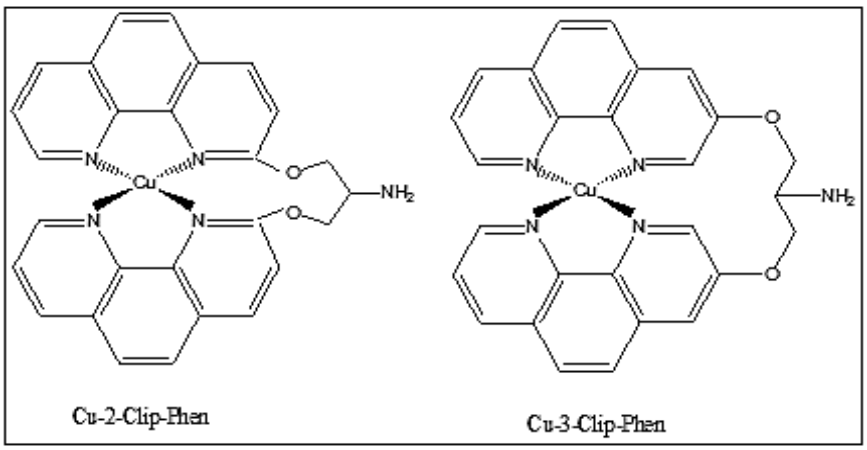

Figure 2.4 Structure of [Cu-2-Clip-Phen, Cu-3-Clip-Phen] [98].

.

2.2.2.1 The mechanism of action of copper compounds

The cancer-fighting properties of copper(I) complexes can be attributed to various functions, chiefly the potential to generate active oxygen species (ROS). Cu(I) ions are able to decrease hydrogen peroxide to form hydroxyl radical. In the same way, Cu(II)

ions can turn to Cu(I) through superoxide anion (O_2^-), or glutathione. As a result, forming of reactive oxygen species such as OH· are driven by the copper, regardless of the form in which it is initially introduced into the body be it Cu^+, or Cu^{2+}.

$$Cu^{2+} + O_2^- \rightarrow Cu^+ + O_2 \quad (2.1)$$

$$Cu^+ + H_2O_2 \rightarrow Cu^{2+} + OH\cdot + OH^- \quad (2.2)$$

Superoxide anion (O_2^-) can be obtained upon the reduction of the molecular oxygen as it takes place in numerous biological settings. Next, it is changed to hydrogen peroxide upon dismutation. These two can generate of ROS a different kind of active oxygen group, that is the hydroxyl radical (OH·), upon catalysis by Cu or Fe ions. A radical like this has been reported as the primary condition that harms DNA in cells under oxidative stress [101, 102].

2.3 Quinoxaline

Quinoxalines have been studied extensively for the last decade [14]. It is also known as 1,4-benzodiazine, benzoparadiazine, phenpiazine and benzopyrazine (Figure 2.5), forming a heterocyclic circular complex comprising a benzene ring and a pyrazine [15]. Along with its derivatives, quinoxaline account for a major group of nitrogen-based heterocycles. With heteroatoms in rings, they possess a rather reduced orbits serving as ideal receptors of metal d-orbital density [103]. Due to this feature, they are often applied for bridging in homobimetallic as well as heterobimetallic compounds [17].

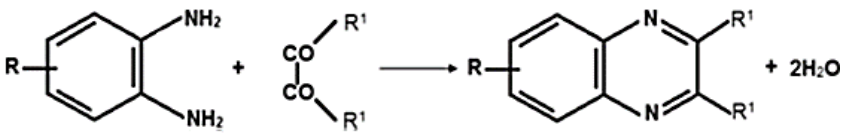

Figure 2.5 Structure of benzopyrazine [15].

Molecular weight of the quinoxaline is 130.15 and is expressed as $C_8H_6N_2$, being of white and crystal powder appearance under normal settings [104]. It is a low melting

point (29-30° C), can be purified, and has a fraction of boiling point at (220-223° C) [105]. Quinoxaline varieties are soluble in water to form mono-quaternary salts upon applying quaternization with dimethyl sulfate and methyl p-toluene sulphonate. These salts of 2-alkylquinoxalines are steady and may be changed to a variety of colored materials upon oxidation [105]. It is acidic with a pKa of 0.60 in water at 20° C, while nitration takes place just upon forcing (Conc. HNO_3, Oleum, 90° C) to release 2 complexes: namely, 5-nitroquinoxaline (1.5%) and 5,7-dinitro-quinoxaline (24%) [15]. The 2^{nd} pKa is 5.52, which implies that quinoxaline can be largely diprotonated in the presence of very potent acidic solutions [108].

Research on (QXs) or benzopyrazines, along with their byproducts is also a major field now owing to the large number of biological and therapeutic uses found for them. For instance, echinomycin contains quinoxalinyl moiety while certain drugs, such as Brimonidins, can reduce glaucoma [104].

Antimicrobial property is very essential as regards the global public health, in part due to a reckless use of drugs made for the goal [106], thus calling for relentless research to find improved antimicrobial formula that can withstand and fight pathogeny. Many quinoxaline derivatives can be use for this purpose [107].

Apart from antimicrobial properties, quinoxaline derivatives are essential in treatment of several cases of both chronic and metabolic disorders like diabetes, neurological illnesses, atherosclerosis and inflammation [108].

Quinoxaline nucleuses have some cancer-fighting benefits, thus setting them apart for use in this way [109]. To this end, a new group of 2-alkylcarbonyl and 2-benzoyl-3-trifluromethylquinoxaline-1,4-di-N-oxide byproducts is formed and assessed clinical use against a 3-cell line panel (MCF7 (breast), NCIH 460 (lung) and SF-268 (CNS)) [108], a number of studies demonstrate the application of pyridine platinum(II) compounds to be imitated by cisplatin is effective; one of them is applied as peridyl-quinoxaline as agent to contain metal [20]. The Interactions taking place between platinum(II) compounds and quinoxaline bonding ligands have proved to be essential

in both biological and biochemical terms and, hence, for massive drug production in the past decade or so [21].

2.4 DNA Binding

Drugs interact with DNA through two different ways, covalent and/or non-covalent modes.

2.4.1 Covalent binding

Covalent bonds occur between the sugar of one nucleotide and the phoshate of an adjacet nucleotide. When nucleotides are incorporated into DNA, adjacent nucleotides are linked by a phosphodiester bond: a covalent bond is formed between the 5′, phosphate group of one nucleotide and the 3′-OH group of another.

DNA as carrier of genetic information is a major target for anticancer drug interaction because of the ability to interfere with transcription and DNA replication, a majer step in cell growth and division. The covalent type of binding of drug-DNA is irreversible and invariably causes the complete inhibition of DNA processes and subsequent cell death. A major advantage of covalent binders is the high binding strength. However, covalent bulky adducts can cause DNA backbone distortion, which affect both transcription and replication (disrupting protein complex recruitment). The covalent binders are also called alkylating agents due to adduct formation because they are used in cancer treatment to attach an alkylating agents due to adduct formation because they are used in cancer treatment to attach an alkyl group (C_nH_{2n+1}) to DNA [110]. for examples carboplatin and cyclophosphamide.

2.4.2 Non- Covalent binding

Non- Covalent binders interact through small aromatic ligand molecules that bind to DNA double helical structures by different ways: (i) intercalation, and (ii) groove binding. Non- Covalent DNA interction agents are generally considered less cytotoxic than agents producing covalent DNA adducts; non-covelent DNA interacting agents can change DNA conformation, DNA torsional tension, interrupt protein-DNA interaction, and potentially lead to DNA strand breaks [110].

2.4.2.1 Groove Binding

DNA Groove Binding involves temporary non-covalent interaction through intermolecular physical forces of attraction by a protein or low molecular weight ligand with double stranded DNA in either the major or minor groove formed by the double helical structure, in either a sequence dependent or independent fashion. These grooves allow proteins to bind to and recognize DNA sequences from the outside of the helix. The grooves expose the edges of each base pair located inside the helix, which allows proteins to chemically recognize specific DNA sequences. There are two grooves that run the length of the DNA double helix. Each groove is lined by potential hydrogen-bond donor and acceptor atoms, and these interact with DNA-binding proteins that recognize specific DNA sequences. Major groove is the wider of the two grooves in a DNA double helix. It has the nitrogen and oxygen atoms of the base pairs pointing inward toward the helical axis, whereas in the minor groove, the nitrogen and oxygen atoms point outwards; important because the major groove is more dependent on base composition and may be the site for protein recognition of specific DNA sequences or regions. [111].

Electrostatic interaction:

Minor Groove Binders or MGBs are crescent-shaped molecules that selectively bind non-covalently to the minor groove of DNA, a shallow furrow in the DNA helix. DNA binding with specific sequences, mostly AT, takes place by means of a combination of directed hydrogen bonding to base pair edges, van der Waals interactions with the minor groove walls and generalized electrostatic interactions.

For example, endonucleases bind electrostatically to the minor groove of the double-helical DNA.The major and minor grooves are opposite each other, and each runs continuously along the entire length of the DNA molecule. They arise from the antiparallel arrangement of the two backbone strands. The grooves are important in the attachment of DNA Binding Proteins involved in replication and transcription [112, 113] (Figure 2.6).

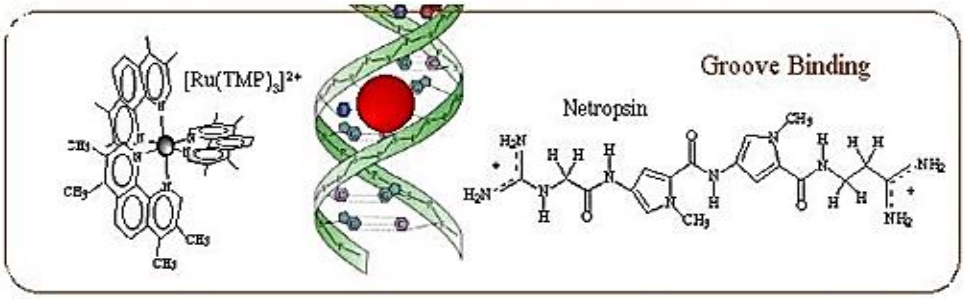

Figure 2.6 Adsorption of the complex in the DNA grooves [112].

Hydrogen bond

The hydrogen bonding between complementary bases holds the two strands of DNA together. Hydrogen bonds occur between an H and two strongly negatively charged groups (e.g., N, O, F). Over short distances and can be easily formed and broken. Although individually eash hydrogen bond is much weaker than the covalent bond, they can stabilize the double helix because of their large numbers. But, when several hydrogen bonds occur simultaneously, they can increase the strength and stability of a drug-receptor interaction substantially. Netropsin is known to bind specifically to the DNA minor groove by selective hydrogen bonds [114].

2.4.2.2 Intercalators

Intercalation is the insertion of molecules between the planar bases of deoxyribonucleic acid (DNA). This process involves positioning planar molecules between deoxyribonucleic acid base couples to decrease the winding within the deoxyribonucleic acid helix and elongate it instead [115]. They involve heterocyclic sets, some of which within the planar aromatic or hetero-aromatic category can find their way between the base couples of deoxyribonucleic acid to steady the duplex while maintaining the coupled shape as it is, replication and transcription by disrupting the topoisomerases. Intensively studied DNA intercalators include berberine, ethidium bromide, proflavine, daunomycin, doxorubicin, and thalidomide. DNA intercalators are used in chemotherapeutic treatment to inhibit DNA replication in rapidly growing cancer cells. Examples include doxorubicin (adriamycin) and daunorubicin (both of

which are used in treatment of Hodgkin's lymphoma), and dactinomycin (used in Wilm's tumour, Ewing's Sarcoma, rhabdomyosarcoma) [116] (Figure 2.7).

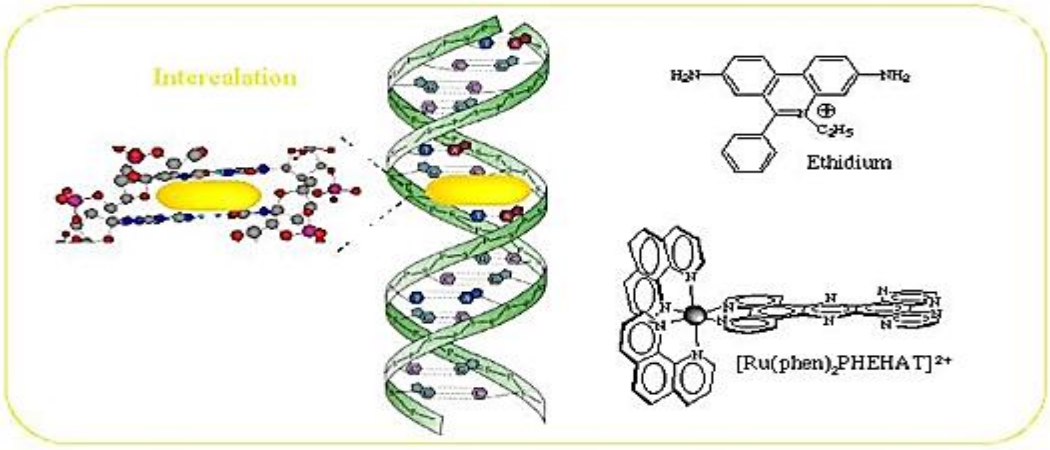

Figure 2.7 Intercalation of a planar ligand of the complex in the DNA base pairs stack [117].

2.5 DNA Cleavage

Cleavage of DNA is an essential process in all living systems. For example, topoisomerase enzymes resolve topological problems of DNA in replication, transcription and other cellular transactions by cleaving one or both strands of the DNA [118]. Another example is restriction enzymes (or restriction endonucleases), which protect the cell against virus infection by cleavage of the foreign DNA. DNA cleavage is widely observed in dying cells that display apoptotic morphological changes. In contrast to the random DNA degradation that occurs in necrotic cells, DNA degradation in apoptotic cells most often involves generation of large DNA fragments-so-called domain-sized 50- to 300-kilobase pair fragments followed by the appearance of a ladder of low molecular weight fragments that are multiples of 180 base pair (bp) and reflect double-strand cleavage of linker DNA between nucleosomes [119]. The activity of many anticance drugs rely on their ability to introduce extended damage to the DNA in the (affected) cells (e.g. bleomycin) [120], which can trigger apoptosis [121], leading to the cell death. In general, three different types of DNA cleavage can be distinguished, namely, i) hydrolytic cleavage, ii) oxidative cleavage, and iii) photochemical cleavage.

2.5.1 Hydrolytic Cleavage

This process is described as DNA splitting on the phosphor diester bonds to make pieces in an aqueous solution, as shown in (Figure 2.8), for relegation. The half-life pertaining to any given phosphate diester bond within the DNA in such a solution and at room temperature of 25°C can exceed billions of years – an indication that a catalyst is required to speed up the process about 1017 times to materialize successful hydrolysis of the phosphate in a way that is practically sound and feasible.

To achieve this, requires metal ions to serve as Lewis Acids and stimulate the phosphates for nucleophilic reaction, activate water or hydroxide as nucleophile, or alternatively intensify the departure of the alcohol. A common way for DNA hydrolysis is through nucleophilic invasion within the DNA phosphate backbone so as to generate a 5-coordinate medium for subsequent steadying through catalysis. Next, splitting the 3'-PO – as is often the case for enzymes - or the 5'-PO can yield a strand scission. Once this invasion is complete, one group departs in the form of alcohol [122].

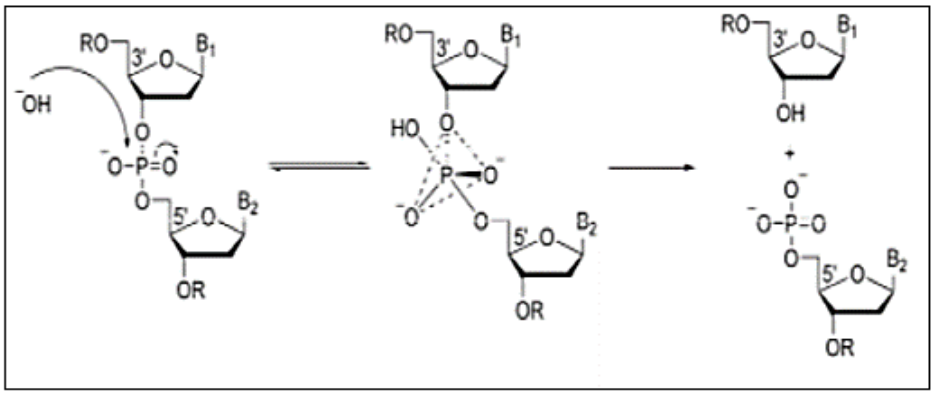

Figure 2.8 Proposed reaction mechanism for the hydrolysis of DNA [122].

2.5.2 Oxidative Cleavage

This approach comprises oxidizing a deoxy ribose upon the removal of sugar hydrogen or oxidizing the nucleobases, often requiring other additives and other agents such as direct light sources or H_2O_2 to start the splitting. Similar hydrolytic cleavage, here the DNA pieces are not religated, and the process can take place at the carbohydrate level

and/or at the nucleic base level. This, nevertheless, may harm the entire nucleobases or the deoxy ribose sugar. As a whole, Hydroxyl radical groups of O_2 (OH) take part in oxidative cleavage, which can be done in three different ways: by hydrogen abstraction, removing or supplying electron delivery. In case of cleavage at the deoxyribose sugar, should this happen within the carbohydrate, removing a hydrogen from the deoxyribose will be sufficient. (Figure 2.9) refers to the process after removing the C-3' of deoxyribose. As for oxidizing at the nucleic base level, it is better to apply it at guanine due to its lower oxidation potential. Once supplied, hydroxyl radical reacts with the heterocyclic bases in DNA. In pyramidines, OH intensifies to the C5 or C6 double bond, which causes cleavage. As for purines, the hydroxyl ion attaches to the C4, C5 & C8 [123].

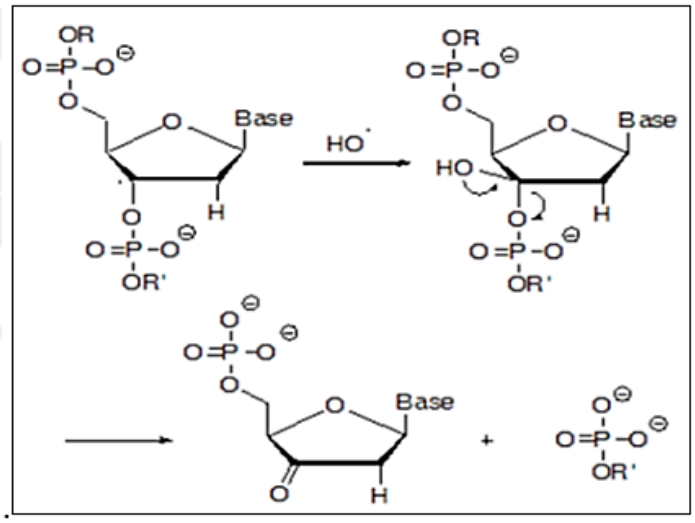

Figure 2.9 Cleavage at nucleobases [122].

2.5.3 Photoinduced DNA Cleavage

This operation involves applying light so as to initiate nuclease response, conducted by means of normal or near-UV light to investigate transcription as well as nucleic acid formations that are also known as photo-footprinting or photo-sequencing agents. Apart from this, photosensitization carried out using drugs has been proved to serve against tumor development as well. Photo-cleavage is often materialized in different

ways [124], namely by removing hydrogen atoms from the sugar ring through photo-chemically induced radicals, directly carrying electrons from the base – oftentimes, guanine - to the photoexcited cleaver [125], generating one oxygen by carrying energy from the activated photocleaver, and [126] generating of base adducts. The harm caused to DNA due to photo-sensitization is often grouped as (Figure 2.10) type I, which involves a single electron, and type II that comprises a path with one oxygen [127].

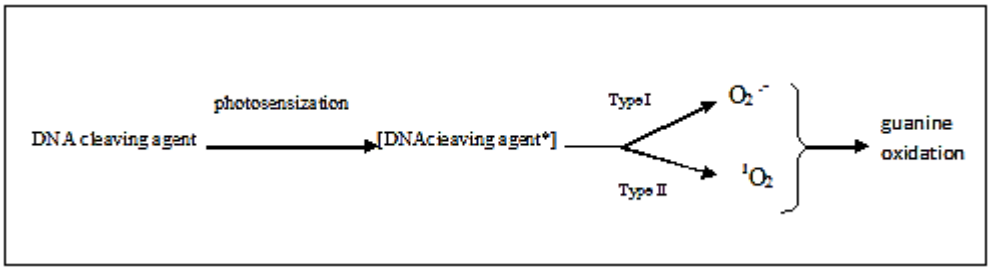

Figure 2.10 Type I and II photochemical cleavage of DNA [127].

2.6 Serum Albumin

A very stable protein, albumin appears in blood as a one-protein molecule that is self-sufficient in operational terms and comprises 585 amino acids with over fifty minor variations of the series. The appearance of human serum albumin (HSA) can be seen using high-resolution X-ray crystallography [128] to reveal the tertiary structure. Albumins among other living forms resemble one another as regards the order of amino acid, secondary and tertiary structures (Figure 2.11). Nonetheless, the most minute of changes within the amino acid can alter its capabilities for attaching to various solutes, thus proving critical to have a sufficiently high-resolution image for additional studies on the protein and its properties. Serum albumin is believed to be adaptable and not be affected in structure due to the surroundings or upon ligand binding. Albumin is resilient structure and can flex upon disulphide links to enhance its structural integrity, in particular in different physiological settings. Upon damage, the molecule repairs the links and retrieves its original form [129]. Denaturation might

only take place upon dramatic and non-physiological fluctuations within the ambient temperature, pH, and ionic or chemical configuration of the surroundings.

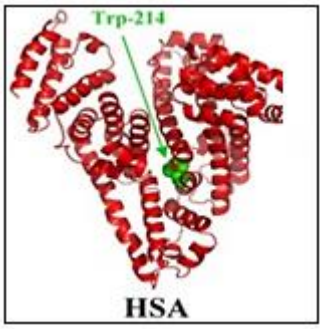

Figure 2.11 Three-dimensional structures of HSA with tryptophan residues shown in green [129].

2.6.1 The importance of Albumin

This protein accounts for about 75 to 80 % of all osmotic pressure within blood vessels to maintain the flow and avoid leakage, thus making it a vital ingredient within plasma and interstitial fluid [129]. Albumin is key to carrying drugs, ligands, hormones, and vitamins as it attaches to them and, in this way, decreases the serum amount of these compounds. Four main binding points appear on albumin, each of a specific importance for a certain compound. In cases, the competitive binding of substances struggles among themselves for such bonding spots, thereby leading to issues related to conformity, such as the case with warfarin and diazepam. In this way, albumins serve as transporters for many exogenous and endogenous complexes within the blood [128]. Albumin constitutes a major provider for the sulfhydryl series, making "thiols" into collectors of free radicals like nitrogen and oxygen groups, not to mention sepsis [129]. This protein is negatively charged and is abundant in the plasma, which feature makes it a major contributor to the so-called “anion gap” phenomenon formulated as (Na + K) − (Cl) = AG (mEq/l). it is important that there be an even distribution of cations and anions within the plasma, where the rest of the latter originates mainly from albumin, inorganic phosphate and hemoglobin - the protein in red blood cells that account for the color. Therefore, under hypoalbuminemic conditions – in other words,

elevated albumin within the plasma - the anion gap requires a narrowed [129]. Albumin contributes to the reduction of fluid seeping through capillary beds induced increase occur in the perviousness of the vessels triggered by stress. Put differently, the endothelial cells' power to manage such perviousness within the walls and the spaces in between depends upon the amount of albumin in circulation. In this way, the protein can seal the gap or affect the process owing the negativity it bears, hence resulting in the notion that colloids can play a role in the maintaining vascular architecture [129].

2.6.2 HSA Binding

Albumins are heavily attracted to metals, though bond efficiency relies on their main structure since metal ions have selective coordination properties when it comes to the side- chain of amino acids. Any secondary structural component, in this way, can be decreased as opposed to its original state, which forces albumin to bind in reverse preference in case of soft metal ions as opposed to hard ones [130]. Human serum albumin comprises some 585 amino acid residues shaped in three configurations: I, II and III, where ever one has two subdomins A and B (exactly like Bovine serum albumin, BSA). The places for bonds on HSA are such that there is major efficiency in carrying, dispensing, and processing of any drug [127]. In this sense, the molecules interact either with the polar amino acids – that is, make firm bonds with the protein through electrostatic processes and opposite charges in amino acids – or with non-polar ones – that is, hydrophobic process [131] (Figure 2.12). The binding sites where the bonds form are within domain I, arranged by side chains of aspartic and glutamic remainders of the acid as they remain uncovered on the surface of the protein. [132].

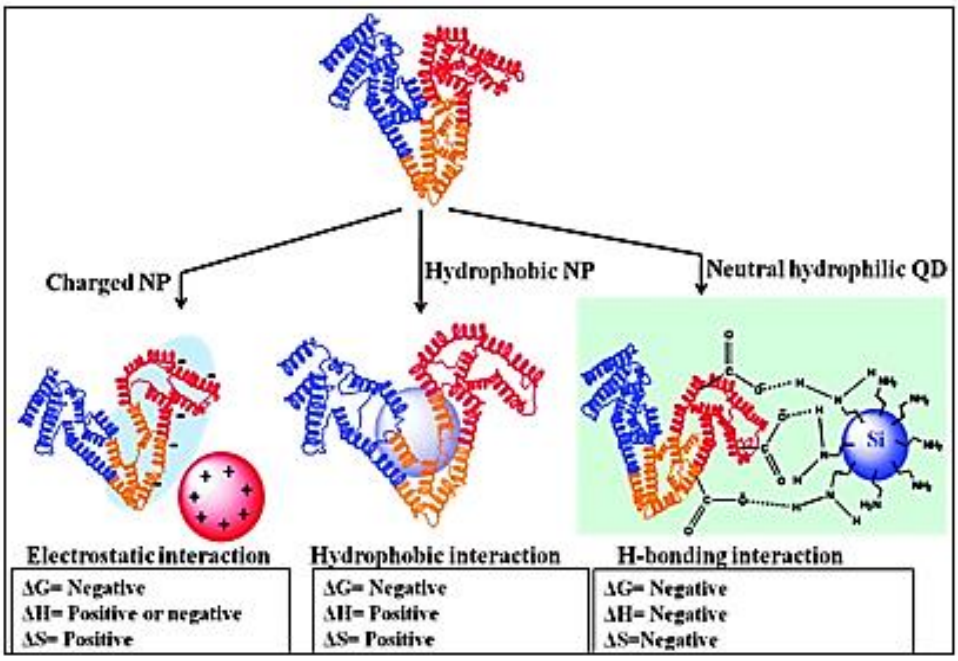

Figure 2.12 Types of HSA Binding [131].

CHAPTER 3

3 EXPERIMENTAL PART

3.1 Material

3.1.1 Instruments and Apparatus

The glassware (conical flasks, measuring cylinders, beakers, petriplates and test tubes) were autoclaved at 121°C for 20 min, and instruments and apparatus, which used throughout the experiments was carefully sterilized.

3.1.2 Chemicals

The pure and analytical grade chemicals were used directly without any further purification in all experiments.

3.2 Synthesis

3.2.1 Synthesis of [2,3-di-pyridin-2-yl-quinoxaline](dpq), [2,3-di-thenyl-2-yl-quinoxaline] (dtq).

Synthesis of dpq and dtq were performed using the methods described in the literature. Details of the synthesis and the identification of the compounds can be found elsewhere [133-134]. After the crystallization in toluene, the yield of dpq and dtq was calculated as 76.96%, and 80.77%, respectively (Figure 3.1).

3.2.2 Synthesis of [2,3,2',3'-Tetra-pyridin-2-yl-[6,6']biquinoxaline] (tpbq), [2,3,2',3'-Tetra-thenyl-2-yl-[6,6']biquinoxaline] (ttbq).

A mixture of 2 mmol 2-dipyridyl ethandione, or mixture of 2 mmol 2’-dithienyl ethandione, with 1mmol 3,3’-diaminobenzidine and two drops of glacial acetic acid

was refluxed in 25 ml ethanol for 5 hours. After reflux period, reaction mixture was poured into 75 ml ice water and neutrailized with 30 % NH_4OH solution. The resultant precipitate was filtered and recrystallized with methanol. Green crystals of dpbq were obtained with 87 % yield; Yellow crystals of dtbq were obtained with 65 % yield (Figure 3.2).

(tpbq): Anal. calc. for $C_{36}H_{22}N_8$ (%): C, 76.240; H, 3.883; N, 19.766. Found C, 74.80; H, 4.03; N, 19.20. **IR (ν/cm^{-1}):** 3100w, 3054w, 3003w, (Ar-H), 1609m (C=N), 1585s (C=C), 1148m (C-N), 1469s (ph), 1277m (C-H),1073m, 995m (C-H out of plane ring), 790s, 748vs (C-C out of plane), 1347s (C-H in plane), 1433s (C-CH in plane). **^{1}H NMR** (600 MHz, $CDCl_3$) δ 8.65 (2H, s, 5- & 5′-H), 8.41 (4H, d, J = 6 Hz, 4x6′′-H), 8.38 (2H, d, J = 12 Hz, 8- & 8′-H), 8.30 (2H, d, J = 12 Hz, 7- & 7′-H), 8.08 (4H, t, J = 12 Hz, 4x 4′′-H), 7.91 (4H, 2xd, J = 12 Hz, 4x 3′′-H), 7.31 (4H, m, 4x 5′′-H).**^{13}C-NMR** ($CDCl_3$, 400 MHz, δ, ppm): 123.43, 124.67, 127.77, 130.25, 137.45, 141. 41, 141.74, 147.88, 156.63 (Figure B1). **ESI–MS** (m/z, DCM): 566.63 (calc. 566.82) $[M]^+$, 567.628 (calc. 567.20) $[tpbq)+H^+]$.

(ttbq): **Anal. calc. for $C_{32}H_{18}S_4N_4$ (%):** C, 65.442; H, 3.068; N, 9.544; S, 21.814. Found C, 65.10; H, 2.96; N, 9.09; S, 18.60. **IR (ν/cm^{-1}):** 3095w, 3062w, 2921w (Ar-H), 1610m (C=N), 1519m (C=C), 1184w (C-N), 1477s (ph), 1299s (C-H),1079w, 1058w, 1041w (C-H out of plane ring), 748s, 698vs (C-C out of plane), 1358s (C-H in plane), 1431s (C-CH in plane), 833m (C-S-C). **^{1}H NMR** (600 MHz, $CDCl_3$) δ 8.55 (2H, s, 5- & 5′-H), 8.28 (2H, d, J = 6 Hz, 8- & 8′-H), 8.21 (2H, d, J = 6 Hz, 7- & 7′-H), 7.56 (4H, d, J = 6 Hz, 4x5′′-H), 7.36 (4H, s, 4x3′′-H), 7.08 (4H, s, 4x4′′-H).**^{13}C-NMR** ($CDCl_3$, 400 MHz, δ, ppm): 123.50, 126.92, 127.31, 129.25, 129.70, 139.30, 142.25, 144.81 (Figure B2). **ESI–MS** (m/z, DCM): 586.78 (calc. 587.05) $[M]^+$, 587.78 (calc. 588.05) $[ttbq)^+H^+]$.

3.2.3 Synthesis of [bis(2,3-di-pyridin-2-yl-quinoxaline)dichlorocopper(II)]: $[Cu(dpq)_2Cl_2]$

0.128g (0.4519 mmol) dpq was completely dissolved in 10 ml ethanol and then added to 10 ml aqueous copper chloride ($CuCl_2.6H_2O$) (0.03 g, 0.223 mmol) solution

dropwise while stirring. Afterwards that mixture was refluxed for 24 h at about 45-50˚ C. The greenish precipitate of the copper complex was collected under vacuum and wash with cold water and ethanol, and dried at room temperature. The yield was 40.66%.

Anal. calc. for $C_{36}H_{24}N_8Cl_2Cu$ (%): C, 61.5; H, 3.4; N, 15.9. Found C, 61.9; H, 3.3; N, 16.2. **IR (ν/cm^{-1}):** 3099w, 3071w, 3018w, (Ar-H), 1597m (C=N), 1560s (C=C), 1159m (C-N), 1480s (ph), 1281m (C-H), 1083m, 992m (C-H out of plane ring), 782s, 751vs (C-C out of plane), 1354s (C-H in plane), 1431s (C-CH in plane), 3424w (HOH). **Dispersive Raman** (785 cm^{-1}): 240w, 346 vw (M-Cl), 473m (M-N), 141m (Cl-M-Cl), 220w (Cl-M-N), 115m (N-M-N). **^{1}H NMR** (400 MHz, $CDCl_3$) δ 8.37 (4H, m, 2x5-H & 2x8-H), 8.22 (4H, dd, J = 4 & 8 Hz, 2x6-H & 2x7-H), 7.96 (12H, m, 4x3′, 4x4′- & 4x6′-H), 7,43 (4H, m, 4x5′-H). **UV-vis** (H_2O) λmax/nm (ε_{max}/M^{-1}cm^{-1}): 246 (49072.7), 272 (30845.5), 338 (16000). **ESI–MS** (m/z, EtOH): 703.1 (calc. 704.0) $[M]^+$, 382.3 (calc. 382.0) $[Cu(dpq)Cl]^+$, 666.6 (calc. 666.1) $[Cu(dpq)2Cl]^+$, 630.2(calc. 631.1) $[Cu(dpq)_2]^{+2}$, 181.3 (calc. 182.0) $[CuCl]^+$+EtOH, 347.9 (calc. 347.0) $[Cu(dpq)]^{+2}$, 284.3 (calc. 285.1) [dpq].

3.2.4 Synthesis of [bis(2,3-di-thenyl-2-yl-quinoxaline)dichloro copper(II)]: $[Cu(dtq)_2Cl_2]$

0.031g (0.1061 mmol) dtq was dissolved in10 ml ethanol, and added to 10 ml aqueous copper chloride ($CuCl_2.6H_2O$) (0.0071 g, 0.0528 mmol) solution dropwise while stirring. The mixture then was refluxed for 24 h at 45-50˚C. The yellowish precipitate of $Cu(dtq)_2Cl_2$ collected and dried under vacuum and washing with cold water and cold ethanol. (Yield: 79.75 %)

Anal. calc. for $C_{32}H_{20}S_4N_4Cl_2Cu$ (%): C, 53.2; H, 2.8; N, 7.7; S, 17.7. Found C, 53.5; H, 2.4; N, 7.6; S, 17.7. **IR (ν/cm^{-1}):** 3071w, (Ar-H), 1591m (C=N), 1560m (C=C), 1130w (C-N), 1471s (ph), 1312s (C-H), 1078w, 1015w, 989w (C-H out of plane ring), 761s, 704vs (C-C out of plane), 1351s (C-H in plane), 1435s (C-CH in plane), 819m (C-S-C). **Dispersive Raman** (785 cm^{-1}): 313w, 325m (M-Cl), 460m, 527w (M-N), 173m (Cl-M-Cl), 206w (Cl-M-N), 118m (N-M-N). **^{1}H NMR** (400 MHz, $CDCl_3$) δ

8.07 (4H, 2xd, J = 4 Hz, 2x5-*H* & 2x8-*H*), 7.86 (4H, dd, J = 4 & 6 Hz, 2x6-*H* & 2x7-*H*), 7.62 (4H, d, J = 4 Hz, 4x5′-*H*), 7.24 (4H, d, J = 4 Hz, 4x3′-*H*), 7.13 (4H, t, J = 4 Hz, 4x4′-*H*).**UV-vis** (Acetonitrile) λ_{max}/nm (ε_{max}/$M^{-1}cm^{-1}$): 257 (30260), 286 (26110), 378 (18537.5). **ESI–MS** (m/z, Acetonitrile): 723.1 (calc. 722.5) $[M]^+$, 428.5 (calc. 430.2) $[Cu(dtq)Cl_2]$, 392.9 (calc. 392.0) $[Cu(dtq)Cl]^+$, 651.6 (calc. 652.9) $[Cu(dtq)_2]^{+2}$, 726.1 (calc. 727.5) $[Cu(dtq)_2Cl]^+ + K^+$, 745.4 (calc. 745.5) $[Cu(dtq)_2]^{+2} + Na^+$, 294 (calc. 295.0) [dtq].

3.2.5 Synthesis of [bis(2,3-di-pyridin-2-yl-quinoxaline)dichloro platinum(II)]: $[Pt(dpq)_2Cl_2]$

100 mg (0.241 mmol), K_2PtCl_4 was dissolved in 5 mL of double distilled water. Next, 163.7 mg (0.964mmol) $AgNO_3$ was added directly to the aqueous platinum solution and stirred at room temperature at the dark overnight. Then precipitated AgCl was removed by filtration. 5 mL DMF solution of 0.1377 g (0.482 mmol) dpq was added dropwise to the filtrate by string and the mixture was refluxed at 40°C for another 24 h. The precipitate of $Pt(dpq)_2Cl_2$ was collected under vacuum and dried at room temperature. The percent yield for the $[Pt(dpq)_2Cl_2]$ is 34.37%.

Anal. calc. for $C_{36}H_{24}N_8Cl_2Pt$ (%): C, 51.8; H, 2.9; N, 13.4. Found C, 51.1; H, 3.0; N, 13.1. **IR (ν/cm^{-1}):** 3107w, 3082w, 3065w, (Ar-H), 1606m (C=N), 1550s (C=C), 1185w (C-N), 1474s (ph), 1301m (C-H),1096w, 1012w (C-H out of plane ring), 783s, 759vs (C-C out of plane), 1419s (C-H in plane), 1435s (C-CH in plane). **Dispersive Raman** (785 cm^{-1}): 343m (M-Cl), 422m (M-N), 112m (Cl-M-Cl), 200w (Cl-M-N), 253m (N-M-N). **^{1}H NMR** (600 MHz, $CDCl_3$) δ 8.37 (4H, m, 2x5-H & 2x8-H), 8.22 (4H, dd, J = 4 & 8 Hz, 2x6-H & 2x7-H), 7.96 (12H, m, 4x3′-, 4x4′- & 4x6′-H), 7,43 (4H, m, 4x5′-H).UV-vis (Acetonitrile) λmax/nm (ε_{max}/$M^{-1}cm^{-1}$): 275 (42285.7), 334 (19900). **ESI–MS** (m/z, EtOH): 834.6 (calc. 833.4) [M]+, 799.2 (calc. 801.0) $[Pt(dpq)_2Cl]^+$, 763.7 (calc. 763.1) $[Pt(dpq)_2]^{+2}$, 841.8(calc. 843.6) $[Pt(dpq)_2]^{+2} + 2K^+$, 845.3 (calc. 846.0) $[Pt(dpq)_2Cl]^+ + EtOH$, 809.8 (calc. 810.0) $[Pt(dpq)_2]^{+2} + 2EtOH$, 284.3 (calc. 285.1) [dpq].

3.2.6 Synthesis of [bis(2,3-di-thenyl-2-yl quinoxaline)dichloroplatinum(II)]: [$Pt(dtq)_2Cl_2$]

163.7 mg (0.964mmol) $AgNO_3$ is dissolved in 5 mL aqueous solution of 100 mg (0.241 mmol), K_2PtCl_4 at dark and stirred overnight. Then recipitated AgCl was filtered out. 5 mL DMF solution of 0.1418 g (0.482 mmol) dtq ligand was added dropwise in to the filthate. The resultant mixture was refluxed at 40°C for 24 h. The greenish precipitate of $Pt(dtq)_2Cl_2$.collected and dried under vacuum. The percent yield for the [$Pt(dtq)_2Cl_2$] is 31.67%.

Anal. calc. for $C_{32}H_{20}S_4N_4Cl_2Pt$ (%): C, 44.9; H, 2.4; N, 6.6; S, 15.0. Found C, 44.7; H, 2.4; N, 8.9; S, 14.4. **IR (ν/cm^{-1}):** 3071w, 2920w, (Ar-H), 1594w (C=N), 1519w (C=C), 1132w (C-N), 1474m (ph), 1298m (C-H),1061w, 1045w, 981m (C-H out of plane ring), 760s, 709vs (C-C out of plane), 1354m (C-H in plane), 1433m (C-CH in plane), 844m (C-S-C), 3347w (HOH). **Dispersive Raman** (785 cm^{-1}): 324m (M-Cl), 416m (M-N), 114m (Cl-M-Cl), 200w (Cl-M-N), 251m (N-M-N). **^{1}H NMR** (400 MHz, $CDCl_3$) δ 8.06 (4H, 2xd, J = 4 Hz, 2x5-H & 2x8-H), 7.86 (4H, dd, J = 4 & 6 Hz, 2x6-H & 2x7-H), 7.62 (4H, d, J = 4 Hz, 4x5′-H), 7.24 (4H, d, J = 4 Hz, 4x3′-H), 7.13 (4H, t, J = 4 Hz, 4x4′-H).**UV-vis** (Acetonitrile) λmax/nm (ε_{max}/M^{-1}cm^{-1}): 288 (49100), 382 (34171.4). **ESI–MS** (m/z, CH_2Cl_2): 854.6 (calc. 855.1) [M]$^+$, 783.1 (calc. 783.0) [$Pt(dtq)_2$]$^{+2}$, 829.1 (calc. 830.3) [$Pt(dtq)_2$]$^{+2}$+2Na+, 559.9 (calc. 602.3) [$Pt(dtq)Cl_2$]$^{+2}$, 829.2 (calc. 830.5) [Pt(dtq)2]$^{+2}$+EtOH, 294 (calc. 295.0) [dtq].

3.2.7 Synthesis of [2,3,2',3'-Tetra-pyridin-2-yl-[6,6']biquinoxaline(dichloro) copper(II)]: [$Cu(tpbq)Cl_2$]

0.128g (0.2268 mmol) tpbq was dissolved in about 10 ml ethanol and added to 10 ml aqueous 0.0305 g (0.2268 mmol) copper chloride ($CuCl_2.6H_2O$) solution dropwise while stirring. Then the solution was refluxed for 24 h at about 45-50˚C. The solid formed during this stage was collected by filtration and dried under vacuum after washing with cold water and cold ethanol. The percent yield was 13.71 % for [$Cu(tpbq)\ Cl_2$].

Anal. calc. for $C_{36}H_{22}N_8Cl_2Cu$ (%): C, 61.676; H, 3.163; N, 15.983. Found C, 61.466; H, 3.341; N, 15.137. **IR (v/cm^{-1}):** 3054w, 3005w, 2924w, (Ar-H), 1706m (C=N), 1577s (C=C), 1149m (C-N), 1472s (ph), 1290m (C-H),1072m, 993m (C-H out of plane ring), 789s, 742vs (C-C out of plane), 1386s (C-H in plane), 1430s (C-CH in plane), 3366w (HOH). **Dispersive Raman** (785 cm^{-1}): 246m, 353m (M-Cl), 394m, 460m (M-N), 186m (Cl-M-Cl), 220w (Cl-M-N), 114m (N-M-N). ^{1}**H-NMR** (DMSO-d_6, 400 MHz, δ, ppm): δ :7.61 (d, 2H, H-5, 5′), 7.80 (m, 4H, H-3, 3′, H-4,4′), 8.24(d, 2H, H6,6′), 8. 41 (m, 2HC_6H_3),8.60 (s, HC_6H_3). **UV-vis** (DMF) λ_{max}/nm (ε_{max}/M^{-1}cm^{-1}): 285 (2310), 373 (13490). **ESI–MS** (m/z, EtOH): 702.1 (calc. 702.07) [M]$^+$, 382.32 (calc. 382.0) [Cu(tpbq)Cl]$^+$, 699.41 (calc. 700.07) [Cu(tpbq)Cl]$^+$-2H, 630.12(calc. 631.16) [Cu(tpbq)]$^{+2}$, 417.22.3 (calc. 418.76) [$CuCl_2$]$^+$, 567.20 (calc. 566.63) [(tpbq)$_2$], 284.32 (calc. 283.31) [tpbq].

3.2.8 Synthesis of [2,3,2',3'-Tetra-thenyl-2-yl[6,6']biquinoxaline(dichloro) copper(II)]: [Cu(ttbq) Cl_2]

0.0312g (0.0532 mmol) ttbq was dissolved in 10 ml ethanol and added to 10 ml aqueous solution of 0.0072 g (0.535 mmol) ($CuCl_2.6H_2O$) dropwise and resultant solution was refluxed for 24 h at 45-50˚C, the solid was collected by filtration and dried under vacuum after washing with cold water and cold ethanol at room temperature. The percent yield was calculated as 26.08 %.

Anal. calc. for $C_{32}H_{18}S_4N_4Cl_2Cu$ (%): C, 53.291; H, 2.516; N, 7.768; S, 17.783. Found C, 53.655; H, 3.211; N, 7.548; S, 18.50. **IR (v/cm^{-1}):** 3053w, 2922w (Ar-H), 1607m (C=N), 1519m (C=C), 1179w (C-N), 1473s (ph), 1296s (C-H),1045w, 978w, 934w (C-H out of plane ring), 744s, 696vs (C-C out of plane), 1368s (C-H in plane), 1423s (C-CH in plane), 835m (C-S-C), 3462w (HOH). **Dispersive Raman** (785 **cm^{-1}**): 239m, 280m (M-Cl), 381m, 417m (M-N), 146m (Cl-M-Cl), 206w (Cl-M-N), 120m (N-M-N). **^{1}H-NMR** (DMSO-d_6, 400 MHz, δ, ppm): 7.21 (d, 2H, H-3,3′), δ: 7.30 (t,2H, H-4,4′), 8.00 (dd, 2H, H-5,5′), 8.48 (dd, 2H, C_6H_3),8.60 (s, HC_6H_3). **UV-vis** (DMF) λ_{max}/nm (ε_{max}/M^{-1}cm^{-1}): 287 (55990), 415 (58830). **ESI–MS** (m/z, Acetonitrile): 721.9 (calc. 721.23) [M]$^+$, 723.51 (calc. 722.23) [Cu(ttbq)Cl_2]+H, 685.44 (calc. 685.78) [Cu(ttbq)Cl]$^+$, 649.18 (calc. 650.33) [Cu(ttbq)]$^{+2}$, 743.52 (calc. 744.23)

$[Cu(ttbq)Cl_2]^{+2}+Na^+$,663.46 (calc. 662.78) $[Cu(ttbq)]^{+2}$-(Cl+Na), 587.05 (calc. 586.78) $[(ttbq)_2]$.

3.2.9 Synthesis of [2,3,2',3'-Tetra-pyridin-2-yl-[6,6']biquinoxaline(dichloro) platinum(II): [Pt(tpbq)Cl$_2$]

163.7 mg (0.964 mmol) $AgNO_3$ is dissolved in 5 mL aqueous solution of 100 mg (0.241 mmol), K_2PtCl_4 at dark. The solution was kept overnight at room temperature and then formed AgCl was filtered out. To this solution, 5 mL DMF solution of 0.136 g (0.482 mmol) tpbq was added slowly and the mixture was refluxed at 40°C during 24 h. The Pt(tpbq)Cl_2 was collected under vacuum and dried at room temperature. The percent yield for the [Pt(tpbq)Cl_2] was 16.45%.

Anal. calc. for $C_{36}H_{22}N_8Cl_2Pt$ (%): C, 51.932; H, 2.663; N, 13.458. Found C, 49.237; H, 3.013; N, 13.930. **IR (ν/cm^{-1}):** 3200w, 3055w, 2915w, (Ar-H), 1707m (C=N), 1580s (C=C), 1152w (C-N), 1472s (ph), 1293m (C-H),1076w, 1042w (C-H out of plane ring), 789s, 744vs (C-C out of plane), 1380s (C-H in plane), 1426s (C-CH in plane), 3365w (HOH). **Dispersive Raman** (785 nm): 340m (M-Cl), 404m (M-N), 113m (Cl-M-Cl), 213w (Cl-M-N), 240m (N-M-N). **^{1}H-NMR** (DMSO-d_6, 400 MHz, δ, ppm): δ :7.59 (d, 2H, H-5, 5′), 7.83 (m, 4H, H-3, 3′, H-4,4′), 8.27 (d, 2H, H6,6′), 8. 50 (m, 2HC_6H_3), 8.68 (s, HC_6H_3). **UV-vis** (DMF) λ_{max}/nm (ε_{max}/M^{-1}cm^{-1}): 287 (67930), 373 (43540). **ESI–MS** (m/z, EtOH): 833.11 (calc. 832.62) $[M]^+$, 799.01 (calc. 797.65) $[Pt(tpbq)Cl]^+$, 762.04 (calc. 762.20) $[Pt(tpbq)]^{+2}$, 764.04 (calc. 764.20) $[Pt(tpbq)]^{+2}$+2H, 587.51 (calc. 587.63) $[(tpbq) +2Cl]^+$-2H, 567.20 (calc. 566.63) [(tpbq)], 284.10 (calc. 283.31) [tpbq].

3.2.10 Synthesis of [2,3,2',3'-Tetra-thenyl-2-yl-[6,6']biquinoxaline(dichloro) platinum(II): [Pt(ttbq)Cl$_2$]

100 mg (0.241 mmol), K_2PtCl_4 was dissolved in 5 mL of double distilled water. 163.7 mg (0.964 mmol) $AgNO_3$ was dissolved in that equeous platinum solution and stirred at room temperature at the dark overnight. The precipitate of AgCl was removed by filtration. Afterwards 5 mL DMF solution of 0.1413 g (0.482 mmol) ttbq was added dropwise to this and the refluxed at 40°C for another 24 h, and the precipitate of

$Pt(ttbq)Cl_2$ was collected under vacuum and dried at room temperature. The percent yield for the $[Pt(ttbq)Cl_2]$ was 13.19%.

Anal. calc. for $C_{32}H_{18}S_4N_4Cl_2Pt$ (%): C, 45.071; H, 2.128; N, 6.570; S, 15.039. Found C, 45.246; H, 2.368; N, 6.509; S, 16.33. **IR (v/cm^{-1}):** 3054w, 2924w, (Ar-H), 1606w (C=N), 15198w (C=C), 1178w (C-N), 1473m (ph), 1295m (C-H),1048w, 978w, 933m (C-H out of plane ring), 744s, 695vs (C-C out of plane), 1368m (C-H in plane), 1422m (C-CH in plane), 835m (C-S-C), 3358w (HOH). **Dispersive Raman** (785 cm^{-1}): 388m (M-Cl), 528m (M-N), 118m (Cl-M-Cl), 200w (Cl-M-N), 250m (N-M-N). **^{1}H-NMR** (DMSO-d_6, 400 MHz, δ, ppm): 7.15 (d, 2H, H-3,3′), δ: 7.36 (t, 2H, H-4,4′),8.15(dd, 2H, H-5,5′), 8.50 (dd, 2H, C_6H_3),8.60 (s, HC_6H_3). **UV-vis** (DMF) λ_{max}/nm (ε_{max}/M^{-1}cm $^{-1}$): 284 (49140), 414 (48890). **ESI–MS** (m/z, CH_2Cl_2): 852.95 (calc. 852.77) $[M]^+$, 815.51 (calc.815.32) $[Pt(ttbq)Cl_2]$ -[Cl+2H], 910.39 (calc. 910.75) $[Pt(ttbq)Cl_2]$ +[Na+K]-5H, 851.39 (calc. 851.77) $[Pt(ttbq)Cl_2]$ -H, 891,54 (calc. 892.76) $[Pt(ttbq)Cl_2]$ +K, 587.05 (calc. 586.78) [(ttbq)].

3.3 Solubility

Solubility of all the complexes was studied in different solvents such as acetonitrile, ethanol, methanol, acetone and DMF. As observed from the (Table 3.1) that all the complexes are very soluble in common organic solvents; methanol, ethanol and DMF. Almost all complexes are insoluble in H_2O, but all are very soluble in DMF.

Table 3.1 Solubility of the complexes

Complexes	AN	H_2O	EtOH	MeOH	Acetone	DMF
$[Cu(dpq)_2Cl_2]$	SS	VS	VS	VS	SS	VS
$[(Cu(dtq)_2Cl_2]$	VS	NS	VS	VS	VS	VS
$[Pt(dpq)_2Cl_2]$	NS	NS	VS	VS	NS	VS
$[Pt(dtq)_2Cl_2]$	VS	NS	VS	VS	SS	VS
$[Cu(tpbq)Cl_2]$	NS	NS	SS	SS	NS	S
$[Cu(ttbq)Cl_2]$	SS	NS	S	S	S	VS
$[Pt(tpbq)Cl_2]$	VS	S	S	S	S	S
$[Pt(ttbq)Cl_2]$	NS	NS	SS	SS	S	S
SS: Slightly Soluble; VS: Very Soluble and NS: Not Soluble						

3.4 Methods

3.4.1 DFT studies

For the computational analysis of the metal ligand complexes, density functional theory calculations were performed by utilizing the hybrid functional B3LYP [135-136]. First, the lowest energy structures of the isolated dpq, dtq, tpbq and ttbq ligands in their neutral form were obtained through the conformational analysis using Pople's triple zeta quality basis set, 6-311++G(d,p) [137]. Conformers of the metal-ligand complexes were prepared by using the minimum energy structures of the dpq, dtq, dpbq and dtbq ligands, and they were fully optimized at the B3LYP/LANL2DZ level of theory. For the calculations on the complexes, the LANL2DZ basis set was used due to the unavailability of the 6-311++G(d,p) basis set for the metal atoms Cu and Pt and for its performance on similar systems [138-139]. Hessian calculations were also performed on optimized metal-ligand complexes, both to verify if the geometries were true minima and to obtain zero point vibrational energies that were used in the calculation of the relative energies of the different conformers. Following the conformational analyses, reorganization energies and ligand binding energies were calculated at the B3LYP/LANL2DZ level of theory. All DFT calculations included Grimme's empirical dispersion corrections with Becke-Johnson damping, and they were performed by using the Gaussian 09 Rev. D.01 software package [140]. Molecules were visualized by GaussView 5.0.9 [141].

3.4.2 DNA and HSA interaction

3.4.2.1 Electronic absorption spectroscopy (EAS)

Conventionally, one can look for any interaction among DNA and metal-based compounds by detecting changes in absorption bands in the presence of nucleic acid. To do so, the compounds were diluted in a mixture of DMF for all copper and platinum compounds except $[Cu(dtq)_2]Cl_2$ in AN, and $[Cu(dpq)_2]Cl_2$ in H_2O with Tris–HCl by 1:1 by volume buffer (5 mM Tris–HCl; 50 mM NaCl, pH 7.11). EAS monitoring was carried out with an HP Agilent®8453 Spectrophotometer. Any variation in EAS values was monitored upon maintaining the concentration accumulation of compounds at a

fixed level at the same time as while increasing the concentration of Calf Thymus DNA (CT-DNA) (R= [DNA]/[Complex]= 0-10). The intrinsic binding constant (K_b) of the compounds with CT-DNA is found with the help of this formula [142].

$$[DNA]/(\varepsilon_a-\varepsilon_f) =[DNA]/(\varepsilon_b-\varepsilon_f) +1/K_b[(\varepsilon_a-\varepsilon_f)] \quad (3.1)$$

Here, ε_a is the apperent extinction coefficient; ε_f and ε_b show the extinction coefficients of both free and bound compound respectively; and K_b is determined based on the proportion of the slope to the intercept gained from a series of $[DNA]/(\varepsilon_a-\varepsilon_f)$ vs [DNA]. Selected incubation times for each platinum and copper complex are given in (Table 3. 2). Thermodynamic parameters were also obtained by EAS experiments conducted at 310, 320, 330, and 340 K. The standard Gibbs free energy (ΔG^o) was calculated by using the following equation (3.2):

$$\Delta G^o = -R\ T\ Ln\ K_b \quad (3.2)$$

The binding enthalpy and entropy were determined from the slope and the intercept of the Van't Hoff [143] equation (3.3):

$$Ln(K_b)= (-\Delta H^o/RT)+(\Delta S^o/R) \quad (3.3)$$

Table 3.2. Experimental Concentration of the complexes and the CT- DNA

Complexes	**Concentration (M)**		**Incubation Time (min)**
	Complexes	**Calf thymus DNA**	
$[Cu(dpq)_2Cl_2]$	3.04×10^{-3}	$0\text{-}1.25 \times 10^{-3}$	45
$[Cu(dtq)_2Cl_2]$	2.74×10^{-3}	$0\text{-}7.80 \times 10^{-4}$	30
$[Pt(dpq)_2Cl_2]$	3.00×10^{-3}	$0\text{-}5.02 \times 10^{-4}$	30
$(Pt(dtq)_2Cl_2]$	3.22×10^{-3}	$0\text{-}5.86 \times 10^{-4}$	30
[Cu(tpbq) Cl_2]	3.00×10^{-3}	$0\text{-}9.60 \times 10^{-4}$	45
[Cu(ttbq) Cl_2]	0.50×10^{-3}	$0\text{-}4.20 \times 10^{-4}$	30
[Pt(tpbq) Cl_2]	3.00×10^{-3}	$0\text{-}8.00 \times 10^{-4}$	60
[Pt(ttbq) Cl_2]	3.00×10^{-3}	$0\text{-}1.19 \times 10^{-3}$	45

UV-titration with HSA were monitored with the same spectrometer applied for the DNA test. Additionally, the compounds were diluted in a mixture of DMF for all copper and platinum compounds except $[Cu(dtq)_2]Cl_2$ in AN, and $[Cu(dpq)_2]Cl_2$ in H_2O with Tris–HCl by 1:1 by volume buffer (5 mM Tris–HCl; 50 mM NaCl, pH 7.11). Under these circumstances, the EAS variations were recorded while maintaining fixed the HSA concentration (2.12×10^{-5} M) and altering that of the compound between 0 and 2.12×10^{-6} M. Furthermore, the concentration of the representative EA band of HSA at about 280 nm was monitored - with the series being twice reciprocal of $1/(A–A_o)$ as versus to 1/[complex] [144], in which A and A_o represent absorption values both in the presence and absence of the compounds, respectively. The intrinsic binding constant (K_b) of the compounds to the protein was found based on spectral variations and determined as the proportion of the slope to the intercept as appearing in the series. Selected incubation times for each platinum and copper complex are given in (Table 3.3). In order to understand the nature of the interaction between the complexes, CT-DNA, and HSA, thermodynamic experiments were also performed and the temperature dependent binding constant (K'_b) was determined at 310, 320, 330 and 340 K.

Table 3.3 Experimental Concentration of the complexes and the HSA.

Complexes	**Concentration (M)**		**Incubation Time (min)**
	Complexes	**Human serum albumin (HSA)**	
$[Cu(dpq)_2Cl_2]$	3.13×10^{-3}	2.12×10^{-5}	30
$(Cu(dtq)_2Cl_2]$	3.27×10^{-4}	2.12×10^{-5}	30
$(Pt(dpq)_2Cl_2]$	2.99×10^{-4}	2.12×10^{-5}	45
$(Pt(dtq)_2Cl_2]$	2.57×10^{-4}	2.12×10^{-5}	45
$[Cu(tpbq)Cl_2]$	3.18×10^{-4}	2.12×10^{-5}	60
$[Cu(ttbq)Cl_2)$	2.77×10^{-4}	2.12×10^{-5}	30
$[Pt(tpbq)Cl_2]$	3.00×10^{-4}	2.12×10^{-5}	60
$[Pt(ttbq)Cl_2]$	3.05×10^{-4}	2.12×10^{-5}	30

3.4.2.2 Viscosity measurements

These tests were done to additionally shed light on the processes taking place between metal compounds and DNA [145], with an (AND® SV-10 VIBRO Viscometer) at room temperature. The concentration values for each compound changed from 0 to 70 μm whereas that of CT-DNA remained the same at 60 μm at 1:1 (V / V) 5mM tris hydrochloric acid: 50 mM NaCl buffer mixture at pH = 7.11. The viscosity of the CT-DNA with (η) and without (η_o) the compounds present was checked automatically and the values of $(\eta/\eta_o)^{1/3}$ compared to 1/R and set against [complex]/[DNA] concentration ratio, Here, η is the DNA viscosity with and η_o without the compounds present. Accordingly, similar assessments were made for HSA in the same manner.

3.4.2.3 Thermal Denaturation

Thermal study specimens were made with 1:1 (V/V) 5 mM Tris HCl:50 mM NaCl buffer mixture at pH=7.11. The absorbance at 260 nm was monitored with and without the compounds present with the help of an Agilent®8453 Spectrophotometer and a HAAKE circular bath. Throughout the procedure, CT-DNA value remained the same at 60 μM and those of the compounds changed from 10 to 160 μM. Temperatures were elevated by 1℃ min^{-1}. In case of samples containing HSA, the absorbance of the peak of albumin at 280 nm was followed as temperature was raised. The ultimate concentration of this solution stood at 2.12×10^{-5} M and that of the compounds at 2.12×10^{-6} μM based on 1:1 (V/V) 5 mM Tris HCl:50 mM NaCl buffer mixture at pH=7.11.

3.4.2.4 Fluorescence Titration

The scope of fluorescence of ethidium bromide (EB) was applied to see DNA binding scopes occurring in the metal-based compounds and DNA [146]. EB releases sharp fluorescence rays in the presence of DNA thanks to robust processes occurring between the joined DNA base couples. Research has shown that increased fluorescence may be suppressed through supplying another molecule [147, 148]. Fluorometric assessments were carried out, as such, using a Thermo Scientific® Lumina Fluorescence Spectrometer and keeping constant the EB pretreated CT-DNA

concentration and changing those of the compounds in 1:1 (V/V) 5 mM Tris HCl:50 mM NaCl buffer mixture at pH=7.11. These assessments also incorporated an excitation wavelength of 478 nm with an emission scope fixed from 500 to 800 nm using a luminous software wave scan. The final spectra were examined based on the common Stern–Volmer Eq [149].

$$I_o / I = 1 + K_{sv}.r \qquad (3.4)$$

In which, I_0 and I represent fluorescence intensities at 605 nm with and without quencher, respectively; K_{sv} represents the linear Stern – Volmer quenching constant; r is the concentration of quencher.

In case of protein specimens, the HSA value was kept constant at 1 μM while assessments took place, whereas those of the compounds were altered between 0 and 50 μM in 1:1 (V/V) 5 mM Tris HCl:50 mM NaCl buffer mixture at pH= 7.11. The HSA fluorescence spectra was determined upon keeping constant the agitation wavelength at 280 nm and the release was monitored between 200 and 500 nm.

3.4.3 Biological Activity

3.4.3.1 MTT Cell Viability Assay

Cell culture conditions: Several cancer cell lines from different origins including human glioblastoma A172 (CRL-1620), LN229 (CRL-2611), U87 (HTB-14) cell lines; human lung A-549 (CCL-185), human breast MDA -231 (HTB-26), human cervix HeLa (ATCC, CCL-2), human prostate PC-3 (ATCC, CRL-1435) cell lines; and Chinese hamster ovary CHOK1 cell line (CCL61) used as an control were purchased from American Type Culture Collection (ATCC, USA). They were cultured in Dulbecco's modified Eagle's Medium-F12 (DMEM/F12, #D0547, Sigma- Aldrich) supplemented with 5% Fetal Bovine Serum (FBS, # 10500, Gibco) and 1% antibiotic-antimycotic (#15240, Gibco) and incubated at 37 ^{o}C and 5% CO_2. They were subcultured and used for the following assays when they reached 70-80% confluency.

MTT Cell Viability Assay: A172, LN229, U87, A549, MDA-231, HeLa, PC-3 and CHO-K1 were seeded at a cell density of 6 x 10^3 cells/well in the 96-well plates and

incubated at 37 ^{o}C and 5% CO_2 for 24 h. The following day, copper(II) and platinium(II) compounds were applied to the cell monolayers at concentrations of 6.25, 12.5, 25, 50, and 100 μM in DMEM-F12 and incubated at 37 ^{o}C and 5% CO_2 for 24, 48, and 72 h. To examine the cytotoxic effects of our compounds, the colorimetric agent MTT (3-[4,5-dimethylthiazol-2-yl]-2,5-diphenyltetrazolium bromide, # M5655, Sigma-Aldrich) tetrazolium salt converted into a purple formazan product after reduction by the mitochondrial enzymes of the metabolically active live cells was dissolved in phosphate buffer solution (PBS, 5 mg/ml, w/v). After each incubation period, MTT (5 μg/ml) in DMEM was added to each well and incubated at 37 °C and 5% CO_2 for 4 h. The formazan crystals dissolving solution, dimethyl sulfoxide (DMSO # D 8418, Sigma-Aldrich), was added into each well and placed in the shaker for 2 h. The absorbance was measured on a microplate reader with a test wavelength of 570 nm and a reference wavelength of 630 nm.

3.4.3.2 Oxidative stress testing (DCFDA assay)

The reactive oxygen species (ROS) formation on the selected cell lines upon exposure to the synthetized Cu and Pt complexes was investigated using the oxidation-sensitive dye 2′, 7′-dichlorofluorescein diacetate (DCFDA, #D6883 Sigma-Aldrich). The cell lines (A172, LN229, U87, HeLa, MDA-231, PC-3, A549, and CHO-K1) were seeded (6 x 10^3 cells/well) into the 96-well plates and incubated at 37^{o}C and 5% CO_2 for 24 h. After that, the Cu and Pt complexes at a concentration range of 6.25 to 100 μM were added on the cell monolayers. Hydrogen peroxide (H_2O_2) at concentrations from 50 to 500 μM was utilized as a positive control. Following day, 5 μM of DCFDA in PBS was added into the cell monolayers and then the plate was incubated for 30-45 min. Consequently, the fluorescence intensity was measured with 485 nm excitation and 535 nm emission wavelengths using a microplate reader. The fluorescence values of each treatment was normalized to the negative control including only growth medium without any treatment. The assay was repeated in triplicate.

3.4.3.3 TUNEL assay

The sensitive cell lines selected according to the results of the cell viability assay, U87 and HeLa in $5x10^4$ cells, were seeded on 12 mm round cover slips in the 24-well plate and incubated at 37 ºC, and 5% CO_2 for 24 h. The following day, the cell monolayers were treated with freshly prepared the Cu and Pt complexes at 50 and 100 μM and incubated for 24 h. The day after, the cell monolayers were fixed in 4% paraformaldehyde (15 min at room temperature). Then, DNA fragmentation associated with apoptosis was examined by the terminal deoxynucleotidyltransferase (TdT)-mediated dUTP nick end labeling (TUNEL) method using a commercial assay kit, In Situ Cell Death Detection Kit (Roche, #11767291910), following the manufacturer's instructions. The experiment was repeated at two independent times with the tested cell lines. Images were taken using a Leica DMI 6000 fluorescence microscope with 40X magnification.

3.4.3.4 Matrigel invasion analysis

To assess the metastatic potential of tumor cells, Matrigel invasion analysis is useful to evaluate cell invasion of malignant cells. Matrigel invasion assay was performed using a transwell inserts with 8 μm pore size polycarbonate membrane (Corning Costar, Cambridge, MA). First of all, transwell inserts were coated with 1/5 of Matrigel (Beckton Dickinson, Bedford, MA) in FBS free DMEM-F12 and they were air-dried at room temperature for 4 to 5 h. Selected sensitive U87 and HeLa cell lines (3×10^5 cells/insert) with previously prepared Cu or Pt complexes at concentrations of 6.25 or 12.5 μM in the medium containing 1% FBS were added to the apical side of the inserts. The basolateral side of the inserts was filled with DMEM-F12 including 10% FBS and incubated at 37ºC in a humidified incubator with 5% CO_2 for 24 h. After that, the cell monolayers in the transwell inserts were fixed with ice-cold methanol and then stained with 0.05% crystal violet. The invasion of the cells to the basolateral side of the inserts was imaged with the light microscope with 40X magnification. The experiment was repeated twice.

3.4.3.5 In vitro scratch wound healing

Cell migration, invasion, and adhesion are crucial steps in cancer development and progression, invasion, and metastasis therefore, it is very important to inhibit these mechanisms using novel drugs to overcome the disease. HeLa cells (3×10^4 cells/insert) were seeded into 96-well plates. When they reached 80–90% confluence, scratches were created by using AutoScratch™ (BioTek) in a straight line. Then cell monolayers were washed with PBS to remove floating cells. After that, the cell monolayers were exposed to the Cu or Pt complexes at concentrations of 6.25 or 12.5 μM and incubated at 37ºC and 5% CO_2 in a humidified incubator for 24 h, 48 h, and 72 h. Images were taken at the beginning of the exposure (time 0), and every 24, 48 and 72 incubation periods.

3.4.4 Analysis of DNA Damage

3.4.4.1 In-vitro comet assay

A gel electrophoresis-based method (comet assay) was performed to detect DNA damage in the used cell lines as described by Olive and Banath [211], with some minor modification. The selected cell lines were seeded at a cell density of 4×10^4 cells in a 24-well plate and incubated at 37°C, in 5% CO_2 for 24 h. The freshly prepared concentrations of the 50 and 100 μM of cupper and platinum compounds were added to the cell monolayers and incubated for another 24 h. The cells were treated with Ethyl methanesulfonate (EMS, Merck-Millipore #8.20774) at a concentration of 40 μM for 1 h and serviced as a positive control. As a negative control, the cells were only treated with the medium. By the end of the exposure period, the cells were trypsinized and suspended at a concentration of 1.6×10^4 cells/mL in DPBS. The cell suspensions were mixed with 1% low-gelling-temperature agarose (#A-4018 Sigma-Aldrich) at 40°C at a ratio of 1:3 and spread all over the slides. After agarose gellification, the slides were submerged into the lysis solution (1.2 M NaCl, 100 mM Na_2EDTA, 0.1% sodium lauryl sarcosinate, 0.26 M NaOH, pH > 13) at 4°C in the dark for 18-20 h. The day after, the slides were washed three times in an alkaline carrier buffer at pH=13 for 20 min and then submerged in a fresh alkaline solution (0.03 M

NaOH, 2 mM Na_2EDTA, pH ~12.3). The slides were placed in an electrophoresis chamber filled with a consistent volume of the buffer, and electrophoresis was conducted in the alkaline solution for 25 min at a voltage of 0.6 V/cm. The slides were washed with distilled water and stained with propidium iodide (10 µg/mL, #P4864 Sigma-Aldrich) for 20 min. The slides were analyzed at Ex/Em = ~535/~617 nm, and the images were taken using a fluorescence microscope. The experiment was performed in triplicate, and 50 cells were individually examined in each repeat.

3.4.4.2 Plasmid DNA interaction assay

DNA cleavage activities of the synthetized Cu or Pt complexes were evaluated by determining their ability of converting the plasmid DNA in the supercoiled form (SC) to the its nick circular form (NC) and the linear form (LF). In this assay, pBI-CMV1 plasmid (3.1 kb, #631630, Clontech) was grown in E-coli and then purified using a Machery Nagel DNA isolation kit. The 100 and 200 µM concentrations of the copper and platinum compounds were incubated with 200 ng of plasmid DNA in double-distilled water (ddH_2O) for 16 h at RT in a total volume of 20 µL. After that, the studied samples were electrophoresed on 1% agarose gels by means of a Tris-acetate-EDTA (TAE) buffer at 100 V for 1 h. The gel eventually was stained using ethidium bromide, and the images of the bands were captured using a ChemiDoc imaging system (BioRad). The testing was done in two repeats [150].

3.4.5 Statistical analysis

Significance analyses were performed by means of one-way analysis of variance (ANOVA) and Tukey's post hoc test. The level of statistical significance was $p < 0.05$.

CHAPTER 4

4 RESULTS & DISCUSSION

4.1 Computational studies

The DFT calculation gives more suitable information about structural features, in the absence of crystal data, in addition to the energy minimized conformation, such as coordination behaviour in metal complexes and HOMO–LUMO energy gap [151].
The lowest energy structures of the $Cu(dpq)_2Cl_2$, $Cu(dtq)_2Cl_2$, $Pt(dpq)_2Cl_2$, $Pt(dtq)_2Cl_2$, $Cu(tpbq)_2Cl_2$, $Cu(ttbq)_2Cl_2$, $Pt(tpbq)_2Cl_2$, and $Pt(ttbq)_2Cl_2$ complexes based on the calculations at the B3LYP/LANL2DZ level of theory are given in (Figure 4.1).

As can be seen from Figure 4.1, while the $Cu(dtq)_2Cl_2$, $Pt(dpq)_2Cl_2$, and $Pt(dtq)_2Cl_2$ structures seem to have square planar geometry around the metal center, the $Cu(dpq)_2Cl_2$ geometry significantly deviates from planarity due to the additional interaction between Cu^{2+} and the nitrogen atom in the pyridyl group with a distance of 2.26 Å, which does not exist in the other systems. This deviation is also apparent from the N1-Cl4-N2-Cl3 dihedral, which was calculated to be 14.4° for $Cu(dpq)_2Cl_2$ as given in (Table 4.1). $Pt(dpq)_2Cl_2$ slightly deviates from planarity by an N1-Cl4-N2-Cl3 dihedral of only 1.6°, while $Cu(dtq)_2Cl_2$ and $Pt(dtq)_2Cl_2$ seem to be perfectly planar. Pt^{2+} interacts with the nitrogen atoms in the quinoxaline group and chlorine atoms through a longer distance by comparing with Cu^{2+}. For example, Pt-N distance was calculated to be 2.04 and 2.05 Å while Cu-N distance was found to be 2.01 and 2.02 Å. Similarly, Pt-Cl distances are 2.42 Å above, and Cu-Cl distances are 2.39 Å below.

Geometry optimized structures of $[Cu(tpbq)Cl_2]$ and $[Pt(tpbq)Cl_2]$ display a deviation from the square planar structure around the metal center. This deviation become

significant for [Cu(tpbq)Cl_2] with the N1-Cl4-N2-Cl3 dihedral angle of 49.3°. Deviation from planarity for Pt(dpq)$_2Cl_2$ is rather slight by an N1-Cl4-N2-Cl3 dihedral of only 3.6° (Table 4.1).

In these complexes Pt^{2+} interacts with the chlorine atoms through a longer distance by comparing with Cu^{2+} and Pt-N distances were calculated as 2.03 and 2.04 Å while Cu-N distances were found to be 2.10 and 2.02 Å. The optimized geometry calculations for [Cu(ttbq)Cl_2] and [Pt(ttbq)Cl_2], on the other hand, exhibited coordination between the metal ions and a H atom of the quinoxaline as well as a nitrogen atom coordination of the same unit. The chlorine atoms filled the empty coordination sites as depicted in Figure 4.1. The interaction of the metal ions with the H-atom led the deviation of from the planarity, which was also proved by high N1-Cl4-N2-Cl3 dihedral of 59.8° and 59.5° for [Cu(ttbq)Cl_2] and [Pt(ttbq)Cl_2], repectively. For both complexes M^{2+}-N and M^{2+}-H distances were obtained almost equal, while longer metal ion-Cl distances were calculated for the platinum complex than that of the copper complex (Table 4.1).

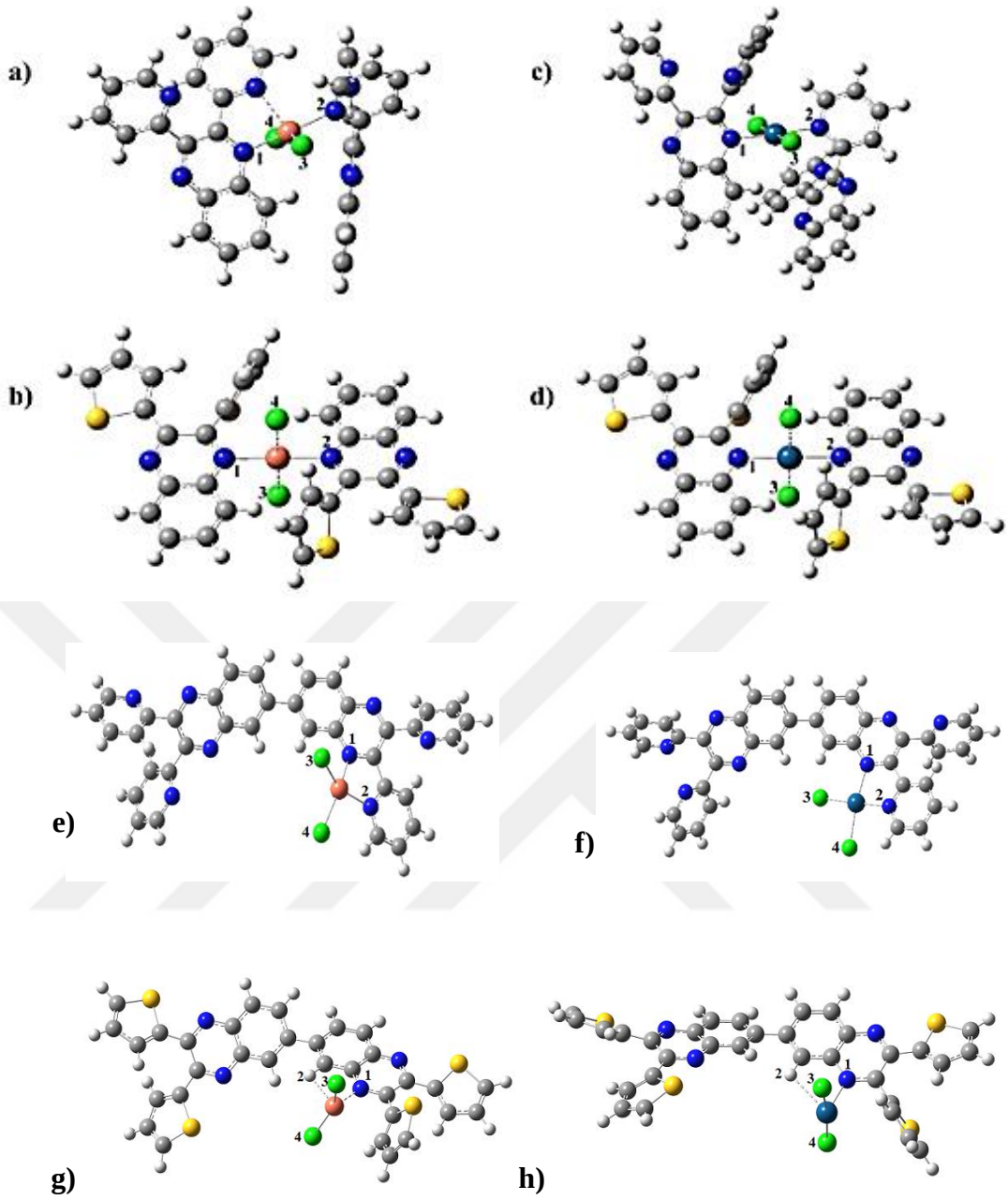

Figure 4.1 Optimized structures of (a) $Cu(dpq)_2Cl_2$, (b) $Cu(dtq)_2Cl_2$, (c) $Pt(dpq)_2Cl_2$, (d) $Pt(dtq)_2Cl_2$ (e) $Cu(tpbq)Cl_2$, (f) $Pt(tpbq)Cl_2$, (g) $Cu(ttbq)Cl_2$, and (h) $Pt(ttbq)Cl_2$ neutral complexes.

Table 4.1 Selected geometrical parameters for the metal-ligand complexes (bondlengths are in Å, bond angles and dihedrals are given in °).

Complexes	**Geometrical Parameter**							
	M-N1	**M-N2**	**M-Cl3**	**M-Cl4**	**N1-M-N2**	**Cl3-M-Cl4**	**N1-M-Cl4**	**N1-Cl4-N2-Cl3**
[Cu(dpq)$_2$Cl$_2$]	2.02	2.01	2.39	2.39	174.2	160.4	86.9	14.4
[Cu(dtq)$_2$Cl$_2$]	2.01	2.01	2.34	2.36	178.2	180.0	90.9	0.0
[Pt(dpq)$_2$Cl$_2$]	2.05	2.04	2.42	2.44	176.2	178.2	90.4	1.6
[Pt(dtq)$_2$Cl$_2$]	2.04	2.04	2.42	2.45	179.4	180	90.3	0.0
[Cu(tpbq)Cl$_2$]	2.10	2.02	2.28	2.28	78.9	101.8	144.5	49.3
[Pt(tpbq)Cl$_2$]	2.05	2.03	2.40	2.40	79.6	87.7	172.6	3.6
	M-N1	**M-H2**	**M-Cl3**	**M-Cl4**	**N1-M-H2**	**Cl3-M-Cl4**	**N1-M-Cl4**	**N1-Cl4-H2-Cl3**
[Cu(ttbq)Cl$_2$]	1.99	2.65	2.22	2.24	68.7	148.7	102.6	59.8
[Pt(ttbq)Cl$_2$]	1.97	2.60	2.40	2.39	70.3	171.3	95.4	59.5

M: Metal center (Cu^{2+} or Pt^{2+})

4.2 Identification of the complexes

4.2.1 Mass spectrometry

Mass spectrometry is a robust method to find out molecular weight of compounds. The complete process involves the conversion of the sample into gaseous ions, with or without fragmentation, which are then characterized by their mass to charge ratios (m/z) and relative abundances [152].

Mass spectrum measurements of our complexes demonstrate the molecular ion peaks corresponding to M^+ species confirmed that all the compounds were synthesized successfully. Molecular mass and the main mass fractions observed in the mass spectrum of the complexes were listed in Table 4.2 and mass spectrum of selected compounds were presented in Figures 4.2-4.5. The mass spectrum results indicated coordination of the dpq, dtq, tpbq, and ttbq ligands to Cu(II) and Pt(II) ions with two chlorines by supporting the data presented by theoretical calculations (Figures A1-A6).

Table 4.2 Mass Spectral data for the complexes. (Calculated molecular weight of the fractions are given in parentheses next to the experimental values.)

Complexes	Theoretical Mwt (g/mol)	Complex ion peak (m/z)	Other main ions (m/z)
tpbq	566.63	$[M^+]$ (566.82)	567.628 (567.20) $[tpbq+H^+]$
ttbq	586.78	$[M^+]$ (587.05)	587.78 (588.05) $[ttbq+H^+]$
$[Cu(dpq)_2Cl_2]$	703.1	$[M^+]$ (704.034)	$[Cu(dpq)_2Cl]^+$, 666.64(666.11) $[Cu(dpq)_2]^{+2}$, 630.19(631.14) $[Cu(dpq)Cl]^+$, 382.32(382.00) $[Cu(dpq)]^{+2}$, 347.87(347.03) [dpq], 284.320(285.11)
$[Cu(dtq)_2Cl_2]$	723.1	$[M^+]$ (722.51)	$[Cu(dtq)_2Cl]^+ + K^+$, 726.09(727.46) $[Cu(dtq)_2]^{+2}$, 651.55(652.99) $[Cu(dtq)Cl_2]$, 428.452(430.242) $[Cu(dtq)Cl]^+$, 392.99(392.04) [dtq], 294 (295.04)
$[Pt(dpq)_2Cl_2]$	834.63	$[M^+]$ (833.36)	$[Pt(dpq)_2Cl]^+$, 799.18 (801.04) $[Pt(dpq)_2]^{+2}$, 763.73 (763.11) [dpq], 284.32 (285.11)
$[Pt(dtq)_2Cl_2]$	854.63	$[M^+]$ (855.06)	$[Pt(dtq)_2]^{+2}$, 783.08(783.01) $[Pt(dtq)Cl_2]$, 559.98(602.27) [dtq], 294(295.04)
$[Cu(tpbq)Cl_2]$	702.1	$[M^+]$ (702.07)	$[Cu(tpbq)Cl]^+ - 2H^+$, 699.41(700.07) $[Cu(tpbq)]^{+2}$, 630.12(631.16) [tpbq], 567.20(566.63)
$[Cu(ttbq)Cl_2]$	721.9	$[M^+]$ (721.23)	$[Cu(ttbq)Cl_2]+H$, 723.51(722.23) $[Cu(ttbq)Cl]^+$, 685.44(685.78) $[Cu(ttbq)]^{+2}$, 649.18(650.33) [ttbq], 587.05 (586.78)
$[Pt(tpbq)Cl_2]$	833.11	$[M^+]$ (832.62)	$[Pt(tpbq)Cl]^+$,799.01 (797.65) $[Pt(tpbq)]^{+2}+2H$,764.04(764.20) [tpbq],567.20 (566.63)
$[Pt(ttbq)]Cl_2$	852.95	$[M^+]$ (852.77)	$[Pt(ttbq)Cl_2]+K^+$, 891.54 (892.76) $[Pt(ttbq)Cl]^+ – [2H^+]$, 815.51(815.32) [ttbq], 587.05(586.78)

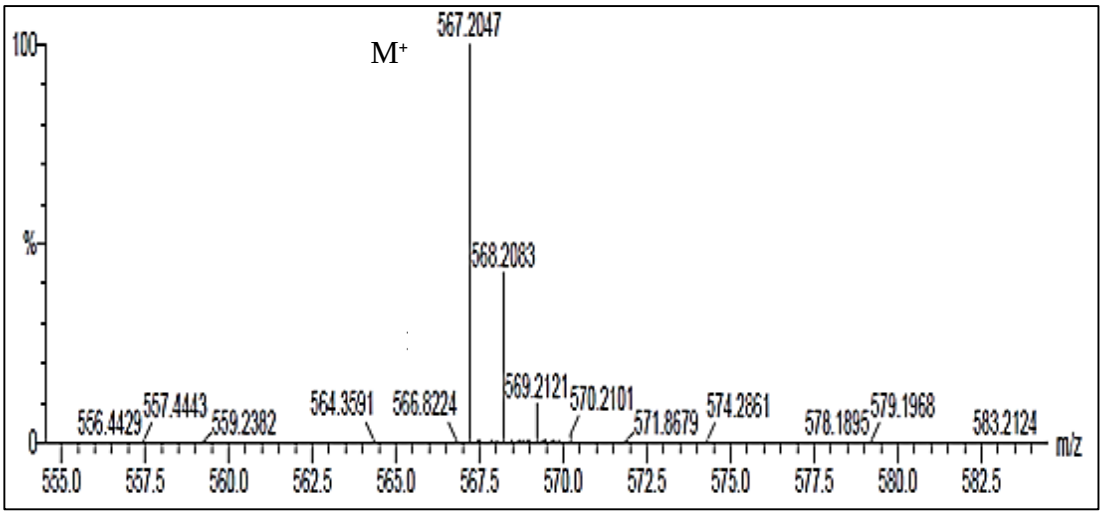

Figure 4.2 Mass spectrum of tpbq.

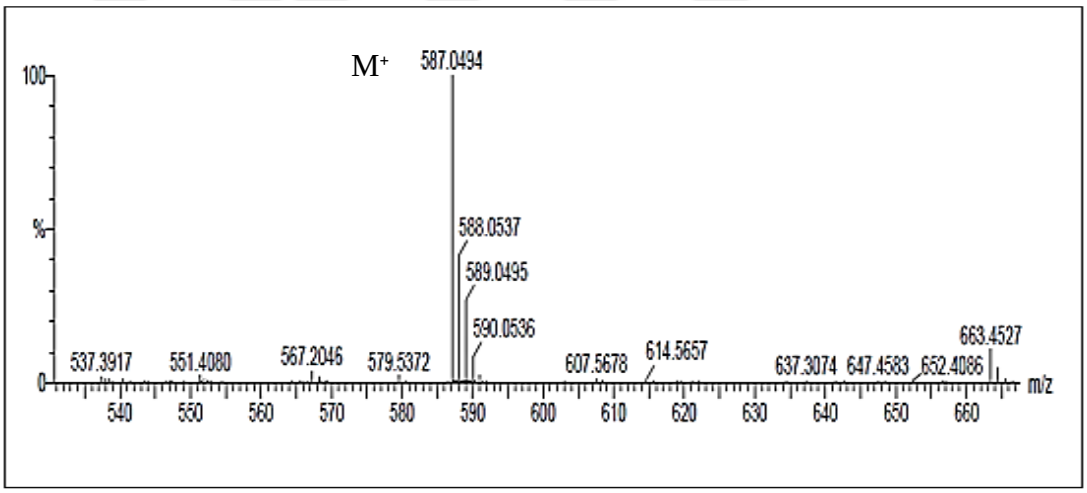

Figure 4.3 Mass spectrum of ttbq.

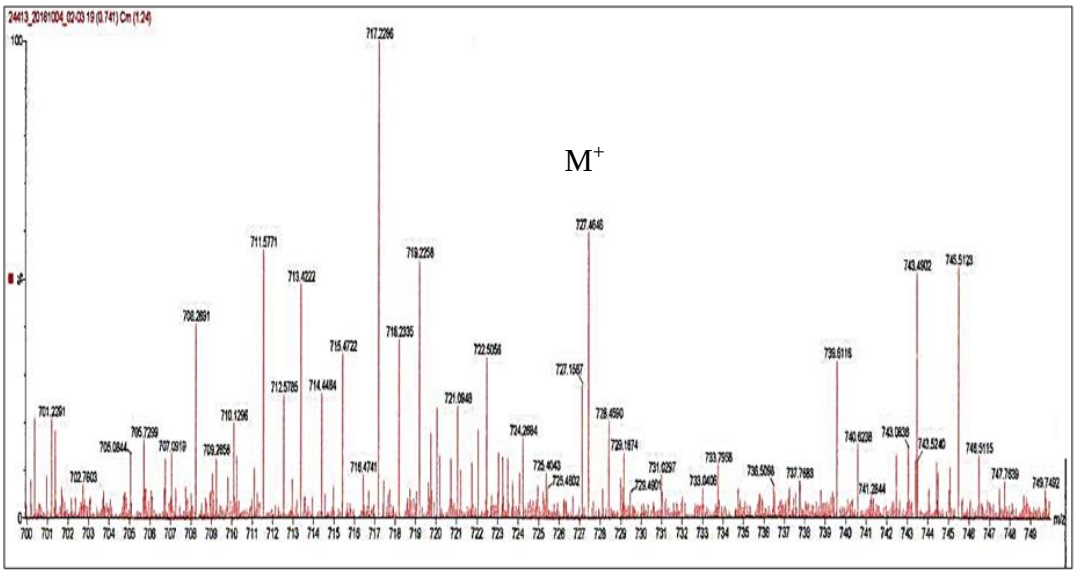

Figure 4.4 Mass spectrum of $[Cu(dtq)_2Cl_2]$.

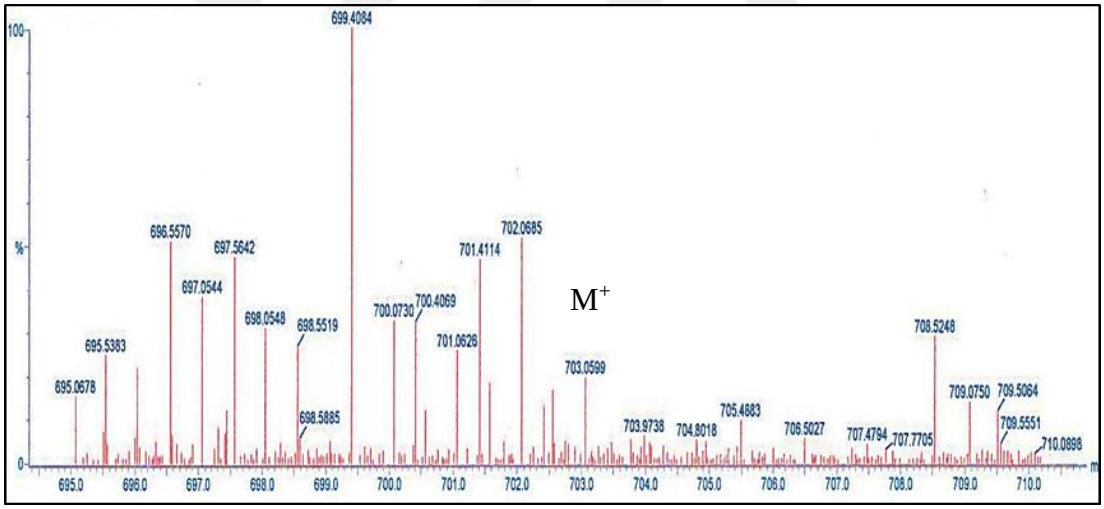

Figure 4.5 Mass spectrum of $[Cu(tpbq)Cl_2]$.

4.2.2 ^{1}H-NMR Nuclear Magnetic Resonanance Spectrometry

^{1}H-NMR spectrum is a technique used to determine the number of H atoms in molecular structure, and give information about structure of any molecular containing hydrogen. Proton NMR of dpq, dtq, tpbq, ttbq were compared with that of our complexes to prove the coordination of these ligands to Cu(II) and Pt(II) ions. The ^{1}H-NMR data of dpq and dtq can be found elsewhere [154, 155] and the proton NMR data of all our ligands are tabulated in Table 4.3. This table shows that, the ^{1}H-NMR Spectrum of dpq contains aromatic signals between δ: 7.25-8.38 ppm [153-155], and the signal positions moved to δ: 7.42 and 8.34 by the coordination of dpq. Correspondingly, ^{1}H-NMR signals of dtq observed at around δ: 7.02-8.13 ppm appeared at δ: 7.23-8.07 ppm (Figures 4.8, 4.9 and B3, B4) for our complexes.

As for the ^{1}H-NMR spectrum of tpbq, protons have signals between δ: 7.29-8.65 ppm (Figre 4.6) whose position changed to δ: 7.42 and 8.34 upon the tpbq coordination with metal ions. Likewise, ^{1}H-NMR spectrum of ttbq contains the signals between δ: 7.24-8.54 ppm (Figure 4.7), and the coordination of ttbq to copper and platinum ions caused shift of these aromatic signals towards δ: 7.15 and 8.60 ppm (Figures B5-B8).

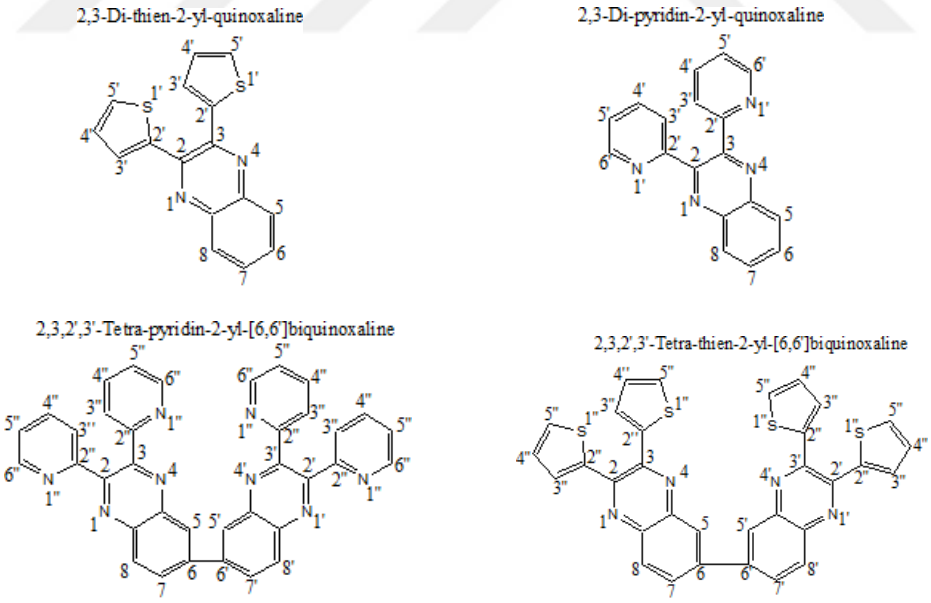

Scheme 4.1 Numbering system used in ^{1}H-NMR assignments

Table 4.3 ^{1}H-NMR spectral data for the complexes in d_6-DMSO.

Complexes	^{1}H-NMR (d_6-DMSO)
dpq	δ: 7.25 (m, 2H, H-5, 5′), 7.97 (d, 2H, H-3, 3′), 7.83 (m, 4H, H-4,4′, H-1,1′), 8.38 (d, 2H, H-6,6′), 8.25 (m, 2H, H-2, 2′) [154,155].
dtq	δ: 7.76-7.68 (m, 2H, H-5, 5′), 7.52-7.49 (m, 2H, H-3, 3′), 8.13-8.04 (m, 2H, H-4,4′), 7.27-7.25 (m, 2H, H-1,1′), 7.07-7.02 (m, 2H, H-2, 2′) [162a].
tpbq	δ 8.65 (2H, s, 5- & 5′-H), 8.41 (4H, d, J = 6 Hz, 4x6′′-H), 8.38 (2H, d, J = 12 Hz, 8- & 8′-H), 8.30 (2H, d, J = 12 Hz, 7- & 7′-H), 8.08 (4H, t, J = 12 Hz, 4x 4′′-H), 7.91 (4H, 2xd, J = 12 Hz, 4x 3′′-H), 7.31 (4H, m, 4x 5′′-H).
ttbq	δ 8.55 (2H, s, 5- & 5′-H), 8.28 (2H, d, J = 6 Hz, 8- & 8′-H), 8.21 (2H, d, J = 6 Hz, 7- & 7′-H), 7.56 (4H, d, J = 6 Hz, 4x5′′-H), 7.36 (4H, s, 4x3′′-H), 7.08 (4H, s, 4x4′′-H).
[Cu(dpq)$_2$Cl$_2$]	δ 8.37 (4H, m, 2x5-H & 2x8-H), 8.22 (4H, dd, J = 4 & 8 Hz, 2x6-H & 2x7-H), 7.96 (12H, m, 4x3′-, 4x4′- & 4x6′-H), 7,43 (4H, m, 4x5′-H).
[Cu(dtq)$_2$Cl$_2$]	δ 8.07 (4H, 2xd, J = 4 Hz, 2x5-H & 2x8-H), 7.86 (4H, dd, J = 4 & 6 Hz, 2x6-H & 2x7-H), 7.62 (4H, d, J = 4 Hz, 4x5′-H), 7.24 (4H, d, J = 4 Hz, 4x3′-H), 7.13 (4H, t, J = 4 Hz, 4x4′-H).
[Pt(dpq)$_2$Cl$_2$]	δ 8.37 (4H, m, 2x5-H & 2x8-H), 8.22 (4H, dd, J = 4 & 8 Hz, 2x6-H & 2x7-H), 7.96 (12H, m, 4x3′-, 4x4′- & 4x6′-H), 7,43 (4H, m, 4x5′-H).
[Pt(dtq)$_2$Cl$_2$]	δ 8.06 (4H, 2xd, J = 4 Hz, 2x5-H & 2x8-H), 7.86 (4H, dd, J = 4 & 6 Hz, 2x6-H & 2x7-H), 7.62 (4H, d, J = 4 Hz, 4x5′-H), 7.24 (4H, d, J = 4 Hz, 4x3′-H), 7.13 (4H, t, J = 4 Hz, 4x4′-H).
[Cu(tpbq)Cl$_2$]	δ :7.61 (d, 2H, H-5, 5′), 7.80 (m, 4H, H-3, 3′, H-4,4′), 8.24(d, 2H, H6,6′), 8. 41 (m, 2HC$_6$H$_3$),8.60 (s, HC$_6$H$_3$).
[Cu(ttbq)Cl$_2$]	7.21 (d, 2H, H-3,3′), δ: 7.30 (t, 2H, H-4,4′), 8.00 (dd, 2H, H-5,5′), 8.48 (dd, 2H, C$_6$H$_3$),8.60 (s, HC$_6$H$_3$).
[Pt(tpbq)Cl$_2$]	δ :7.59 (d, 2H, H-5, 5′), 7.83 (m, 4H, H-3, 3′, H-4,4′), 8.27 (d, 2H, H6,6′), 8. 50 (m, 2HC$_6$H),8.68 (s, HC$_6$H$_3$).
[Pt(ttbq)Cl$_2$]	7.15 (d, 2H, H-3,3′), δ: 7.36 (t, 2H, H-4,4′), 8.15(dd, 2H, H-5,5′), 8.50 (dd, 2H, C$_6$H$_3$),8.60 (s, HC$_6$H$_3$).

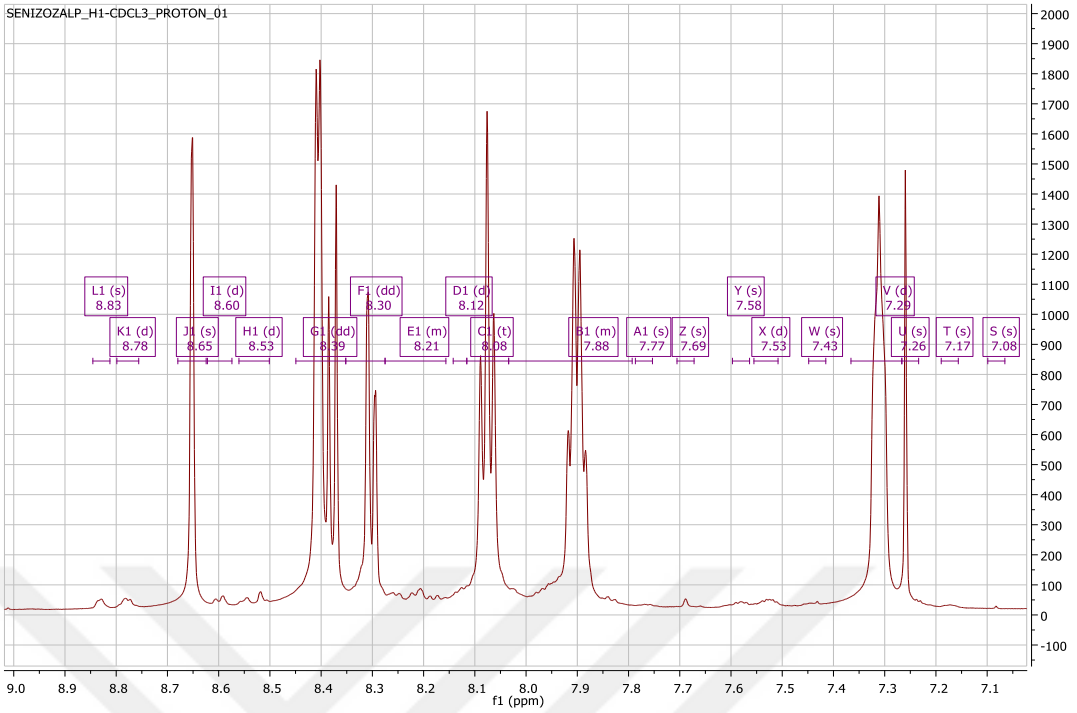

Figure 4.6 ^{1}H-NMR spectrum of tpbq in $CDCl_3$.

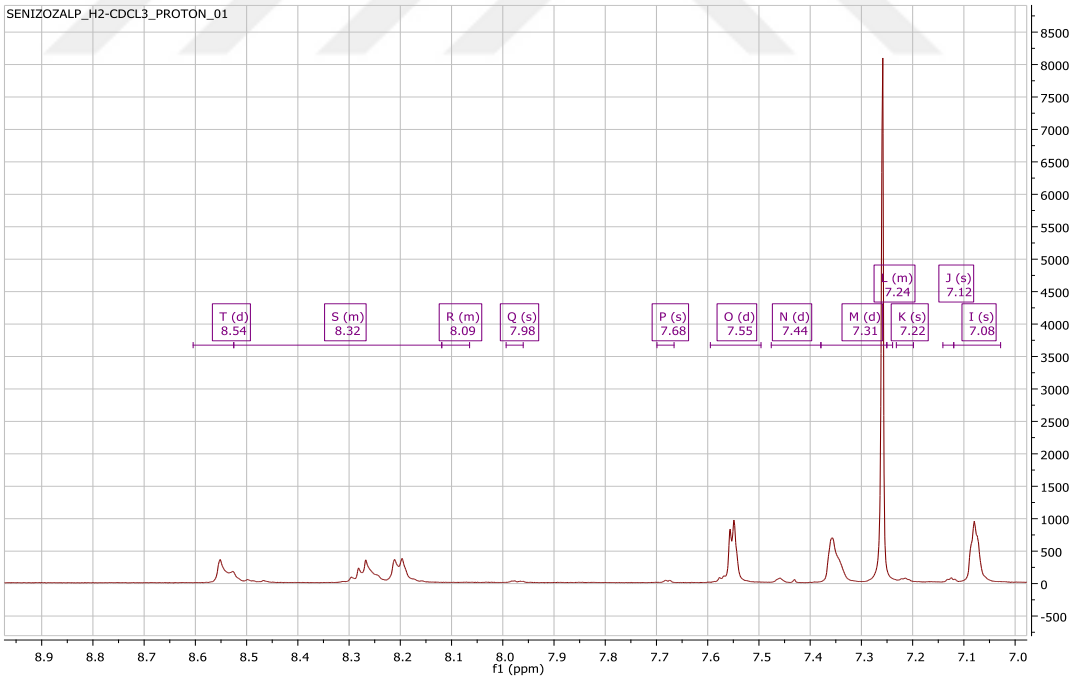

Figure 4.7 ^{1}H-NMR spectrum of ttbq in $CDCl_3$.

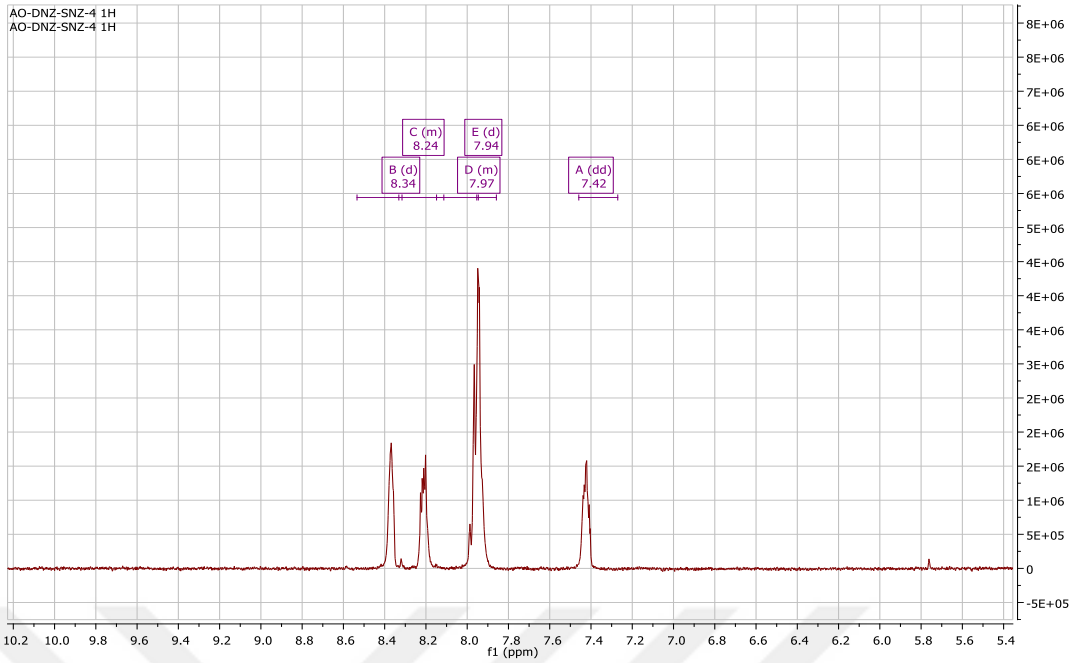

Figure 4.8 ^{1}H-NMR spectrum of $[Cu(dpq)_2Cl_2]$ complex in d_6-DMSO

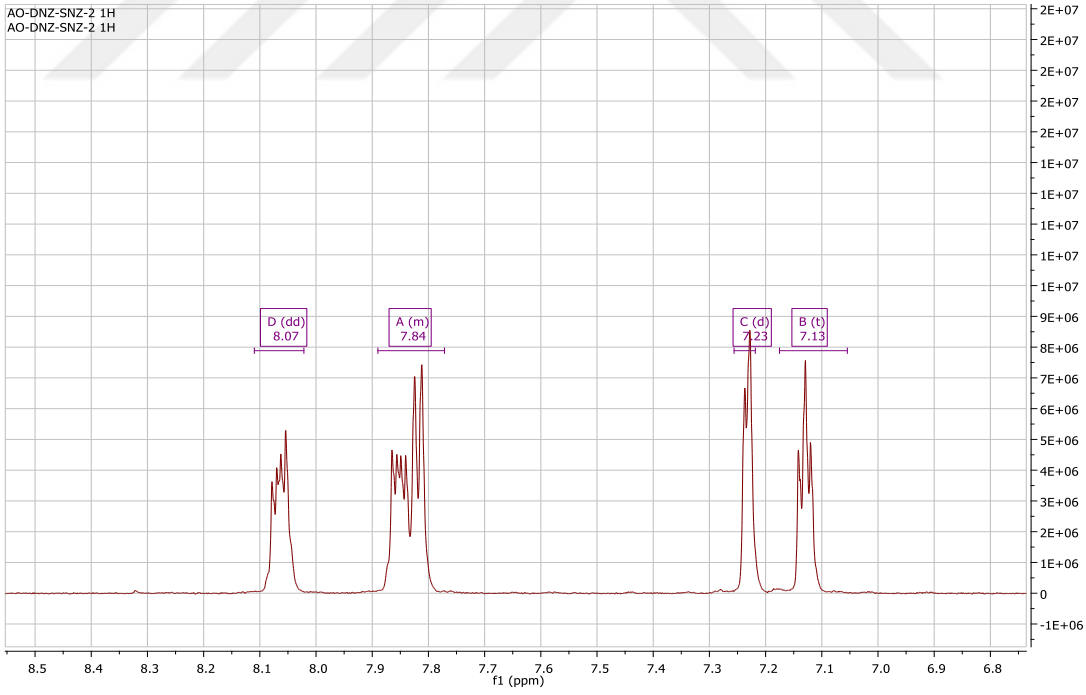

Figure 4.9 ^{1}H-NMR spectrum of $[Cu(dtq)_2Cl_2]$ complex in d_6-DMSO.

4.2.3 UV–Vis spectroscopy

The $Cu(dpq)_2Cl_2$ and $Cu(dtq)_2Cl_2$ complexes exhibit three absorption bands in their electronic absorption spectrum. The bands observed at around 246 and 272 nm in water for $Cu(dpq)_2Cl_2$ and 257 and 286 nm in AN for $Cu(dtq)_2Cl_2$ were attributed to $\pi\rightarrow\pi^*$ charge transfer transitions. Additionally, the bands obtained at about 338 and 378 nm are assigned as $n\rightarrow\pi^*$ transitions of $Cu(dpq)_2Cl_2$ and $Cu(dtq)_2Cl_2$, respectively (Figure 4.10). $Pt(dpq)_2Cl_2$ and $Pt(dtq)_2Cl_2$ have two main electronic transition bands in DMF. The bands that were observed at about 275 and 288 nm for $Pt(dpq)_2Cl_2$ and $Pt(dtq)_2Cl_2$, respectively, were recognized as $\pi\rightarrow\pi^*$ transitions and those obtained at 334 and 382 nm were assigned as $n\rightarrow\pi^*$ transitions of $Pt(dpq)_2Cl_2$ and $Pt(dtq)_2Cl_2$, respectively [156]. Correspondingly, there are two main absorption bands within the electronic absorption spectrum of the Cu(II) and Pt(II) with tpbq and ttbq which were monitored in DMF. The bands appearing at about 285, 287, 287 and 284 nm for $Cu(tpbq)Cl_2$, $Cu(ttbq)Cl_2$, $Pt(tpbq)Cl_2$ and $Pt(ttbq)Cl_2$, respectively, were attributed to the $\pi\rightarrow\pi^*$ charge transfer transitions [157]. Furthermore, the band observed at around 373 nm for $Cu(tpbq)Cl_2$ and $Pt(tpbq)Cl_2$ complexes were attributed as $n\rightarrow\pi^*$ transitions (Figure 4.11). However, $n\rightarrow\pi^*$ transitions band was shifted to 415 nm for $Cu(ttbq)Cl_2$ and $Pt(ttbq)Cl_2$ complexes [158,159]. The spectral data given in Table 4.4.

Table 4.4 Electronic absorption spectral data for the platinum and copper complexes

Band No.	$\lambda_{(nm)}$	$\bar{\nu}$ (nm^{-1})	$\varepsilon_{(M^{-1}cm^{-1})}$
$[Cu(dpq)_2Cl_2]$ in water			
I	246	4065.04	49072.73
II	272	3676.47	30845.455
III	338	2958.58	16000
$[Cu(dtq)_2Cl_2]$ in acetonitrile			
I	257	3891.05	30260
II	286	3496.50	26110
III	378	2645.50	18537.5
$[Pt(dpq)_2Cl_2]$ in DMF			
I	275	3636.36	42285.71
II	334	2994.01	19900
$[Pt(dtq)_2Cl_2]$ in DMF			
I	288	3472.22	49100
II	382	2617.80	34171.43
$[Cu(tpbq)Cl_2]$ in DMF			
I	285	3508.77	2310
II	373	2680.96	13490
$[Cu(ttbq)Cl_2]$ in DMF			
I	286	3496.5	55990
II	415	2409.64	58830
$[Pt(tpbq)Cl_2]$ in DMF			
I	287	3484.32	67930
II	373	2680.96	43540
$[Pt(ttbq)Cl_2]$ in DMF			
I	284	3521.13	49140
II	414	2415.46	48890

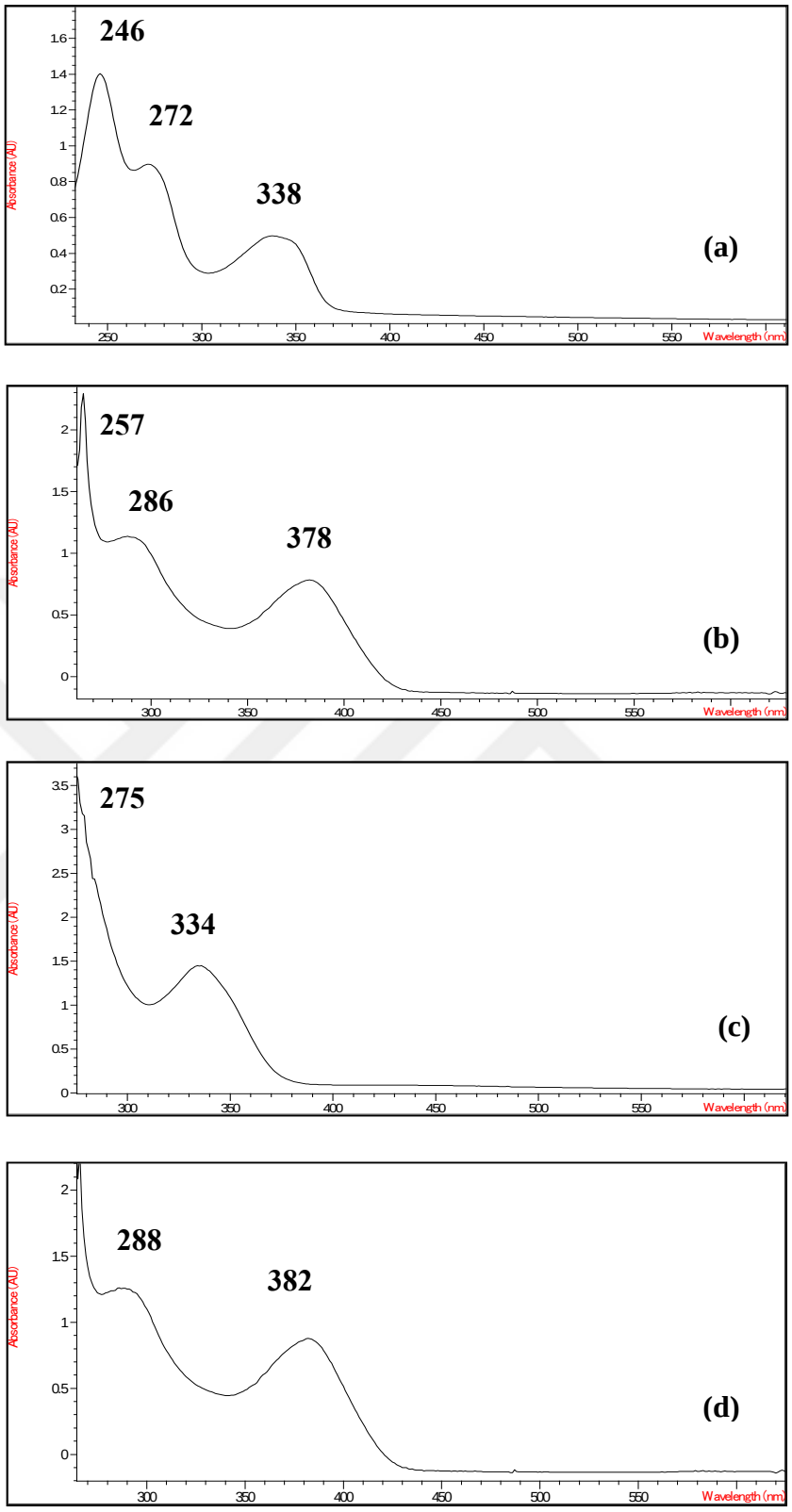

Figure 4.10 Electronic absorption spectrum of (a) $[Cu(dpq)_2Cl_2]$ in water, (b) $[Cu(dtq)_2Cl_2]$ in AN, (c) $[Pt(dpq)_2Cl_2]$ in DMF, (d) $[Pt(dtq)_2Cl_2]$ in DMF.

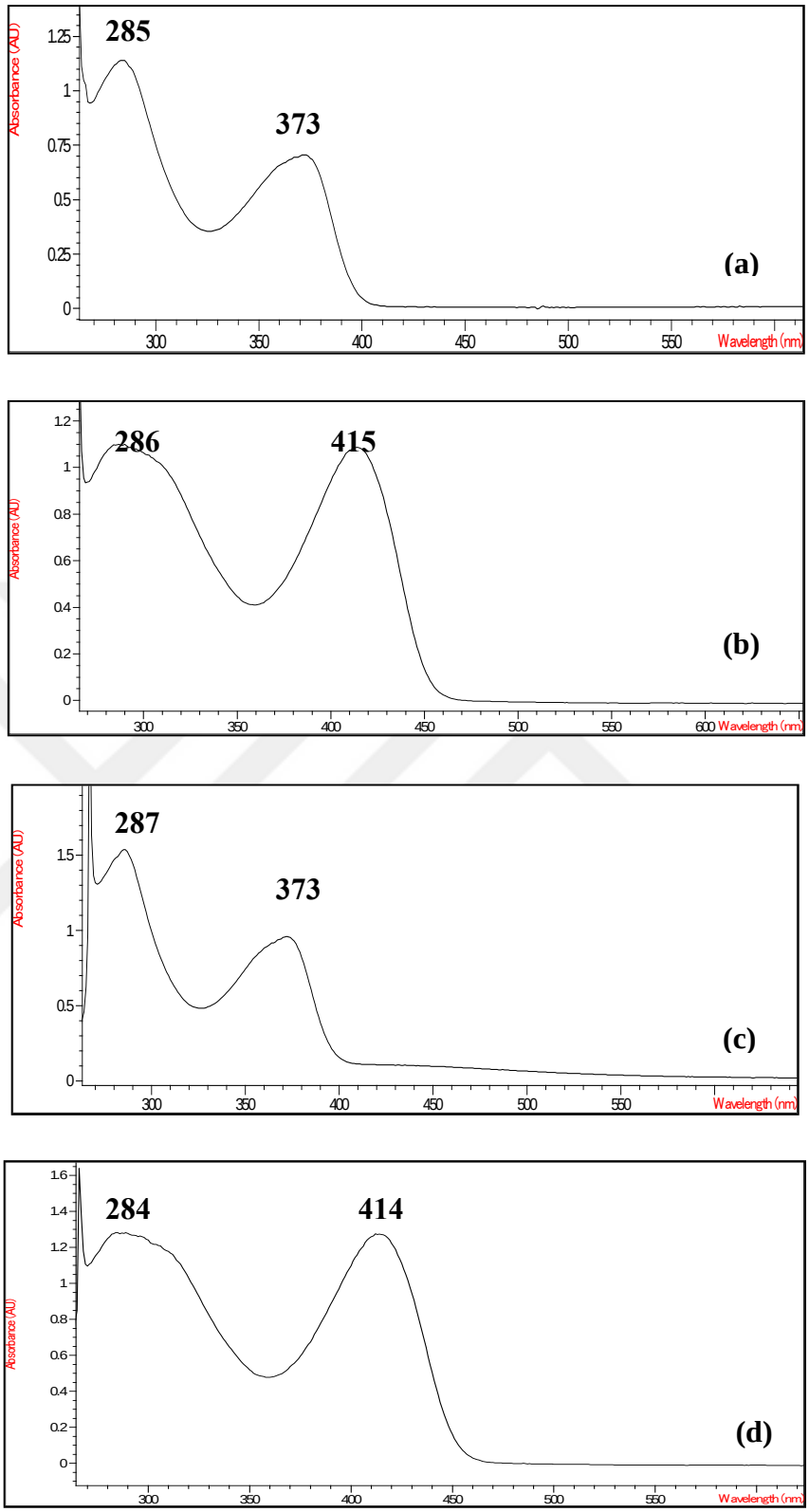

Figure 4.11 Electronic absorption spectrum of (a) [Cu(tpbq)Cl_2] in DMF, (b) [Cu(ttbq)Cl_2] in DMF, (c) [Pt(tpbq)Cl_2] in DMF, (d) [Pt(ttbq)Cl_2] in DMF.

4.2.4 Infrared Spectrometry

FTIR spectrum of the complexes exhibit all the characteristic absorption peaks of dpq, dtq, tpbq and ttbq, especially, observed small deviations in aromatic ring C-H, C=N, C=C, C-S-C peak positions confirm the coordination of the metals to these ligands. Bond frequency of which confirmed the main groups of the ligands and the complexes given in Table 4.5.

FTIR spectrum of dpq contains absorption peaks of aromatic C-H vibrations at around 3098, 3056, and 3002 cm^{-1} [160, 161]. For both copper and platinum coordinated dpq, these absorption peaks appeared in the range of 3100 and 3065 cm^{-1}. While the peak of aromatic C=N vibration is observed at 1590 cm^{-1} for dpq, the same vibration led an absorption at 1597 and 1606 cm^{-1} upon Cu(II) and Pt(II) coordination of dpq, respectively. The $\nu_{(C=C)}$ stretching vibration of dpq is displayed at about 1555 cm^{-1}; on the other hand, the $\nu_{(C=C)}$ absorption was obtained at around 1560 cm^{-1} for $Cu(dpq)_2Cl_2$ (Figure 4.12) and 1550 cm^{-1} for $Pt(dpq)_2Cl_2$ (Figure C1). Observation of shift in the peak position of $\nu_{(C-N)}$ (1145 cm^{-1}) toward 1159 and 1185 cm^{-1} in the IR spectrum of copper and the platinum, respectively, is a good indication and confirmation for the coordination of dpq to the metal.

As reported earlier [162a], the absorption peaks appeared at around 3093 cm^{-1} and 3054 cm^{-1} in the FTIR spectrum of the dtq is attributed to the aromatic $\nu_{(C-H)}$ vibrations [160-161]. Through the coordination of dtq to both Cu(II) and Pt(II), $\nu_{(C-H)}$ vibrations shifted to 3071 cm^{-1}. Similarly, the aromatic $\nu_{(C=N)}$ vibration frequency at 1600 cm^{-1} of dtq was detected at around 1591 and 1594 cm^{-1} in the spectrum of $Cu(dtq)_2Cl_2$ (Figure C2) and $Pt(dtq)_2Cl_2$ (Figure C3), respectively. The $\nu_{(C=C)}$ stretching vibration frequency of the aromatic groups at around 1520 cm^{-1} deviates about 40 cm^{-1} and was observed at about 1560 cm^{-1}. Likewise, the peak determined at about 840 cm^{-1}, which is attributed to the $\nu_{(C\text{-}S\text{-}C\ ring)}$ for dtq, was observed at 842 cm^{-1} for $Cu(dtq)_2Cl_2$ and at 844 cm^{-1} for $Pt(dtq)_2Cl_2$.

The FTIR spectrum of tpbq (Figure 4.13) exhibited absorption peaks of aromatic C-H vibrations at about 3100, 3054 and 3003 cm^{-1}. Concerning copper- and platinum-

coordinated tpbq, the stated peaks were shown up at around 3200, 3055 and 2924 cm^{-1}. Whereas, the peak of aromatic C=N vibration appears around 1609 cm^{-1} for tpbq and caused an absorption at 1606 cm^{-1} upon the coordination to Cu(II) and Pt(II). The $\nu_{(C=C)}$ stretching vibration of tpbq appeared at around 1585 cm^{-1} whereas $\nu_{(C=C)}$ absorption does so at about 1577 cm^{-1} for $Cu(tpbq)Cl_2$ (Figure 4.14) and at 1580 cm^{-1} for $Pt(tpbq)Cl_2$ (Figure C4). Additionally, $\nu_{(C-N)}$ vibration at 1148 cm^{-1} shifted to 1149 and 1152 cm^{-1} in the tpbq coordinated copper and platinum complexes, respectively.

These absorption peaks emerged at about 3095, 3062, 2921 cm^{-1} in the FTIR spectrum of the ttbq (Figure 4.15) were attributed to the aromatic $\nu_{(C-H)}$ vibrations. Owing to metal-ttbq coordination here, the $\nu_{(C-H)}$ vibrations were shifted to 3053, 2924, 2856 cm^{-1} (Figures C5 and C6). In a similar vein, the aromatic $\nu_{(C=N)}$ vibration frequency at 1600 cm^{-1} of ttbq was seen at around 1607 cm^{-1} in the IR spectrum of $Cu(ttbq)Cl_2$ and $Pt(ttbq)Cl_2$. The $\nu_{(C=C)}$ vibration frequency of the aromatic groups observed at about 1520 cm^{-1} for $Cu(ttbq)Cl_2$ and $Pt(ttbq)Cl_2$.

Apart from this, a peak appeared at around 833 cm^{-1} was related to the $\nu_{(C\text{-}S\text{-}C\ ring)}$ for ttbq and was identified at 835 cm^{-1} for $Cu(ttbq)Cl_2$ and $Pt(ttbq)Cl_2$, showing no bond formation between metal and sulfur atom.

Based on all observations, it can be stated that these complexes were synthesized successfully, and IR results supported the geometry-optimized structures of all our complexes.

Table 4.5 Selected infrared vibration frequencies (cm^{-1}) for ligands and copper(II) and platinum(II) complexes

Frequencies	dpq (cm^{-1})	$[Cu(dpq)_2Cl_2]$ (cm^{-1})	$[Pt(dpq)_2Cl_2]$ (cm^{-1})	dtq (cm^{-1})	$[Cu(dtq)_2Cl_2]$ (cm^{-1})	$[Pt(dtq)_2Cl_2]$ (cm^{-1})	tpbq (cm^{-1})	$[Cu(tpbq)Cl_2]$ (cm^{-1})	$[Pt(tpbq)Cl_2]$ (cm^{-1})	ttbq (cm^{-1})	$[Cu(ttbq)]Cl_2$ (cm^{-1})	$[Pt(ttbq)]Cl_2$ (cm^{-1})
$\nu_{(HOH)}$		3424				3347		3366	3365		3462	3358
$\nu_{(C-H)}$ aromatic	3098 3056 3002	3099 3071 3018	3107 3082 3065	3093 3054	3071	3071 2920	3100 3054 3003	3054 3005 2924	3200 3055 2915	3095 3062 2921	3053 2922 2856	3054 2924 2851
$\nu_{(C=N)}$ aromatic	1590	1597	1606	1600	1591	1594	1609	1606	1607	1610	1607	1606
$\nu_{(C=C)}$ aromatic	1555	1560	1550	1520	1560	1519	1585	1577	1580	1519	1519	1518
$\nu_{(ph)}$	1493	1480	1474	1474	1471	1474	1469	1472	1472	1477	1473	1473
$\delta_{(C-CH)}$ in plane	1412	1431	1435	1422	1435	1433	1433	1430	1426	1431	1423	1422
$\delta_{(C-H)}$ in plane bending	1351	1354	1419	1338	1351	1354	1347	1386	1380	1358	1368	1368
$\nu_{(C-N)}$ aromatic	1145	1159	1185	1129	1130	1132	1148	1149	1152	1184	1179	1178
$\delta_{(C-H)}$ out of plane ring	1081 995	1083 992	1096 1012	1061 1013 981	1078 1015 989	1061 1045 981	1073 995	1072 993	1076 1042	1079 1058 1041	1045 978 934	1048 978 933
$\delta_{(C-C)}$ out of plane	786 741	782 751	783 759	845	842	844	790 748	789 742	789 744	833	835	835

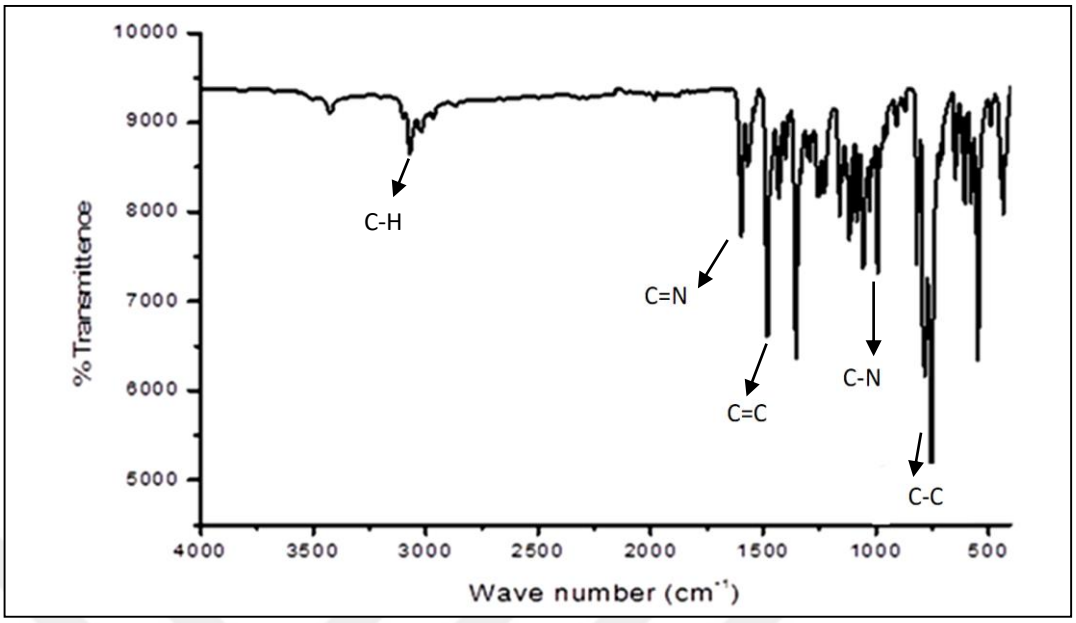

Figure 4.12 Infrared spectrum of $[Cu(dpq)_2Cl_2]$ in the range of 4000-400cm^{-1}.

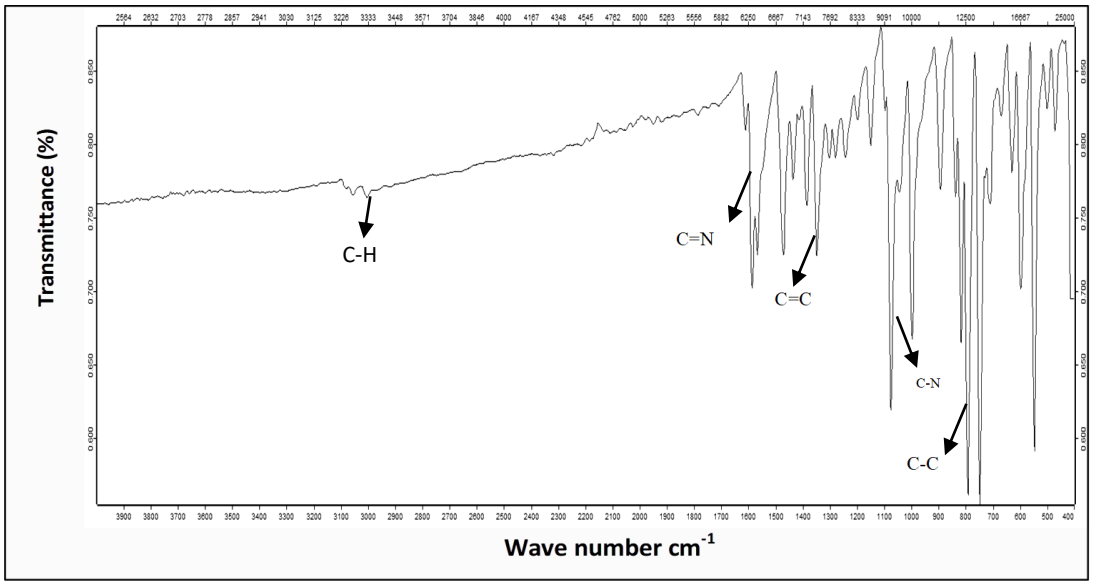

Figure 4.13 Infrared spectrum of tpbq in the range of 4000-400cm^{-1}

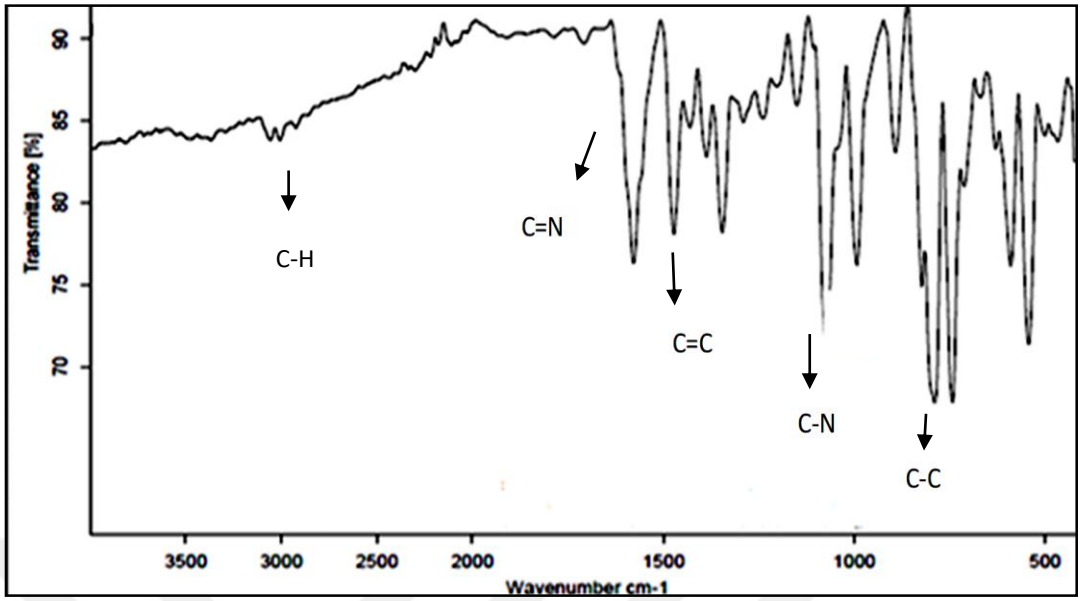

Figure 4.14 Infrared spectrum of [Cu(tpbq)Cl_2] in the range of 4000-400 cm^{-1}.

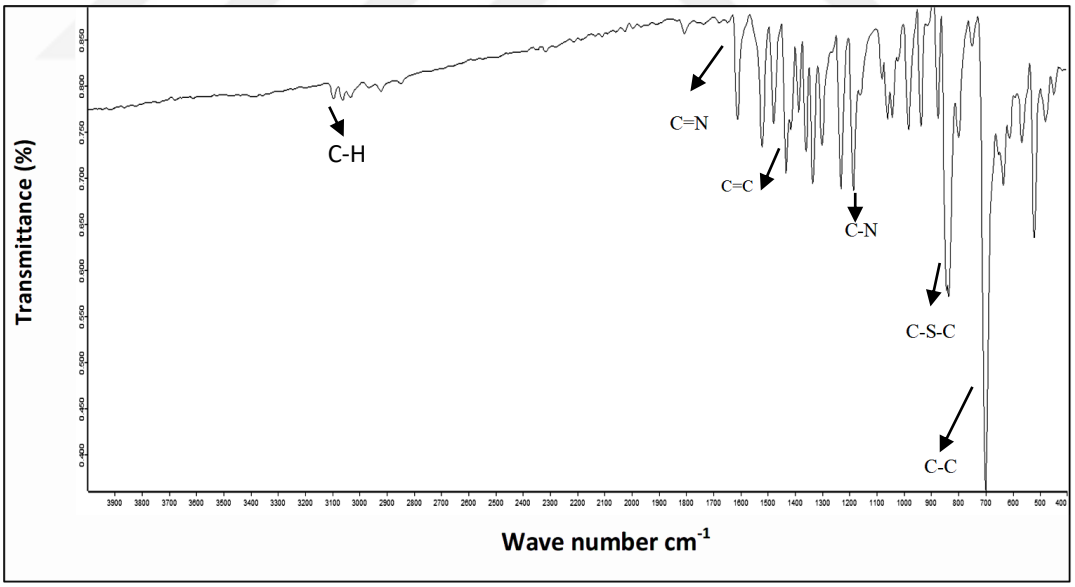

Figure 4.15 Infrared spectrum of ttbq in the range of 4000-400cm^{-1}

4.2.5 Raman Spectrometry

Raman Spectrometry was measured in order to identify the structure of our complexes by maintaining possible band vibrations between the metal and -N, -S or -Cl atoms. The Raman Spectrometry data for our complexes were given in Table 4.6.

The vibrational modes appeared at around 112 and 118 cm^{-1} in Raman spectrum were assigned to $\nu_{(Cl\text{-}Pt\text{-}Cl)}$ stretchings for all Pt–complexes. Cl-Cu-Cl absorption, on the other hand, were observed at about 141-186 cm^{-1} [162g-i]. These vibrations clearly indicated the direct coordination of chlorine atoms to the metal ions. Similarly, $\nu_{(N\text{-}Cl)}$ band vibrations were obtained at around 313-346 cm^{-1} for dpq and dtq complexes and at 340 -381 cm^{-1} for tpbq and ttbq complexes [162a-d].

Cl-M-N vibrations were detected at around 200 – 220 cm^{-1}, while the absorption bands of M-N vibrations for symmetric and assymetric modes were seen at around 416 to 528 cm^{-1} (Table 4.6 and Figures D1-D8). Likewise, N-M-N vibrational modes were obtained at around 115–120 cm^{-1} for Cu(II) complexes and at about 240–253 cm^{-1} for Pt(II) complexes.

The data presented in Table 4.6 and the Figures in Appendix D suggested that all the ligands coordinated to the metal ions through the N–atom of quinoxaline units, and the chlorine atoms interacted to the metal centers directly in the inner shell of the complexes. It was very interesting that no absorption band appeared at around 265 cm^{-1} for $Cu(dtq)_2Cl_2$ and $Cu(ttbq)Cl_2$ and at about 280 cm^{-1} for $Pt(dtq)_2Cl_2$ and $Pt(ttbq)Cl_2$ complexes; this could be attributed to Cu–S and Pt–S vibrations, respectively [162a-f].

These results clearly showed that the thenyl– quinoxaline ligands were not coordinated to the metal ions through S-atoms in our complexes. The similar results were obtained from the symmetry optimized structures of the complexes.

Table 4.6 Raman Spectroscopy data for the Pt(II) and Cu(II) complexes

Complexes	Cl-M-Cl	Cl-M-N	N-M-N	M-Cl	M-N
$[Cu(dpq)_2Cl_2]$	141	220	115	240, 346	473
$[Cu(dtq)_2Cl_2]$	173	206	118	313, 325	460, 527
$[Pt(dpq)_2Cl_2]$	112	200	253	343	422
$[Pt(dtq)_2Cl_2]$	114	200	251	324	416
$[Cu(tpbq)Cl_2]$	186	220	114	246, 353	394, 460
$[Cu(ttbq)Cl_2]$	146	206	-	239, 280, 381	417
$[Pt(tpbq)Cl_2]$	113	213	240	340	404
$[Pt(ttbq)Cl_2]$	118	200	-	388	528

4.3 DNA- Binding Studies

4.3.1 Electronic Absorption Spectroscopy (EAS)

The drug compound attaches to the DNA in various positions either covalently or non-covalently. In order to demonstrate the affinity of our copper and platinum quinoxaline complexes to CT-DNA, electronic absorption spectroscopy was used.

It is known that intercalation interaction between the metal compound and DNA leads to hypochromism (decrease of the intensity band), a stacking interaction between the base pairs of DNA and an aromatic group, while hydrogen bonding, electrostatic interactions and groove binding attraction between the drug and DNA has been attributed to hyperchromism (increase of the intensity band) [163, 164].

The UV-Vis absorption spectrum of DNA contains a sharp band at 280 nm in the UV region as a result of electronic shifts inside chromophoric groups in the pyrimidine and purine bases. The band position and intensity depend on pH or ionic strength within the medium [142].

The binding ability of our copper(II) and platinum(II) complexes to CT-DNA was studied by UV- titration method, where the change in the EAS of our complexes was monitored during the addition of increased amount of CT-DNA (R=[DNA]/[compound]=0-10).

The change in the electronic absorption bands at around 400 nm for our complexes during the UV titration studies performed at 37 ^{o}C were shown in Figures 4.16 and 4.17. The UV titration of all our complexes exhibited hyperchromic change in the presence of the DNA, without any change in the peak position. Since hyperchromism is generally correlated with the non-covalent mode of binding [165], the observed increase in the electronic absorption band intensity may indicate an electrostatic interaction between our complex cations and the phosphate groups in CT-DNA duplex [166] after releasing one or two labile chloride ligand(s) from the complex structure.

The intrinsic binding constant (K_b) of our complexes was determined of using the equation (4.1)

$$[DNA]/(\varepsilon_a-\varepsilon_f)=[DNA]/(\varepsilon_b-\varepsilon_f)+1/K_b[(\varepsilon_a-\varepsilon_f)] \quad (4.1)$$

The plot $[DNA]/(\varepsilon_a-\varepsilon_f)$ versus [DNA]) was drawn for all complexes and K_b value was calculated from the slope-to-intercept of these profiles, in which ε_a is the apparent extinction coefficient; ε_f and ε_b show the extinction coefficients of both free and bound compound.

The obtained K_b values at 37°C were tabulated in Table 4.7 and it was observed that K_b values changed between 7.5 x10^2 to 7.5 x10^3 for dpq and dtq complexes, and 6.76 x10^2 to 6.00 x10^3 for tpbq and ttbq complexes. The careful inspection of the K_b values for dpq- and dtq-Cu(II) and Pt(II) complexes indicated that the complexes having dpq-ligand binded to the DNA duplex more strongly than their counterparts having dtq; for instance, $Cu(dpq)_2Cl_2$ was interacted with CT-DNA approximately three times stronger than $Cu(dtq)_2Cl_2$ and K_b of $Pt(dpq)_2Cl_2$ was two times more than that of $Pt(dtq)_2Cl_2$.

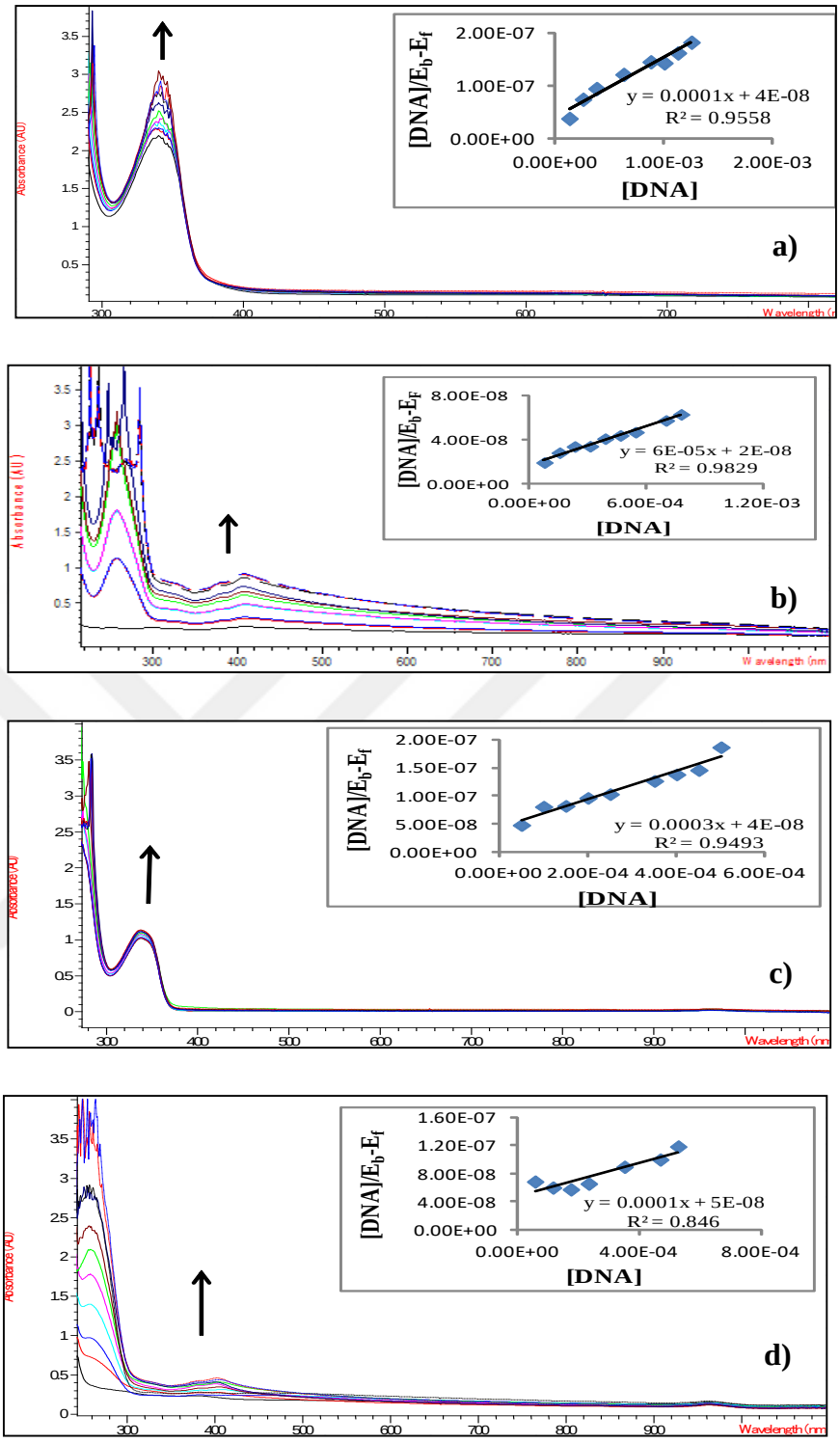

Figure 4.16 The change in the electronic absorption spectra of (a) $[Cu(dpq)_2Cl_2]$, b) $[Cu(dtq)_2Cl_2]$, c) $[Pt(dpq)_2Cl_2]$ and d) $[Pt(dtq)_2Cl_2]$ in Tris-HCl buffer (pH = 7.10) at 37 ^oC in the absence and in the presence of CT-DNA (R=0-10). Inset: Plot of [DNA]/ $[\varepsilon_a - \varepsilon_f]$ *vs.* [DNA].

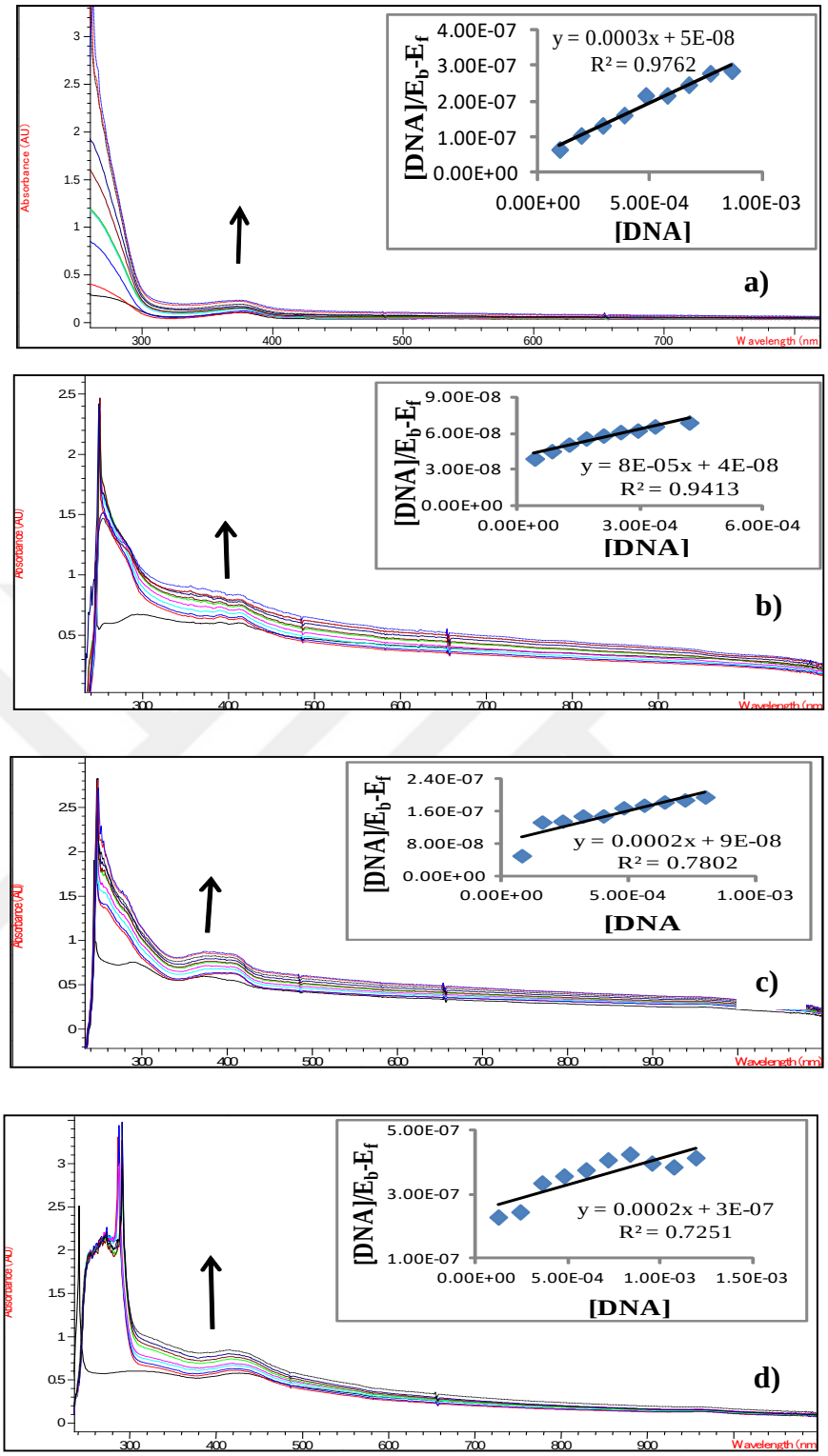

Figure 4.17 The change in the electronic absorption spectra of (a) $[Cu(tpbq)_2Cl_2]$, b) $[Cu(ttbq)_2Cl_2]$, c) $[Pt(tpbq)_2Cl_2]$ and d) $[Pt(ttbq)_2Cl_2]$ in Tris-HCl buffer (pH = 7.10) at 37 °C in the absence and in the presence of increasing amounts of CT-DNA (R=0-10). Inset: Plot of $[DNA]/ [\varepsilon_a - \varepsilon_f]$ *vs.* [DNA].

On the other hand, platinum(II)-dtq and dpq complexes have higher tendency toward CT-DNA compared to that of the Cu(II) complexes. Table 4.8 presents the binding constants of platinum(II) and copper(II) complexes containing tpbq and ttbq. The similar trend in K_b values of the complexes was obtained when the ligands changed with tpbq and ttbq.

Platinum and copper complexes having tpbq exhibited three times more affinity towards to CT-DNA with respect to the complexes containing ttbq. It was also observed that the copper(II) tpbq and ttbq complexes maintained stronger interactions with the CT-DNA than that of platinum(II) complexes.

The obtained K_b values indicated that dpq and tpbq derivatives of the copper and platinum compounds are higher than that of the dtq and ttbq derivatives, which might be attributed to the different donation ability of pyridine and thienyl containing quinoxaline ligands to the metal ions.

Intrinsic binding constants obtained for all our complexes are even lower than the K_b values reported for well-known intercalators such as ethidium bromide ($K_b = 7x10^7\ M^{-1}$) and daynomycin ($K_b = 4.9\times10^6\ M^{-1}$) [167–169]. Conversely, the K_b values of our complexes are close to that of $[Ru(phen)_2(cdpq)]^+$ ($K_b = 4.67\times10^3\ M^{-1}$) and $[Ru(phen)_3]^{+2}$ ($K_b = 9.7\times10^3\ M^{-1}$) which were cited as groove binders [170, 171]. These results clearly suggested the non-covalent interaction between our complexes and CT-DNA as well.

In order to verify the nature of the binding affinity of the complexes toward CT-DNA, temperature dependent binding constants (K_b) were obtained by means of the electronic absorption titration experiments carried out at 37, 47, 57 and 67^o C, where the ratio (R) of the concentrations of our complexes to that of CT-DNA were varied between 0 and 10 with the optimized incubation time (Figures E1-E8).

Thermodynamic parameters were also obtained by EAS experiments conducted at 310, 320, 330, and 340 K. The standard Gibbs free energy (ΔG^o) was calculated by using the following equation (4.2):

$$\Delta G^o = -R\ T\ Ln(K'_b) \quad (4.2)$$

Here, R is the gas constant (8.314 J/mol. K) and T stands for the temperature (K). The binding enthalpy and entropy were determined from the slope and the intercept of the van't Hoff [143] equation (4.3):

$$Ln(K'_b) = (-\Delta H^o/RT) + (\Delta S^o/R) \quad (4.3)$$

Based on the values for ΔH^o and ΔS^o, one can determine the mode of interaction taking place between compounds and biomolecules such as DNA in this way: (1) $\Delta H^o > 0$ and $\Delta S^o > 0$, hydrophobic forces; (2) $\Delta H^o < 0$ and $\Delta S^o < 0$, van der Waals reaction and hydrogen bonds; (3) $\Delta H^o < 0$ and $\Delta S^o > 0$, electrostatic reactions [173].

The ΔG^o values were obtained in a range of (-15.4 to 26.0 kJ) (Table 4.7 and 4.8) for all complexes, suggesting the spontaneous formation of DNA-complex adducts. Generally, dpq- and dtq-containing Cu(II) and Pt(II) complexes have more negative ΔG^o than those containing tpbq and ttbq.

The ΔH^o values, on the other hand varied between (-2.19 and 50.19 kJ/mol), while the ΔS^o values change between 60.36 to 218.89 J/mol K (Table 4.7 and Figure E9) for $Pt(dpq)_2Cl_2$, $Pt(dtq)_2Cl_2$, $Cu(dpq)_2Cl_2$ and $Cu(dtq)_2Cl_2$ complexes. Positive ΔS^o with the positive/negative ΔH^o values confirmed the electrostatic interaction that took place between those complexes and the CT-DNA, thus implying that the binding was mainly enthalpy-driven in the presence of unfavorable entropy conditions. The ΔH^o values were calculated in the range of (-11.45 to -85.29 kJ/mol) for $Pt(tpbq)Cl_2$, $Pt(ttbq)Cl_2$, and $Cu(tpbq)Cl_2$ respectively (Table 4.8 and Figure E10). The ΔS^o values of these complexes, on the other hand, changed between -39.74 to -207.58 J/ K, except $Cu(ttbq)Cl_2$ complex with 26.8 J/K. Negative ΔH^o and ΔS^o values of the $Pt(tpbq)Cl_2$, $Pt(ttbq)Cl_2$, and $Cu(tpbq)Cl_2$ suggested van der Waals and hydrogen bond interaction, whereas the positive ΔS^o with negative ΔH^o value of $Cu(ttbq)Cl_2$ was attributed to electrostatic interaction to DNA [173].

These thermodynamic data obtained for our complexes are very close to the reported values for several groove binders with electrostatic interaction or van der Waals interaction. For instance, ΔH^o value of the DB293 is -15.06 kJ/mol with a negative ΔG^o of -40.17 kJ/mol, and the ΔH^o value of the DB75 is -9.20 kJ/mol with a negative ΔG^o of -37.66 kJ/mol [174].

Table 4.7 $\Delta G°$, ΔH^o and ΔS^o data for $Pt(dpq)_2Cl_2$, $Pt(dtq)_2Cl_2$, $Cu(dpq)_2Cl_2$, and $Cu(dtq)_2Cl_2$.

Compound	**Temp (^{o} C)**	**K'_b (M^{-1})**	**ΔG^o (kJ)**	**ΔH^o (kJ)**	**ΔS^o (J/ K)**
$[Cu(dpq)_2Cl_2]$	37	1.00×10^4	-23.74	8.15	99.72
	47	5.00×10^4	-28.78		
	57	5.00×10^3	-23.37		
	67	1.02×10^4	-26.04		
$[Cu(dtq)_2Cl_2]$	37	7.50×10^2	-17.06	50.19	218.89
	47	2.67×10^4	-20.29		
	57	2.67×10^3	-21.64		
	67	500×10^3	-24.07		
$[Pt(dpq)_2Cl_2]$	37	7.50×10^3	-22.99	-8.76	46.91
	47	1.00×10^3	-18.38		
	57	5.00×10^3	-23.37		
	67	1.00×10^4	-26.04		
$[Pt(dtq)_2Cl_2$	37	3.75×10^3	-21.21	-2.19	60.36
	47	2.00×10^3	-20.22		
	57	2.86×10^3	-21.84		
	67	3.00×10^3	-22.63		

Table 4.8 ΔG°, ΔH° and ΔS° data for $Cu(dpbq)Cl_2$, $Cu(dtbq)Cl_2$, $Pt(dpbq)Cl_2$, and $Pt(dtbq)Cl_2$.

Compound	Temp(° C)	K'b (M^{-1})	ΔG° (kJ)	ΔH° (kJ)	ΔS° (J/ K)
[Cu(tpbq)Cl_2]	37	6.00 x 10^3	-22.40	-85.29	-207.58
	47	4.50 x 10^2	-16.25		
	57	5.00 x 10^2	-17.05		
	67	2.33 x 10^2	-15.41		
[Cu(ttbq)Cl_2]	37	2.00 x 10^3	-19.60	-11.45	26.78
	47	2.50 x 10^3	-20.29		
	57	1.60 x 10^3	-20.24		
	67	1.40 x 10^3	-20.48		
[Pt(tpbq)Cl_2]	37	2.22 x 10^3	-19.90	-38.25	-59.89
	47	1.00 x 10^3	-18.38		
	57	1.11 x 10^3	-19.24		
	67	5.00 x 10^2	-17.57		
[Pt(ttbq)Cl_2	37	6.76 x 10^2	-16.80	-28.75	-39.74
	47	3.33 x 10^2	-15.45		
	57	3.00 x 10^2	-15.65		
	67	2.33 x 10^2	-15.45		

4.3.2 Viscosity measurements

Viscosity measurements provide a clear view of the type of interaction, since they show fluctuations as the molecule dimensions change. The classical intercalation mode of action of the drugs cause separation between the base strands. The elongation of the DNA helix, thus leads an increase in the viscosity [175].

On the contrary, compounds with limited binding in the DNA grooves formed through partial or nonclassical intercalation processes may cause bend or kink in the DNA helix, thus reducing its length as well as viscosity or, alternatively, resulting in no shifts in its viscosity. Furthermore, in the case of electrostatic interaction the aggregation reduces the number of freely moving DNA molecules, leading the decrease in DNA viscosity. [176].

In order to gain further insight to the binding mode of our complexes to CT-DNA, viscosity measurements of CT-DNA were carried out in the presence (η) and the absence (η_o) of our complexes, [R, [DNA]/[compound] =0-10]. Then relative viscosity $(\eta / \eta_o)^{1/3}$ vs. 1/R, plots were drown to obtain the slopes.

The measured relative viscosity slopes were 0.032, 0.033, 0.044 and 0.159 for $Pt(dtq)_2Cl_2$, $Cu(dtq)_2Cl_2$, $Cu(dpq)_2Cl_2$ and $Pt(dpq)_2Cl_2$, respectively, while 0.027, 0.028, 0.030 and 0.044 for $Cu(ttbq)Cl_2$, $Cu(tpbq)Cl_2$, $Pt(ttbq)Cl_2$ and $Pt(tpbq)Cl_2$, respectively, as seen in Figures 4.18 and 4.19. It was observed that the slope of the relative viscosity plots of CT-DNA were slightly increased with the effect of our compounds, suggesting an electrostatic groove binding, similar to netropsin and causing slight or no changes in DNA solution viscosity [177a]. Also, in another study, $[Ni(hhmh)_2]$ and $[Ni(PPh_3)(hpeh)]$ complexes were reported as groove binder via electrostatic interaction which produced no significant slopes [177b]. Thus, an intercalative DNA binding mode could unequivocally be excluded, because slopes for intercalators reach up to 1 [176, 178].

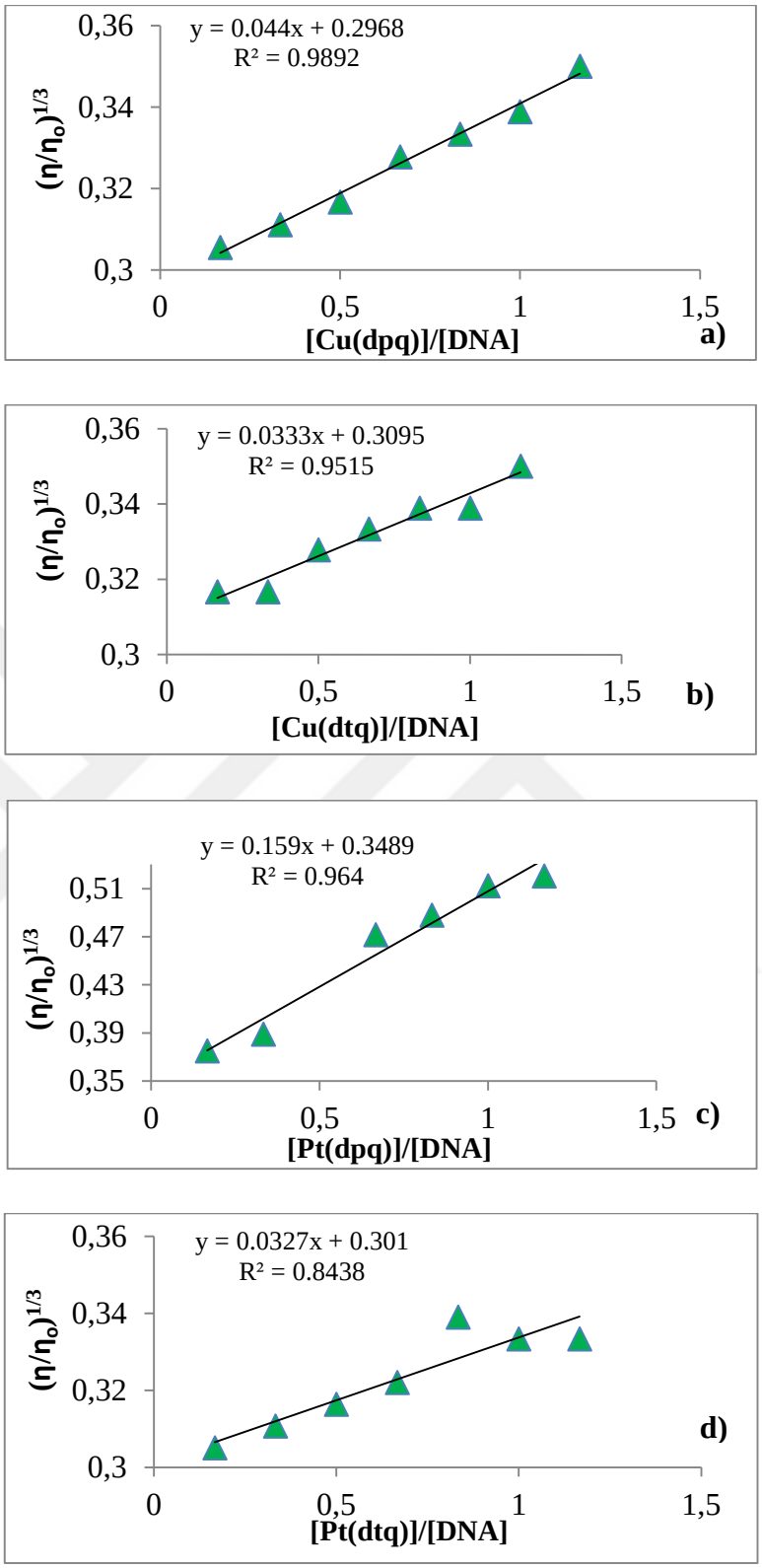

Figure 4.18 The changes in the relative viscosity of the CT-DNA in the presence of a) $[Cu(dpq)_2Cl_2]$, b) $[Cu(dtq)_2Cl_2]$, c) $[Pt(dpq)_2Cl_2]$, d) $[Pt(dtq)_2Cl_2]$.

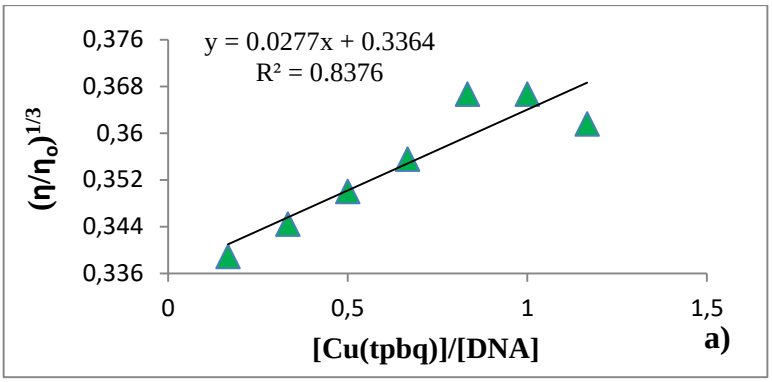

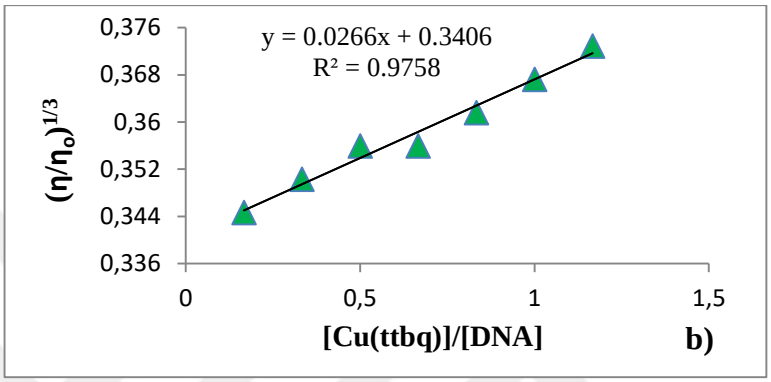

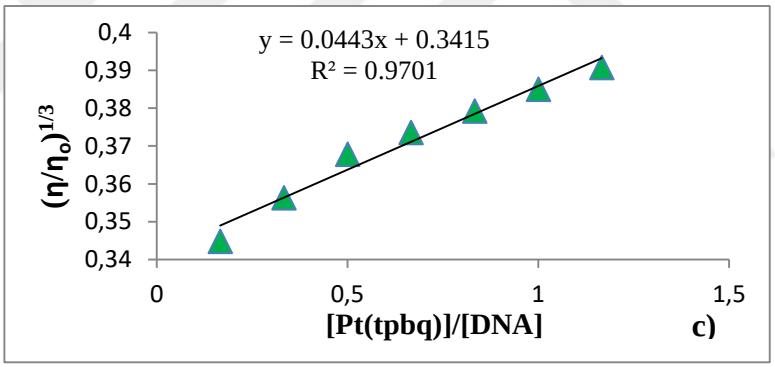

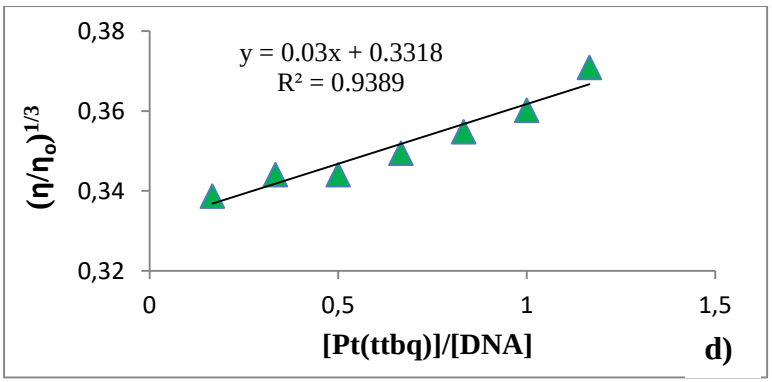

Figure 4.19 The changes in the relative viscosity of the CT-DNA in the presence of a) $[Cu(tpbq)Cl_2]$, b) $[Cu(ttbq)Cl_2]$, c) $[Pt(tpbq)Cl_2]$, d) $[Pt(ttbq)Cl_2]$.

4.3.3 Thermal Denaturation

The conformational changes on the DNA strands were studied by following the change in the electronic absorption band of the CT-DNA at 260 nm in the existence of the complexes between 30 and 90^{o} C in Tris HCl buffer. The melting temperature (T_m) is considered to be the one at which 50% of DNA is denaturalized or melted, half of the nucleic acid being found in the double-stranded state and the other half in the single-stranded state [181].

The magnitude of the T_m value of DNA in the presence of any binder further indicates the binding mode [179]. Based on these facts, a rise in T_m reveals an intercalative or phosphate binding mode, whereas a drop in the temperature signifies base-binding [180].The intercalative mode can maintain the dual helix formation and cause T_m to rise at about 5 to 8° C; on the other hand, a non-intercalative binding results no obvious increase in T_m [182, 183].

The thermal denaturation experments of CT-DNA were conducted in the presence and absence of our complexes in various concentration. The melting temperature of DNA was measured as 79 - 80^{o} C in absence of complexes.

Then under the same conditions, complexes were added to the CT-DNA Tris-buffer solution and absorbance values at 260 were noted for each 1 °C temperature rise within every 2 min. Afterwerds, the melting temperature of CT-DNA was determined from the plot of absorbance *versus* temperature by choosing the temperature value corresponding to the midpoint of the curve. Figure 4.20 highlight the melting curves of the CT-in the existence of our dpq- and dtq-containing complexes. The melting temperature of CT-DNA was obtained as 80°C, for $[Pt(dpq)_2Cl_2]$, $[Pt(dtq)_2Cl_2]$ and 81°C and 82.5°C for $[Cu(dpq)_2Cl_2]$ and $[Cu(dtq)_2Cl_2]$, respectively. As can be easily understood, the change in T_m, $\Delta T_m = T_{m\ (complex)} - T_{m\ (CT\text{-}DNA)}$, was a maximum 2.5, indicating electrostatic interaction [179].

The melting curves obtained for CT-DNA in the presence of tpbq and ttbq Cu(II) and Pt(II) complexes reveals no change was occurred in the melting point of CT-DNA

upon the addition of complexes (Figure 4.21). The maximum ΔT_m values was obtained for [Pt(ttbq)Cl_2] with 1.5°C. The insignificant change in T_m was further attributed to the weak electrostatic interaction of those compounds [184-186].

The extent of the change in the melting temperature (ΔT_m) of DNA with the interactions of some Cu(II) complexes of two tridentate ligands, N-((1H-imidazole-2-yl)methyl)-2-(pyridine-2-yl)ethanamine and N-((1-methyl-1H-imidazole-2-yl)methyl)-2-(pyridine-2-yl)ethanamine, reveal minor structural changes of CT- DNA in presence of complexes. This is also indicative of an electrostatic interaction with the compounds through the phosphate groups in the grooves [184 – 186].

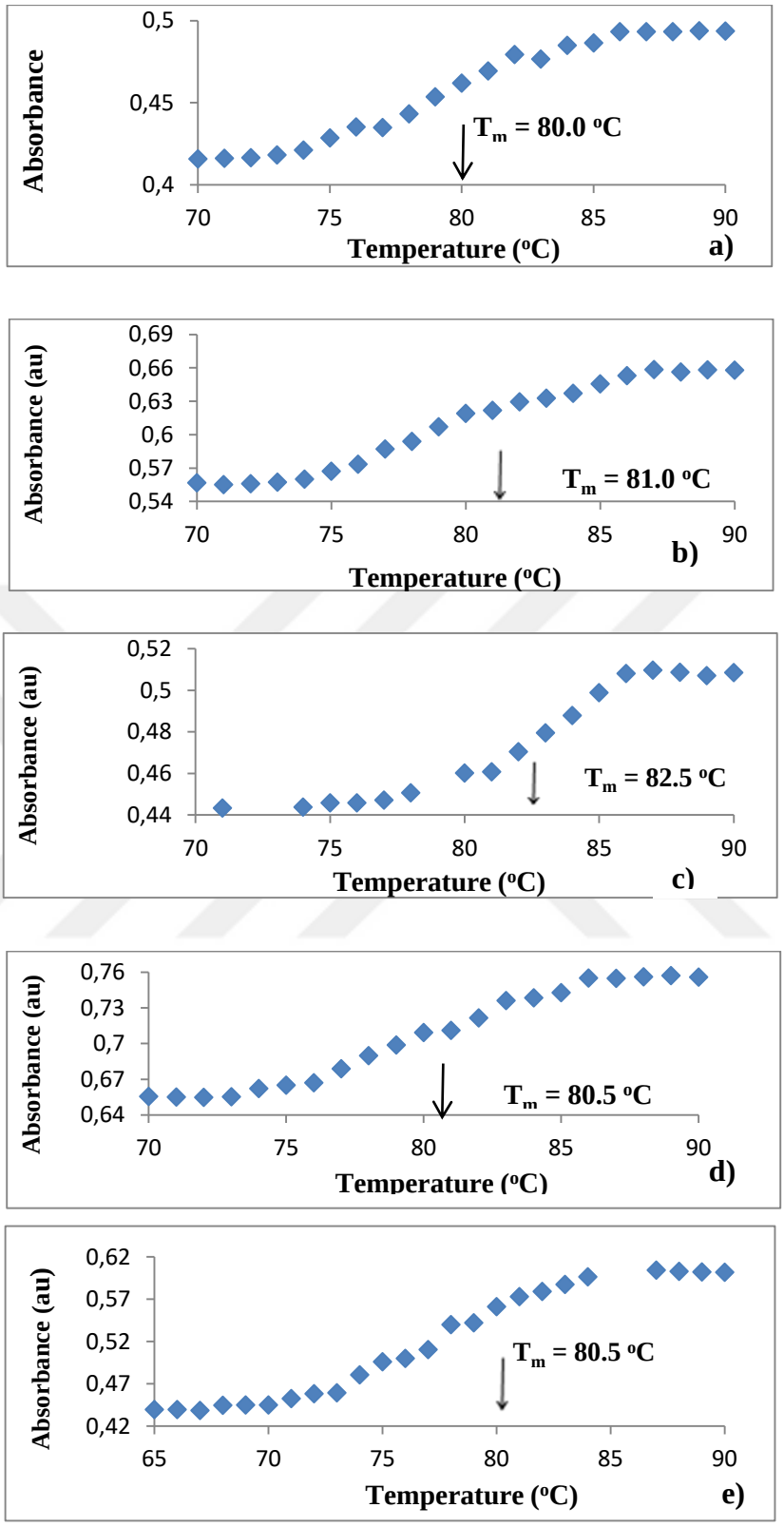

Figure 4.20 Thermal denaturation plots obtained for a) CT-DNA b) $[Cu(dpq)_2Cl_2]$, c) $[Cu(dtq)_2Cl_2]$, d) $[Pt(dpq)_2Cl_2]$ and e) $[Pt(dtq)_2Cl_2]$.

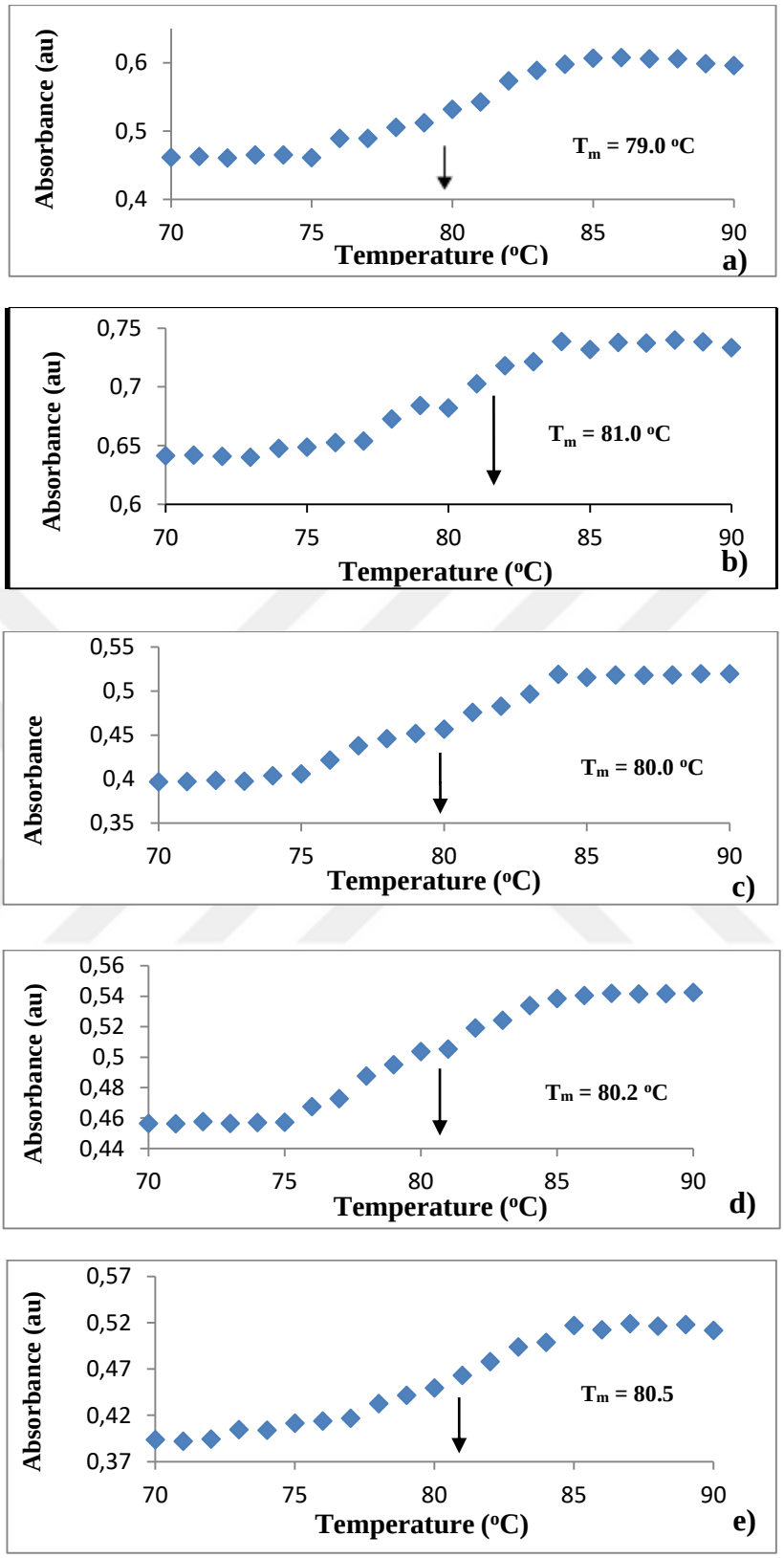

Figure 4.21 Thermal denaturation of a) DNA b) [Cu(tpbq)Cl_2], c) [Cu(ttbq)Cl_2], d) [Pt(tpbq)Cl_2], and e) [Pt(ttbq)Cl_2].

4.3.4 Fluorescence Titration

Fluorescence spectroscopy is a very helpful method to study the interactions between a metal complex and DNA. For this purpose, ethidium bromide EtBr pretreated CT-DNA is used to find the binding affinity of compounds to DNA [187 The EtBr intercalates between the adjacent DNA base pairs and releases sharp fluorescence, which could be quenched upon the addition of another molecule. The presence of another species with an affinity towards DNA may result in a change in the emission intensity of the EtBr-DNA adduct, which is caused by either a competition for binding sites, a change in the DNA conformation, or through a photoelectron transfer mechanism. It is possible to observe a decrease in the fluorescence intensity in the EtBr-DNA, in the case of groove binding, electrostatic, hydrogen bonding or hydrophobic interaction [188,189] due to the inhibition of the EtBr-intercalated sides of DNA by the large complexes.

In order to evaluate the binding ability of our complexes, fluorescence titration studies were performed at 37°C. The EtBr pretreated CT-DNA solution were incubated with our complexes in different concentrations [0 - 50M] in Tris HCl buffer at pH=7.11. The EtBr - DNA solution was excited at 478 nm in the presence and absence of our complexes and the changes in the Fluorescence Spectrum were recorded between 500-800 nm regions by using Thermo Scientific® Lumina Fluorescence Spectrometer. Those spectral data were then used to find out the Stern–Volmer quenching constant K_{sv}, by using the equation below [190].

$$I_o / I = 1 + K_{sv}.r \qquad (4.4)$$

Here, r is the ratio of concentration of the quencher to DNA while I_o is the fluorescence intensity in the absence of quencher and I is the fluorescence intensity in the presence of quencher.

A decrease in the emission intensity of the EtBr pretreated CT-DNA occured in the presence copper(II) and platinum(II) complexes during the fluorometric titration as depicted in the Figures 4.22 and 4.23.

Quenching might be associated with the potential intercalation of the aromatic groups of our complexes by substitution of EtBr or the covering of the EtBr- binding sites of DNA by our complexes through electrostatic interactions [188-189].

The plots of I_o/I *versus* complex concentration was drawn to calculate K_{sv} values directly from the ratio of slope-to-intercept for each plots.

K_{SV} values with a magnitude of 10^3 M^{-1} or greater are generally regarded as indicating a strong interaction between metal complexes and DNA [191], but the results suggested that the interaction of our complexes with DNA was rather weak. The obtained Stern–Volmer quenching constants, K_{sv}, were 5.16 x 10^{-3}, 9.70 x 10^{-4}, 6.16 x10^{-3} and 2.83 x 10^{-3} for $Cu(dtq)_2Cl_2$, $Cu(dpq)_2Cl_2$, $Pt(dtq)_2Cl_2$, and $Pt(dpq)_2Cl_2$, respectively. Likewise, the Ksv values were 1.05x10^{-2}, 1.37x10^{-2}, 8.2x10^{-3} and 1.43x10^{-2} for $Cu(tpbq)Cl_2$, $Cu(ttbq)Cl_2$, $Pt(tpbq)Cl_2$, and $Pt(ttbq)Cl_2$, respectively. These low K_{SV} values of complexes confirmed the electrostatic interaction via groove binding [188, 189] as observed in the spectroscopic and viscometric results obtained previously.

Although $Cu(dtq)_2Cl_2$, $Pt(dtq)_2Cl_2$, $Cu(ttbq)Cl_2$ and $Pt(ttbq)Cl_2$ complexes have stronger binding affinity compared to that of their dpq and tpbq colleagues, one can say that all the complexes inhibit in the fluorescence of EtBr bound CT-DNA by surface binding [190].

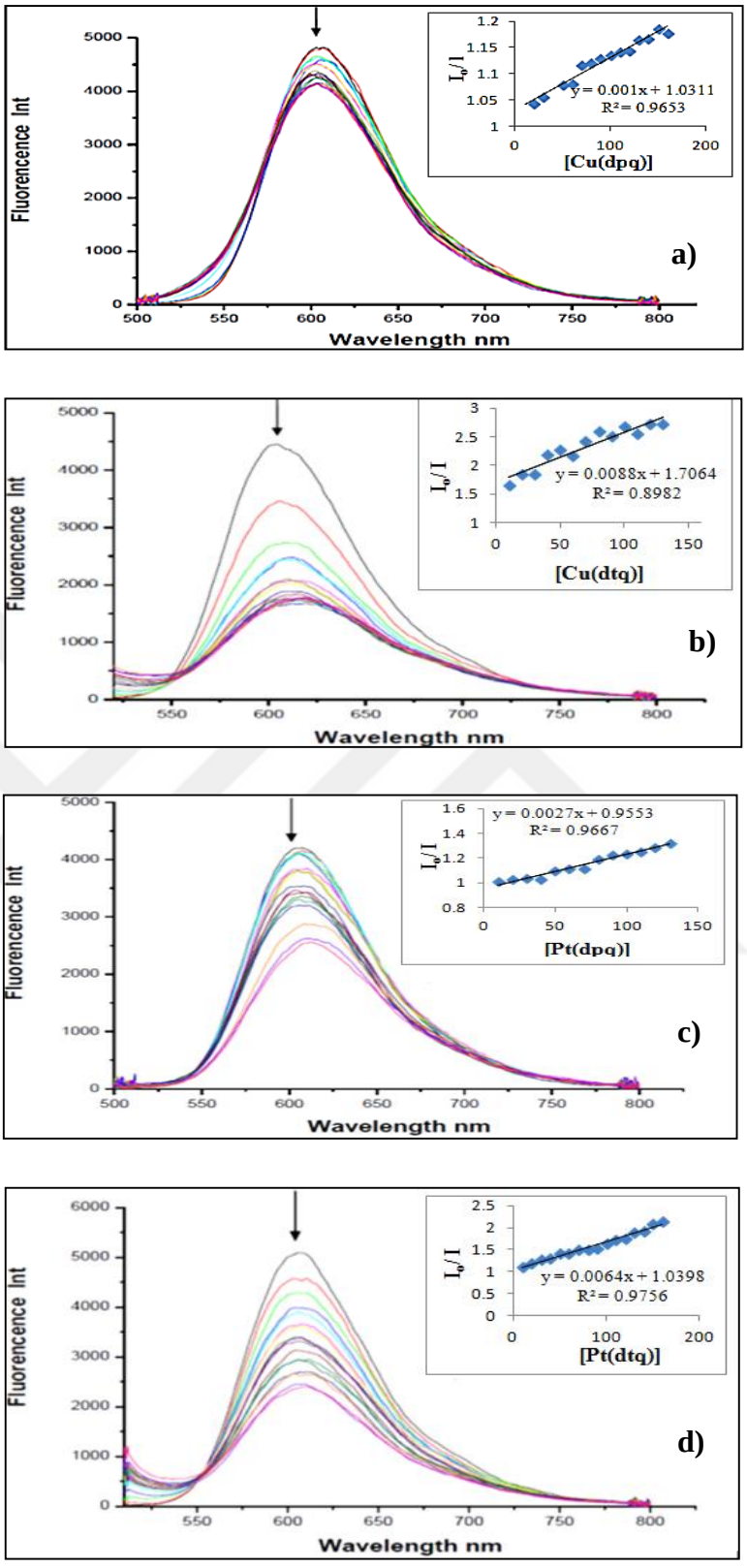

Figure 4.22 The change in the Fluorescence spectrum of a) $[Cu(dpq)_2Cl_2]$, b) $[Cu(dtq)_2Cl_2]$, c) $[Pt(dpq)_2Cl_2]$, d) $[Pt(dtq)_2Cl_2]$.

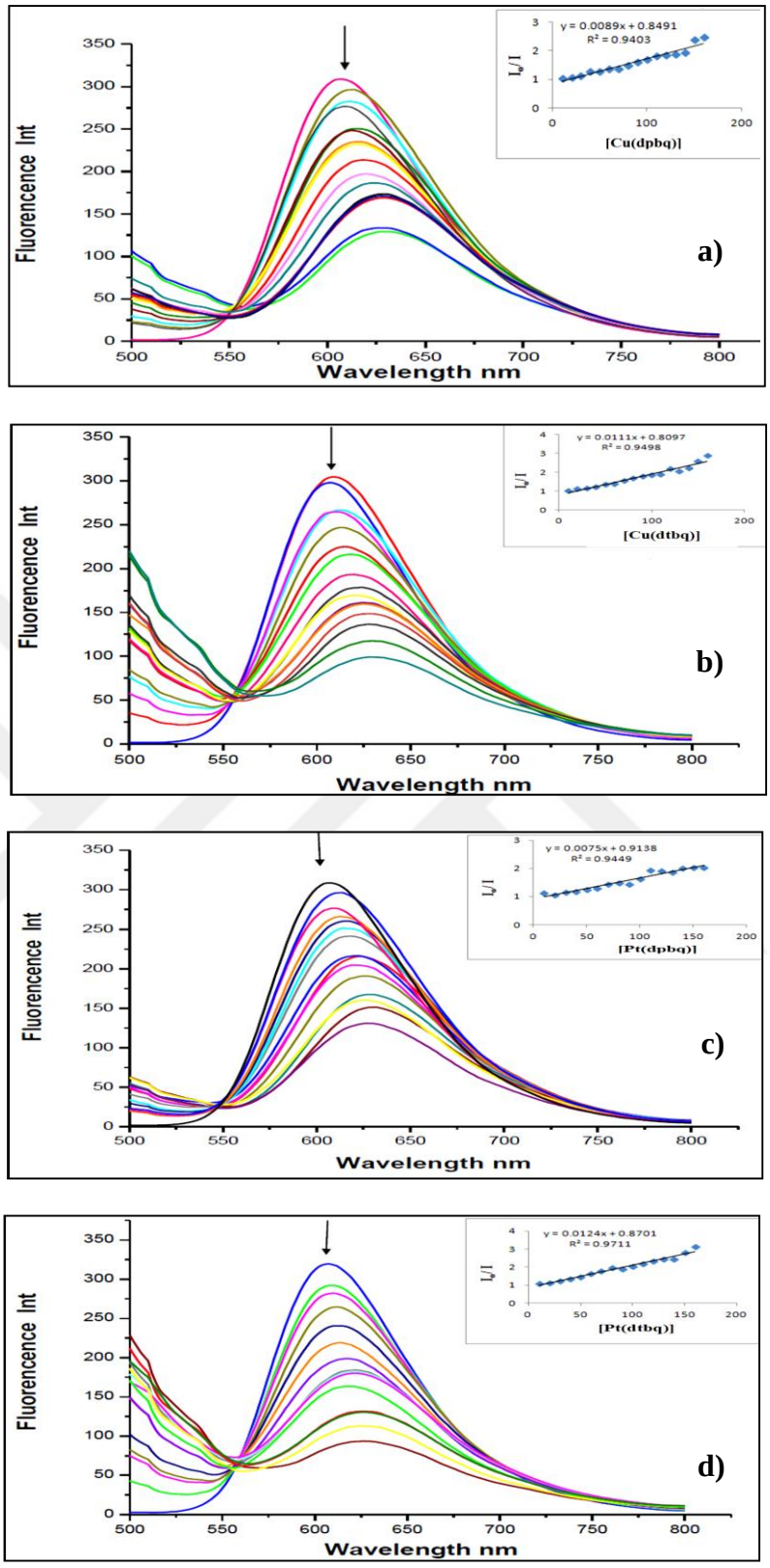

Figure 4.23 The change in the Fluorescence spectrum of a) [Cu(tpbq)Cl_2], b) [Cu(ttbq)Cl_2], c) [Pt(tpbq)Cl_2], d) [tt(dtbq)Cl_2].

4.4 HSA- Binding Studies

4.4.1 Electronic Absorption Spectroscopy (EAS)

Binding affinity of our complexes toward a plasma transport protein HSA was demonstrated by EAS. To establish the nature of this process, UV titration was conducted by using a fixed amount of HSA ($2.12x10^{-5}$ M) and varying the concentrations of the compounds ($2.12x10^{-4}$ - $2.12x10^{-3}$ M). The spectral changes were, then, displayed at the representative absorption band of the protein, 280 nm [192].

The observed decline in the band intensity is attributed the formation of a surface adduct of compound-protein in general; this, however, causes no restrictions to the movement of the compound on the protein (HSA). In addition, this effect can imply that the amount of polarity circling the tryptophan residue increased and the hydrophobicity dropped [193], hence the joining of compounds to hydrophobic areas of the protein and changing the HSA configuration [194]. On the contrary, a rise in the absorption or the hyperchromic effect can take place upon supplying the HSA with compounds and, owing to their reactions on the protein through external contact, possibly through electrostatic processes in the protein's second structure [195].

The spectroscopic titration tests were performed in a molar ratio of the HSA to the platinum and copper compounds (R= [HSA]/[complexes]) between 1 and 10 and an optimum incubation period ranging between 30 and 45 minutes. Band intensity at 279 nm was seen to drop once the compounds are added to the protein solution at R=1 to 10, as depicted in Figures 4.24 and 4.25.

The hypochromic effect detected on the addition of our complexes can be related to hydrophobic processes caused by a π-π stacking relation between the aromatic rings in our compounds and the phenyl rings in tryptophan, tyrosine, and phenylalanine residues within the joint groove of the protein [195].

The intrinsic binding constant, K_b, of the complexes was calculated from the ratio of the intercept to the slope of the linear plot of $1/(A–A_o)$ versus 1/[complex].

K_b was calculated for all HSA-complex adducts at around 10^3 M^{-1} (see Tables 4.9 and 4.10), and indicated relatively high affinity of all the complexes toward HSA as observed for other drugs having strong affinity to words HSA with binding constants ranging from 10^5 to 10^6 [196]. There exist such protein conformational transitions upon the cisplatin binding to HSA in the literature [197]. As shown in Tables 4.9 and 4.10 the intrinsic binding constant K_b of the complexes increases with the function of temperature, suggesting an endothermic process taken place between the complexes and HSA (Figures F1-F8) [198]. Four types of interactions - hydrogen bond, hydrophobic interaction, van der Waals interaction, and ionic interaction - may be related to the noncovalent protein association reactions [198]. To clarify the major interaction mode, thermodynamic data were collected related to our complexes. Standard enthalpy (ΔH^o) and entropy changes (ΔS^o) were also calculated according to the slope and intercept of the linear van't Hoff series [143] related to ln K_b *versus* 1/T in precisely the same way as explained previously for DNA-binding experiments (Figures F9 and F10). The variations in standard Gibbs Free Energy (ΔG^o) related to protein binding were examined based on the equation 4.5;

$$\Delta G^o = - RT \, Ln K_b \qquad (4.5)$$

UV titration experiments, conducted at four different temperatures between 310 and 340 K demonstrated spontaneous affinity of our complexes toward HSA with negative ΔG^o value [199]. Based on the thermodynamic assessments shown in Tables 4.9 and 4.10, such positive indicators of ΔS^o and ΔH^o represented entropy-driven electrostatic binding processes occurring between the compounds and HSA and also a significant hydrophobic effect [200]. Our complexes contain aromatic rings, implying that hydrophobic interactions and π–π stacking with amino acid residues such as Trp present in the hydrophopic region in HSA are reasonable, in contrast with cisplatin that mainly forms irreversible adducts with HSA through covalent bonds [198].

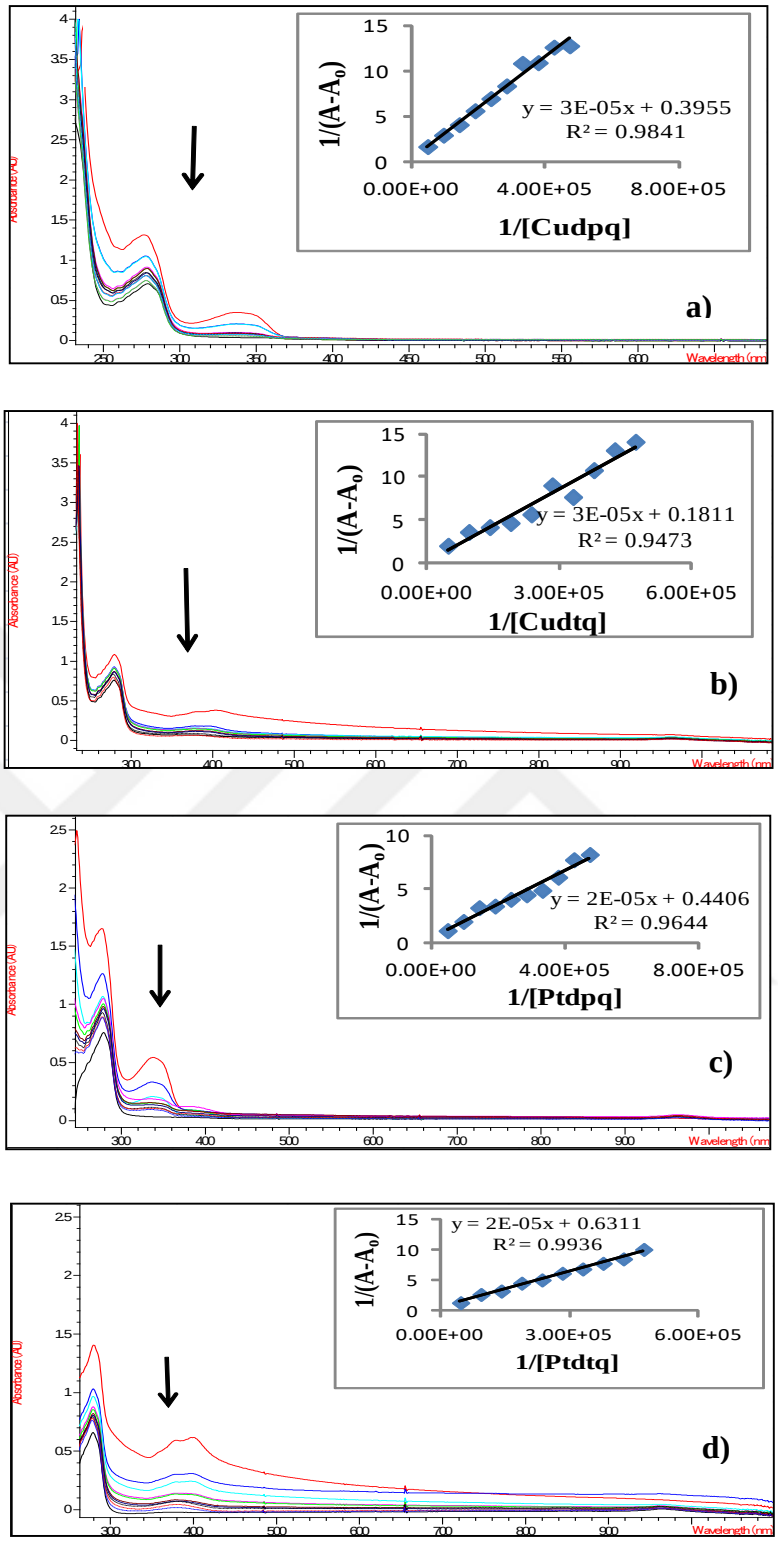

Figure 4.24 The change in the electronic absorption spectrum of (a) $[Cu(dpq)_2Cl_2]$, b) $[Cu(dtq)_2Cl_2]$, c) $[Pt(dpq)_2Cl_2]$ and d) $[Pt(dtq)_2Cl_2]$ in Tris-HCl buffer (pH = 7.10) at 37 ^oC in the absence and in the presence HSA (R=0-10). Inset: Plot of $1/(A–A_o)$ vs 1/[complex].

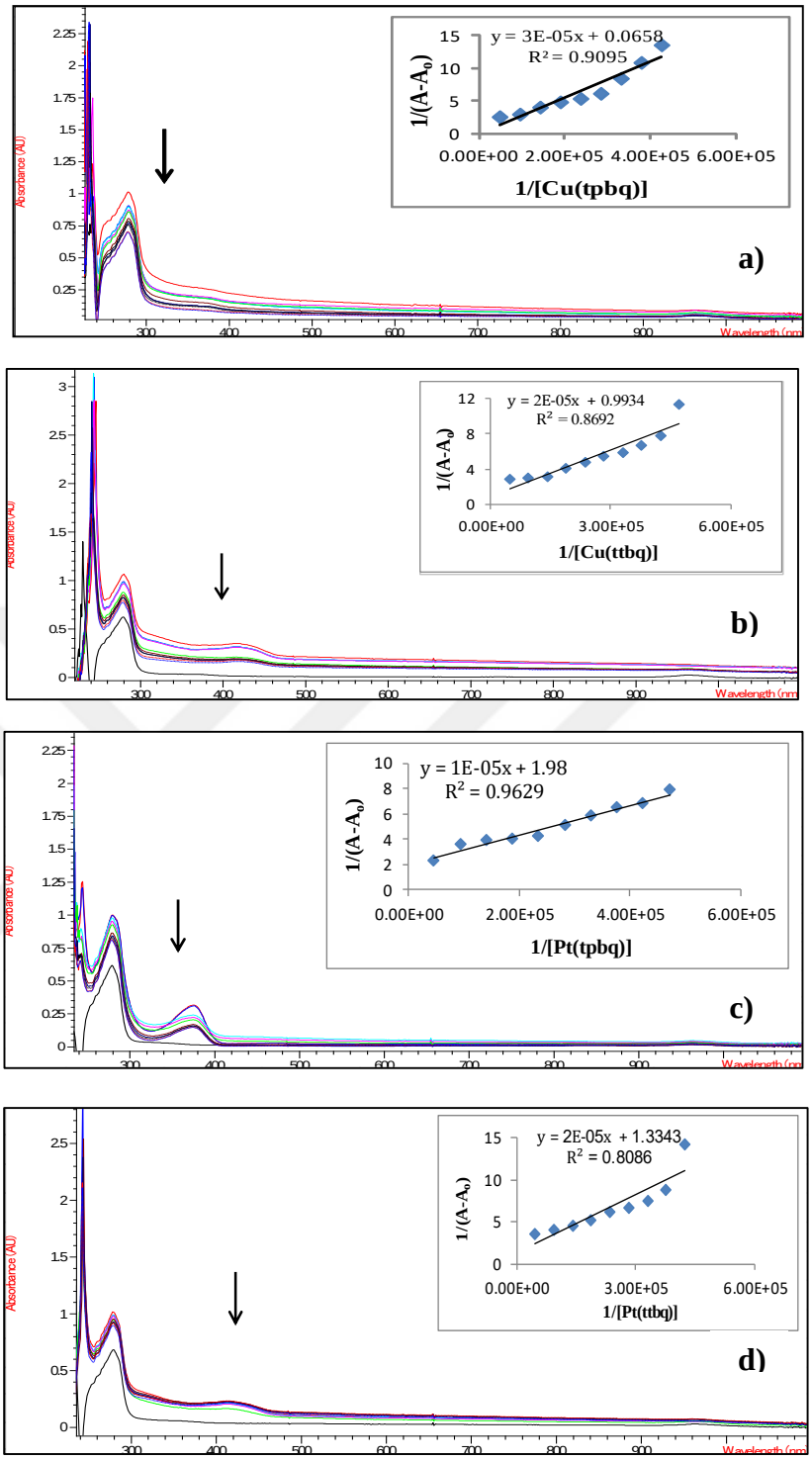

Figure 4.25 The change in the electronic absorption spectrum (a) $[Cu(tpbq)_2Cl_2]$, b) $[Cu(ttbq)_2Cl_2]$, c) $[Pt(tpbq)_2Cl_2]$ and d) $[Pt(ttbq)_2Cl_2]$ in Tris-HCl buffer at 37°C (pH = 7.10) in the absence and in the presence of HSA (R=0-10). Inset: Plot of $1/(A–A_o)$ vs 1/[complex].

Table 4.9 ΔG°, ΔH° and ΔS° data for $[Cu(dpq)_2Cl_2]$, $[Cu(dtq)_2Cl_2]$, $[Pt(dpq)_2Cl_2]$, and $[Pt(dtq)_2Cl_2]$.

Compound	Temp (°C)	K'$_b$ (M^{-1})	ΔG° (kJ)	ΔH° (kJ)	ΔS° (J/K)
$[Cu(dpq)_2Cl_2]$	37	1.32×10^4	-24.45	60.61	278.19
	47	8.27×10^4	-30.12		
	57	9.83×10^4	-31.54		
	67	1.21×10^5	-33.08		
$[Cu(dtq)_2Cl_2]$	37	6.04×10^3	-22.44	135.02	504.22
	47	9.45×10^3	-24.35		
	57	1.02×10^5	-31.64		
	67	4.77×10^5	-36.96		
$[Pt(dpq)_2Cl_2]$	37	2.20×10^4	-25.80	39.74	211.22
	47	3.32×10^4	-27.69		
	57	6.00×10^4	-30.18		
	67	8.18×10^4	-31.98		
$[Pt(dtq)_2Cl_2]$	37	3.16×10^4	-26.80	84.18	359.89
	47	1.84×10^5	-32.25		
	57	2.58×10^5	-34.19		
	67	6.84×10^5	-37.98		

Table 4.10 $\Delta G°$, ΔH^o and ΔS^o data for [Cu(tpbq)Cl_2], [Cu(ttbq)Cl_2], [Pt(tpbq)Cl_2] and [Pt(ttbq)Cl_2].

Compound	**Temp (°C)**	**K'$_b$ (M^{-1})**	**ΔG^o (kJ)**	**ΔH^o (kJ)**	**ΔS^o (J/ K)**
[Cu(tpbq)Cl_2]	37	2.19×10^3	-19.82	120.78	458.15
	47	2.37×10^4	-26.79		
	57	1.05×10^5	-33.14		
	67	1.76×10^5	-32.68		
[Cu(ttbq)Cl_2]	37	4.97×10^4	-27.87	53.11	258.51
	47	3.99×10^4	-28.19		
	57	1.32×10^5	-32.36		
	67	2.56×10^5	-35.20		
[Pt(tpbq)Cl_2]	37	1.98×10^5	-31.43	22.92	174.97
	47	1.68×10^5	-32.77		
	57	3.60×10^5	-35.10		
	67	4.04×10^5	-36.49		
[Pt(ttbq)Cl_2]	37	6.67×10^4	-28.63	33.16	198.00
	47	7.49×10^4	-29.86		
	57	9.63×10^4	-31.50		
	67	2.20×10^5	-34.77		

4.4.2 Viscosity measurements

Viscosity measurements were selected as another effective method to confirm the nature of binding between the copper and the platinum compounds and the albumin structure. The electrostatic processes taking place between the metal compounds and HSA may cause a rise in the relative viscosity in the mixture [201]. Insignificant positive or negative fluctuations in related values can be seen once bindings are formed in the HSA groove [202]. Yet, should there be minor increases in relative specific viscosity once compound concentrations also rise, then the binding with HSA can be said to have occurred by means of hydrophobic processes [203].

The viscometric titration was carried out on the proteins to see the nature of binding between the compounds and HSA, all compound was incubated at 37^{o} C for half an hour to record the variations in viscosity with the help of an SV-10 VIBRO instrument. The relative viscosity in $(\eta/\eta^{o})^{1/3}$ (η and η^{o} point to specific viscosity addition from serum albumins both with and without compounds being present, respectively) *versus* the ratio of the increasing concentrations of complexes to HSA concentration. Figures 4.26 and 4.27 depict the relative viscosity change of HSA in the existence of our complexes.

It was observed that the addition of our complexes to the albumin solutions result in a slight increasing in the viscosity values of the solution. The measured relative viscosity slopes were 0.031, 0.036, 0.038 and 0.046 for $Cu(dpq)_2Cl_2$, $Pt(dtq)_2Cl_2$, $Cu(dtq)_2Cl_2$ and $Pt(dpq)_2Cl_2$, respectively, while 0.049, 0.051, 0.052 and 0.066 for $Cu(ttbq)Cl_2$, $Cu(tpbq)Cl_2$, $Pt(tpbq)Cl_2$ and $Pt(ttbq)Cl_2$, respectively. In this way, the minor increases obtained in the slope of the plot of relative viscosity revealed the processes were indeed taken place in the hydrophobic area for all complexes [204].

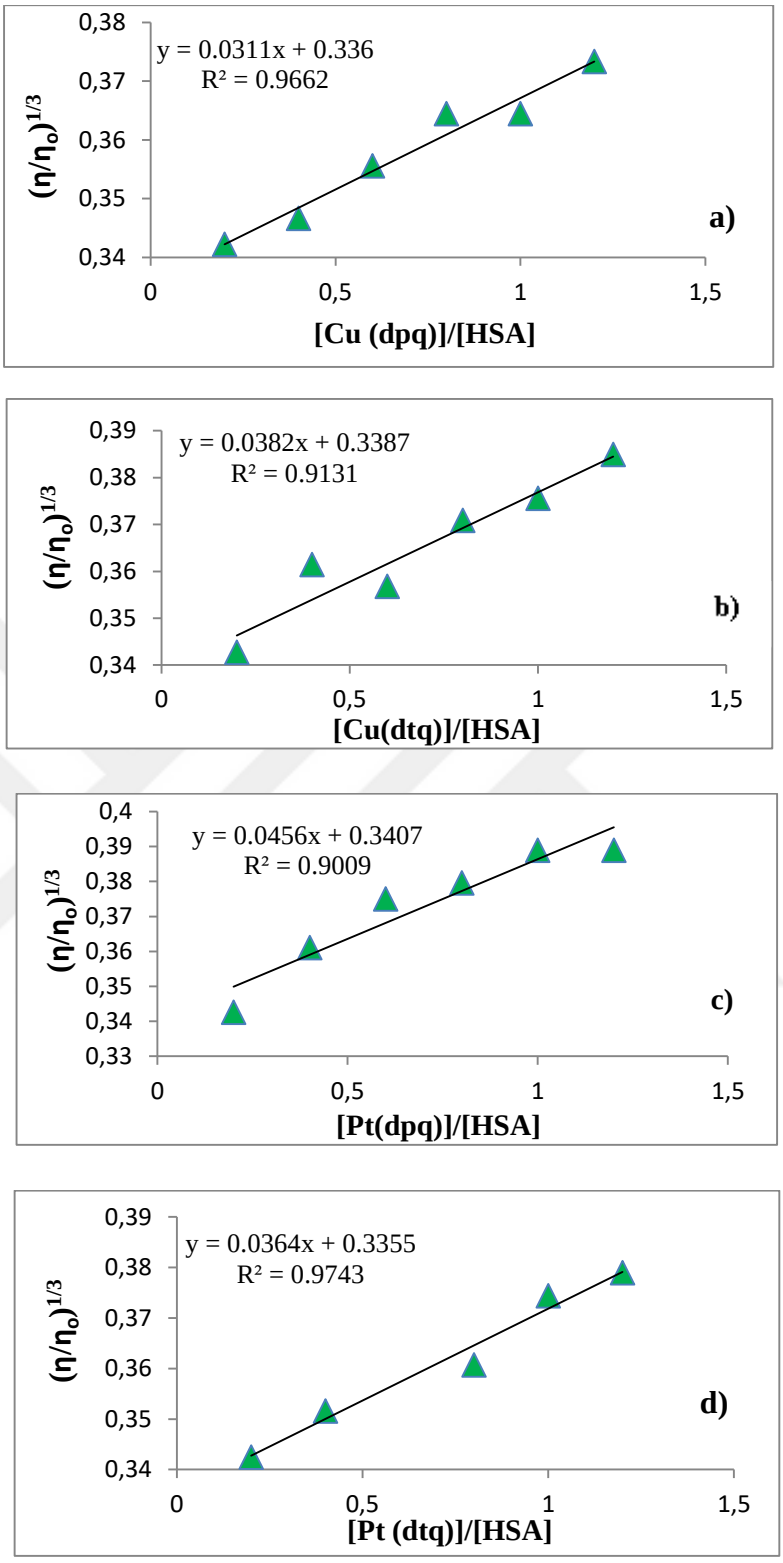

Figure 4.26 The changes in the relative viscosity of the HSA in the presence of a) $[Cu(dpq)_2Cl_2]$, b) $[Cu(dtq)_2Cl_2]$, c) $[Pt(dpq)_2Cl_2]$, and d) $[Pt(dtq)_2Cl_2]$.

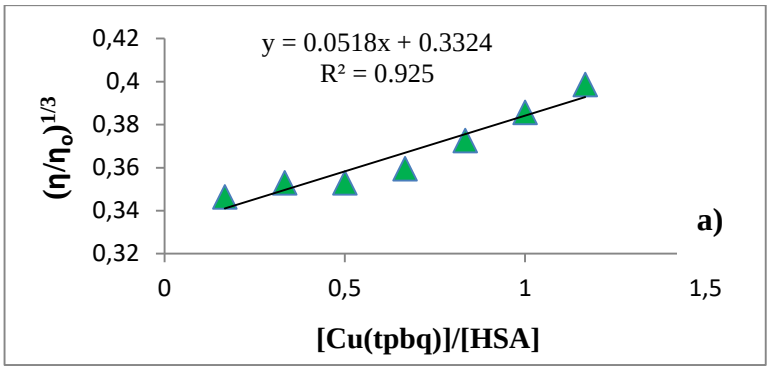

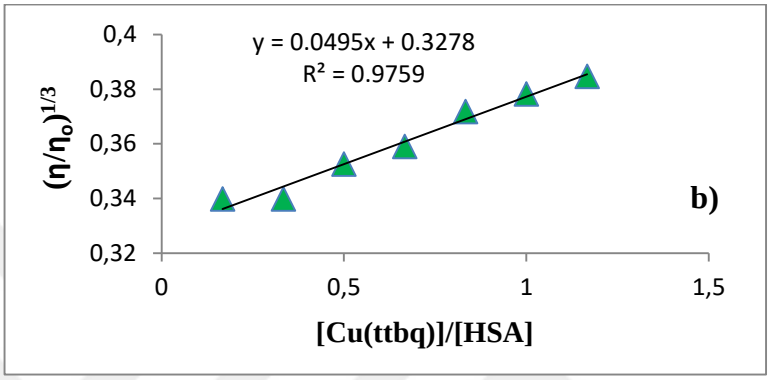

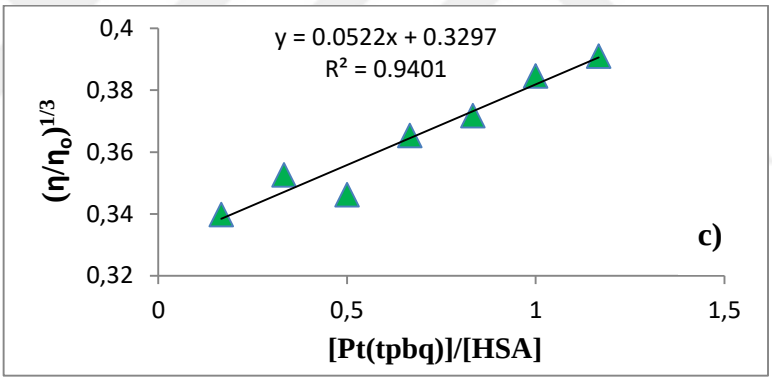

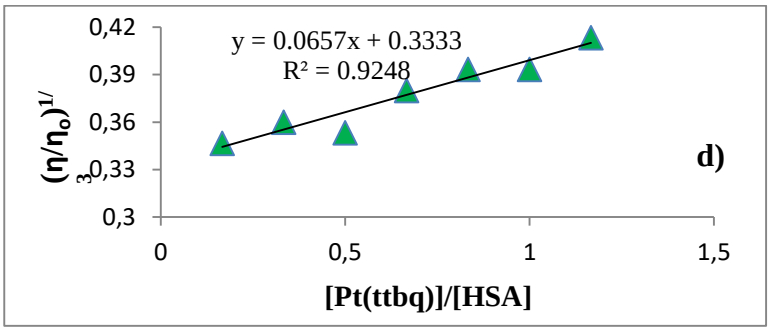

Figure 4.27 The changes in the relative viscosity of the HSA in the presence of a) [Cu(tpbq)Cl_2], b) [Cu(ttbq)Cl_2], c) [Pt(tpbq)Cl_2], d) [Pt(ttbq)Cl_2].

4.4.3 Thermal Denaturation

The thermal denaturation in the proteins possesses a major challenge on segregating/reposition of proteins, biotransformation, biosensing, drug manufacturing, and finally food production. As a whole, once a compound binds with a protein at a native state, it stabilizes the temperature, thus improving the related index.

According to other researchers, temperature of HSA decreasing after the addition of the drug is an indication that the drug is gradually denaturating the protein [205]. As to this study, the HSA thermal denaturation was examined with and without compounds to see the extent of thermal stabilization within the proteins upon binding. The related diagrams were obtained upon measuring the variations in absorbance levels of the HSA at 279 nm as the function of temperature, and the melting temperature of HSA was studied between 30 - 140^{o} C in our laboratory conditions.

Thermal denaturation studies carried out in this work indicated a drop in the melting point of HSA from 113^{o} C to 112° C, 108° C, 102° C, and 98° C by the effects of $Pt(dpq)_2Cl_2$, $Cu(dpq)_2Cl_2$, $Cu(dtq)_2Cl_2$, and $Pt(dtq)_2Cl_2$, respectively (Figure 4.28). In addition, the melting point declined gradually in the presence of $Cu(ttbq)Cl_2$, $Cu(tpbq)Cl_2$, $Pt(tpbq)Cl_2$, and $Pt(ttbq)Cl_2$ to 111° C, 110° C, 109° C and 105° C, respectively, as seen in Figure 4.29.

In the light of these findings, it can be stated that albumin lost its stability slightly upon binding with platinum and copper complexes.

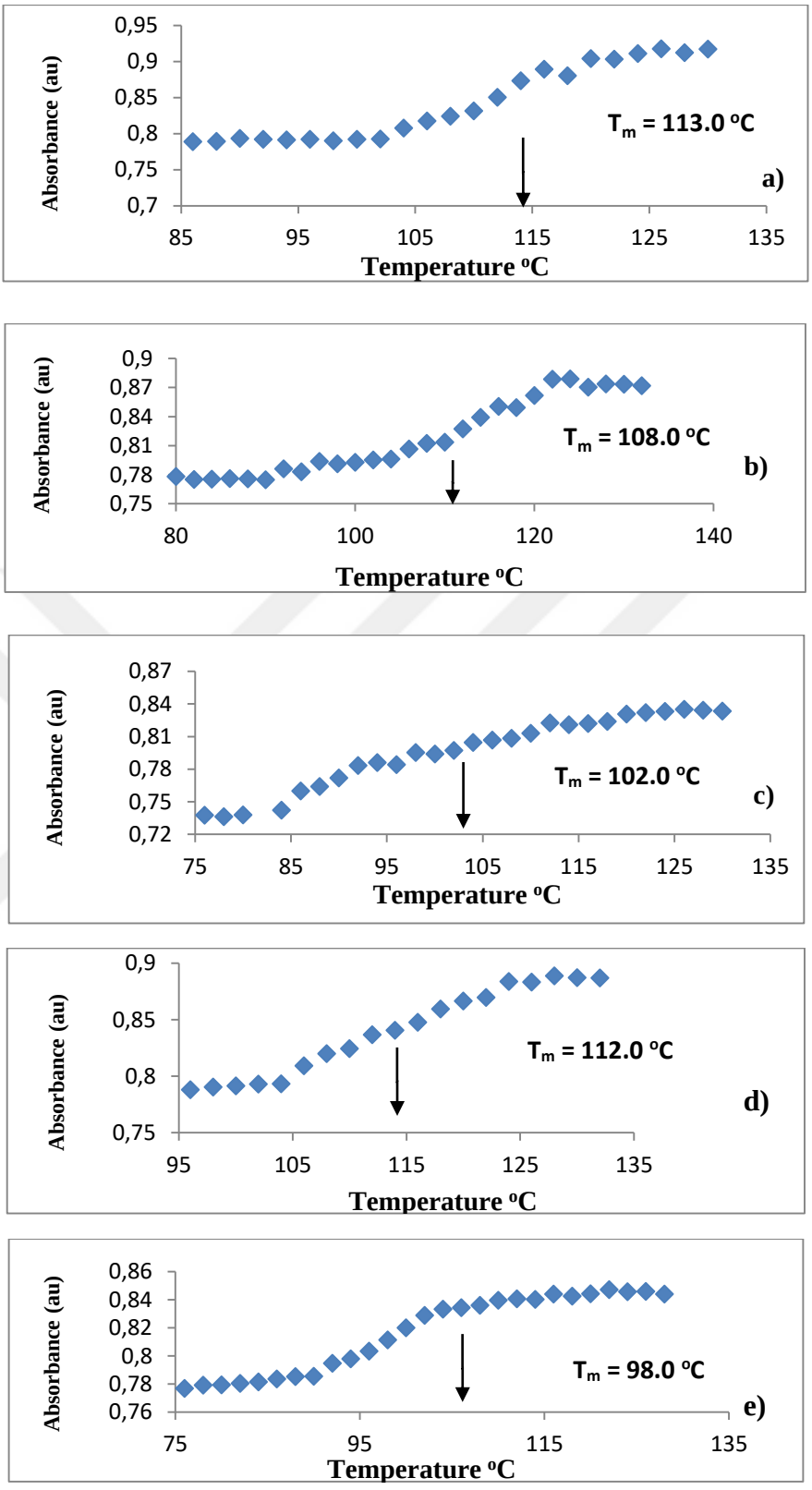

Figure 4.28 Thermal denaturation plots obtained for a) HSA, b) $[Cu(dpq)_2Cl_2]$, c) $[Cu(dtq)_2Cl_2]$, d) $[Pt(dpq)_2Cl_2]$ and e) $[Pt(dtq)_2Cl_2]$.

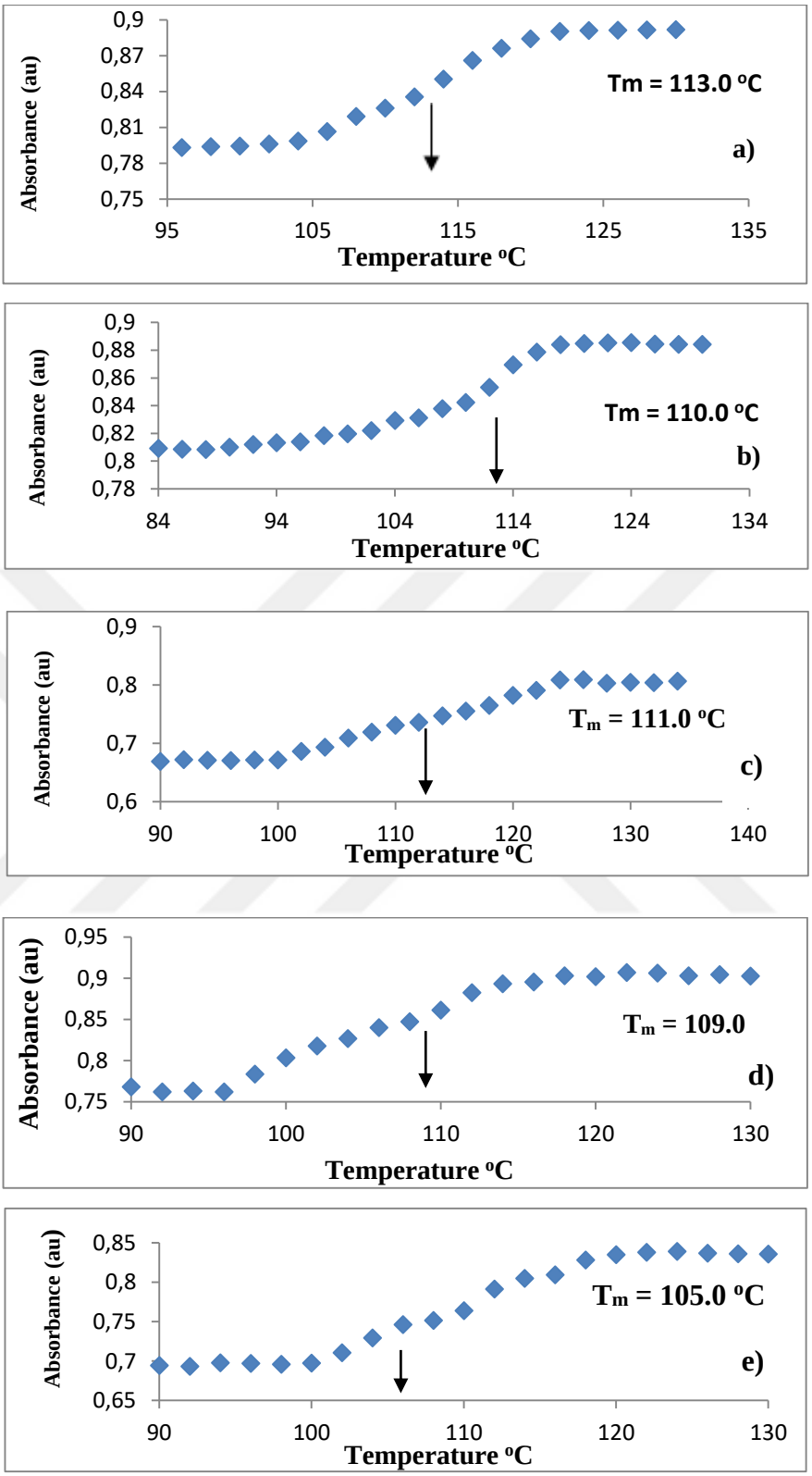

Figure 4.29 Thermal denaturation of a) HSA b) [Cu(tpbq)Cl_2], c) [Cu(ttbq)Cl_2], d) [Pt(tpbq)Cl_2], and e) [Pt(ttbq)Cl_2].

4.4.4 Fluorescence Titration

The Fluorescence quenching tests for albumin are significant since they show the processes the protein can engage with any drugs [206]. In most cases, such fluorescence appears due to three inherent features: namely tryptophan, tyrosine and phenylalanine remains. In practice, the sheer fluorescence in most proteins is primarily formed by tryptophan and no others; yet, given the very low quantum yield of phenylalanine, fluorescence of a tyrosine can be entirely removed by ionizing [207].

Related tests were carried out for HSA upon examining the variations in the emission intensity of the band at 346 nm in the presence and in the absence of our complexes in different concentration. The emission intensity of the representative band related to protein at 346 nm dropped accordingly with added concentrations in a step-by-step manner as depicted in Figures 4.30 and 4.31.

Furthermore, the highest emission wavelength of HSA did not differ throughout the process, which indicates that our complexes quenched the intrinsic fluorescence of the protein (HSA) without altering the environment [207].

Quite often, the albumin fluorescence reduction with many compounds can be represented with a linear Stern-Volmer (SV) series and calculated with the classical Stern-Volmer formula as explained for DNA studies. The K_{sv} values related to $Cu(dtq)_2Cl_2$, $Cu(dpq)_2Cl_2$, $Pt(dtq)_2Cl_2$, and $Pt(dpq)_2Cl_2$ were found as 0.0066, 0.1626, 0.0112 and 0.8769, respectively. Those values for $Cu(tpbq)Cl_2$, $Cu(ttbq)Cl_2$, $Pt(tpbq)Cl_2$, and $Pt(ttbq)Cl_2$ were calculated as 0.0059, 0.0720, 0.0261 and 0.0589, respectively. The observed values of K_{SV} were very close to the quenching constant of various kinds of quencher such as $[Pt_3LCl_3](ClO_4)_3$ (L=(N,N,NI,NI,NII,NII-hexakis(2-pyridylmethyl)-1,3,5-tris(aminomethyl)benzene) (K_{sv}=1.04 x 10^{-4} M^{-1}) [208]. Evidently, our complexes reduced the emission intensity without insignificant shifts in the peak position, suggesting that they interacted with HSA by producing non-fluorescent adducts [209]; that is, the copper and platinum complexes interacted with the serum albumin via the hydrophobic region located inside the protein [208].

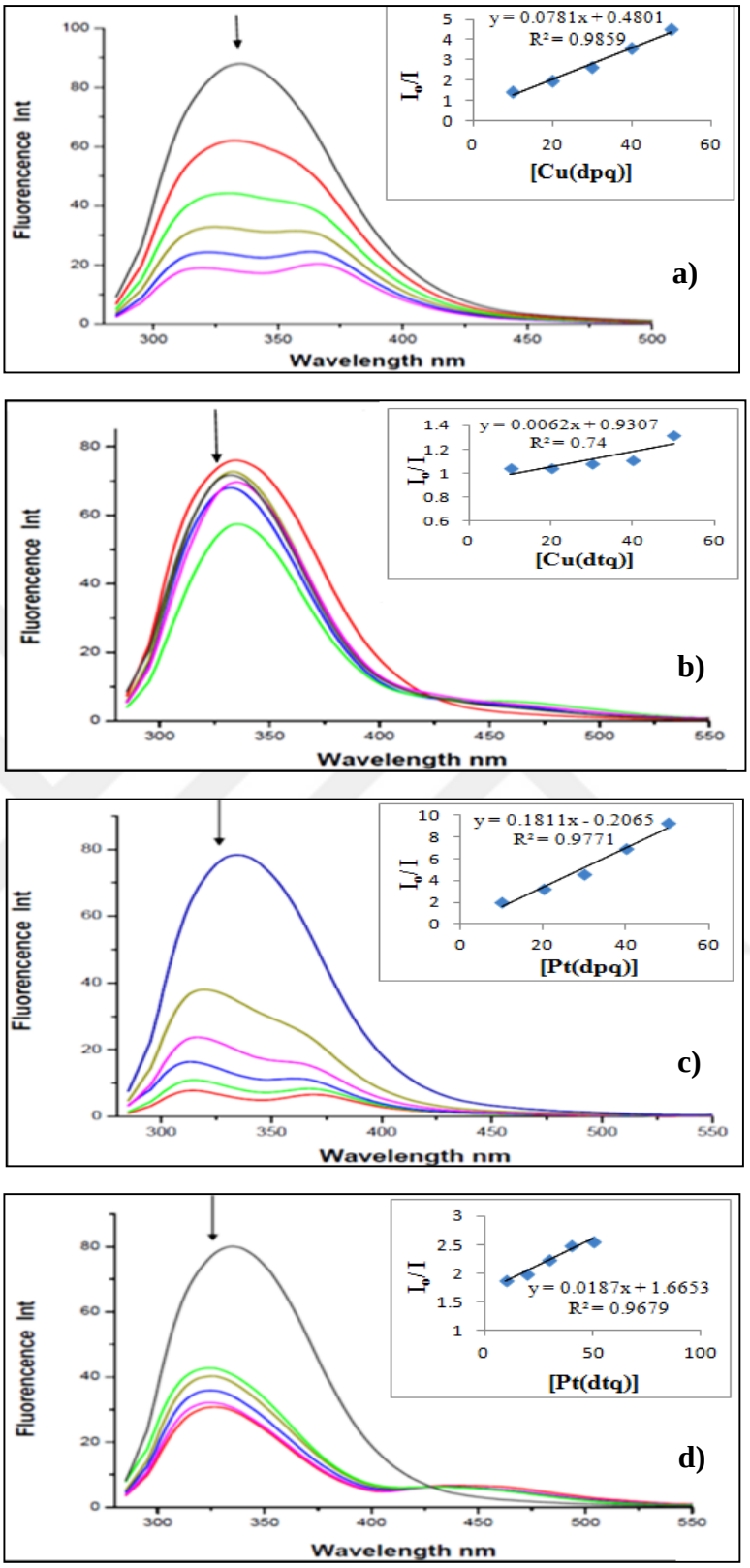

Figure 4.30 The change in the Fluorescence spectrum of a) $[Cu(dpq)_2Cl_2]$, b) $[Cu(dtq)_2Cl_2]$, c) $[Pt(dpq)_2Cl_2]$, d) $[Pt(dtq)_2Cl_2]$.

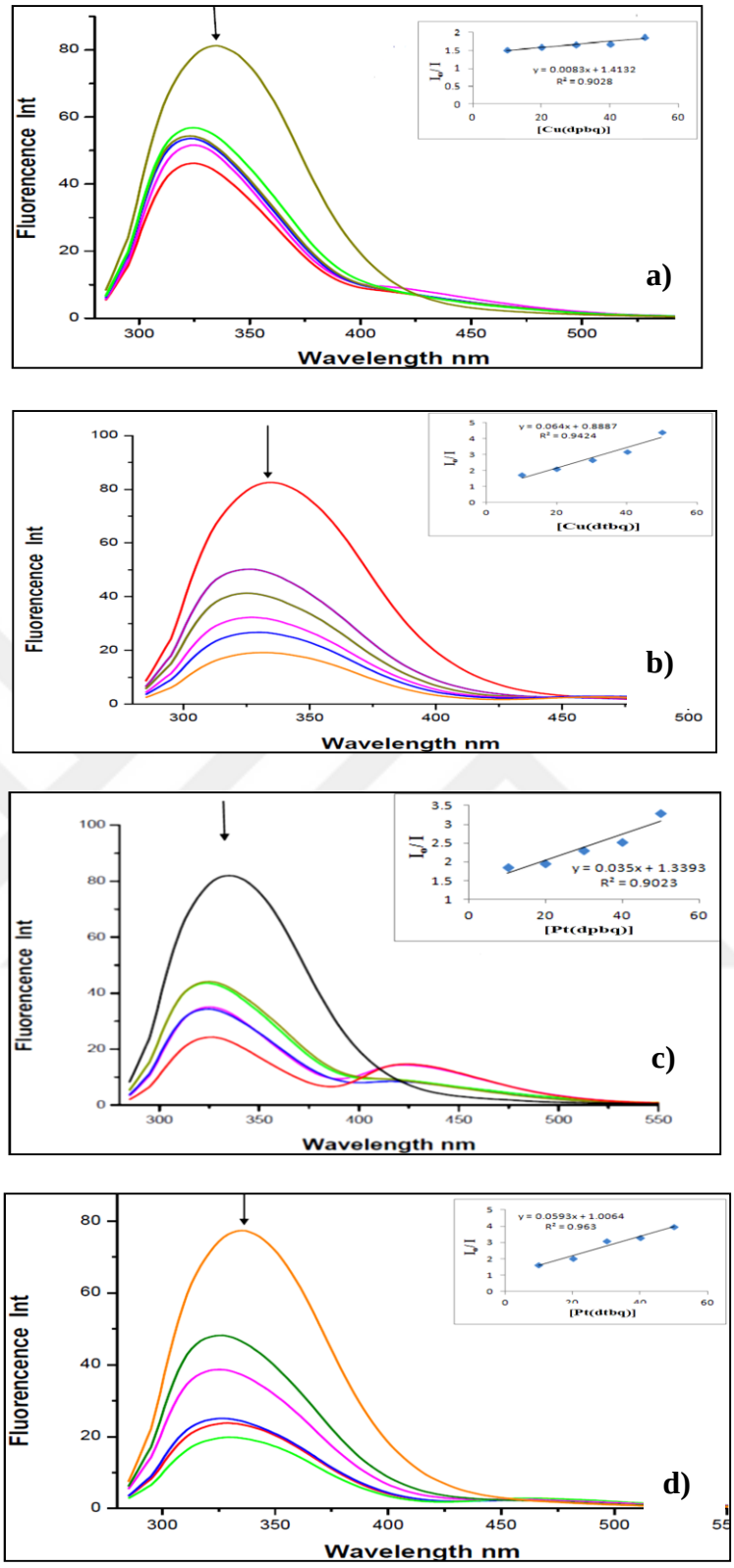

Figure 4.31 The change in the Fluorescence spectrum of a) $[Cu(tpbq)Cl_2]$, b) $[Cu(ttbq)Cl_2]$, c) $[Pt(tpbq)Cl_2]$, d) $[Pt(ttbq)Cl_2]$.

4.5 Cytotoxicity

4.5.1 Cell Viability

The cytotoxicity of $Cu(dpq)_2Cl_2$, $Cu(dtq)_2Cl_2$, $Pt(dpq)_2Cl_2$, $Pt(dtq)_2Cl_2$, $Cu(tpbq)Cl_2$, $Cu(ttbq)Cl_2$, $Pt(tpbq)Cl_2$ and $Pt(ttbq)Cl_2$ complexes was investigated by using MTT assay. For this purpose, the human cancer cell lines, glioblastoma (A172, LN229, U87), cervix (HeLa), breast (MDA- 231), lung (A-549), prostate (PC-3) and non-cancer Chinese hamster ovary CHO-K1 cell line as a control were used and the half-maximal inhibitory concentrations (IC_{50}) of our copper and platinum complexes were obtained from the plots for each compound for 24, 48, and 72 h exposure period was obtained from the dose-response curve. MTT assay was conducted by separating the complexes into two subgroups; (i) dpq and dtq containing Cu(II) and Pt(II) complexes and (ii) tpdq and ttbq containing Cu(II) and Pt(II) complexes.

Based on these calculations, the cytotoxic effect of the compounds in the first group was found to increase in the order of $Cu(dpq)_2Cl_2$ < $Pt(dpq)_2Cl_2$ < $Pt(dtq)_2Cl_2$ < $Cu(dtq)_2Cl_2$ in cancer cells compared to non-cancer CHO-K1 cell lines, as seen in Figure 4.32. It clearly indicated that dtq derivatives of the copper and platinum compounds have higher cytotoxicity compared to the dpq derivatives for the chosen cell lines (Table 4.11).

The cytototocity of the compounds in the second group, on the other hand, was changed in the order of $Cu(ttbq)Cl_2$ > $Pt(tpbq)Cl_2$ > $Pt(ttbq)Cl_2$ > $Cu(tpbq)Cl_2$ (Figure 4.33 and Table 4.12). Contrary to the first group complexes, no relationship was found between the cytotoxicy and the type of the ligands. In another words, ttbq derivative of the Cu(II) was more cytotoxic than that of the tpbq derivatives while the cytotoxicity of tpbq derivative of the Pt(II) was higher than that of its ttbq derivative.

In the both groups, dtq and its combined form, ttbq, containing Cu(II) chloride complexes were found to have the most anti-cancer potential among the examined complexes across the tested cell lines. The most sensitive cancer cells upon exposure to all complexes were found to be U87 and HeLa cell lines which were then, selected to use for the further assays. $Cu(ttbq)Cl_2$ also exerted high cytotoxic effect on

MDA231 cell line which was not sensitive to the other complexes studied in this work. These results indicated that our complexes selectively exerted their cytotoxicity towards glioblastoma, cervix and breast tumor cell lines.

The non-cancer control CHO-K1 cell line was less responsive one among the all examined cell lines as expected.

In the literature, it is possible to find many Cu(II) and Pt(II) complexes containing nitrogen and/or sulphur donor ligands showing cytotoxic effect towards several cell lines. For instance, symmetric and asymmetric the Cu(II) complexes with 2-(2′-pyridyl quinoxaline) (2,2′-pq) ligand were found more cytotoxic on human breast MCF-7 and human embryonic kidney HEK-293 cell lines than that of cis-platin used as a positive control [210]. Another Cu(II) complex with 3-(2-pyridyl)pyrazole-based ligand was shown to have a considerable inhibitory effect and cytotoxic specificity against six different cancer cell lines (HL-60 cells, PC-3M-1E8 human prostate tumor cells, BGC-832 cells, MDA cells, Bel-7402 human hepatoma cells and HeLa human cervix cancer cells) [211]. Similarly, platinum(II) terpyridine complexes were reported as strongly cytotoxic to the human cancer cell lines, HCT116 (colorectal), SW480 (colon), NCI-H460 (non-small cell lung), and SiHa (cervix). Their IC_{50} values were ranged from 0.05 to 4.4 μM [212]. Several platinum-based complexes containing various types of ligands revealing excellent anticancer activity against MCF-7, A549, and HCT-116 cell lines in comparison with clinically used cisplatin and oxaliplatin [213]. As a result, one can say that our Cu(ttbq)Cl_2 complex is almost twice as much as active against U87 human glioblastoma (Table 4.12) compared to cisplatin (IC_{50}: 5.88 μM). Likewise, Cu(tpbq)Cl_2 has slightly lower cytoxicity towards U87 than cisplatin and all our complexes were much more active to this cell line compared to carboplatin [214].

Table 4.11 IC_{50} values of the tested compounds examined by MTT cell viability assay using the cancer cell lines from different origins such as A172, LN229, U87 A549, Hela, MDA231, PC3 and the control non-cancer cell line CHO-K1 upon exposure for 24 hr, 48 hr and 72 hr.

Cell lines	Exposure hr	$Cu(dpq)_2Cl_2$	$Cu(dtq)_2Cl_2$	$Pt(dpq)_2Cl_2$	$Pt(dtq)_2Cl_2$
A172	24	> 100	66.66±0.38	> 100	67.82±27.11
	48	> 100	56.63±7.28	> 100	66.66±0.38
	72	> 100	34.97±1.27	> 100	83.69±4.00
LN229	24	> 100	> 100	> 100	92.84±5.25
	48	> 100	48.79± 5.78	> 100	71.16± 3.16
	72	> 100	36.79±10.83	> 100	93.98±4.72
U87	24	> 100	> 100	23.67±6.97	38.37±9.13
	48	> 100	73.11±5.43	78.31±28.26	19.17±5.78
	72	> 100	53.85±1.22	35.46±3.18	15.02±0.89
A549	24	> 100	71.92±5.61	> 100	> 100
	48	> 100	35.22±6.63	> 100	> 100
	72	> 100	39.32±4.01	> 100	> 100
HeLa	24	> 100	24.82±4.32	> 100	60.22±26.59
	48	> 100	24.19±0.83	> 100	72.78±22.62
	72	> 100	25.55±6.63	> 100	60.94±11.51
MDA231	24	> 100	57.67±1.13	> 100	83.36±0.98
	48	> 100	28.03±5.60	> 100	> 100
	72	> 100	24.19±7.51	> 100	> 100
PC3	24	> 100	> 100	> 100	78.78±057
	48	> 100	> 100	> 100	81.37±1.43
	72	> 100	> 100	> 100	> 100
CHO-K1	24	> 100	> 100	> 100	> 100
	48	> 100	> 100	> 100	> 100
	72	> 100	> 100	> 100	> 100

Table 4.12 IC_{50} values of the tested compounds examined by MTT cell viability assay using the cancer cell lines from different origins such as A172, LN229, U87 A549, Hela, MDA231, PC3 and the control non-cancer cell line CHO-K1 uponexposure for 24 hr, 48 hr and 72 hr

Cell lines	**Exposure hr**	**IC_{50} Values, µM**			
		Cu(tpbq)Cl_2	**Cu(ttbq)Cl_2**	**Pt(tpbq)Cl_2**	**Pt(ttbq)Cl_2**
A172	24	> 100	69.44±0.19	94.29±12.27	93.50±18.37
	48	> 100	63.88±3.56	39.38±15.82	65.52±17.73
	72	92.04±7.46	57.41±13.68	73.67±0.28	49.47±5.73
LN229	24	> 100	42.04±13.99	> 100	67.86±16.32
	48	> 100	36.00±6.38	91.89±049	44.78±11.61
	72	> 100	54.01±3.1	83.85±3.16	38.76±1.46
U87	24	79.46±26.38	31.18±0.43	58.35±11.81	> 100
	48	5.49±0.01	2.95±0.97	34.68±2.16	9.24±4.16
	72	13.53±6.06	5.75±0.03	22.09> 10016.24	5.95±1.68
A549	24	> 100	73.55±1.35	> 100	95.02±2.93
	48	> 100	70.68±4.09	58.44±5.35	> 100
	72	> 100	66.90±8.70	40.26±3.42	> 100
HeLa	24	> 100	67.52±2.78	> 100	88.85±8.31
	48	> 100	74.22±0.45	57.97±26.86	79.69±24.21
	72	> 100	64.99±2.75	42.86±1.69	> 100
MDA231	24	72.14±26.04	20.59±2.39	94.81±2.57	85.00±10.81
	48	> 100	32.11±1.05	> 100	> 100
	72	> 100	40.95±0.60	99.37±5.71	> 100
PC3	24	> 100	65.75±5.35	> 100	> 100
	48	> 100	75.50±3.16	> 100	> 100
	72	> 100	62.31±4.02	> 100	> 100
CHO-K1	24	> 100	> 100	> 100	> 100
	48	> 100	> 100	86.63±1.98	> 100
	72	> 100	> 100	77.52±0.87	> 100

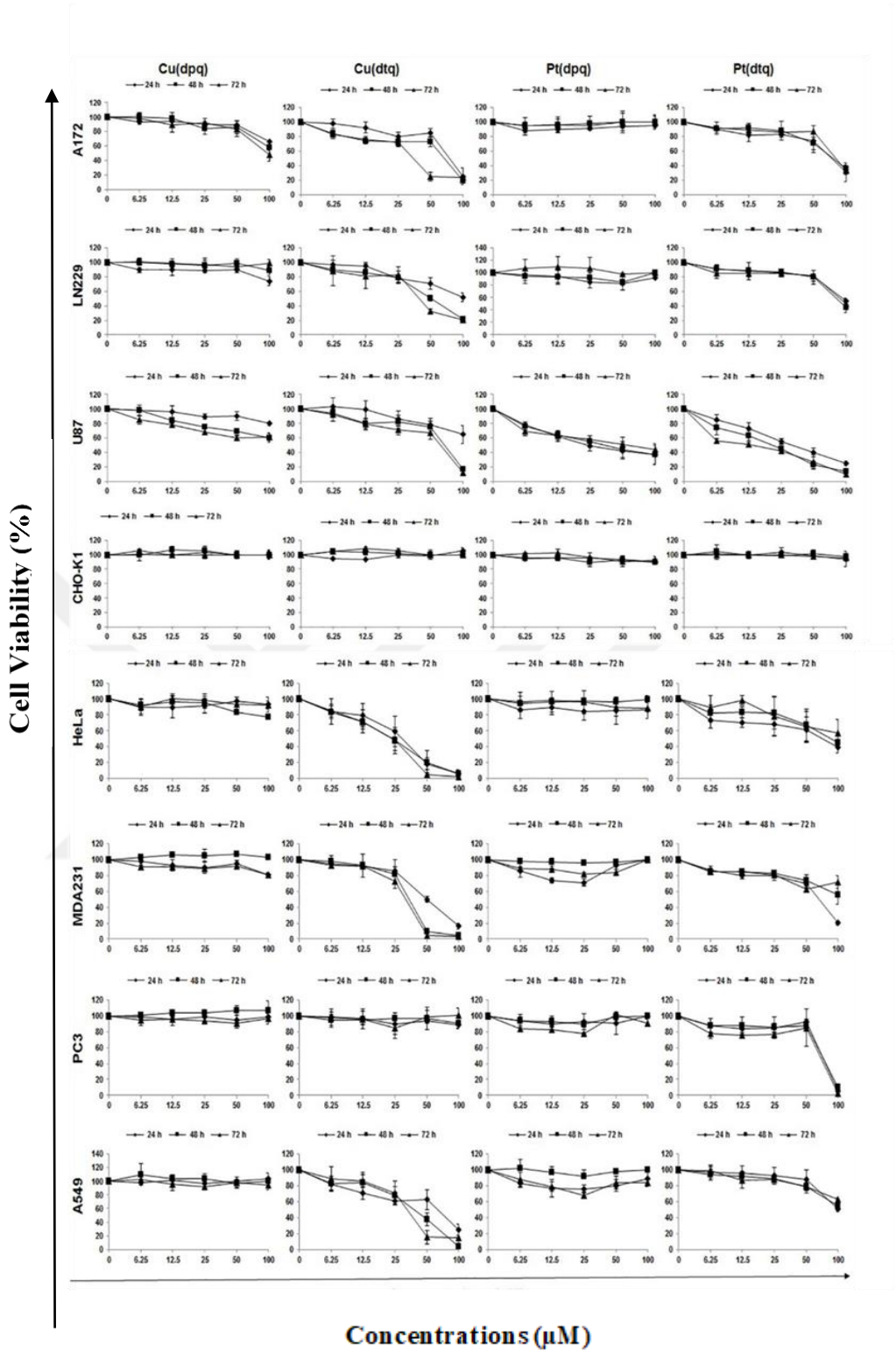

Figure 4.32 The dose-response curves for the synthetized Cu and Pt complexes using cell lines from different origins (A172, LN229, U87, A549, HeLa, MDA-MB-231, PC3, CHO-K1) were obtained upon exposure for 24 h, 48 h, and 72 h by MTT cell viability assay.

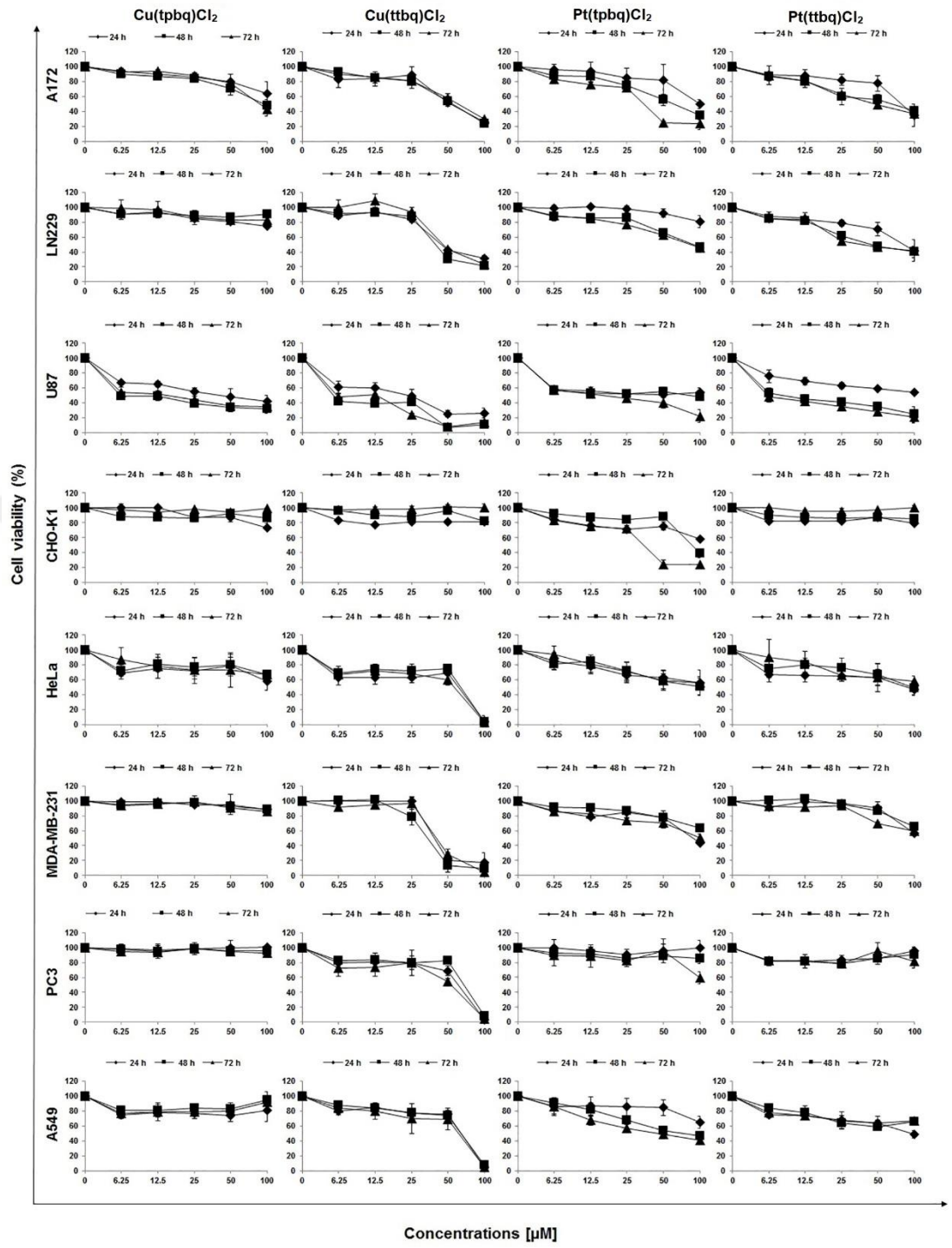

Figure 4.33 The dose-response curves for the synthetized Cu and Pt complexes using cell lines from different origins (A172, LN229, U87, A549, HeLa, MDA-MB-231, PC3, CHO-K1) were obtained upon exposure for 24 h, 48 h, and 72 h by MTT cell viability assay.

4.5.2 Oxidative stress testing (DCFDA assay) (ROS Production – DCFDA Assay)

Cancer cells exhibit various differences in cellular biological activities, including the level of reactive oxygen species (ROS), which is involved in redox balance, cellular proliferation, and cancer progression. Cellular oxidative stress is generally demonstrated by using the fluorescent marker H(2)DCF-DA (dihydrodichlorofluorescein diacetate) [215], which is then de-esterified and oxidized to fluorescent DCF (2',7'-dichlorofluorescein) in plasma. The oxidation process observed in this process is generally considered to involve ROS. Hence, it is an indirect method to measure total ROS generation [216]. In this method, in order to determine DCFDA activity that increases in response to H_2O_2 treatment (positive control), the determined DCFDA signal for a particular condition is referenced to the corresponding proliferation counts. In our work, A172, LN229, U87, A549, HeLa, MDA-231, and PC-3 cell lines were used for ROS experiments. The doses used in cell viability assays were administered for 24 h for ROS formation, which was measured in a fluorescence spectrophotometer using DCFDA. The results are shown in Figures 4.34 and 4.35.

We detected substantial initiation of ROS production in cells in response to our $Cu(dpq)_2Cl_2$, $Cu(dtq)_2Cl_2$, $Pt(dpq)_2Cl_2$, and $Pt(dtq)_2Cl_2$ complexes. Interestingly, compounds generated different amounts of ROS in different cells compared to the negative control, including growth medium DMEM_F12. For instance, neither platinum nor copper compounds produced an ROS response in PC3 cells. However, $Pt(dtq)_2Cl_2$ significantly increased ROS production in human glioblastoma A172, LN229, U87, cervix HeLa, and breast MD-A231 cells. $Cu(dpq)_2Cl_2$ did not induce any ROS formation on the examined cell lines, whereas $Cu(dtq)_2Cl_2$ caused approximately fourfold ROS formation on only A172 cells and approximately twofold increase in human lung A549 cells with respect to the negative control. $Pt(dpq)_2Cl_2$ increased the amount of ROS in human glioblastoma U87 and breast MDA231 cells approximately by twofold.

The level of ROS generation in the cells compared to the negative control including growth medium in response to $Cu(tpbq)Cl_2$, $Cu(ttbq)Cl_2$, $Pt(tpbq)Cl_2$, and $Pt(ttbq)Cl_2$

complexes (Figure 4.35) indicated that tetrathenyl derivatives (ttbq) of Cu(II) and Pt(II) complexes produced more ROS than the terapyridyl counterparts (tpbq) of the Cu(II) and Pt(II) complexes. Generally, Cu(ttbq)Cl_2 caused the highest level of ROS formation, which was followed by Pt(ttbq)Cl_2 and Cu(tpbq)Cl_2 in the used cell lines. Cu(ttbq)Cl_2 and Pt(ttbq)Cl_2 increased the ROS production by 3 to 5.5 folds in human glioblastoma (A172, LN229, U87) and induced almost 2 folds ROS production in the lung A549, cervix HeLa, and breast MD-A231 cells. Pt(tpbq)Cl_2 did not display any ROS formation in these cell lines.

Careful inspection of the results indicated that ROS formation significantly enhanced almost in all cell line tested when they treated with Cu(II) or Pt(II)-ttbq complexes. At this stage, it has to be remembered that ttbq is the combined form of two dtp units. For instance, Cu(ttbq)Cl_2 and Pt(ttbq)Cl_2 led approximately 5.5 and 5 fold ROS formation in A172 cells, while Cu(dtq)$_2Cl_2$ and Pt(dtq)$_2Cl_2$ yielded 3.5 and 3 fold ROS in the same cell line, respectively. Similarly, Cu(ttbq)Cl_2 rised ROS formation from 2 fold to about 5 fold in human lung A549 cells compared to its dtq counterpart, Cu(dtq)$_2Cl_2$, with respect to the negative control. It was also observed that ROS generation increased nearly four times upon exposure of Cu(ttbq)Cl_2 and Pt(ttbq)Cl_2 in human glioblastoma LN 229 cell line. Moreover, Cu(tpbq)Cl_2 triggered three times better ROS formation in human glioblastoma U87 while Cu(ttbq)Cl_2 and Pt(ttbq)Cl_2 led 4 times higher ROS generation in the same cell line. ROS formation was also better in cervix HeLa cell lines in the presence of Cu(ttbq)Cl_2 and Pt(ttbq)Cl_2 with respect to that could only be observed in the presence of Pt(dtq)$_2Cl_2$. Remarkably, prostate PC3 cells were unresponsive to all our complexes with respect to ROS generation. As depicted in Figure 4.34 and 4.35, H_2O_2 was tested as a positive control and caused 3 fold ROS generation only at high (500 μM) concentration. As a result, it can be said that the complexes caused oxidative stress in tested cells lines and increased the amount of ROS in the cells, causing disruption of mitochondrial membrane polarization and death of cells via apoptosis because of oxidative damage on DNA double strand [217].

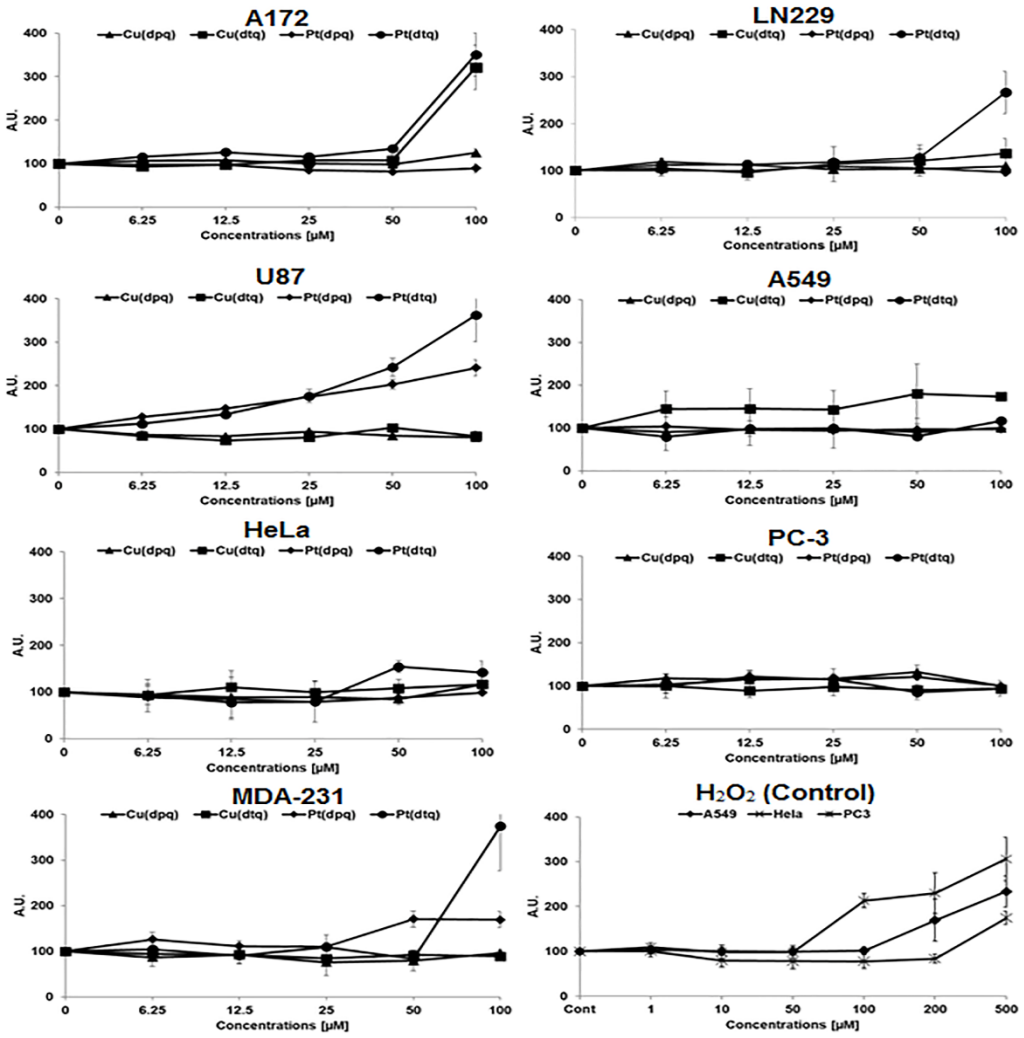

Figure 4.34 The ROS production of the cancer cell lines from different origins such as A172, LN229, U87, A549, HeLa, MDA-231, PC-3, and the control non-cancer cell line CHO-K1 upon exposure to the tested copper and platinum compounds for 24 h was measured by the DCFDA assay. For positive control, H_2O_2 was used at indicated doses.

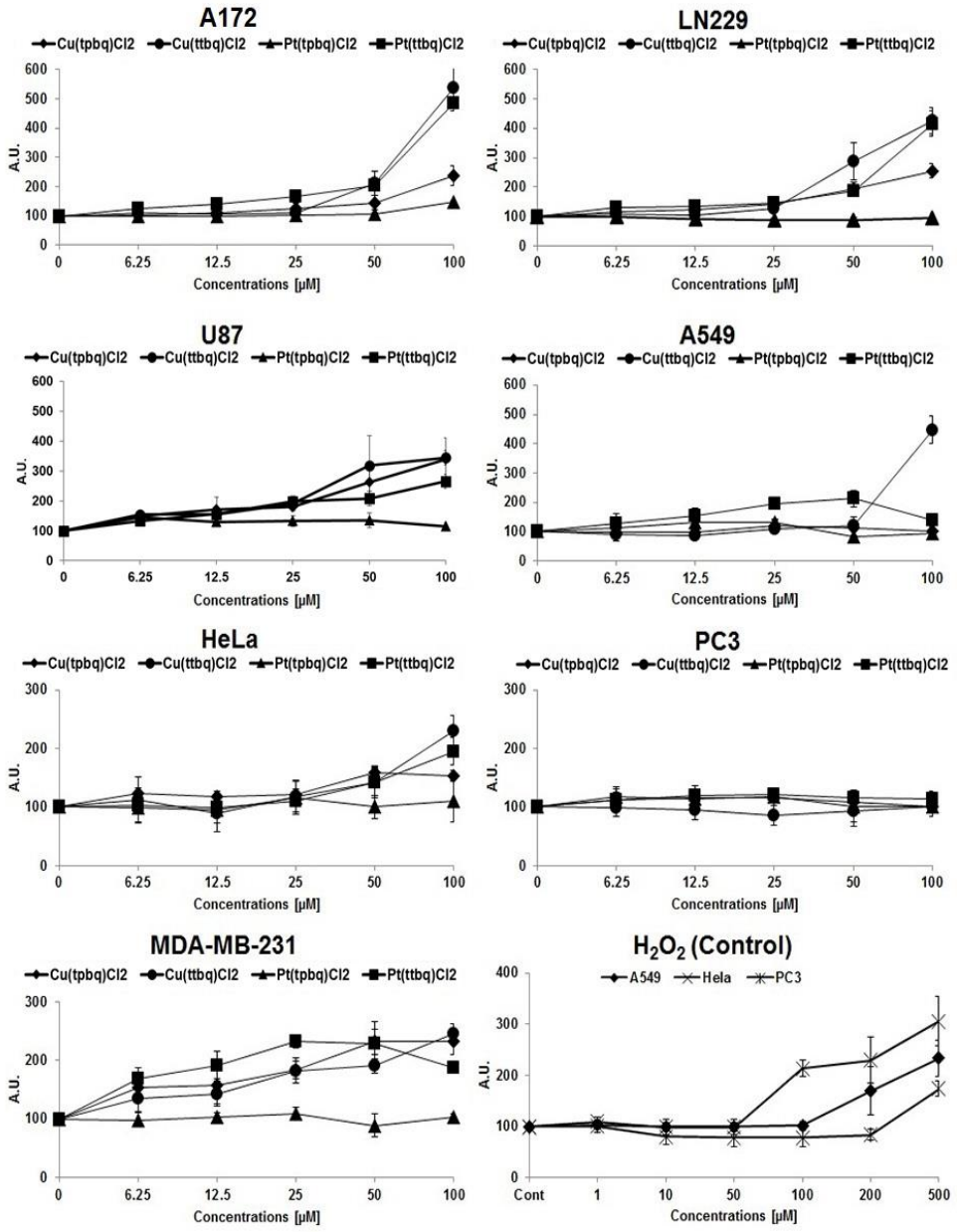

Figure 4.35 The ROS generation of the used cell lines from different origins (A172, LN229, U87 A549, HeLa, PC3, and MDA231) upon exposure to the tested Cu and Pt complexes for 24 h was determined by the DCFDA assay. H_2O_2 was used as a positive control at the indicated doses.

4.5.3 Apoptosis - TUNEL assay

There two known main cell death patterns: necrosis and apoptosis. Apoptosis is a cellular suicide process triggered by specific proteins. However, toxins or insufficient blood supply may lead to necrosis [218]. In order to investigate the cell death pathway of our copper and platinum quinoxaline chloride complexes, we completed the terminal deoxynucleotidyl transferase dUTP nick end staining (TUNEL). TUNEL assay designed to detect apoptotic cells that undergo extensive DNA fragmentation during the late stages of apoptosis resulting from the activation of endonucleases and the DNA fragmentation patterns of the U87 and HeLa cells were analyzed after 24 h exposure to the copper and platinum compounds (Figure 4.36). A significant difference in the cellular DNA degradation potency of $Cu(dtq)_2Cl_2$ was observed compared to that of the other copper and platinum complexes tested here at the concentrations of 50 and 100 μM according to the different DNA fragmentations as seen in Figure 4.36.

$Cu(dtq)_2Cl_2$ caused DNA fragmentation to a greater extent than in the negative control in both concentrations. Indeed, $Cu(dtq)_2Cl_2$ induced higher DNA fragmentation at higher concentration (100 μM) with respect to one obtained at low concentration (50 μM), and insignificant differences were observed in the DNA degradation potency of $Cu(dtq)_2Cl_2$ in both used cell lines, U87 and HeLa. Since U87 and HeLa cells were found to be sensitive to the TUNEL assay upon exposure to $Cu(dtq)_2Cl_2$, inducing the apoptotic cell death, $Cu(dtq)_2Cl_2$ might be a good anticancer drug candidate.

The DNA fragmentations were too low for the $Cu(dpq)_2Cl_2$, $Pt(dpq)_2Cl_2$, and $Pt(dtq)_2Cl_2$ complexes; hence, their results were not contained in Figure 4.36.

Figure 4.37 depicts the apoptotic potential of the U87 cells after $Cu(ttbq)Cl_2$ and $Pt(tpbq)Cl_2$ treatments at 50 μM and 100 μM concentrations. On the other hand, apoptosis on HeLa cells was only observed upon exposure of the $Pt(ttbq)Cl_2$ at the selected concentrations. $Cu(tpbq)Cl_2$ and $Pt(ttbq)Cl_2$ on the U87 cells, and $Cu(ttbq)Cl_2$, $Cu(tpbq)Cl_2$, $Pt(tpbq)Cl_2$ on the HeLa cells were not induced any apoptosis upon 24 h treatment (data were not presented here) under the same experimental conditions.

Relatively higher DNA fragmentations were detected in HeLa and U87 cell lines after the treatment of the 100 μM concentrations of our active complexes compared to one obtained after 50 μM complex accumulation. These results were similar to those were reported as potential anti-cancer agents in the available literature for some platinum(II) complexes containing pyrazole ligands that were induced cell cycle arrest and apoptosis in breast cancer MCF-7 and MDA-MB-231 cells [219].

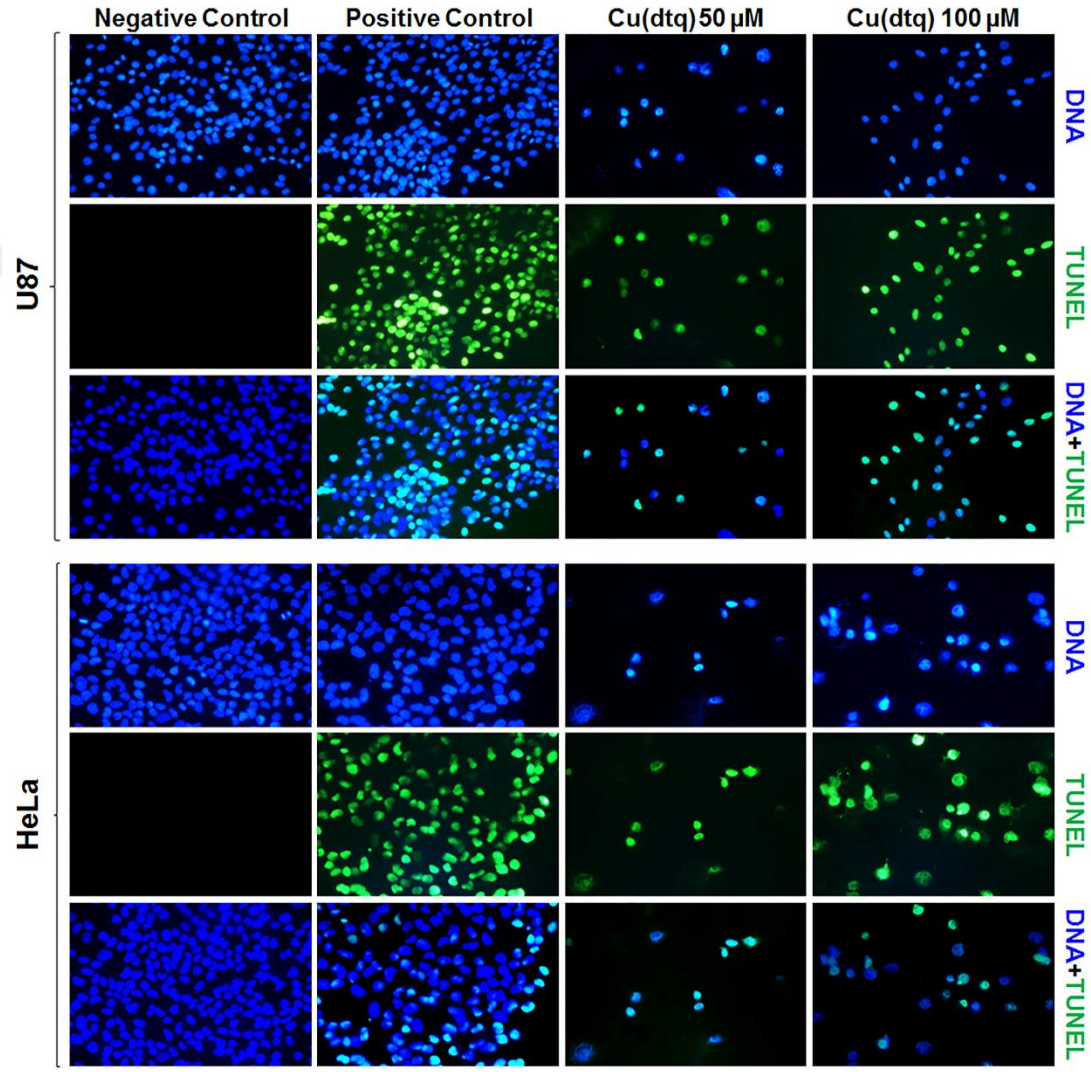

Figure 4.36 Apoptosis – DNA fragmentation on U87 and HeLa cells treated at the concentrations of 50 and 100 μM [$Cu(dtq)_2Cl_2$] for 24 h – was evaluated by using terminal deoxynucleotidyl transferase dUTP nick end labeling assay (TUNEL). Negative control was treated only with growth medium and the positive control was treated with Dnase. The pictures of the DNA fragmentation were taken with 40X magnification using a fluorescence microscope.

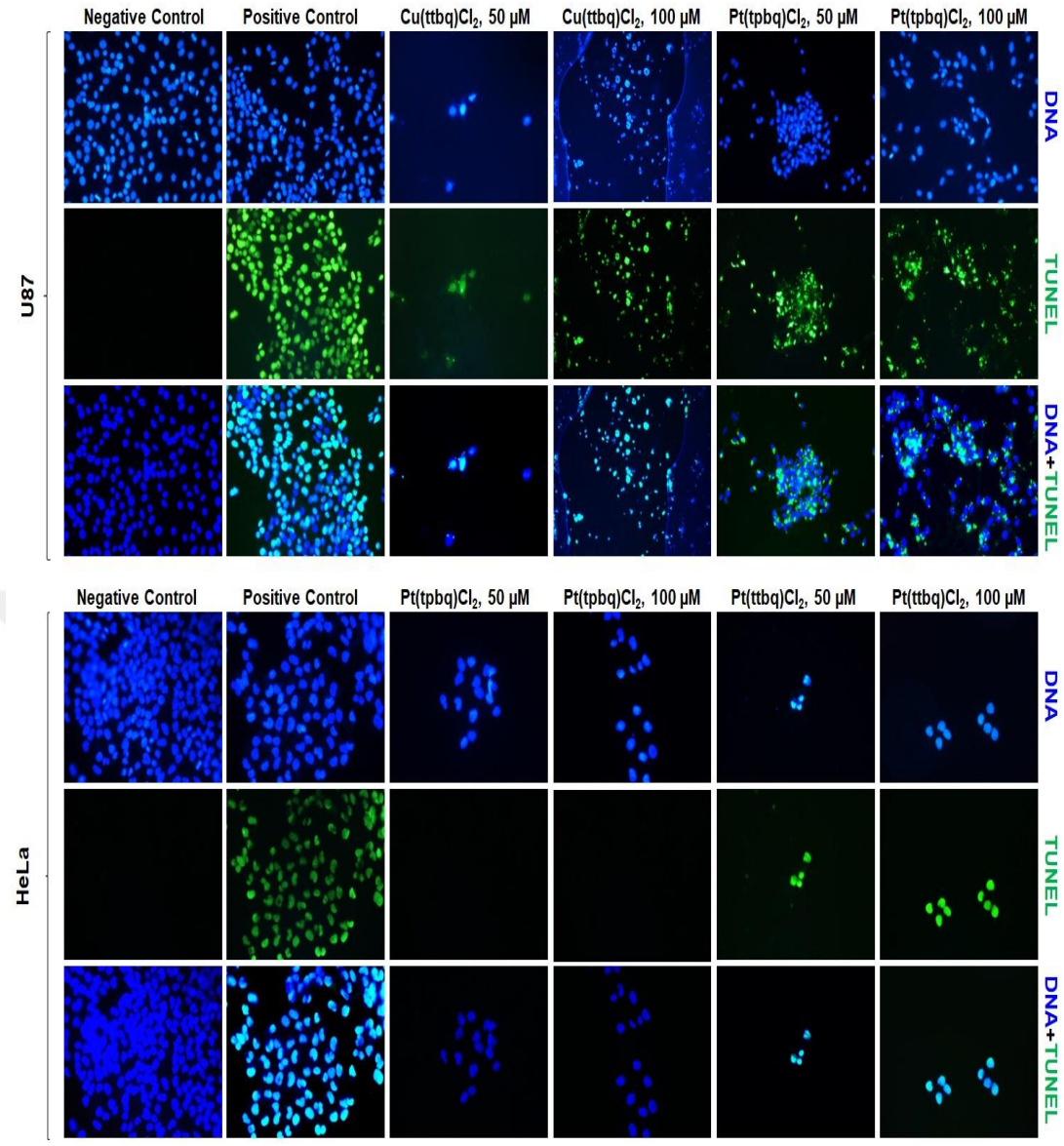

Figure 4.37 Apototic potency of the U87 and HeLa cells treated with Cu and Pt complexes at concentrations of 50 and 100 µM for 24 hr evaluated by applying TUNEL assay. Negative control was treated with only growth medium and positive control was treated with Dnase. Images were taken with 40X magnification using fluorescence microscope.

4.5.4 In vitro cell invasion and migration assays

Since the main cause of death in cancer patients is related to metastatic progression, cell migration studies are important in cancer research. For cancer to spread throughout the body, cancer cells must migrate and invade through the extracellular matrix (ECM)

and enter the bloodstream, attach to a distant site, and spread out of the vessel. Tumor metastasis is one of the biggest obstacles in anticancer treatment [220, 221]. The first step in tumor metastasis is the migration and the invasion of tumor cells. Various biological methods can be used to study cell migration in detail. Among them, in vitro cell invasion assay is a widely used method of providing an assessment of cell invasive capacity in vitro, where the Corning® Matrigel® matrix acts as an in-vitro membrane that prevents non-invasive cells from migrating. However, invading cells (malignant and non-malignant) enzymatically degrade the Corning Matrigel matrix and spread through the membrane pores. The behavior of cells can be examined under a microscope [222] (Figure 4.38). Matrigel Invasion Analysis was accomplished in the presence of our most effective complexes, $Cu(dtq)_2Cl_2$ and $Pt(dtq)_2Cl_2$ in the first group and $Cu(ttbq)Cl_2$, $Pt(tpbq)Cl_2$ and $Pt(ttbq)Cl_2$ in the second group.

In this study, the invasion potency of U87 and HeLa cell lines across the Matrigel after 24 h treatment of 6.25 and 12.5 μM $Cu(dtq)_2Cl_2$ or $Pt(dtq)_2Cl_2$ was investigated firstly, as shown in Figure 4.38. Both compounds at the tested concentrations negatively regulated the invasion potential of the HeLa cell line as compared with the negative control, whereas the treatment of $Cu(dtq)_2Cl_2$ resulted in a higher potency to prevent the invasion of HeLa cells with respect to the $Pt(dtq)_2Cl_2$ treatment, as seen in Figure 4.38. There were no differences between the anti-invasive effects on the HeLa cells upon exposure to both tested concentrations of the copper and platinum compounds. According to these results, one can say that $Cu(dtq)_2Cl_2$ has more anticancer potential than the $Pt(dtq)_2Cl_2$ under selected conditions. The inhibitory effects of $Cu(dtq)_2Cl_2$ and $Pt(dtq)_2Cl_2$ compounds at the same concentrations on the U87 cell invasion was also examined, and no difference observed between the tested compounds and control treatments on U87.

The invasion potency of U87 and HeLa cell lines across the Matrigel after 24 h treatment of 6.25 and 12.5 μM $Cu(ttbq)Cl_2$, $Pt(tpbq)Cl_2$ and $Pt(ttbq)Cl_2$ was also explored and shown in Figure 4.39. Careful assessment of the results indicated that $Cu(ttbq)Cl_2$ and $Pt(tpbq)Cl_2$ complexes have high anti-invasive effects on the HeLa

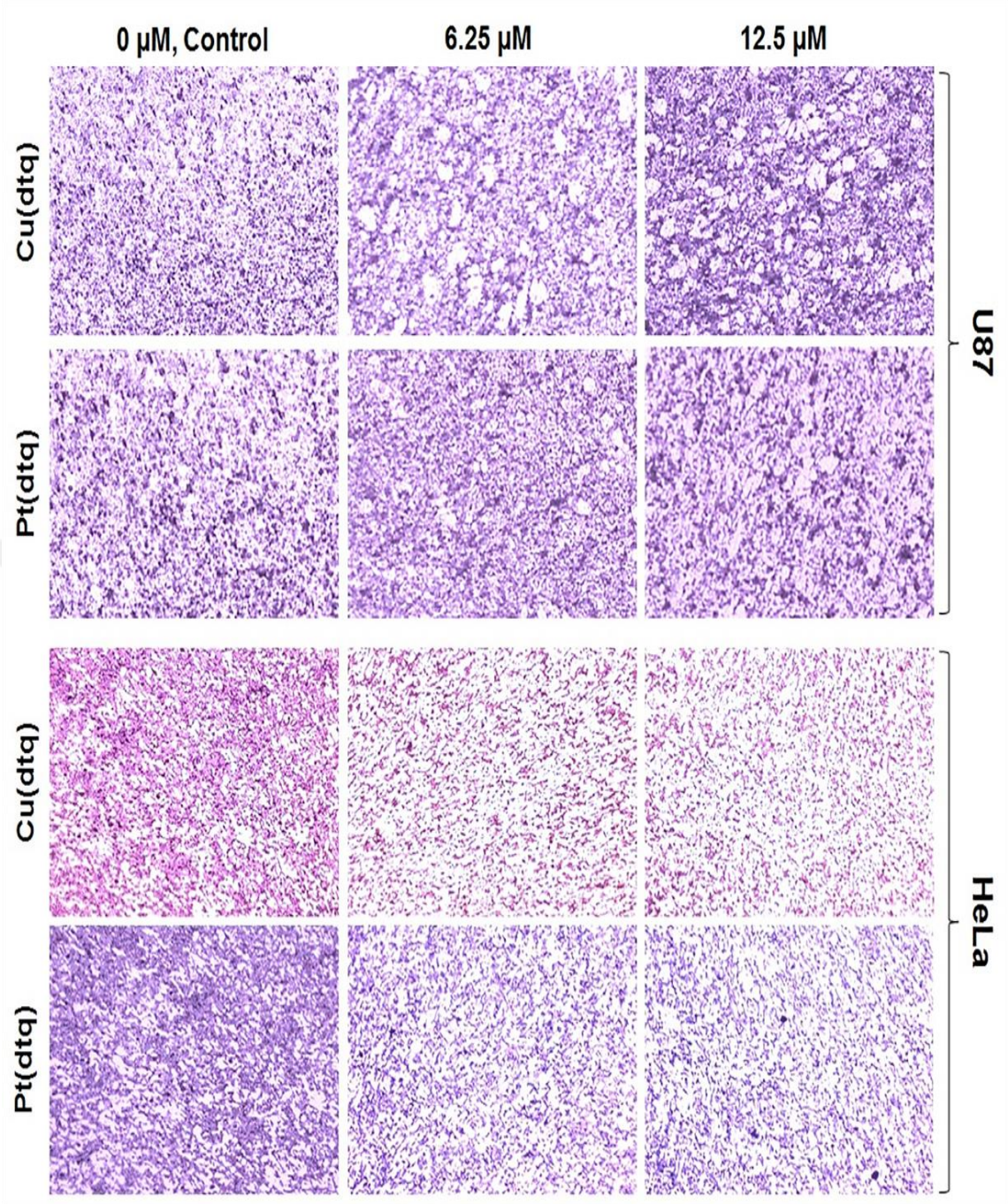

Figure 4.38 In vitro U87 and HeLa cell invasion toward the Matrigel after 24 h treatment with $[Cu(dtq)_2Cl_2]$ or $[Pt(dtq)_2Cl_2]$ at concentrations of 6.25 and 12.5 µM. Both compounds at the tested concentrations negatively regulated the invasion potential of the HeLa cell line as compared with the negative control, whereas the treatment of $[Cu(dtq)_2Cl_2]$ resulted in higher potency to prevent the invasion of HeLa cells than did $[Pt(dtq)_2Cl_2]$ treatment, as seen in the image. There was no difference between the treatments of $[Cu(dtq)_2Cl_2]$/$[Pt(dtq)_2Cl_2]$ and the control in U87 cell invasion shown in the image.

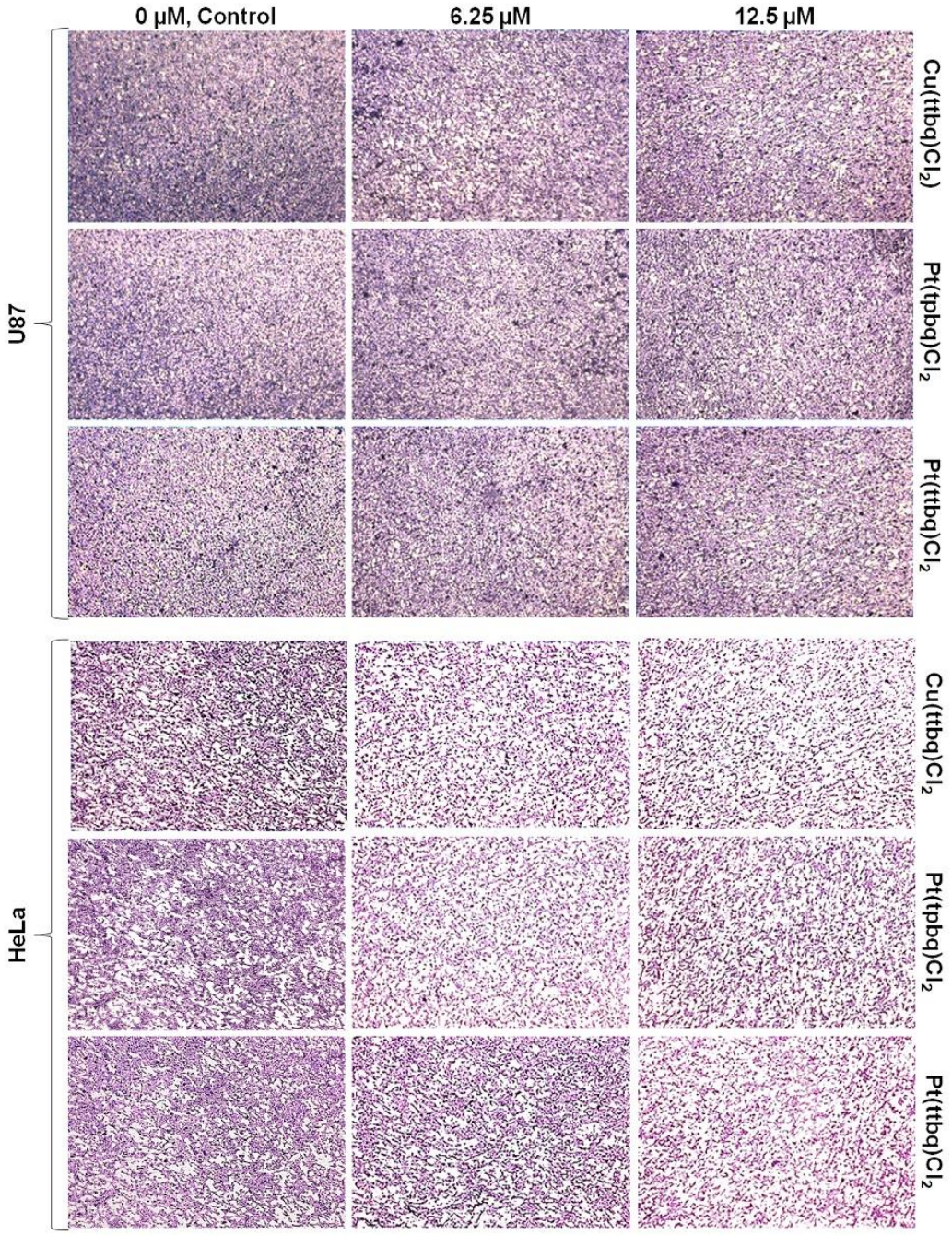

Figure 4.39 The anti-invasive effects of [Cu(ttbq)Cl_2], [Pt(tpbq)Cl_2], and [Pt(ttbq)Cl_2] at concentrations of 6.25 and 12.5 µM on U87 and HeLa cells across the matrigel during 24 h treatment was determined by matrigel invasion assay as compared with the negative control. The images were taken with 40x magnification.

cell monolayer at both concentrations with respect to the negative control. Indeed, no significant difference was observed between the anti-invasive capacity of $Cu(ttbq)Cl_2$ and $Pt(tpbq)Cl_2$ complexes on the HeLa cells in relation with the concentrations, except $Pt(dtbq)Cl_2$ which was only effective at 12.5 μM.

Unfortunately, $Cu(ttbq)Cl_2$, $Pt(tpbq)Cl_2$ and $Pt(ttbq)Cl_2$ did not demonstrate anti-invasive effect on U87 cells at concentrations of 6.25 and 12.5 μM. In the second group $Cu(tpbq)Cl_2$ did not have any anti-invasive effect on both cell lines and hence, data were not presented here. Interestingly, some studies in the literature also reported that the copper compounds inhibited the invasion abilities of HeLa cells, whereas there was no significant difference found in the U87 cell line [223].

The cell culture scratch wound-healing assay is widely used for screening the novel anticancer compounds. It can provide the necessary data that may allow for an understanding of how well a particular cell type can spontaneously migrate or respond to a chemo-attractant and directionally migrate toward it. Because the invasion potential of the HeLa cell line was unregulated by the tested compounds, this cell line was chosen to use for the cell migration assay. The potential inhibitory effects of platinum and copper compounds on the migration of HeLa are presented in Figures 4.40 and 4.41.

As a result of the cell migration assay, the migration capacity of HeLa cells decreased in the treatment of $Cu(dtq)_2Cl_2$, $Pt(dtq)_2Cl_2$, $Cu(ttbq)Cl_2$, $Pt(ttbq)Cl_2$, and $Pt(tpbq)Cl_2$ at concentrations of 6.25 and 12.5 μM during 24 h, 48 h and 72 h compared to the control including growth medium. The number of HeLa cells migrating toward the scratch zone on treatment with $Cu(dtq)_2Cl_2$ diminished with increasing concentrations. On the other hand, this decrease in the migration was found to be independent from concentration of $Pt(dtq)_2Cl_2$, $Cu(ttbq)Cl_2$, $Pt(ttbq)Cl_2$, and $Pt(tpbq)Cl_2$, as demonstrated in Figures 4.40 and 4.41.

As a summary, the examined Cu(II) and Pt(II) complexes had an anti-migration potential on the HeLa cell line. Henceforth, they could be anti-cancer drug candidates for further investigation.

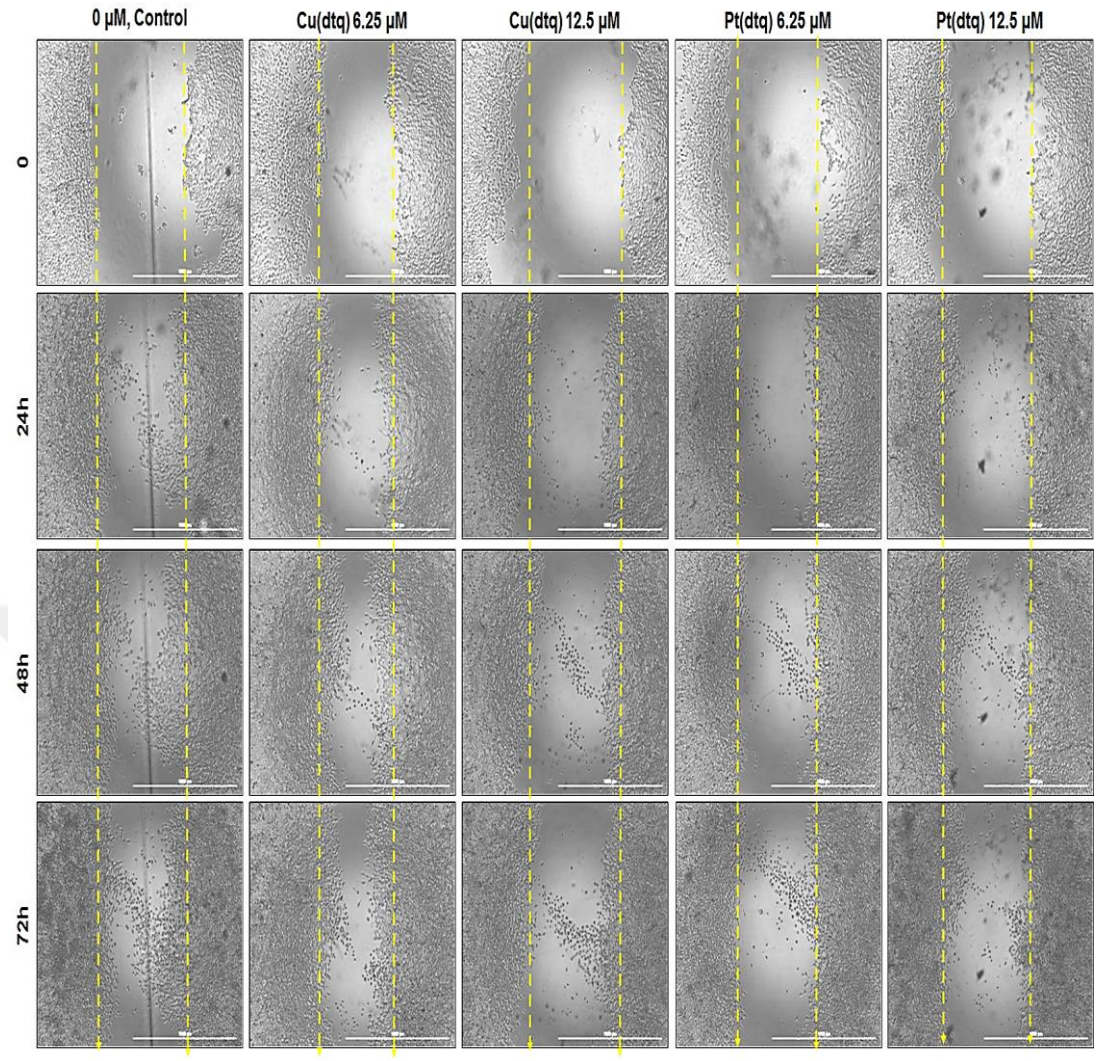

Figure 4.40 In vitro cell migration assay using cervical cancer HeLa cell line after 24 h treatment with $[Cu(dtq)_2Cl_2]$ or $[Pt(dtq)_2Cl_2]$ at concentrations of 6.25 and 12.5 μM. $[Cu(dtq)_2Cl_2]$ had an increasing anti-migration potential with increasing concentrations, but the same increased potential was not observed on $[Pt(dtq)_2Cl_2]$ treatment. Images were acquired at 0, 24, 48, and 72 h in wound healing assay.

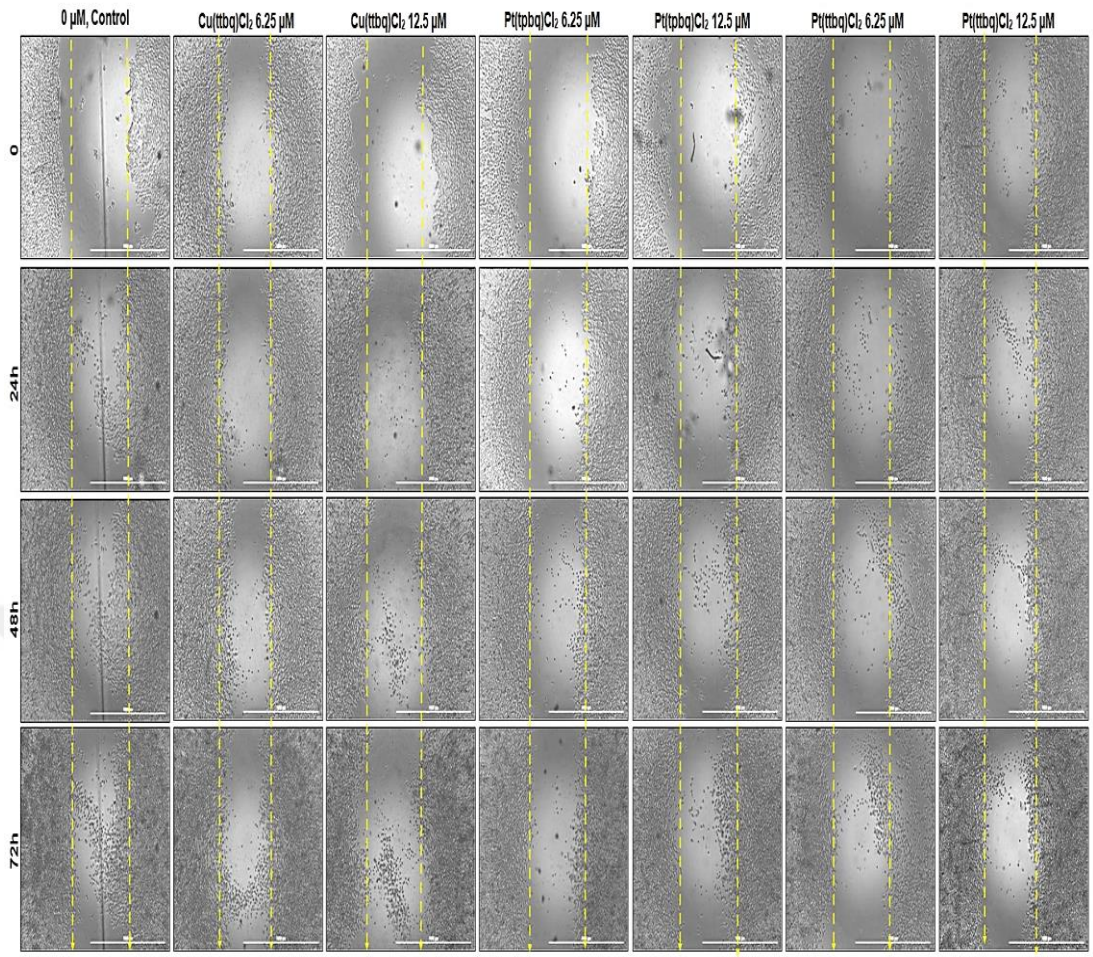

Figure 4.41 In vitro cell migration assay using human cervix HeLa cell line after 24 h treatment with [Cu(ttbq)Cl_2], [Pt(tpbq)Cl_2], and [Pt(ttbq)Cl_2] at concentrations of 6.25 and 12.5 μM. Images were acquired at 0, 24 h, 48 h, and 72 h with inverted microscope.

4.6 Genotoxicity

4.6.1 In-vitro comet assay

To assess DNA damage analysis, a crucial confounding factor in defining the genotoxic potential of the synthetized complexes was investigated by means of a comet assay which precisely detected the DNA damage and reflected the genotoxic potential [224]. The effective anti-cancer potential of 25 and 50 μM $Cu(dtq)_2Cl_2$, $Pt(dtq)_2Cl_2$, $Cu(ttbq)Cl_2$, $Pt(ttbq)Cl_2$, and $Pt(tpbq)Cl_2$ complexes was determined on the HeLa and U87 cell lines using in vitro comet assay.

Among these complexes $Cu(dtq)_2Cl_2$ $Pt(dtq)_2Cl_2$ and $Pt(tpbq)Cl_2$ were found to be non-genotoxic on both cell lines. $Cu(ttbq)Cl_2$ and $Pt(ttbq)Cl_2$ caused DNA damage on the U87 cells at both concentrations. The genotoxicity of $Cu(ttbq)Cl_2$ and $Pt(ttbq)Cl_2$ enhanced as the concentration of the complexes increased. On the other hand, $Cu(ttbq)Cl_2$ was detected as only genotoxic compound on the Hela cells but at high concentration (50 μM) (Figure 4.42). Briefly, $Cu(ttbq)Cl_2$ showed more genotoxic potential than the other synthesized complexes by inducing more DNA fragmentation on HeLa and U87 cell lines.

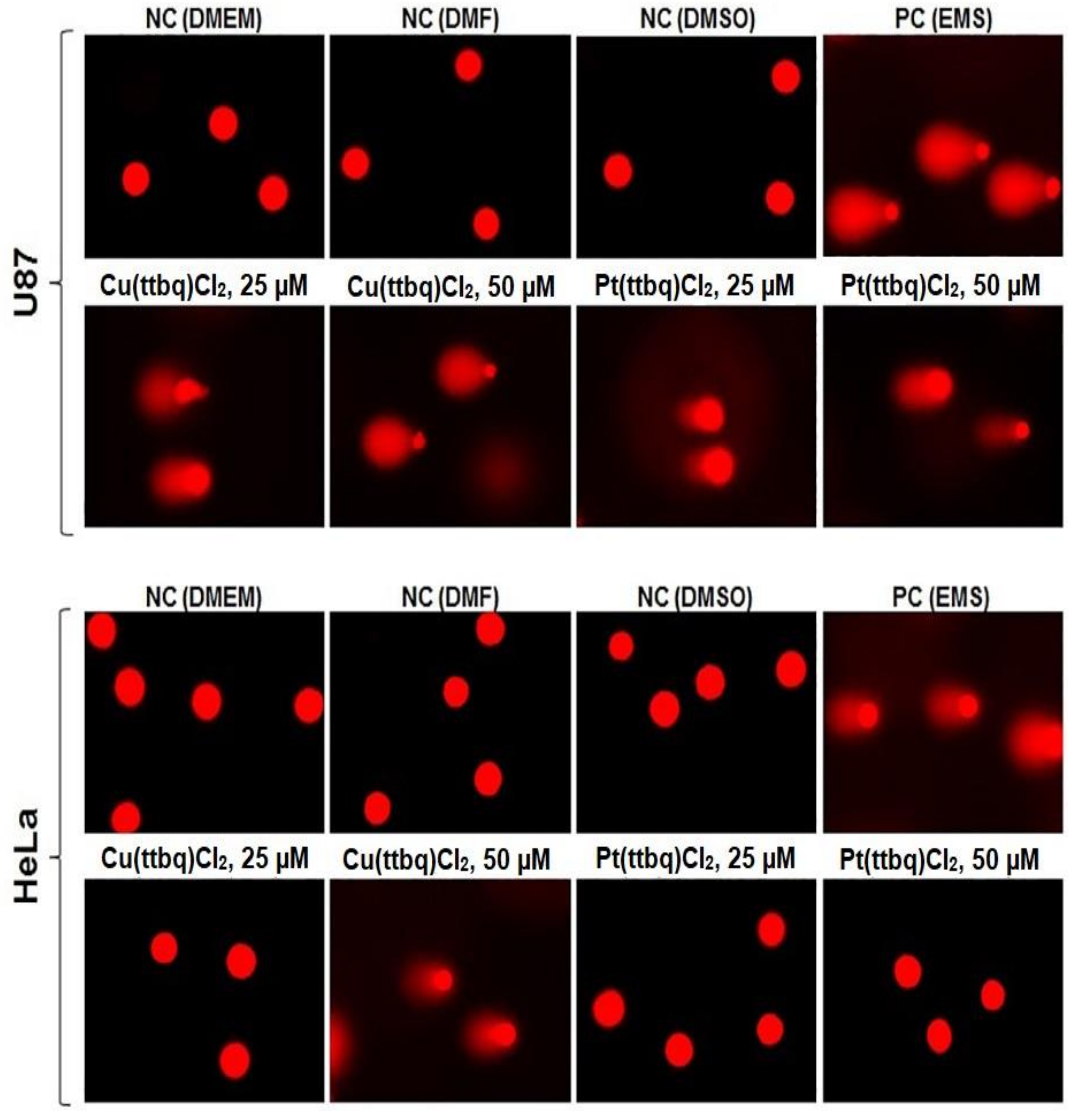

Figure 4.42 Single-cell gel electrophoresis of U87 and HeLa cell lines following treatment with synthetized Cu and Pt complexes for 24 h. Negative control: Growth Medium, Positive control: Ethyl methanesulfonate (EMS) treated cells. Representative microscopic images of cells were taken at magnification 40x with fluorescence microscope.

4.6.2 Plasmid DNA interaction assay

The potentials of the $Cu(dpq)_2Cl_2$, $Cu(dtq)_2Cl_2$, $Pt(dpq)_2Cl_2$ and $Pt(dtq)_2Cl_2$ compounds at 50 and 100 µM concentrations were examined by agarose gel electrophoresis using pBR322 plasmid DNA as shown in the Figure 4.43. The relative fast migration is observed for the supercoiled form (SC), when circular DNA is subjected to gel electrophoresis. In case of scission occurs on one strand (nicked circular), the supercoiled form will relax to generate a slower moving open circular form (NC). A linear form of the DNA that migrates between the two forms when both strands are cleaved.

The plasmid DNA was cleaved by the $Cu(dtq)_2Cl_2$ at the tested concentrations upon 24 hr incubation as compared with the negative control. The other tested compounds did not show any cleavage potentials under these conditions.

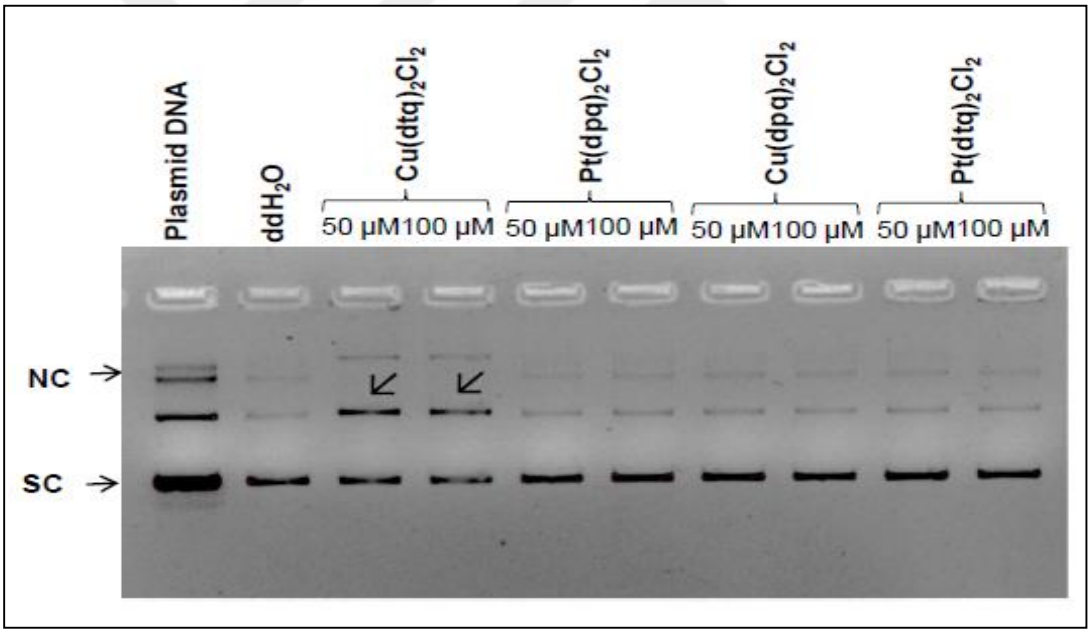

Figure 4.43 Plasmid DNA interaction assay with pBI-CMV1 plasmid (3.1 kb) grown in E-coli and then purified using a Machery Nagel DNA isolation kit. The plasmid DNA incorporation after treatments with 50 and 100 µM concentrations of the cupper and platinum compouds were analyzed and the images of the bands were captured using a ChemiDoc imaging system (BioRad). The testing was done in two repeats. SC: Supercoiled; NC: Nicked circular.

DNA cleavage activities of the $Cu(tpbq)Cl_2$, $Cu(ttbq)Cl_2$, $Pt(tpbq)Cl_2$ and $Pt(ttbq)Cl_2$ complexes at concentrations of 100 and 200 μM were evaluated by observing their ability of converting the plasmid DNA in the supercoiled form to the its open circular form and the linear form in gel electrophoresis (Figure 4.44). The pure plasmid DNA mainly composes of supercoiled (SC) and nicked circular (NC) forms. It mainly led to a decrease in the intensity of nicked circular (NC) bands, possibly due to accumulation of too many nicks leading to DNA degradation composed of mainly supercoiled (SC). $Pt(tpbq)Cl_2$ and $Pt(ttbq)Cl_2$ treatment caused plasmid DNA double strand degradation, which was detected in increased intensity of NC bands and linear form. On the other hand, $Cu(tpbq)Cl_2$ and $Cu(ttbq)Cl_2$ complexes did not cause any plasmid DNA cleavage in the agarose gel.

Although the synthesized $Cu(tpbq)Cl_2$ and $Cu(ttbq)Cl_2$ complexes did not form any strand cleavage on plasmid DNA in this study, the previous studies showed that copper complexes may act via different mechanisms, such as ROS generation, which leads oxidative cell damage and consequently triggers cancer cell death through an apoptotic mechanism [225]. Indeed, $Cu(tpbq)Cl_2$ and $Cu(ttbq)Cl_2$ complexes caused increased level of ROS generation in our study. Although pyridyl quinoxaline containing $Cu(dpq)_2Cl_2$ and $Cu(tpbq)Cl_2$ complexes did not perform DNA strand cleavage, a report in literature showed that the Cu(II)-2-(2′-pyridyl) quinoxaline complexes caused DNA cleavage and were found more cytotoxic on human breast MCF-7 and human embryonic kidney HEK-293 cell lines than that of cis-platin used as a positive control [210]. Similarly, another study on platinum(II)-quinoxaline compounds revealed that they interacted with calf-thymus DNA and demonstrate high level of cytotoxic effects on L1210 murine leukaemia cell line [226].

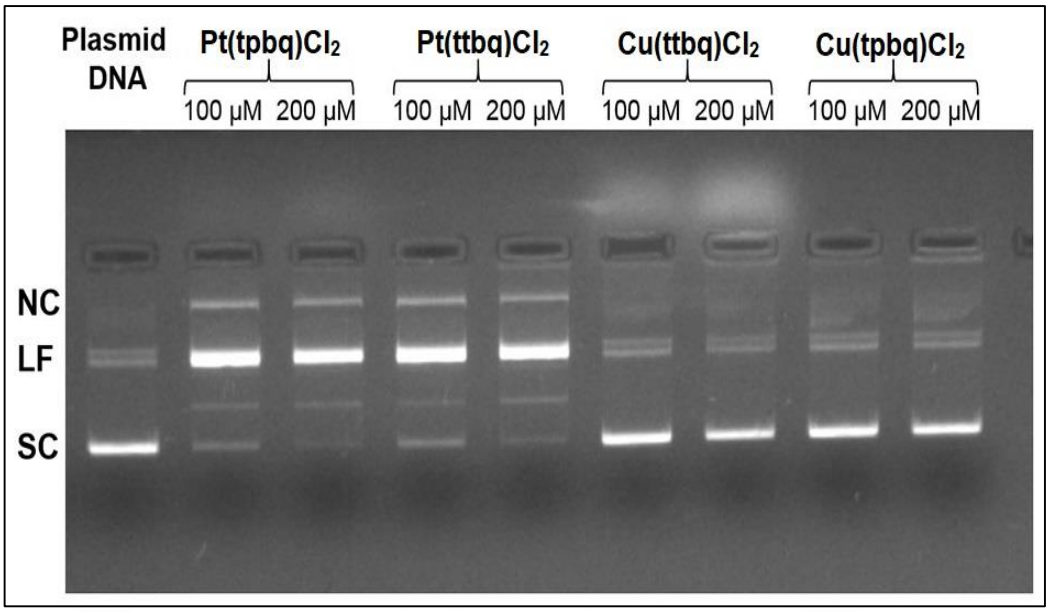

Figure 4.44 Plasmid DNA interaction assay with pBI-CMV1 plasmid (3.1 kb) grown in E-coli and then purified using a Machery Nagel DNA isolation kit. The plasmid DNA incorporation after treatments with 100 and 200 µM concentrations of the Cu and Pt compounds were analyzed and the images of the bands were captured using a ChemiDoc imaging system (BioRad). The testing was done in two repeats. SC: Supercoiled; NC:Nicked circular; LF: Linear form.

CHAPTER 5

5 CONCLUSION

In this study, $Cu(dpq)_2Cl_2$, $Cu(dtq)_2Cl_2$, $Pt(dpq)_2Cl_2$, $Pt(dtq)_2Cl_2$ $Cu(tpbq)Cl_2$, $Cu(ttbq)Cl_2$, $Pt(tpbq)Cl_2$, and $Pt(ttbq)Cl_2$, compounds were synthesised and the characterized, assessed using ultraviolet–visible, mass, ^{1}H-NMR, FTIR, and raman spectroscopy.

The molecular structure of the dedicated complexes was determined theoretically. Calculations at the B3LYP/LANL2DZ level of theory showed that $Cu(dpq)_2Cl_2$ and $Pt(dpq)_2Cl_2$ structures deviate from planarity, while dtq derivatives have perfectly planar geometry. Similarly, $[Cu(tpbq)Cl_2]$ and $[Pt(tpbq)Cl_2]$ displayed a deviation from the square planar structure around the metal center. This deviation became significant for $[Cu(tpbq)Cl_2]$ but slight for $[Pt(tpbq)Cl_2]$. The optimized geometry calculations for $[Cu(ttbq)Cl_2]$ and $[Pt(ttbq)Cl_2]$, on the other hand, exhibited a coordination between the metal center and a H-atom on the quinoxaline as well as a nitrogen atom coordination of the same unit. The interaction of the metal ions with the H-atom led a deviation of from the planarity, which was also proved by the high N1-Cl4-N2-Cl3 dihedral of 59.8° and 59.5° for $[Cu(ttbq)Cl_2]$ and $[Pt(ttbq)Cl_2]$, repectively.

DNA binding potentials of our complexes were determined using spectroscopic methods as well as viscosity measurements. The hyperchromic effect that was observed during the UV titration experiments with the moderate intrinsic binding constant about 10^3 indicate an electrostatic interaction between the complexes and CT-DNA.

In order to assess the nature of the interaction between our complexes and CT - DNA thermodynamic data were taken in account. The standard ΔG^o values were calculated

in terms of temperatures dependent K_b constants obtained from UV titration at various temperatures (310. 320, 330 and 340 K). In this respect, the negative values related to ΔG^o showed spontaneous interaction process, while the positive ΔH^o and positive ΔS^o values indicated mainly entropy driven interaction of our complexes by confirming an electrostatic mode of action.

The viscometric measurement of complex-DNA adducts yielded insignificant changes in the relative viscosity compared to those obtained for DNA alone by the electrostatic interactions of our complexes according to UV titrations experiments.

Thermal denaturation studies showed only small changes in melting temperature of CT-DNA upon addition of the complexes by underlining the electrostatic interactions occuring between the complexes and DNA.

The fluorescence emission intensity of the ethidium bromide-bound DNA decreased gradually as the platinum and copper compounds added in increasing amount. The observed quenching suggested a potential intercalation of the aromatic groups present in our complexes by exchanging EtBr within the DNA-base pairs or electrostatic interactions of our complexes through the grooves of DNA by obscuring the EtBr-binding sites.

The UV titration tests conducted with HSA showed the hydrophobic surface interactions between our complexes and the albumin clearly.

According to the thermodynamic data, the obtained negative values for ΔG^o showed us that the processes taken place between the compounds and HSA were spontaneous in aqueous solution; whereas the positive values for ΔS^o and ΔH^o showed that the binding were mainly entropy driven.

As to the melting temperature of HSA, T_m decreased very slightly with the addition of the Cu(II) and Pt(II) compounds. Decreasing the melting temperature of HSA reaffirmed that the protein structure became destabilized in the presence of our complexes.

The viscometric measurements on HSA were also confirmed the interactions of our complexes with the biomolecule through hydrophobic regions showing minor increases in relative viscosity values.

The fluorescence titration experiments, which were carried out with the HSA solutions in the presence of the complexes, indicated that the maximum emission wavelength did not shift or change significantly. These results clearly showed that the complexes were likely to interact with the albumin via the hydrophobic region located inside the protein and producing non-fluorescent adducts.

Cytotoxicity of the complexes indicated that $Cu(dtq)_2Cl_2$, $Pt(dtq)_2Cl_2$, $Cu(ttbq)Cl_2$ and $Pt(tpbq)Cl_2$ were the most effective complexes, and U87 and HeLa cell lines were determined to be the most effected cell lines by exposure of all the compounds. DNA damage was generated by compounds dependent on ROS formation, and the cell death pattern was identified as apoptosis for U87 and HeLa cell lines upon addition of $Cu(dtq)_2Cl_2$, $Cu(ttbq)Cl_2$, $Pt(tpbq)Cl_2$, and $Pt(ttbq)Cl_2$.

The $Cu(dtq)_2Cl_2$, $Cu(ttbq)Cl_2$, $Pt(tpbq)Cl_2$, and $Pt(ttbq)Cl_2$ complexes demonstrated higher potency to prevent the invasion and migration of HeLa cells. Thus, in accordance with our findings, $Cu(dtq)_2Cl_2$, $Cu(ttbq)Cl_2$, $Pt(tpbq)Cl_2$, and $Pt(ttbq)Cl_2$ have a higher potential to be an anticancer drugs candidate and deserves further detailed studies.

6 REFERENCES

[1] R. Mahesh, V. Perumal, V. Pandy, "Cancer chemotherapy- induced nausea and vomiting: role of mediators, development of drugs and treatment methods". *Pharmazie*, vol 60(2). pp 83–96, Mar. 2005.

[2] I. Kostova, "Platinum Complexes as Anticancer Agents". *Recent Patents on Anti-Cancer Drug Discovery*, vol. 1 (1). pp. 1-22, Jan. 2006.

[3] M. J. McKeage, S. J. Berners-Price, P. Galettis, R. J. Bowen, W. Brouwer. L. Ding, L. Zhuang, and B. Baguley, "Role of lipophilicity in determining cellula uptake and antitumour activity of gold phosphine complexes" *Cancer Chemother Pharmacol*, vol. 46(5), pp. 343–350, Feb. 2000.

[4] A. Pizarro, and P. Sadler, "Unusual DNA binding modes for metal anticancer complexes". *Biochimie*, vol. 91(10), pp. 1198–1211, Oct. 2009.

[5] X. Yao, K. Panichpisal, N. Kurtzman, and K. Nugent, "Cisplatin nephrotoxicity: review". *The American Journal of the Medical Sciences*, vol. 334(2), pp. 115–124, Aug. 2007.

[6] T. Hambley, "Platinum binding to DNA: structural controls and consequences". *Journal of the Chemical Society Dalton Transactions*, vol. 19(19), pp. 2711–2718, Oct. 2001.

[7] M. Devereux, D. O'Shea, M. O'Connor, H. Grehan, G. Connor, M. McCann, G, Rosair, F. Lyng, A. Kellett, M. Walsh,D. Egan , and B. Thati, "Synthesis, catalase, superoxide dismutase and antitumour activities of copper(II) carboxylate complexes incorporating benzimidazole, 1,10-phenanthroline and bipyridine ligands: X-ray crystal structures of $[Cu(BZA)_2(bipy)(H_2O)]$, $[Cu(SalH)_2(BZDH)_2]$ and $[Cu(CH_3COO)_2(5,6\text{-DMBZDH})_2]$ ($SalH_2$ = salicylic acid; BZAH = benzoic acid; BZDH = benzimidazole and 5,6-DMBZDH = 5,6-dimethylbenzimidazole)". *Polyhedron*, vol. 26(15), pp. 4073- 4083, Sept. 2007.

[8] M. Devereux, M. McCann, D. Shea, R. Kelly, D. Egan, C. Deegan, V. McKee, G. Finn, "Synthesis, antimicrobial activity and chemotherapeutic potential of inorganic derivatives of 2-(40 -thiazolyl)benzimidazole{thiabendazole}: X-ray crystal structures

of [Cu(TBZH)2Cl]Cl .H2O . EtOH and TBZH2NO3 (TBZH ¼ thiabendazole)". *J. Inorg. Biochem*, vol. 98(6), pp.1023- 1031, Jun. 2004.

[9] I. Gracia-Mora, L. Ruiz-Ramirez, C. Gomez-Ruiz, M. Tinoco- Mendez, A. Marquez-Quinones, L. R. Lira, A. Marin- Hernandez, L. Masias-Rosales, M. E. Bravo-Gomez, "Knigth's Move in the Periodic Table, From Copper to Platinum, Novel Antitumor Mixed Chelate Copper Compounds, Casiopeinas, evaluated by an in Vitro Human and Murine Cancer Cell Line Panel". *Met. Based Drugs*, vol. 8(1), pp. 19-28, Feb. 2001.

[10] I. Warad, A. Eftaiha, A. L. Al-Nuri. Husein, M. Assal, A. Abu-Obaid, N. Al-Zaqri, T. Hadda, B. Hammouti, "Metal ions as Antitumor Complexes-Review". *J. Mater. Environ. Sci*, vol. 4(4), pp. 542-557, Jan. 2013.

[11] A. R. Nchakravarty, P.A. Reddy, B. Santr, and A. M. Thomas, "Copper complexes as chemical nucleases". *Proc. Indian Acad. Sci. (Chem. Sci.),* vol. 114(4), pp. 391–401, Aug. 2002.

[12] A. E. Porter, A. R. Katritzky, and C.W. Rees, *Comprehensive heterocyclic chemistry*. Pergamon, Oxford, 1984.

[13] D.A. Horton, G.T. Bourne, M. L. Smythe, "The combinatorial synthesis of bicyclic privileged structures or privileged substructures". *Chem Rev,* vol. 103(3), pp. 893–930, Feb. 2003.

[14] D. Sherman, J. Kawakami, Y. H. H, A. Majhi, "Synthesis of unsymmetrical and region defined 2,3,6-quinoxaline and 2,3,7-pyridopyrazine derivatives". *Tetrahedron Letters*, vol. 48(51), pp. 8943–8946, Nov. 2007.

[15] A. K. Patidar, M. Jeyakandan, A. K. Mobiya, G. Selvam, "Exploring potential of quinoxaline moiety". *Int J Pharm Tech Res*, vol. 3(1), pp.386–392. 2011.

[16] C. Justin Dhanaraj, and J. Johnson, "Metal Complexes of Quinoxaline Derivatives: Review (Part-I)". *Research Journal of Chemical Sciences*, vol. 4(11), pp. 80-102, Nov. 2014.

[17] C. Justin Dhanaraj, and J. Johnson, "Metal Complexes of Quinoxaline Derivatives: Review (Part-II)". *Research Journal of Chemical Sciences*, vol. 5(4), pp. 64-84, Apr. 2015.

[18] S. Alavi1, M. H. Mosslemin, R. Mohebat, A. R Massah, "Green synthesis of novel quinoxaline sulfonamides with antibacterial activity". *Springer Science Business. Res Chem Intermed*, vol. 43(8), 4549–4559, Aug. 2017.

[19] V. A. Mamedov, N. A. Zhukova, "Progress in Quinoxaline Synthesis (Part 2)". *Progress in Heterocyclic Chemistry*, 1st ed., vol. 25, G. W. Gribble, J. A. Joule Ed, UK: British Library, 2013, PP. 1-45.

[20] Y. Kim, J. Park, and S. Kim, "Synthesis and biologiactivity of new quinoxaline antibiotics of echinomycin analogues". *Bioorg Med Chem Lett*, vol. 14(2), pp. 541-544, Jan. 2004.

[21] D. Chang, S. Ko, J. Kim, L. Dai, and J. Baek, "Multifunctional quinoxaline containing small molecules with multiple electron-donating moieties: Solvatochromic and optoelectronic properties". *J Synthetic Metals*, vol.162, pp. 1169-1176. Aug. 2012.

[22] R. A Weinberg, *The Biology and Cancer*. New York, W.W. Norton & Company, 2007.

[23] M. Hejmadi, (2010), *Introduction to cancer biology*, (2nd edition), [Online], Available: bookboon.com.

[24] Nptel – Chemistry – Bio-Organic Chemistry of Natural Enediyne Anticancer Antibiotics.II (Syllabus Template). Course Title: Bio-Organic Chemistry of Natural Enediyne Anticancer Antibiotics. Module 4.

[25] C. Orvig, M.J. Abrams, "Medicinal inorganic chemistry: introduction". *Chemical Reviews*, vol .99(9), pp.2201-2203. Sep. 1999.

[26] L. Galluzzi, O. Kepp, I. Martins, J. Michels, I. Vitale, L. Senovilla, M. Castedo, G. Kroemer Molecular mechanisms of cisplatin resistance. *oncogene*, vol. 31, pp. 1869-1883, 2012.

[27] G.B. Kauffman, R. Pentimalli, S. Doldi, M. Hall, "Michele Peyrone (1813-1883), Discoverer of Cisplatin". *Platinum Metals Review*, vol. 54(4), pp.250-256, Oct. 2010.

[28] H. Berke, "Old and New 'Anschauungen in der Anorganischen Chemie'. Ahomage to Alfred Werner's book and intuition: Part I. Alfred Werner's book and coordination theory". *Chimia International Journal for Chemistry*, vol. 63(9), pp. 541–544, Sep. 2009.

[29] L.R. Kelland, N.P. Farrell. *Platinum Based Drugs in Cancer Therapy.* Humana Press: Totowa, NJ, USA, 2000.

[30] C.S. Allardyce, A. Dorcier. C. Scolaro, P.J. Dyson, "Development of organometallic (organo-transition metal) pharmaceuticals". *Appl. Organometal. Chem*, vol. 19, pp. 1–10, Jan. 2005.

[31] E. Wexselblatt, E. Yavin, D. Gibson, "Cellular interactions of platinum drugs". *Inorg. Chim. Acta*, vol.393, pp.75–83, Dec. 2012.

[32] B.W. Harper, A.M. Krause-Heuer, M.P. Grant, M. Manohar, K.B. Garbutcheon-Singh, J.R. Aldrich-Wright, "Advances in Platinum Chemotherapeutics". *Chem. Eur. J*, vol. 16(24), pp. 7064–7077, Jun. 2010.

[33] A. Sigel, H. Sigel, *Metal Ions in Biological Systems: Metal Complexes in Tumor Diagnosis and as Anticancer Agents*, CRC Press: London, UK, 2004.

[34] A. M. Florea, D. Büsselberg. "Cisplatin as an Anti-Tumor Drug: Cellular Mechanisms of Activity, Drug Resistance and Induced Side Effects". *Cancers*. vol. 3(1), pp.1351–1371, Mar. 2011.

[35] S. Acharya, et al, "Synthesis, characterization, X-ray structure and spectroscopic study of platinum (II) complexes with tridentate diazene ligands having O, N, S donor set". *Inorganica Chimica Acta*, vol. 394, pp.757-764, Jan. 2013.

[36] C. Makedonas, C.A. Mitsopoulou. "An Investigation of the Reactivity of [(diimine)(dithiolato)M] Complexes Using the Fukui Functions Concept". *Eur J. Inorg. Chem*, vol. 3, pp.590-598, Feb. 2006.

[37] A. Pasini, G.D. Alfons, C. Manzotti, M. Moret, S. Spinelli, M. Valsecchi, "cytotoxic Diamine-Platinum(II) Complexes with Methylsulfinyl Carboxylates as the Leaving Groups. Synthesis, Characterization, and Reactivity toward Chloride Ions, 5'-GMP, and 9-Methylguanine". *Inorg. Chem*, vol. 33(18), pp. 4140- 4148, Aug. 1994.

[38] G. Faraglia, S. Sitran, D. Montagner, "Pyrrolidine dithiocarbamates of Pd(II)". *Inorg. Chim. Acta*, vol. 358(4), pp. 971-980, Mar. 2005.

[39] C. Metcalfe, J. A. Thomas, "Kinetically inert transition metal complexes that reversibly bind to DNA", *Chem. Soc. Rev*, vol.32(4), pp.215–224, Jul. 2003.

[40] E. Gao, M. Zhu, H. Yin, L. Liu, Q. Wu, Y. Sun, "Synthesis, characterization, interaction with DNA and cytotoxicity in vitro of dinuclear Pd(II) and Pt(II) complexes dibridged by 2,20-azanediyldibenzoic acid". *J. Inorg. Biochem*, vol.102(10), pp. 1958-1964, Oct. 2008.

[41] C. Monneret, "Platinum anticancer drugs. From serendipity to rational design". *Ann Pharm* Fr, vol. 69(6), Pp.286–295, Nov. 2011.

[42] A. Surrah, M. Kettunen, "Platinum Group Antitumor Chemistry: Design and development of New Anticancer Drugs Complementary to Cisplatin". *Curr. Med. Chem*, vol. 13(11), pp.1337-1357, May.2006.

[43] J. Reedijk, "Improved understanding in platinum antitumour chemistry". *Chem. Commun*, vol.7, pp. 801-806, 1996.
[44] L. Kelland, "New platinum antitumor complexes". *Crit. Rev. Oncol. Hematol*, vol. 15(3), pp.191-219, Dec.1993.

[45] B. Evans, K. Raju, A. Calvert, S. Harland, E. Wiltshaw, "Phase II study of JM8, a new platinum analog, in advanced ovarian carcinoma". *Cancer Treat. Rev*, vol. 67(11), pp 997- 1000, Nov. 1983.

[46] K. Harrap, "Preclinical studies identifying carboplatin as a viable cisplatin alternative". *Cancer Treat. Rev*, vol.12, pp.21-33, Sep.1985.

[47] O. Rixe, W. Ortuzar, M. Alvarez, "Oxaliplatin, Tetraplatin, Cisplatin, and Carboplatin: Spectrum of Activity in Drug-Resistant Cell Lines and in the Cell Lines of the National Cancer Institute's Anticancer Drug Screen Panel". *Biochem. Pharmacol*, vol. 52(12), pp. 1855-1865, Dec.1996.

[48] T. Tashiro, Y. Kawada, Y. Sakurai, "Antitumor activity of a new platinum complex, oxalato (trans-l-1,2-diaminocyclohexane) platinum (II): new experimental data". *Biomed. Phsrmacoth*er, vol.43(4), pp. 251- 260, 1989.

[49] T. Uehara, J. Yamate, M. Torii, T. Maruyama, "Comparative nephrotoxicity of cisplatin and nedaplatin: mechanisms and histopathological characteristics". *J Toxicol Pathol*, vol. 24(2), pp. 87–94, Jun. 2011.

[50] T.C. Johnstone, K. Suntharalingam, S.J. Lippard, "The next generation of platinum drugs: targeted Pt (II) agents, nanoparticle delivery, and Pt(IV) prodrugs". *Chem Rev*, vol.116(5), pp. 3436–3486, Feb. 2016.

[51] N. Shah, D.S. Dizon, "New-generation platinum agents for solid tumors". *Future Oncol*, vol. 5(1), pp. 33–42, Feb. 2009.

[52] N.J. Wheate, S. Walker, G.E. Craig, R. Oun, "The status of platinum anticancer drugs in the clinic and in clinical trials". *Dalton Trans*, vol. 39(35), pp. 8113–8127, Sep 2010.

[53] D. Liu, C. Poon, K. Lu, C. He, W. Lin, "Self-assembled nanoscale coordination polymers with trigger release properties for effective anticancer therapy". *Nat Commun*, vol. 25(5), pp.4182, Jun. 2014.

[54] K. Tummalapalli., G. Vuppalapati, P.A. Madhvesh, "Glance on Bio-Significant Metallo- Organic Complexes of Copper(II)". *Research Journal of Pharmaceutical, Biological and Chemical Sciences*, vol. 7(5), pp.12-28, Jun. 2016.

[55] T. R. Rau, A. lsfasser, R. Zahl. van Eldik, "Structural and Kinetic Studies on the Formation of Platinum(II) and Palladium(II) Complexes with L-Cysteine-Derived Ligands". *Inorg. Chem*, vol. 37(17), pp. 4223-4230, Jul. 1998.

[56] J. Reedijk, and J. M. Teuben. *In Cisplatin, Chemistry and Biochemistry of a Leading Anticancer Drug*. ed. B. Lippert, Wiley-VCH, Zurich. 1999, pp. 339–362.

[57] M.I. Duran, E.L.M. Lampers, and J. Reedijk, "Reactivity of chloro- and aqua(diethylenetriamine)platinum(II) ions with glutathione, S-methylglutathione, and guanosine 5'-monophosphate in relation to the antitumor activity and toxicity of platinum complexes". *Inorg. Chem*, vol. 30(12), pp. 2648- 2652, Jun 1991.

[58] M.N. Patel, et al, "Square Planar Platinum (II) Complexes with N, S-Donor Ligands: Synthesis, Characterisation, DNA Interaction and Cytotoxic Activity". *Applied biochemistry and biotechnology*, vol. 172(4), pp1846-1858, Feb.2014.

[59] (a) M.J. Clarke, F. Zhu D R. Frasca, "Non-platinum chemotherapeutic metallopharmaceuticals", *Chem. Rev*.vol .99(9), pp. 2511- 34, Sep. 1999; (b) M.D. Hall, R.C. Dolman, T.W. Hambley, A. Sigel, H. *Sigel Metal Ions in Biological Systems*. vol.42, Dekker, New York. 2004, Pp. 297; (c) K.R. Barnes, S.J. Lippard, in: A. L. Sige, Sigel, H., *Metal Ions in Biological Systems*. vol. 42. Dekker, New York. 2004, pp.143.

[60] M. Hay, *Current Opinion in Endocrine and Metabolic Research*. Invest. Drugs, 1999.

[61] M.P. Shaver, C.M. Vogels, A.I. Wallbank, T.L. Hennigar, K. Biradha, M.J. Zaworotko, S.A. Westcott, "Trans alkenylpyridine and alkenylamine complexes of platinum ". *Can J. Chem*, vol.78(5), pp. 568- 576. 2000.

[62] B. A. Miles, A.E. Patterson, C.M. Vogele, A. Decken, J.C. Waller, J.R. Pier. Morin, A.A. Westcott, " Synthesis, characterization, and anticancer activities of lipophilic pyridinecarboxaldimine platinum(II) complexes". *Polyhedron*, vol. 108, Pp. 23-29, Mar. 2016.

[63] J. L. Butour, and J. P. Macquet, "Differentiation of DNA Platinum Complexes by Fluorescence the Use of an Intercalating Dye as a Probe". *Eur. J. Biochemistry*. 1977. 78(2), pp. 455-463, Sep. 1977.

[64] K. Neplechova, J. Kasparkova, O. Vrana, O. Novakova, A. Habtemariam, B. Watchman, P.J. Sadler, and V. Brabec, "DNA Interactions of New Antitumor Aminophosphine Platinum(II) Complexes". *Mol. Pharmacol*, vol. 56(1), pp. 20-30, Jul. 1999.

[65] (a) V. Brabec, "DNA modifications by antitumor platinum and ruthenium compounds: their recognition and repair". *Prog. Nucleic Acid Res. Mol. Biol*, vol. (71), pp.1–68, 2002. (b) E.R. Jamieson, S. J. Lippard, "Structure, Recognition, and Processing of Cisplatin-DNA Adducts". *Chem R*ev, vol.99(9), pp. 2467–2498, Sep.1999. (c) N. P. Johnson, J.L. Butour, G. Villani, F.L. Wimmer, M. Defais, V. Pierson, V. Brabec," Metal antitumor compounds: The mechanism of action of platinum complexes". Prog. *Clin. Biochem. Med*, vol.10, pp.1–24, 1989.

[66] J.L. García-Giménez, J. Hernández-Gil, A. Martínez-Ruíz, A. Castiñeiras, M. Liu-Gonzáles, F.V. Pallardó, J. Borrás, G. A. Piña, "DNA binding, nuclease activity, DNA photocleavage and cytotoxic properties of Cu(II) complexes of N-substituted sulfonamides". *J. Inorg. Biochem*, vol. 121, pp.167-178, Apr. 2013.

[67] S.M. Fiuza, J. Holy, L.A. Batista de Carvalho, M. P. Marques, "Biologic Activity of a Dinuclear Pd(II)–Spermine Complex Toward Human Breast Cancer". *Chem. Biol. Drug Des*, Vol. 77(6), pp. 477-488, Jun. 2011.

[68] C. Icsel, V.T. Yilmas, Y.S. Kaya, M. Durmus, O. Sarimahmut. E. Buyukgungor "Ulukaya Cationic Pd(II)/Pt(II) 5,5-diethylbarbiturate complexes with bis (2 pyridylmethyl) amine and terpyridine: Synthesis, structures, DNA/ BSA interactions, intracellular distribution, cytotoxic activity and induction of apoptosis". *Journal of Inorganic Biochemistry*, vol .152, pp. 38-52, Nov.2015.

[69] C.H. Hing, Dik-Lung Ma, [b] M. Yang, and Chi-Ming Che C-M. "Synthesis and Biological Activity of a Platinum(II) 6-Phenyl-2,2-bipyridine Complex and Its Dimeric Analogue". *ChemBioChem*, Vol. 4(2), pp. 62–68, Jan. 2003.

[70] M.K. Amir, G. Hogarth, Z. Khan, M. Imran, and Zia-ur-Rehmana, "Platinum(II) dithiocarbamate complexes [Pt(S2CNR2)Cl(PAr3)] as anticancer and DNA damaging agents". *Inorganica Chimica Acta*, Vol. 512, Nov. 2020.

[71] D. Ćoćić, S. Jovanović-Stević, R. Jelić, S. Matić, S. Popović, P. Djurdjević, D. Baskićdg, and B. Petrović, "Homo- and hetero-dinuclear Pt(ii)/Pd(ii) complexes: studies of hydrolysis, nucleophilic substitution reactions, DNA/BSA interactions, DFT calculations, molecular docking and cytotoxic activity". *Dalton Trans*, Vol 49(41), pp. 14411-14431, Oct. 2020.

[72] M. A. Fuertes, C. Alonso, and J.M. Perez, "Biochemical modulation of cisplatin mechanisms of action: enhancement of antitumor activity and circumvention of drug resistance". *Chemical Reviews*, vol. 103(3), pp. 645-662, Mar. 2003.

[73] B. Lippert. "Impact of Cisplatin on the recent development of Pt coordination chemistry: a case study". *Coordination Chemistry Reviews*, vol. 182(1), pp. 263-295, Feb.1999.

[74] J. Reedijk, "Why does cisplatin reach guanine-N7 with competing S-donor ligands available in the cell?". *Chemical Reviews*, vol. 99, pp. 2499-2510, Sep. 1999.

[75] M.A. Jakupec, M. Galanski and B. K. Keppler, "Tumour-inhibiting platinum complexesstate of the art and future perspectives". *Reviews of Physiology, Biochemistry and Pharmacology*, vol. 146, pp. 1-54, Feb.2003.

[76] J. Kozelka, F. Legendre, F. Reeder, J.C. Chottard, "Kinetic aspects of interactions between DNA and platinum complexes". *Coordination Chemistry Reviews*, vol.190-192, pp. 61–82, Sep.1999.

[77] C. T. Johnstone, K. Suntharalingam, "Third row transition metals for the treatment of cancer". *Philosophical Transactions*, Feb. 2015.

[78] X. Lin, T. Okuda, A. Holzer, S. Howell, "The copper transporter CTR1 Regulates cisplatin uptake in Saccharomyces cerevisiae", *Mol Pharmacol*, vol. 62(5), pp. 1154–1159, Nov.2002.

[79] S. Howell, R. Safaei, C. Larson, M. Sailor, "Copper transporters and the cellular pharmacology of the platinum-containing cancer drugs". *Mol. Pharmacol*, vol. 77(6), pp.887–894, Jun. 2010.

[80] K. Filipski, R. Mathijssen, T.S. Mikkelsen, A. Schinkel, "Sparreboom. "Contribution of organic cation transporter 2 (OCT2) to cisplatin-induced Nephrotoxicity". *Clin. Pharmacol. Ther*, vol. 86(4), pp. 396–402, Oct. 2009.

[81] K. Ivy, and J. Kaplan, "A re-evaluation of the role of hCTR1, the human high-Affinity copper transporter, in platinum-drug entry into human cells". *Mol Pharmacol*, vol. 83(6), pp.1237–1246, Jun. 2013.

[82] A. Di Pasqua, J. Goodismanm, D. Kerwood, B. Toms, R. Dubowy, J. Dabrowiak. Activation of carboplatin by carbonate. *Chem. Res. Toxicol*. 2006. 19(1), pp.139–149, Dec. 2006.

[83] S. Cohen, and S. J. Lippard, "Cisplatin: from DNA damage to cancer chemotherapy". *Prog Nucleic Acid Res Mol Biol*. vol. 67. pp. 93- 130, Feb. 2001.

[84] K. Lovejoy, And S. Lippard, "Non-traditional platinum compounds for improved accumulation, oral bioavailability, and tumor targeting". *Dalton Trans*, vol.38(48), pp 10651–10659, Dec. 2009.

[85] A. Basu, and S. Krishnamurthy, "Cellular responses to Cisplatin-induced DNA damage". *J. Nucleic Acids*, pp.1-16, Aug.2010.

[86] M. Al-Sarraf, "Chemotherapeutic management of head and neck cancer". *Cancer Metastasis Rev*, vol. 6(3), pp.181-198, 1987.
[87] J.M. Hill, and R.J. Speer, "Organo-platinum complexes as antitumor agents". *Anticancer Res*, vol. 2(3), pp. 173-186, Jun.1982.

[88] K. Caglar, C. Kinalp, F. Arpaci, M. Turan, K. Saglam, B. Ozturk, S. Komurcu, I. Yavuz, M. Yenicesu, A. Ozet, A. Vural, "Cumulative prior dose of cisplatin as a cause of the nephrotoxicity of high-dose chemotherapy followed by autologous stem-cell transplantation". *Nephrol Dial Transplant*, vol. 17(11), pp. 1931-1935, Nov. 2002.

[89] T. Boulikas, A. Pantos, E. Bellis, P. Christofis, "Designing platinum compounds in cancer: structures and mechanisms". *Cancer Therapy*, vol. 5, pp 537-583, Dec.2007.

[90] M. Devereux, M. McCann, D. Shea, M. Connor, E. Kiely, V. McKee, D. Naughton, A. Fisher, A. Kellett, M. Walsh, D. Egan, C. Deegan, "Synthesis, Superoxide DismutaseMimetic and Anticancer Activities of Metal Complexes of 2,2-Dimethylpentanedioic Acid(2dmepdaH2) and 3,3-Dimethylpentanedioic acid(3dmepdaH2): X-Ray Crystal Structures of $[Cu(3dmepda)(bipy)]_2 \cdot 6H_2O$and $[Cu(2dmepda)(bipy)(EtOH)]_2 \cdot 4EtOH$ (bipy = 2,2_Bipyridine)". *Bioinorg. Chem. Appl*, pp. 1–11, 2006.

[91] C. Deegan, M. McCann, M. Devereux, B. Coyle, D. Egan, "In vitro anti-tumour effect of 1,10-phenanthroline-5,6-dione (phendione), $[Cu(phendione)_3](ClO_4)2 \cdot 4H_2O$ and$[Ag(phendione)_2]ClO_4$ using human epithelial cell lines". *Chemico Biol. Interact*, vol.164(1-2), pp. 115-125, Dec. 2006.

[92] C. Deegan, M. McCann, M. Devereux, B. Coyle, D. Egan, "In vitro cance chemotherapeutic activity of 1,10-phenanthroline (phen), $[Ag_2(phen)_3(mal)]$ $2H_2O$, $[Cu(phen)_2(mal)]$ $2H_2O$ and $[Mn(phen)2(mal)]$ $2H_2O$ (malH2 = malonic acid) using human cancer cells". *Cancer Lett*, vol. 247(2), pp. 224-233, Mar. 2007.

[93] L. Gracia-Mora, Ruiz-Ramirez, C. Gomez-Ruiz, M. Tinoco- Mendez, A. Marquez Quinones, L. Romero de Lira, A. Marin- Hernandez, L. Masias-Rosales, M.E. Bravo-Gomez, *Met. Based Drugs*, 2002.

[94] A. De Vizcaya-Ruiz, A. Rivero-Mueller, L. Ruiz-Ramirez L., G. Kass, L. Kelland, R. Or, M. Dobrota, "Induction of Apoptosis by a Novel Copper- based Anticancer Compound, Casiopeina II, in L1210 Murine Leukaemia and CH1 Human Ovarian Carcinoma Cells". *Toxicol. In Vitro,* vol.14(1), pp. 1-5. Feb. 2000.
[95] B. Coyle, P. Kinsella, M. McCann, M. Devereux, R. O'Connor, M. Clynes, K. Kavanagh, "Induction of apoptosis in yeast and mammalian cells by exposure to 1,10-phenanthroline metal complexes". *Toxicol. In Vitro,* vol. 18(1), pp. 63-70, Feb. 2004.

[96] B. Coyle, K. Kavanagh, M. McCann, M. Devereux, M. Geraghty, "Biometals. Mode of anti-fungal activity of 1,10-phenanthroline and its Cu(II), Mn(II) and Ag(I) complexes". *Biometales,* vol.16(2), pp. 321-329, Jun. 2003

[97] W. Cuia. L. Wanga.G. Xianga. L. Zhoub. X. Ana. D. Caoa, "A colorimetric and fluorescence turn-off" chemosensor for thedetection of silver ion based on a conjugated polymer containing2,3-di(pyridin-2-yl)quinoxaline". *Sensors and Actuators B Chemical* , vol. 207, pp. 281–290, 2015.

[98] M. Pitie, C. Boldron, H. Gornitzka, C. Hemmert, B. Donnadieu, B. Bernard Meunier, "DNA Cleavage by Copper Complexes of 2- and 3-Clip-Phen Derivatives". *Eur. J. Inorg. Chem,* vol. 3, pp. 528-540, Feb. 2003.

[99] P. Biswas, S. Dutta, M. Ghosh, "Influence of counter anions on structural, spectroscopic and electrochemical behaviours of copper(II) complexes of dipyrido[3,2-f: 20,30-h]-quinoxaline (dpq)". *Polyhedron,* vol. 27(9), pp. 2105–2112, Jun. 2008.

[100] C. Molinaro, A. Martoriati, L. Pelinski, and K. Cailliau, "Copper Complexes as Anticancer Agents Targeting Topoisomerases I and II". *Cancers*, vol. 12(10), pp.1-27, Oct. 2020.

[101] M. Plotek, K. Dudek, A. Kyzioł, "Selected copper(I) complexes as potential anticancer agent". *Chemik,* vol. 679(12), pp. 1181–1190, Jan. 2013.

[102] M. B. Baile, N.S. Kolhe, P.P. Deotarse, A.S. Jain, A.A. Kulkarni, "Metal Ion Complex -Potential Anticancer Drug- A Review". *International Journal of Pharma Research & Review,* vol. 4(8), pp. 59-66, Aug. 2015.

[103] C. Justin Dhanaraj, and J. Johnson, "Metal Complexes of Quinoxaline Derivatives: Review (Part-I)". *Research Journal of Chemical Sciences*, vol. 4(11), pp. 80-102, Nov. 2014.

[104] V. K. Maikhuri, A. K. Prasad, A. Jha and S. Srivastava, "Recent advances in the transition metal catalyzed synthesis of quinoxalines: a review". *New Journal of Chemistry*, vol. **45,** 13214 - 13246, Jun. 2021.

[105] G. W. H. Chesseman, *The Chemistry of Heterocyclic Compounds, Condensed Pyrazines*. John Wiley & Sons, Inc, Jan.1979.

[106] C. Ferraz, M. Prudencio, R. Vieira, J. P. Fernandes, Z. Noronha, Petrovski, "Bacterial Resistance". *Biochem. Pharmacol. Open Access J*, vol. 1, pp. 7, Jan. 2012.

[107] J.B. Desmond, A.E. Jonathan, *The Chemistry of Heterocyclic Compounds*. Wiley, 2004.

[108] J. Pereira, A. M. Pessoa, M. N. alia, D. S. Cordeiro, R. Fernandes, C. Prudencio, J. P. Noronha, M. onica M. Vieira, "Quinoxaline, its derivatives and applications: A State of the Art review". *European Journal of Medicinal Chemistry*, vol. 97, pp. 664-672, Jul. 2015.

[109] D. M. Asif Husain, "Recent advances in pharmacological activities of quinoxaline derivatives". *J. Pharm. Res*, vol.4(3), pp. 924 – 929, Mar. 2011.

[110] S. H. Alotaibi, and A. A. Momen, (2019. Nov 11). *Biophysical Chemistry - Advance Applications*, [Online], Available: IntechOpen, Open Access books.

[111] R. Palchaudhuri, P. J. Hergenrotherm, "DNA as a target for anticancer compounds: methods to determine the mode of binding and the mechanism of action". *Current Opinion in Biotechnology*, vol. 18 (6), pp. 497-503, Dec. 2007.

[112] H. Mei, J. Barton, "A Chiral Probe for A-form Helices of DNA and RNA: Tris(tetramethylphenanthroline)ruthenium(II)". *J. Am. Chem. Soc*, Vol. 108, pp. 7414, Nov.1986.

[113] L. Hlaka, M-Jon Rosslee, M. Ozturk, S. Kumar, S. P. Parihar, F. Brombacher, A. I. Khalaf, K. C. Carter, F. J. Scott, C. J. Suckling and R. Guler, "Evaluation of minor

groove binders (MGBs) as novel anti-mycobacterial agents and the effect of using non-ionic surfactant vesicles as adelivery system to improve their efficacy". *J Antimicrob Chemother*, vol. 72, pp. 3334–3341, Dec. 2017. doi:10.1093/jac/dkx326

[114] L. Tabernero, J. Bella, and C. Alemán, "Hydrogen bond geometry in DNA–minor groove binding drug complexes". *Nucleic Acids Research*, vol. 24(17), pp. 3458–3466, Sep. 1996.

[115] A. D. Richards, A. Rodgers, "Synthetic metallomolecules as agents for the control of DNA structure" (PDF)". *Chemical Society Reviews*, vol. 36 (3), pp. 471–83, Mar. 2007.

[116] S. Ulrich, *Metallointercalators and Metalloinsertors: Structural Requirements for DNA Recognition and Anticancer Activity.* In Sigel, Astrid; Sigel, Helmut; Freisinger, Eva; Sigel, Roland K. O. (eds.). Metallo-Drugs: Development and Action of Anticancer Agents. Metal Ions in Life Sciences.18. Berlin: de Gruyter GmbH. 2018, pp. 387–435.

[117] C. Moucheron. Kirsch-De Mesmaeker, "New DNA-binding ruthenium(II) complexes as photo-reagents for mononucleotides and DNA C". *J. Physical Organic Chemistry*, vol. 11, pp. 577-583, Dec. 1998.

[118] K. Fukui, K. Tanaka, "The Acridine Ring Selectively Intercalated into a DNA Helix at Various Types of Abasic Sites: Double Strand Formation and Photophysical Properties". *Nucleic Acids Res*, vol. 24, pp. 3962-3967, Oct. 1996.

[119] T.A. Bickle, D.H. Krüger, "Biology of DNA restriction". *Microbiol. Rev*, Vol. 57, pp. 434-450, Jun. 1993.
[120] K. Samejima, W.C. Earnshaw, "Trashing the genome: the role of nucleases during apoptosis". *Nat. Rev. Mol. Cell. Biol*, Vol. 6, pp. 677-688, Oct. 2005.

[121] J. Chen, J. Stubbe, "Bleomycins: towards better therapeutics". *Nat. Rev. Cancer*, Vol. 5, pp. 102-112, Feb. 2005.

[122] K. R. Gowda, C. N. Blessy Baby Mathew. H.S. Sudhamani, B. Naik, "Mechanism of DNA Binding and Cleavage Sangeetha". *Biomedicine and Biotechnology*, Vol. 2, pp. 1-9, Jun. 2014.

[123] N. K. Kochetkov, E. I. Budovskii, *Reactions Involving the Cleavage or Rearrangement of Heterocyclic Rings of Nucleic Acid Bases and their Derivatives*. Organic Chemistry of Nucleic Acids. Springer, 1972, pp. 381-423.

[124] I.E. Kochevar, A. Dunn. "Photosensitized reactions of DNA: cleavage and addition". *Bioorg. Photochem*, vol. 1, pp. 273, Jun. 1990.

[125] M. J. Fernandez, K. B. Grant, F. Herraiz, X. Yang, A. Lorente, "DNA photocleavage by dicationic bisintercalants". *Tetrahedron Lett*, vol. 42, pp. 5701-04, Aug. 2001.

[126] B. Armitag,"Photocleavage of Nucleic Acids". *Chem. Rev*, vol. 98, pp. 1171, Mar. 1998.

[127] B. Meunier, G. Pratviel, J. Bernadou, "Active Species Involved in Oxidative DNA Cleavage". *Bull. Soc. Chim,* vol. 131, pp. 933-943, Feb. 1994.

[128] T. J. Peters, "Metabolism, Albumin in the body In: All about albumin, Biochemistry Genetics and Medical applications". *San Diego, Academic Press,* vol. 43, pp. 2014-2015, Oct. 1997.

[129] D.C. Carter, and J.X. Ho, "Serum albumin, Ad V". *Protein Chem,* vol. 45, pp. 153-203, Oct. 1994.

[130] B. Saha, S. Chakraborty, and G. J. Das, "A rational approach for controlled adsorption of metal ions on bovine serum albumin – malachite bio- nanocompstie". *Chem. C*, vol. 114(21), pp. 9817-9825, May. 2010.

[131] A. P. J. Middelberg, L. He, A. F. Dexter, S. A. Shen, and R.K. Thomas, "The interfacial structure and Young's modulus of peptide films having switchable mechanical properties". *J. R. Soc. Interface*, Vol. 5, pp. 47-54, Jan. 2008.
[132] B. Dahlbäck, "Protein S and C4b-Binding Protein: Components Involved in the Regulation of the Protein C Anticoagulant System". *Thromb Haemost*, vol. 66(01), pp. 049-061, Jul. 1991.

[133] T. S. Akasheh, P.C. Beaumont, B. J. Parsons, and G. O. Phillips, "Lumine scent charge transfer state of ruthenium –bipyrimidine complexes". *J. Phys. Chem*, vol. 90(22), pp. 5651, Oct. 1986.

[134] F. R. Díaz, M. A. del Valle, C. Núñez, A. Godoy, J. L. Mondaca, A. Toro- Labbe, and C. J. Bernede, "Synthesis, characterization, electropolymerization, and theoretical study of 2,3-di-(2-thienyl)quinoxaline". *Polymer Bulletin*, Vol. 56, pp. 155–162, Dec. 2006.

[135] A. D. Becke, "Density-functional exchange-energy approximation with correct asymptotic behavior". *Physical Review A Gen. Phys*, vol. 38(6), pp. 3098–3100, Sep. 1988.

[136] C. Lee, W. Yang, and R.G. Parr, "Development of the Colle-Salvetti correlation-energy formula into a functional of the electron density". *Phys. Rev. B Condens. Matter*, vol. 37(2), pp. 785–789, Jun. 1988.

[137] R. Krishnan, J. S. Binkley, R. Seeger, and J. A. Pople, "Selfconsistent molecular orbital methods. XX. A basis set for correlated wave functions". *J. Chem. Phys,* vol. 72, pp. 650-654, Jun. 1980.

[138] T. H. Dunning Jr, and P. J. Hay, *In Modern Theoretical Chemistry* Ed. H. F. Schaefer III, (Plenum, New York, 1977, pp. 1-28.

[139] D. A. Erdogan, H. Kayi, and Ş. Özalp-Yaman, "Spectroelectrochemical Investigation of Nuclease Active Pt(II) Complexes Containing Pyrrole Oxime". *Electrochimica Acta*. vol. 158, pp. 333-341, Mar. 2015.
[140] S. A. Popoola, A. A. Al-Saadi,"Spectroscopic Evaluation of the Molecular Structures of di-μ-Chlorobis(1,5-Cyclooctadiene) Iridium (I) and Rhodium (I) Complexes". Journal of Applied Mathematics and Physics, vol. 3, pp. 2, Jan . 2015.

[141] R. Dennington, T. Keith, J. Millam, *Molecular Physical Chemistry: A Computer-based Approach using Mathematica and Gaussion.* J. C. Teixeira-Dias university of Av. Eiro, Baixo Vouga, Portugal, 2017.

[142] Xu X., Xi Z., Chen W., and D. Wang, "Synthesis and Structural characterization of copper (II) complexes of pincer ligands derived from benzimidazole". *J COORD CHEM*, Vol. 60, pp. 2297 – 2308, Sep. 2007.

[143] S. Arounaguiri, and B. Maiya, "Dipyridophenazine Complexes of Cobalt(III) and Nickel(II): DNA-Binding and Photocleavage Studies". *Inorganic Chemistry*, Vol. 35(14), pp. 4267-70, Jul. 1996.

[144] F. Korkmaz, D. A. Erdogan, Ş. Özalp-Yaman, "Interaction of a novel platinum drug with bovine serum albumin: FTIR and UV-Vis spectroscopy analysis". *New J. Chem*, vol. 39, pp. 5676, May. 2015.

[145] Li F, G. Zhao, and H. Wu, "Synthesis, characterization and biological activity of lanthanum(III) complexes containing 2-methylene–1,10 phenanthroline units bridged by aliphatic diamines". *Journal of Inorganic Biochemistry*, Vol. 100, pp. 36–43, Jan. 2006.

[146] S. Christiane, C. Jean, P. Jean, and P. Nicole, "Tuning the mechanism of DNA cleavage photosensitized by ruthenium dipyridophenazine complexes by varying the structure of the two non intercalating ligands". *Journal of Photochemistry and Photobiology B: Biology*, vol. 26. 2, pp.165-174, Nov.1994.

[147] P. Kumar, I. Gorai, M. Santra, B. Mondal, and D. Manna, "DNA binding, nuclease activity and cytotoxicity studies of Cu(II) complexes of tridentate ligands". *Dalton Trans*, vol. 41, pp. 7573-7581, May. 2012.

[148] D. Suh, and J. B. Chaires, "Criteria for the mode of binding of DNA binding agents". *Bioorganic & medicinal chemistry*, Vol. 3(6), pp. 723-728, Jun. 1995.

[149] M. R. Eftink, and C. A. Ghiron, "Fluorescence quenching of indole and model micelle systems". *Journal of Physical Chemistry*, Vol. 80(5), pp. 486–493, Feb. 1976.

[150] P. Lee, J. Costumbrado, H. C. Yuan, and K. Y. Hoon, "Agarose Electrophoresis for the Separa of DNA Fragments". *J VIS EXP*, 2012. Vol. 62, pp. 3923, Apr. 2012.

[151] D. Mahendiran, S. Amuthakala, N. S. P. Bhuvanesh, R. S. Kumar. and A. K Rahiman, "Copper complexes as prospective anticancer agents: in vitro and in vivo evaluation, selective targeting of cancer cells by DNA damage and S phase arrest". *The Royal Society of Chemistry. RSC Adv*, 2018. Vol. 8(30), pp. 16973–16990, May. 2018.

[152] E. Hoffman and V. Stroobant, *Mass Spectrometry Principles and Applications*. John Wiley and sons, 2007, pp. 502.

[153] M. N. AlJibouri, and S.M. Hasun, "Synthesis and characterization of manganese(II), cobalt(II), nickel(II), copper(II) and zinc(II) complexes with new Schiff base derived from 6,7dimethyl quinoxaline2,3(1H,4H) dione and thiosemicarbazide". *European Journal of Chemistry*, vol. 6 (1), pp. 44-47, Dec. 2015.

[154] J. Kandhadi, W. Yan, F. Cheng, H. Wang, H. Liu, "Trans- A 2 B –corrole bearing 2,3-di(2-pyridyl)quinoxaline(DPQ)/phenothiazine moieties: synthesis, characterization, electrochemistry and photophysics", *New J. Chem*, Vol. 42 (12), pp. 9989–9999, Apr. 2018. doi: 0.1039/C8NJ00606G.

[155] J. Granifo, M.E. Vargas, M.T. Garland, R. Baggio, "Coordination mode of some polypyridyl ligands towards the platinum(II) complexes [Pt(dppf)(H 2 O) 2] (CF 3 SO 3) 2 (dppf = 1,1 _ bis (diphenylphosphino)ferrocene) and [Pt(Me 2 SO) 2 Cl 2]. crystal structure of the seven-membered chelate ring complex [Pt(dpq)Cl2] (dpq=2,3-di(2-pyridyl)quinoxaline)". *Inorg. Chim. Acta*, vol. 305 (2), pp. 143–150, Jul. 2000.

[156] T.M. Musa, Synthesis, "characterization and antimicrobia activity of some transition complexes with new Schiffbase derived from Saccharine". *Int. Res. J. Pure and Appl. Chem*, vol. 11 (2), pp. 1–15, Jan. 2016. doi: 10.9734/IRJPAC/2016/23188.

[157] C.J. Dhanaraj, J. Johnson, "Studies on some metal complexes of a quinoxaline based unsymmetrical ONNO donor ligand. synthesis, spectral characteriza- tion, thermal, in vitro biological and DFT studies". *J. Therm. Anal. Calorim*, vol. 127 (2), pp. 1845–1862, Nov. 2017.

[158] M.N. Al-Jibouri, S.M. Hasun, "Synthesis and characterization of manganese(II), cobalt(II), nickel(II), copper(II) and zinc(II) complexes with new Schiffbase derived from 6,7-dimethyl-quinoxaline-2,3(1H,4H)-dione and thiosemicar- bazide". *Eur. J. Chem*, vol. 6, pp. 4–47, Dec. 2015.

[159] P. A. Ajibade, G. A. Kolawole, P. O'brien, M. Helliwell, "Synthesis and characterization of Ni(II), Pd(II) and Pt(II) complexes of 2,4-diamino-5-(3, 4, 5-trimethoxybenzyl)pyrimidine complexes". *J. Coord. Chem*, vol. 59 (14), pp. 1621–1628, Nov. 2006.

[160] D.F. Colton, W.J. Geary, "Transition-metal complexes of the 2,3-dipyridylquinoxalines. Part IV. Cobalt(II), nickel(II), and copper(II) halide derivatives of 6-methyl-2,3-di-(6-methyl-2-pyridyl)quinoxaline and 6,7-dimethyl-2,3-di-(6-

methyl-2-pyridyl)quinoxaline". *J. Chem. Soc. Dalton Trans*, vol. 4, pp. 547–550, Jan. 1972.

[161] W.J. Geary, "Cobalt(II), nickel(II), and copper(II) halide derivatives of 2,3-di-(6-methyl-2-pyridyl)quinoxaline", *J. Chem. Soc. A: Inorg. Phys. Theor*. pp. 2118–2121, Jan. 1969.

[162] (a) F. R. Díaz, M. A. del Valle, C. Núñez, A. Godoy, J. L. Mondaca, A. ToroLabbé and J. C. Bernède, *Polym. Bull*, vol. 56, pp. 155–162, 2006. (b) A. D. Allen, T. Theophanides, *Canadian J. Chem*, vol. 42, pp. 1551-1554, 1964. (c) R. R. Vernooji et al, *Inorg. Chem*, vol, 55(12), pp. 5983-5992, 2016. (d) N. Bélanger-Desmarais, M. Schütz, C. Reber, *J. Phys.Chem*, vol. 123. pp. 5574-5579, 2019. (e) V. Miskowski et al, *Biochemistry*, vol. 14(6), pp.1244-1250, 1975. (f) T. Bardakçı, M. Kumru, S. Güner, *J. Mol.Struc*, vol. 1054-1055, pp.76-82, 2013. (g) Y. Suffren, F. G. Rollet, and C. Reber, *Comments on Inorganic Chemistry*, vol. 32, pp. 246–276, 2011. (h) T. J. thamann, P. franko, L. J. willis, and T. M. loehr. Proc, *NatL Acad. Sci. USA*, vol. 79, pp. 6396-6400, 1982. (i) H. Nawaz, F. k. Bonnier, P. Knief, O. Howe, and F. M. Lyng, *Analyst*, vol. 135, pp.3070-3076, 2010.

[163] M. Sirajuddin, S. Ali, A. Badshah, "Drug-DNA interactions and their study by UV-Visible, fluorescence and cyclic voltammetry". *J. Photochem. Photobiol. B: Biology*, vol. 124, pp. 1-19, Jul. 2013.

[164] F. Arjmand, S. Parveen, M. Afzal, M. Shahid, "Synthesis, characterization, biological studies, DNA binding, cleavage, antibacterial and topoisomerase I) and molecular docking of copper(II) benzimidazole complexes". *J. Photochem. Photobiol. B., Biology*, vol. 114, pp.15-26, Sep. 2012.

[165] P.R. Reddy, A Shilpa, "Oxidative and hydrolytic DNA cleavage by Cu(II) complexes of salicylidene tyrosine schiffbase and 1,10-phenanthroline/bipyridine". *Polyhedron*, vol. 30 (4), pp. 565–572, Mar. 2011.

[166] P. Kalaivani, R. Prabhakaran, F. Dallemer, et al, "DNA, protein binding, cytotoxicity, cellular uptake and antibacterial activities of new palladium(II) com- plexes of thiosemicarbazone ligands: effects of substitution on biological ac- tivity". *Metallomics*, vol. 4 (1). pp. 101–113, Jan. 2012.

[167] M.J. Waring, "Complex formation between ethidium bromide and nucleic acid". *J. Mol. Biol*, vol. 13 (1), pp. 269–282, Aug. 1965.

[168] Y. Baba, C. L. Beathy, A. Kagemoto, C. Gebelien, *Biological Activity of Polymers*. American Chemical Society, Washington, DC, USA, 1982.

[169] W.K. Mudasir, E.T. Wahyuni, N. Yoshioka, H. Inoue, "Salt-dependent binding of iron(II) mixed-ligand complexes containing 1,10-phenanthroline and dipyrido[3,2-*a*:2′,3′-*c*]phenazine to calf thymus DNA Biophys". *Biophysical Chem*, vol. 121, pp. 44-50, Apr. 2006.

[170] S. Satyanarayana, J.C. Dabrowiak, J.B. Chaires, "Neither delta- nor lambdatris(phenanthroline)ruthenium(II) binds to DNA by classical intercalation". *Biochemistry*, vol. 31(39), pp. 9319- 24, Oct. 1992.

[171] An-Guo Zhang, You-Zhuan Zhang, Zhi-Ming Duan, and Ke-Zhi Wang, "Dual Molecular Light Switches for pH and DNA Based on a Novel Ru(II) Complex. A Non-Intercalating Ru(II) Complex for DNA Molecular Light Switch". *Inorg. Chem,* vol. 50(14), pp. 6425–6436, Jun. 2011.

[172] B. Selvakumar, V. Rajendiran, P. U. Maheswari, H. Stoeckli-Evans. M. Palaniandavar, "Structures, spectra, and DNA-binding properties of mixed ligand copper(II) complexes of iminodiacetic acid: The novel role of diimine co-ligands on DNA conformation and hydrolytic and oxidative double strand DNA cleavage". *Journal of Inorganic Biochemistry*, vol. 100. pp. 316–330, Mar. 2006.

[173] N. Shahabadi, S. Akhtarshenas, S. Hadidi, "Synthesis, characterization and DNA interaction studies of new copper complex containing pseudoephedrine hydrochloride drug, Nucleosides". *Nucleosides Nucleotides Nucleic Acids*, vol. 38 (9), pp. 680–699, Apr. 2019.

[174] S. Mazur,F. A. Tanious,D. Ding,A. Kumar,D. W. Boykin, I. J. Simpson,S. Neidle,W. D. Wilson, "A thermodynamic and structural analysis of DNA minor-groove complex formation". *J. Mol. Biol*, vol. 100(2), pp. 321-337, Jul. 2000.

[175] D. Suh, J.B. Chaires, "Criteria for the mode of binding of DNA binding agents". *Bioorg. Med. Chem*, vol. 3 (6), pp. 723–728, Jun. 1995.

[176] M. Harun, G Aysegul, T. Mehmet, O. Mehmet, "Electrochemical investiga- tion and DNA-binding studies of pefloxacin–metal(II/III) complexes". *J. Coord. Chem,* vol. 64 (19), pp. 3393–3407, Jan. 2011.

[177] a) L. J. Lerman, "Structural considerations in the interaction of DNA and acridines". *Mol. Biol*, vol. 3, pp. 18-30, Feb.1961. b) S. H. Alotaibi and A. A, Momen. *Anticancer Drugs' Deoxyribonucleic Acid (DNA) Interactions*. Biophysical Chemistry Advance Applications, 2019. DOI:

[178] L.M. Chen, L. Liu, J.C. Chen, et al, "Synthesis, characterization, DNA- binding and spectral properties of complexes [Ru(L) 4 (dppz)] 2 + (L = Im and MeIm)". *J. Inorg. Biochem*, vol. 102 (2), pp. 330–341, Feb. 2008.

[179] P.R. Reddy, A. Shilpa, "Interaction of DNA with small molecules: Role of copper histidyl peptide complexes in DNA binding and hydrolytic cleavage". *Indian J. Chem. Sec*, vol. 49 (8), pp. 1003–1015, Nov. 2010.

[180] N. Nikolaos, C. Methenitis, G. Pneumatikakis, "Studies on the interaction of altromycin B and its platinum(II) and palladium(II) metal complexes with calf thymus DNA and nucleotides". *J. Inorg. Biochem*, vol. 95 (2), pp. 177–193, Jun. 2003

[181] E. Tselepi, N. Katsaros, "The interaction of [Ru(NH3)5Cl]2+ and [Ru(NH3)6]3+ ions with DNA". *J. Inorg. Biochem*, vol. 37(4), pp. 271-282. Dec. 1989.

[182] C.V. Kumar, R.S. Turner, E.H. Asuncion, "Groove binding of a styrylcyanine dye to the DNA double helix: the salt effect". *J. Photochem. Photobiol A: Chem*, vol. 74 (2–3), pp. 231–238, Sep.1993.

[183] S. Dhar, M. Nethaji and A. R. Chakravarty. "Synthesis, crystal structure and photo-induced DNA cleavage activity of ternary copper (II) complexes of NSO-donor Schiff bases and NN-donor heterocyclic ligands." *Inorganica chimica acta*, vol. 358(7), pp. 2437-2444, Apr. 2005.

[184] P. Kumar, I. Gorai, M. Santra, B. Mondal, D. Manna, "DNA binding, nucle- ase activity and cytotoxicity studies of Cu(II) complexes of tridentate lig- ands". *J. Chem. Soc. Dalton Trans*. vol. 41 (25), pp. 7573–7581, Jul. 2012.

[185] D. Suh, J.B. Chaires, "Criteria for the mode of binding of DNA binding agents". *Bioorg. Med. Chem*, vol. 3 (6), pp. 723–728, Jun.1995.

[186] M. Islami-Moghaddam, H. Mansouri-Torshizi, A. Divsalar and A.A. Saboury, "Synthesis, Characterization, Cytotoxic and DNA Binding Studies of Diimine

Platinum(II) and Palladium(II) Complexes of Short Hydrocarbon Chain Ethyldithiocarbamate Ligand". *J. Iran. Chem. Soc*, Vol. 6 (3), pp. 552-569, Sep. 2009.

[187] J.M. Tercero, A. Matilla, M. A. Sanjuán, et al, "Synthesis, characterization, solution equilibria and DNA binding of some mixed-ligand palladium(II) com- plexes. Thermodynamic models for carboplatin drug and analogous com- pounds". *Inorg. Chim. Acta*, vol. 342, pp. 77–87, 2003.

[188] W. Paw, R. Eisenberg, "Synthesis, characterization, and spectroscopy of dipyridocatecholate complexes of platinum". *Inorg. Chem*, Vol. 36 (11), pp. 2287–2293, May .1997.

[189] S. Arounaguiri, B.G. Maiya, "Dipyridophenazine Complexes of cobalt(III) and nickel(II): DNA-binding and photocleavage studies". *Inorg. Chemi*. vol. 35 (14), pp. 4267–4270, Jul.1996.

[190] S.U. Rehman, Z. Yaseen, M.A. Husain, et al, "Interaction of 6 mercaptopurine with calf thymus DNA–Deciphering the binding mode and photoinduced DNA damage". *PLoS One*, vol. 9 (4), pp. 1-11. Apr. 2014.

[191] J. L. García-Giménez, M. Gonzáles-Alvarez, M. Liu-Gonzáles, J. Macías B, Borrás, G. Alzuet, "Toward the development of metal-based synthetic nucleases: DNA binding and oxidative DNA cleavage of a mixed copper(II) complex with N-(9H-purin-6yl)benzenesulfonamide and 1,10-phenanthroline. Antitumor activity in human Caco-2 cells and Jurkat T lymphocytes. Evaluation of p53 and Bcl-2 proteins in the apoptotic mechanism". *J. Inorg. Biochem*, vol. 103(6). Pp. 923-934, Jun. 2009.

[192] G. Mandal, M. Bardhan, T. Ganguly, "Interaction of bovine serum albumin and albumin-gold nanoconjugates with l-aspartic acid. a spectroscopic approach, Colloids". *Surf B: Biointerfaces*, vol. 81 (1), pp. 178–184, Nov. 2010.

[193] P.B. Kandagal, S. Ashoka, J. Seetharamappa, et al, "Study of the interaction of an anticancer drug with human and bovine serum albumin: spectroscopic approach". *J. Pharm. Biomed. Anal*, vol. 41 (2), pp. 393–399, May. 2006.

[194] A. Buranaprapuk, C.V. Kumar, S. Jockusch, N.J. Turro, "Photochemical protein scissors: role of aromatic on the binding affinity and photocleavage effi- ciency of pyrenyl peptides". *Tetrahedron*, vol. 56 (36), pp. 7019–7025, 2000.

[195] Y. Yue, X. Chen, J. Qin, X. Yao, "Spectroscopic investigation on the binding of antineoplastic drug oxaliplatin to human serum albumin and molecular modelling, Colloids". *Surf. B: Biointerfaces*, vol. 69 (1), pp. 51–57, Feb. 2009.

[196] H. Alsamamra, I. Khalid, R. Alfaqeh, et al, "Spectroscopic investigation of procaine interaction with human serum albumin". *J. Biomed. Sci*, vol. 7 (3:8), pp. 1–10, 2018

[197] P. Kalaivani, R. Prabhakaran, M. V. Kaveri, R. Huang, R. J Staples. and K. Natarajan, "Synthesis, spectral, X-ray crystallography, electrochemistry, DNA/protein binding and radical scavenging activity of new palladium(II) complexes containing triphenylarsine". *Inorg. Chim. Acta*, vol. 405, pp. 415-426, Aug. 2013.

[198] Y. Wang, X. Wang, J. Wang, Y. Zhao, W. He, and Z. Guo, "Noncovalent Interactions between a Trinuclear Monofunctional Platinum Complex and Human Serum Albumin". *Inorg. Chem*. vol. 50(24), pp. 12661−12668, Nov. 2011.

[199] N. Keswani, S. Choudhary, N. Kishore, "Interaction of weakly bound antibiotics neomycin and lincomycin with bovine and human serum albumin: biophysi- cal approach". *J. Biochem*, vol. 148 (1), pp. 71–84, Jul. 2010.

[200] S. Bi, Y. Sun, C. Qiao, H. Zhang, C. Liu, "Binding of several antitumor drugs to bovine serum albumin: fluorescence study". *J. Luminescence*, vol. 129 (5), pp. 541–547, May.2009.

[201] J. Kadokawa, *Ionic Liquids –New Aspects for the Future*, ed., InTechOpen, 2013, pp. 581–593.

[202] C. Metcalfe, C. Rajput, J.A. Thomas, "Studies on the interaction of extended terpyridyl and triazine metal complexes with DNA". *J. Inorg. Biochem*, vol. 100 (8), pp. 1314–1319, Aug. 2006.

[203] D Silva, C.M. Cortez, J.C. Bastos, S.R.W. Louro, "Methyl parathion interaction with human and bovine serum albumin". *Toxicol Lett*, vol. 147 (1), pp. 53–61, Mar. 2004.

[204] E. Froehlich, J.S. Mandeville, C.J. Jennings, R. Sedaghat-Herati, H.A. Tajmir-Riahi, "Dendrimers bind human serum albumin". *J. Phys. Chem. B*, vol. 113 (19), pp. 6986–6993, Apr. 2009.

[205] T. Yotsuyanagi, N. Ohta, T. Futo, et al., "Multiple and irreversible binding of cis-diamminedichloroplatinum(ii) to human serum albumin and its effect on warfarin binding" *Chem. Pharm. Bull*, vol. 39 (11) 3003–3006, 1991.

[206] U. Kragh-Hansen, "Molecular aspects of ligand binding to serum albumin". *Pharmacol. Rev*, vol. 33 (1), pp. 17–53, Mar.1981.

[207] L.S. Lerman, "Structural considerations in the interaction of DNA and acridines". *J. Mol Biol*. vol. 3 (1), pp. 18–30, Feb.1961.
[208] J. R. Lakowich, *Principles of Fluorescence Spectroscopy*, Plenum Press, New York, 1999**,** pp**.** 267.

[209] P.B. Kandagal, S. Ashoka, J. Seetharamappa, S.M.T. Shaikh, Y. Jadegoud, O. B. Ijare, "Study of the interaction of an anticancer drug with human and bovine serum albumin: Spectroscopic approach". *Journal of Pharmaceutical and Biomedical Analysis*, vol. 41(2), pp. 393-399, 2006.

[210] E. Lioli, V. Psycharis, C.P. Raptopoulou, E.K. Efthimiadou, C.A. Mitsopoulou, "Synthesis, characterization, DNA binding and cytotoxicity studies of two novel Cu(II)-2-(2'-pyridyl) quinoxaline complexes". *J Inorg Biochem*, vol. 208, Mar. 2020. 111077.

[211] R. Chen, C.S. Liu, H. Zhang, Y. Guo, X.H Bu, and M. Yang, "Three new Cu(II) and Cd(II) complexes with 3-(2-pyridyl)pyrazole-based ligand: Syntheses, crystal structures, and evaluations for bioactivities". *J. Inorg. Biochem*, vol. 101(3), pp. 412-421, Mar. 2007.

[212] M. Adams, M. P. Sullivan, et al, "Mustards-Derived Terpyridine−Platinum Complexes as Anticancer Agents: DNA Alkylation vs Coordination". *Inorg. Chem*, vol. 60(4), pp. 2414−2424, Jan. 2021.

[213] C. Yu, C. Gao, L. Bai, Q. Liu, Z. Zhang, Y. Zhang, B. Yang, C. Li, P. Dong, X. Sun, Y. Qian, "Design, synthesis and biological evaluation of six dinuclear

platinum(II) complexes". *Bioorganic & Medicinal Chemistry Letters*, vol. 27(4), pp. 963-966, Feb. 2017.

[214] F. Doz, M. E. Berens, D. V. Dougherty, and M. L. Rosenblum, "Comparison of the cytotoxic activities of cisplatin and carboplatin against glioma cell lines at pharmacologically relevant drug exposures". *Journal of Neuro-Oncology*, vol. 11(1), pp. 27–35, Aug. 1991.

[215] J. Wang, B. Luo, X. Li, W. Lu, J. Yang, Y. Hu, P. Huang, and S. Wen, "Inhibition of cancer growth in vitro and in vivo by a novel ROS-modulating agent with ability to eliminate stem-like cancer cells". *Cell Death Dis.* vol. 8(6), pp. 1-9, Jun. 2017.

[216] Y. Cetin, A. M. H. Ibrahim, A. Gungor, Y. Yildizhan, M. Balog, and P. Krizik, "In-vitro evaluation of a partially biodegradable TiMg dental implant: The cytotoxicity, genotoxicity, and oxidative stress". *Materialia*. Vol. 14, pp. 1-9, Dec. 2020.

[217] A. Gegotek, A. Markowska, W. Łuczaj, A. Bielawska, K. Bielawski, E. Ambrozewicz, E. Skrzydlewska, "Effects of dinuclear berenil-platinum(II) complexes on fibroblasts redox status". *Adv. Med. Sci.* vol. 58 (2), pp. 282-291, 2013.

[218] C. P. Matos, Z. Adiguzel, Y. Yildizhan, B. Cevatemre, T. B. Onder, O. Cevik, P. Nunes, L. P. Ferreira, M. D. Carvalho, De. L. Campos, F. R. Pavan, J. C. Pessoa, M. H. Garcia, A. L. Tomaz, I. Correia, C. Acilan, "May iron (III) complexes containing phenanthroline derivatives as ligands be prospective anticancer agents". *European Journal of Medicinal Chemistry*, vol. 176, pp. 492-512, Aug. 2019.

[219] R. Czarnomysy, at el, "The molecular mechanism of anticancer action of novel octahydropyrazino[2,1-a:5,4-a′]diisoquinoline derivatives in human gastric cancer cells". *Invest New Drugs*, vol. 36(6), pp. 970–984, Mar. 2018.

[220] B. L. Fei, S. Tu, Z. Wei, P. Wang, C. Qiao, and Z. F. Chen, "Optically pure chiral copper (II) complexes of rosin derivative as attractive anticancer agents with potential anti-metastatic and anti-angiogenic activities". *European Journal of Medicinal Chemistry*, vol.176, pp.175-186, Aug.2019.

[221] L. M. Balsa, M. C. Ruiz, L. S. M. de la Parra, E. J. Baran, and I. E. León, "Anticancer and antimetastatic activity of copper (II)-tropolone complex against

human breast cancer cells, breast multicellular spheroids and mammospheres". *Journal of Inorganic Biochemistry*, vol. 204. Mar. 2020.

[222] S. Aydinlik, E. Dere, and E. Ulukaya, "Induction of autophagy enhances apoptotic cell death via epidermal growth factor receptor inhibition by canertinib in cervical cancer cells". *Biochim Biophys Acta Gen Subj*, vol.1863(5), pp. 903-91, May.2019.

[223] S. Gu, P. Yu, J. Hu, Y. Liu, Z. Li, Y. Qian, and F. Yang, "Mitochondria-localizing N-heterocyclic thiosemicarbazone copper complexes with good cytotoxicity and high antimetastatic activity". *European journal of medicinal chemistry*, vol.164, pp. 654-664, Feb.2019.

[224] P. L. Olive, and J. P. Banáth, "The comet assay: a method to measure DNA damage in individual cells". *Nature Protocols*, vol. 1(1), pp. 23-29, Feb.2006.

[225] C. Marzano, M. Pellei, F. Tisato, and C. Santini, "Copper complexes as anticancer agents". *Anticancer Agents Med Chem*, vol. 9(2), pp.185-211, Feb.2009.

[226] B. J. Pages, K. B. Garbutcheon-Singh, and J. R. Aldrich-Wright, "DNA Intercalator Pt Complexes, Platinum Intercalators of DNA as Anticancer Agents". *Eur. J. Inorg. Chem*, vol. 12, pp. 1613–1624, 2017.

APPENDIX A

MASS SPECTRA

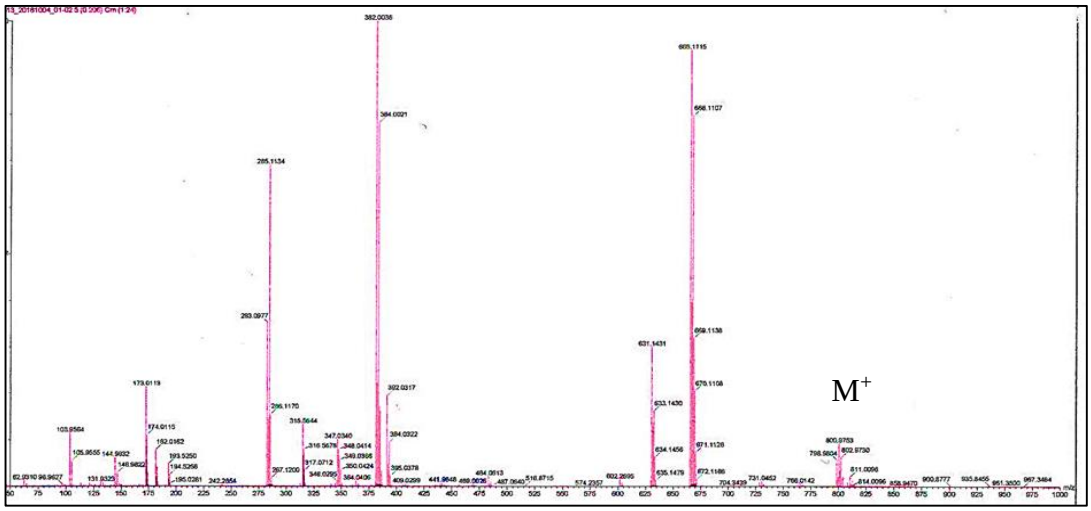

Figure A.1 Mass spectrum of $[Cu(dpq)_2Cl_2]$.

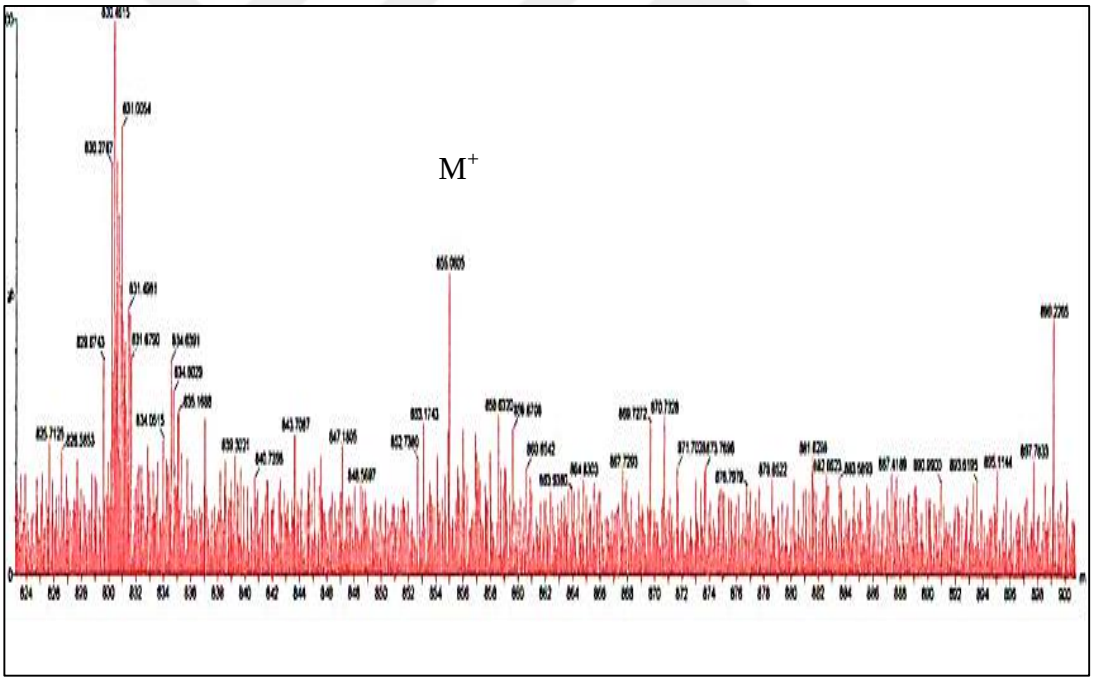

Figure A.2 Mass spectrum of $[Pt(dtq)_2Cl_2]$.

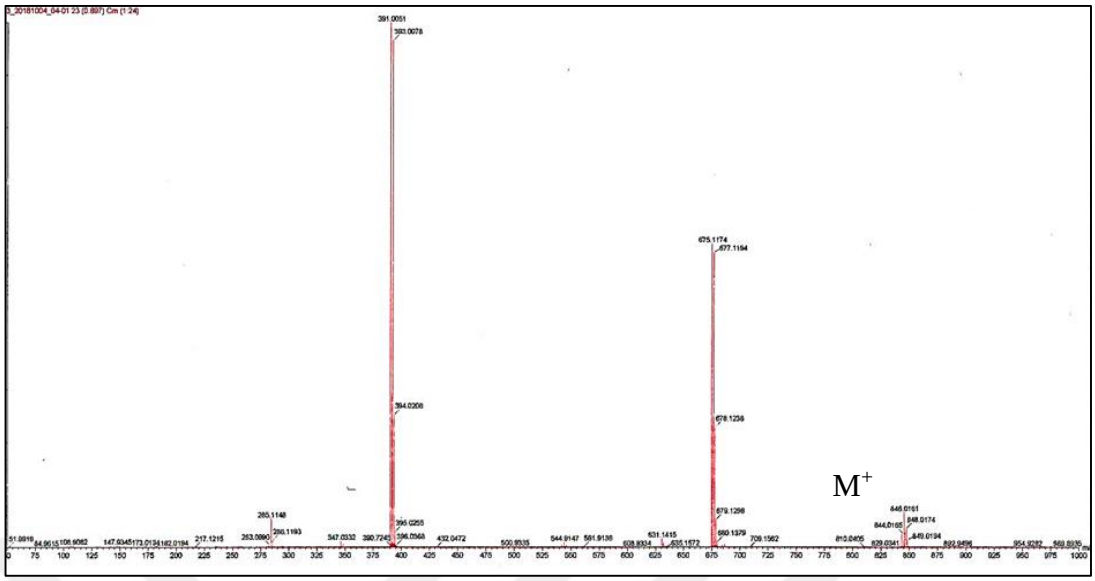

Figure A.3 Mass spectrum of $[Pt(dpq)_2Cl_2]$.

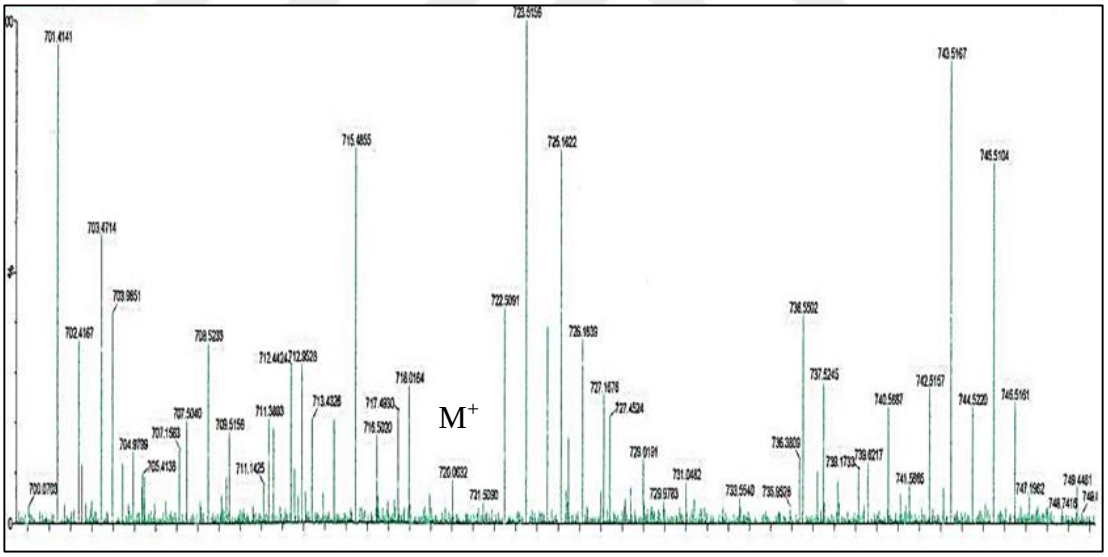

Figure A.4 Mass spectrum of $[Cu(ttbq)Cl_2]$.

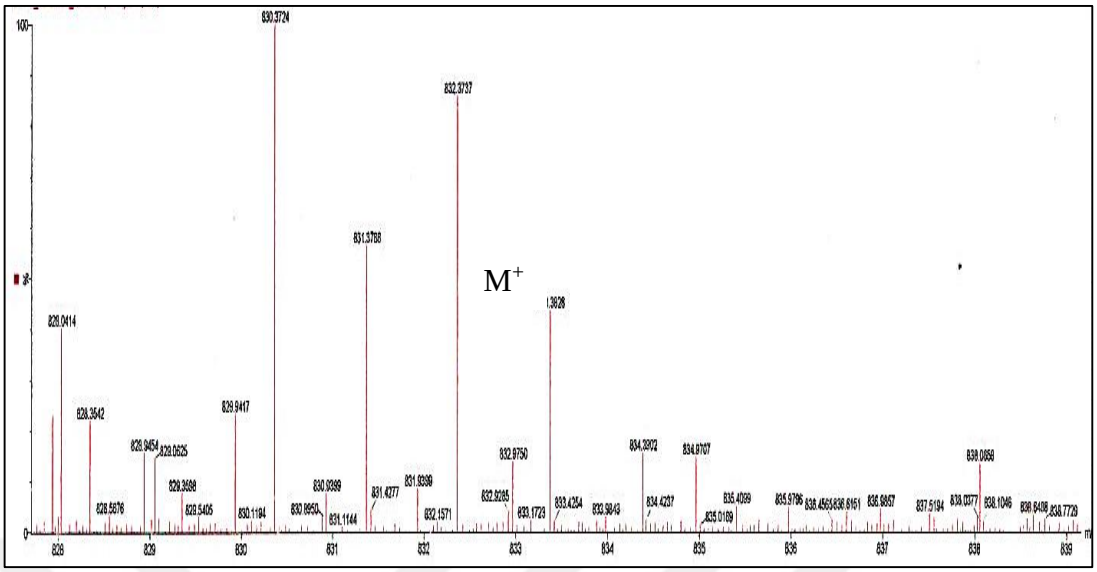

Figure A.5 Mass spectrum of [Pt(tpbq)Cl_2].

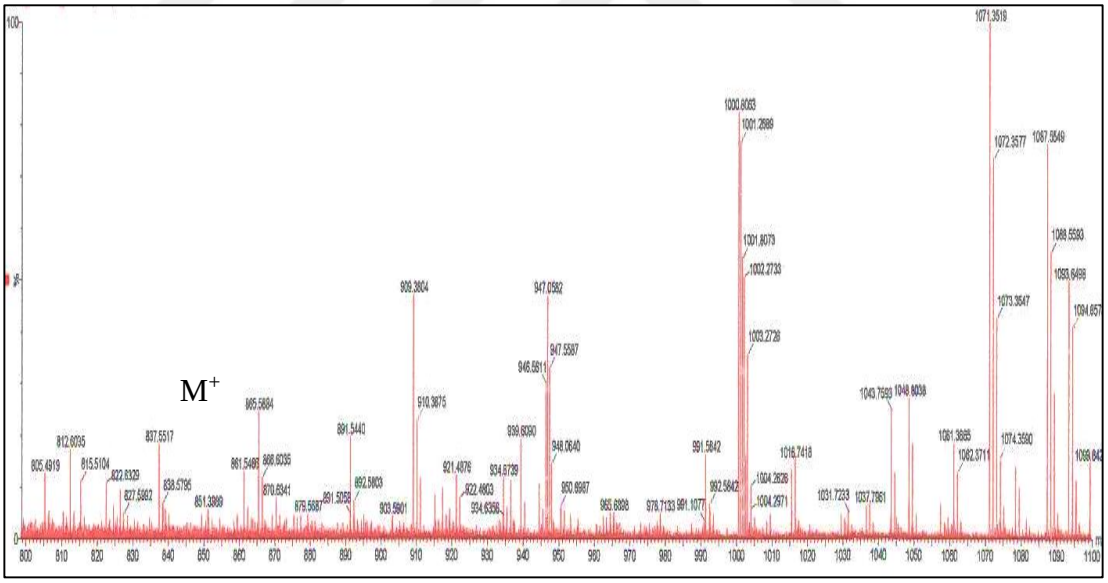

Figure A.6 Mass spectrum of [Pt(ttbq)Cl_2].

APPENDIX B

^{13}C-NMR and ^{1}H-NMR SPECTRA

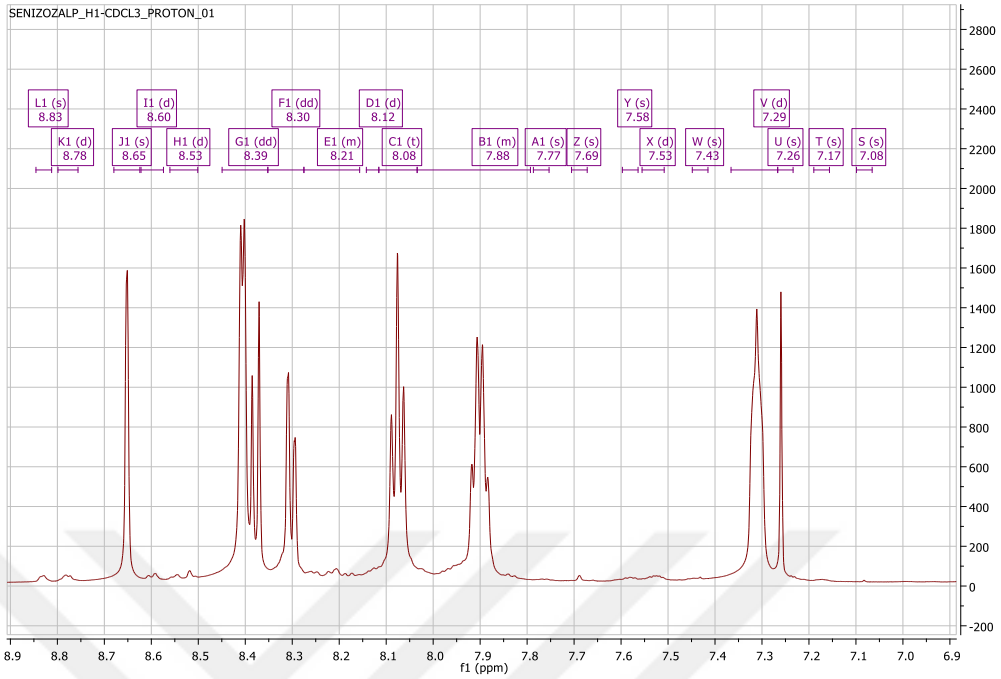

Figure B.1 ^{13}C -NMR spectrum of (tpbq) in d_6-DMSO.

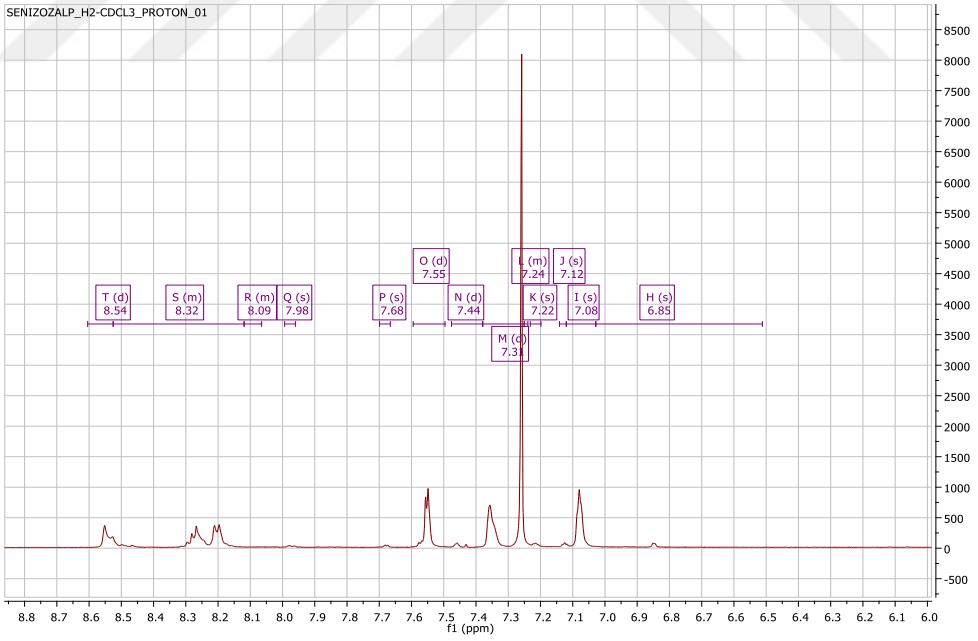

Figure B.2 ^{13}C -NMR spectrum of (ttbq) in d_6-DMSO.

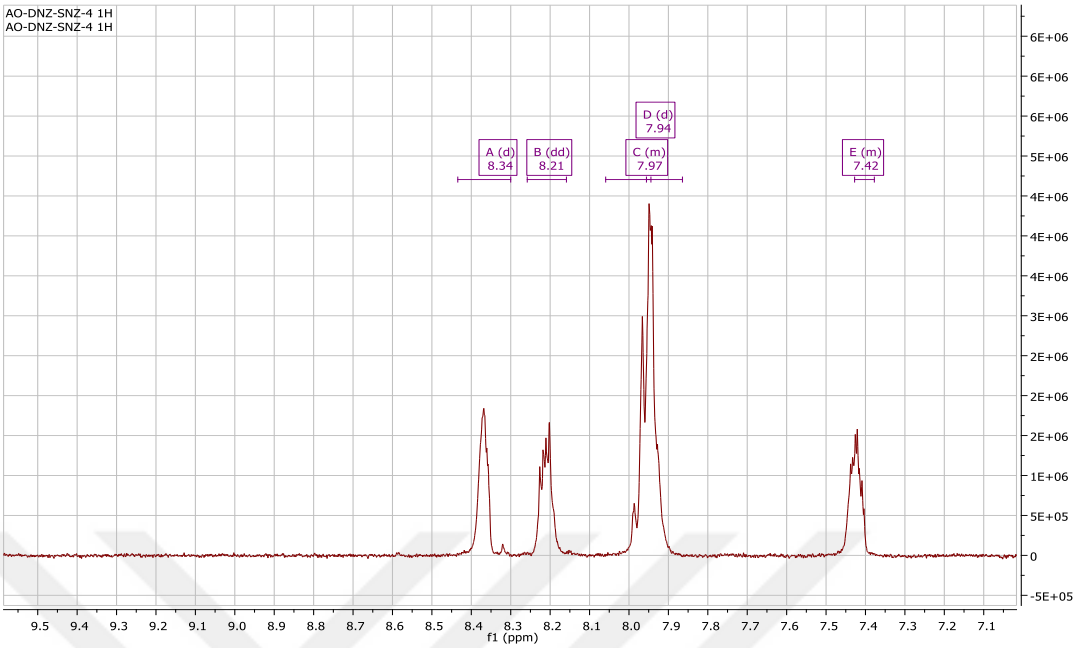

Figure B.3 ^{1}H-NMR spectrum of $[Pt(dpq)_2Cl_2]$ complex in d_6-DMSO.

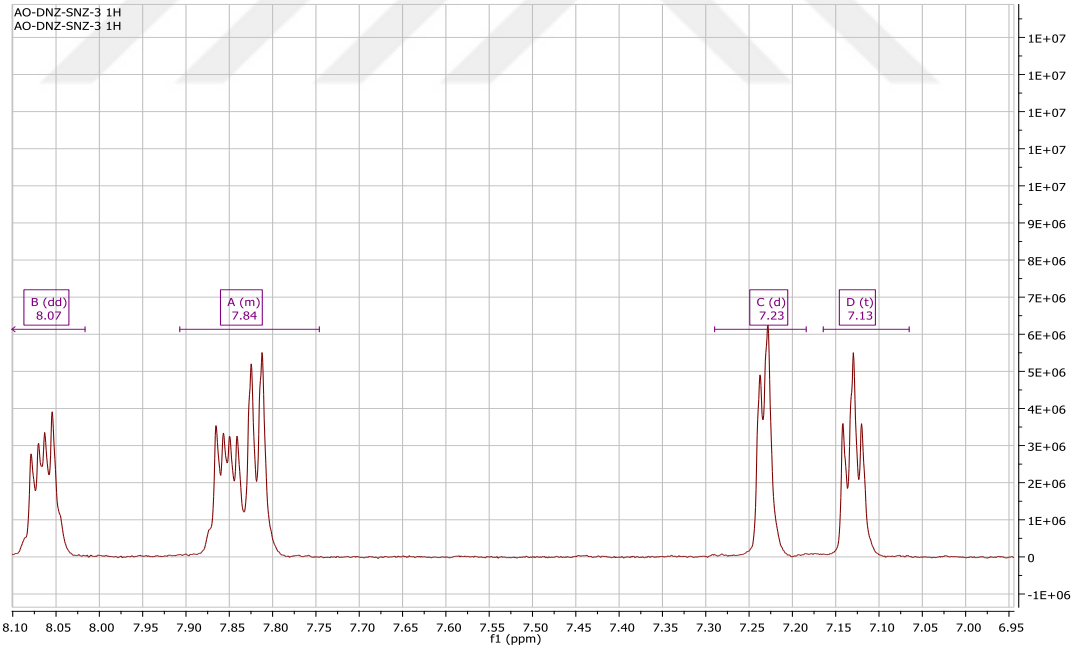

Figure B.4 ^{1}H-NMR spectrum of $[Pt(dtq)_2Cl_2]$ complex in d_6-DMSO.

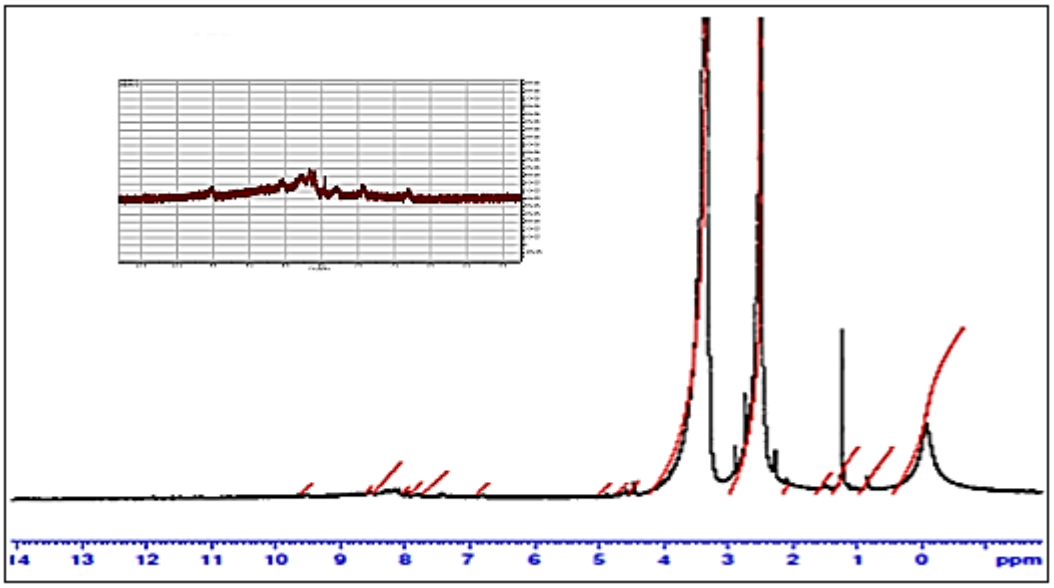

Figure B.5 ^{1}H-NMR spectrum of [Cu(tpbq)Cl_2] complex in d_6-DMSO.

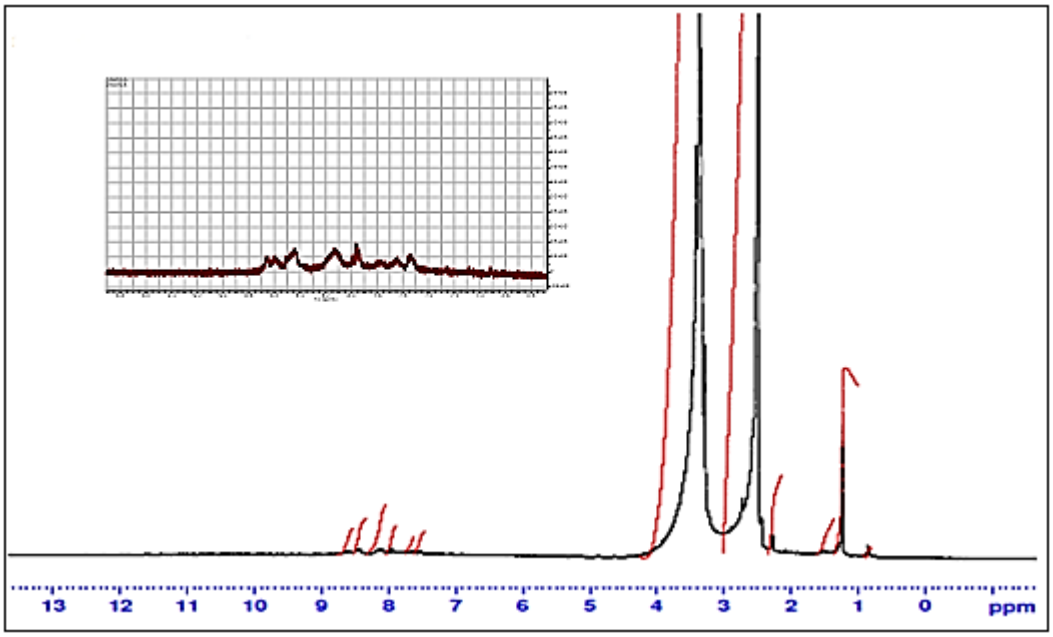

Figure B.6 ^{1}H-NMR spectrum of [Pt(tpbq)Cl_2] complex in d_6-DMSO.

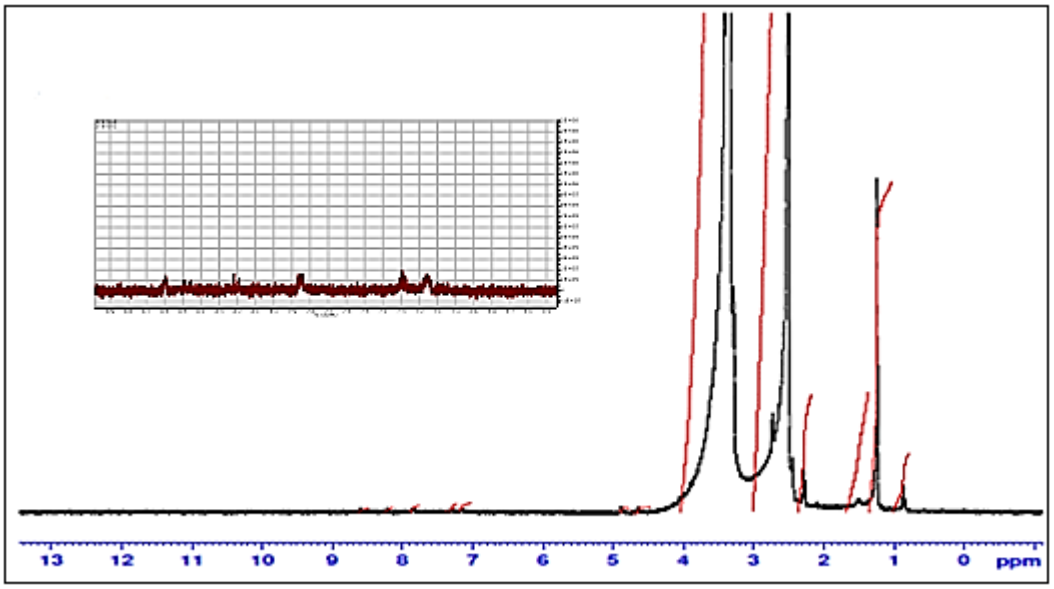

Figure B.7 ^{1}H-NMR spectrum of [Cu(ttbq)Cl_2] complex in d_6-DMSO.

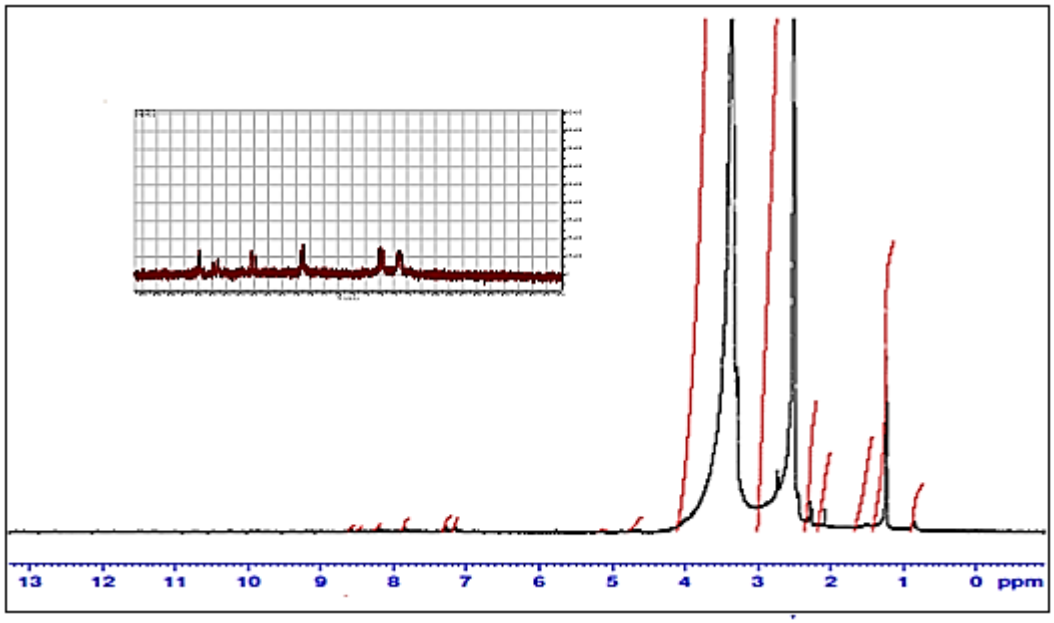

Figure B.8 ^{1}H-NMR spectrum of [Pt(ttbq)Cl_2] complex in d_6-DMSO.

APPENDIX C

INFRARED SPECTRA

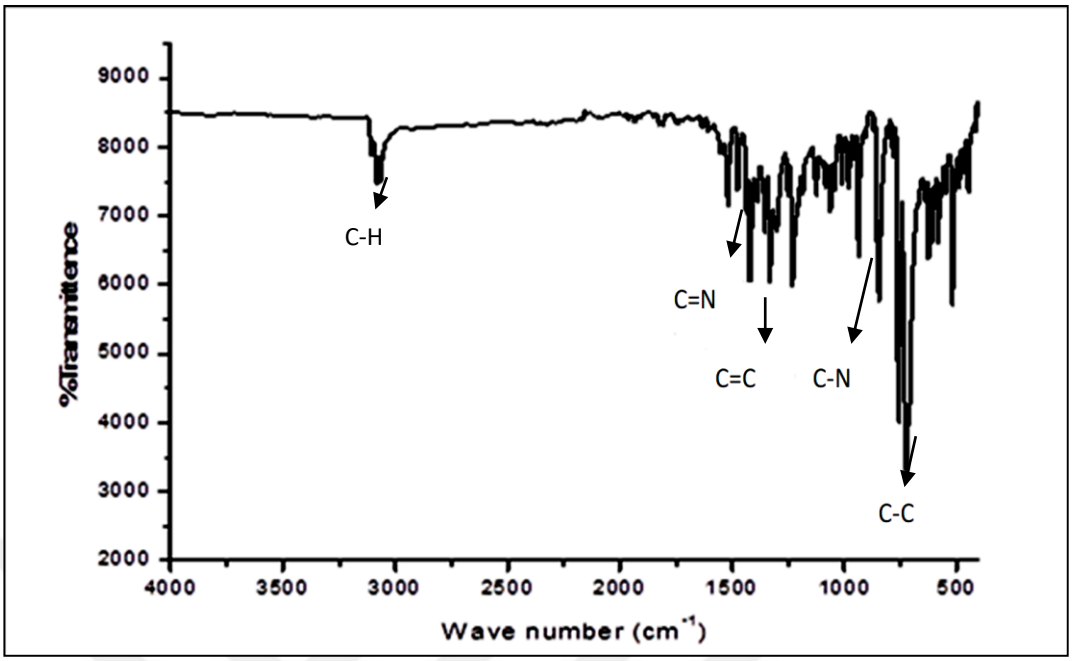

Figure C.1 Infrared spectrum of $[Pt(dpq)_2Cl_2]$ in the range of 4000-400cm^{-1}.

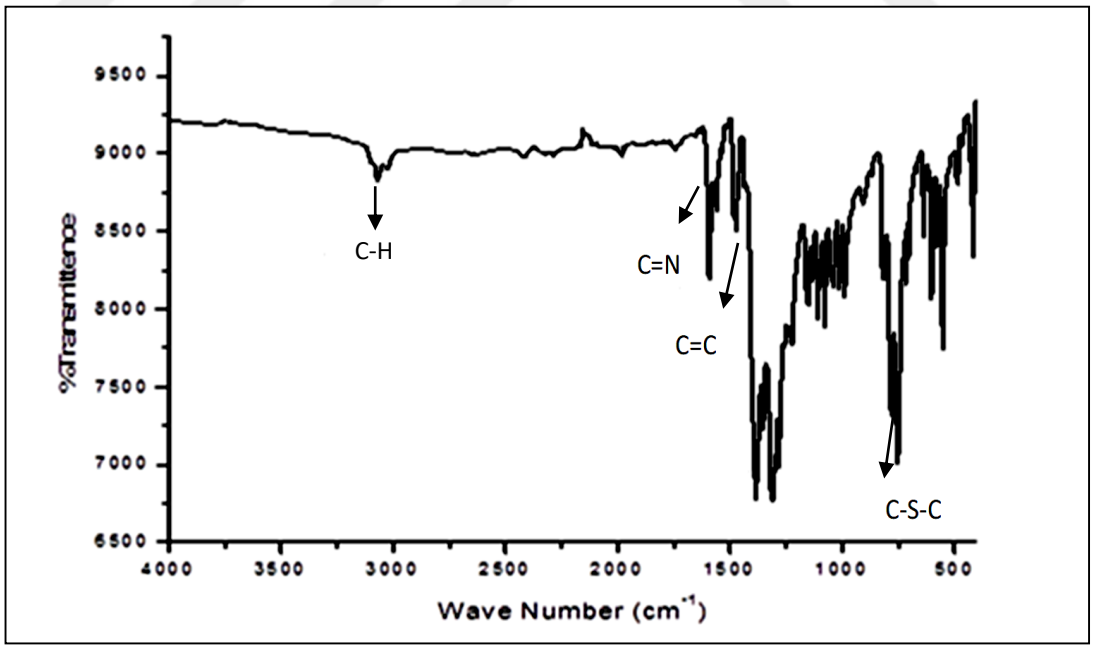

Figure C.2 Infrared spectrum of $[Cu(dtq)_2Cl_2]$ in the range of 4000-400 cm^{-1}

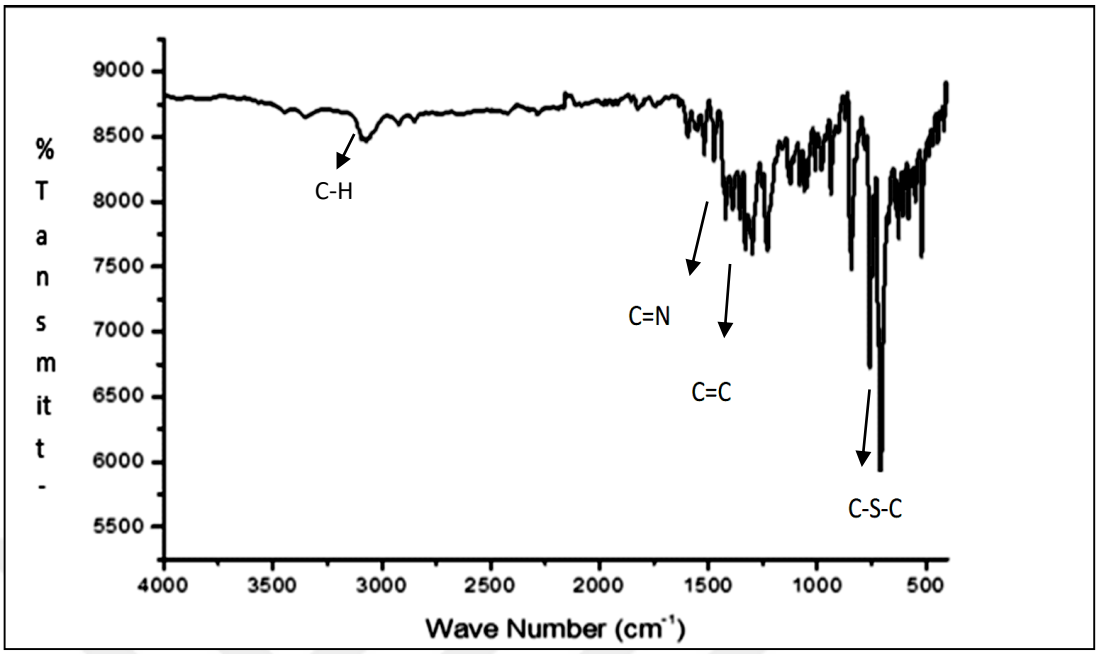

Figure C.3 Infrared spectrum of $[Pt(dtq)_2Cl_2]$ in the range of 4000-400 cm^{-1}.

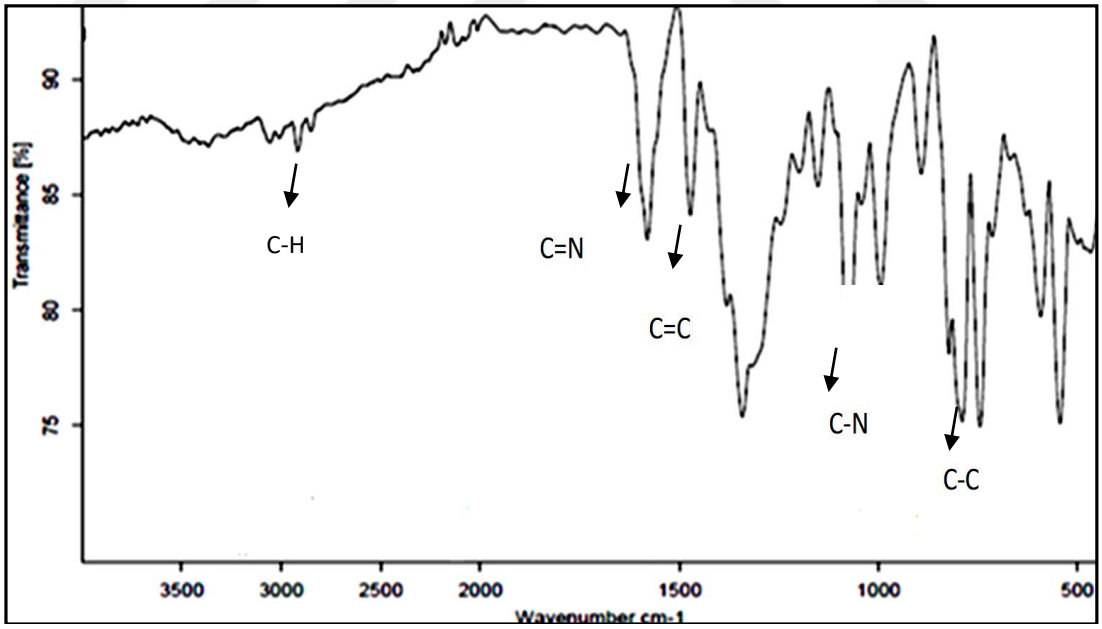

Figure C.4 Infrared spectrum of $[Pt(tpbq)Cl_2]$ in the range of 4000-400 cm^{-1}.

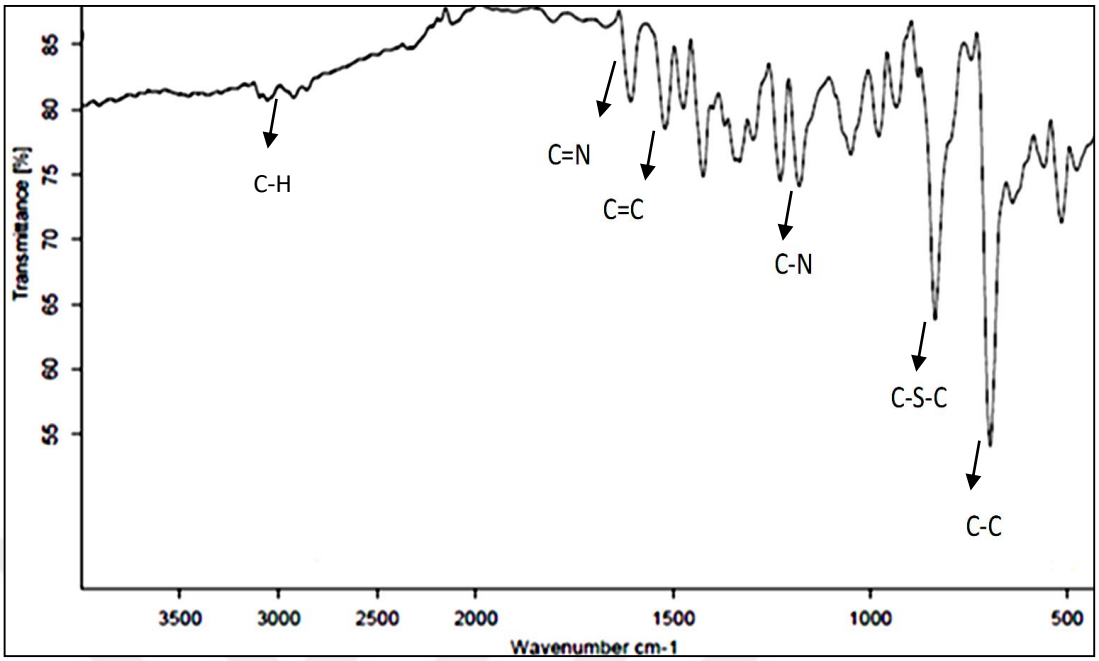

Figure C.5 Infrared spectrum of [Cu(ttbq)Cl_2] in the range of 4000-400 cm^{-1}.

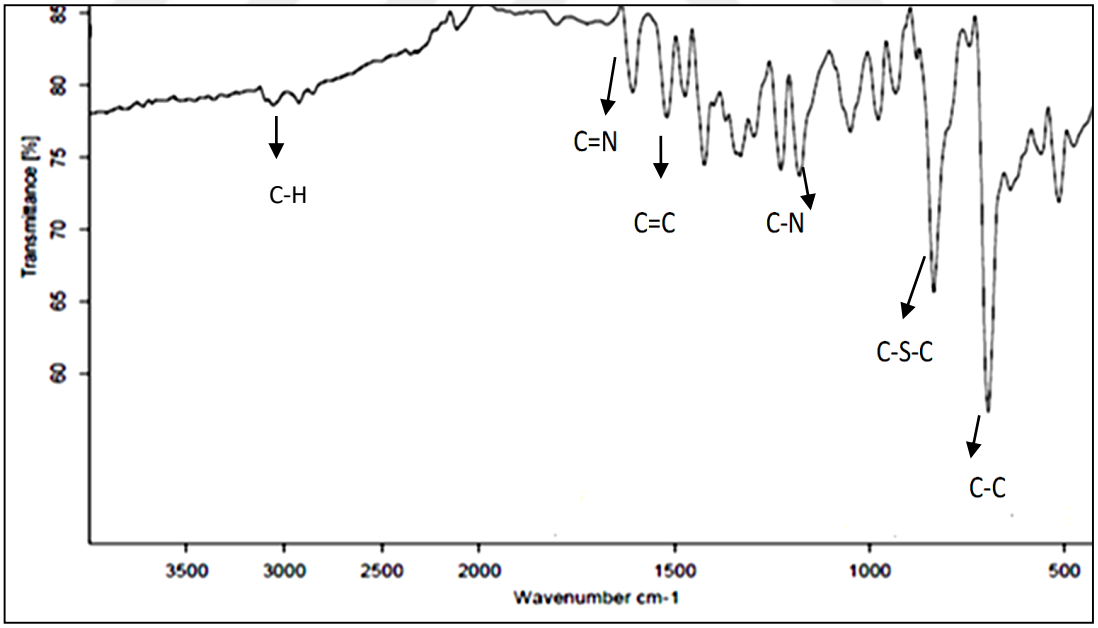

Figure C.6 Infrared spectrum of [Pt(ttbq)Cl_2] in the range of 4000-400 cm^{-1}.

APPENDIX D

RAMAN SPECTRA

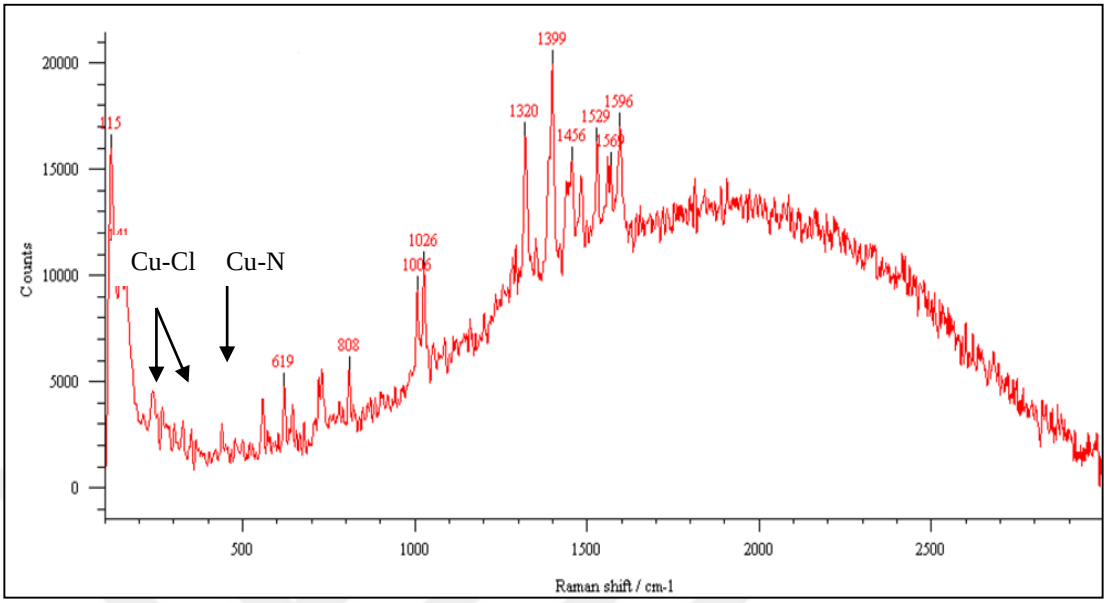

Figure D.1 Raman spectrum of $[Cu(dpq)_2Cl_2]$.

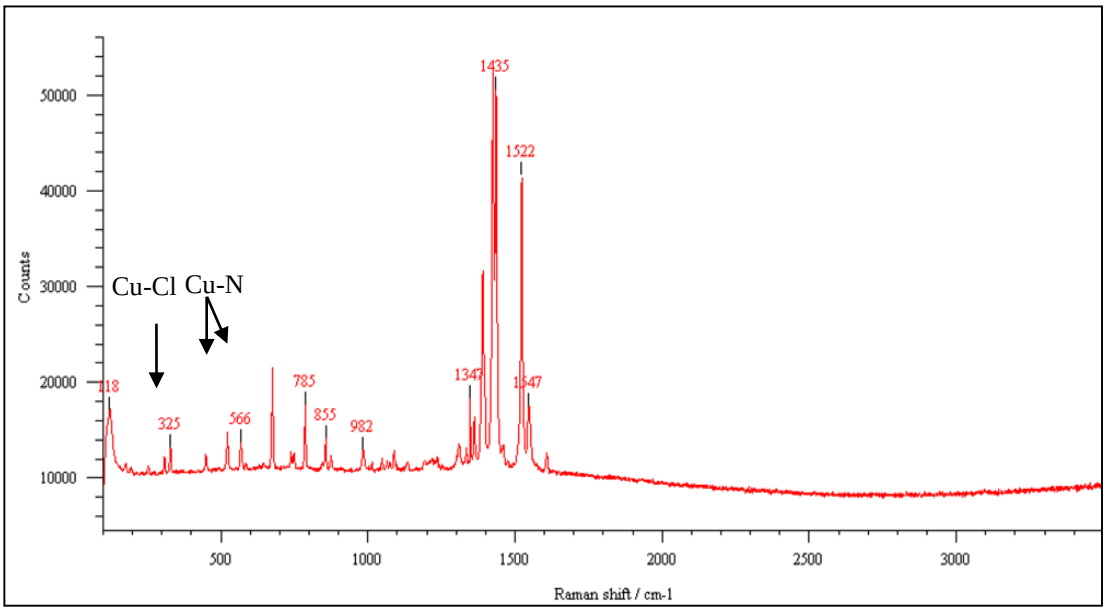

Figure D.2 Raman spectrum of $[Cu(dtq)_2Cl_2]$.

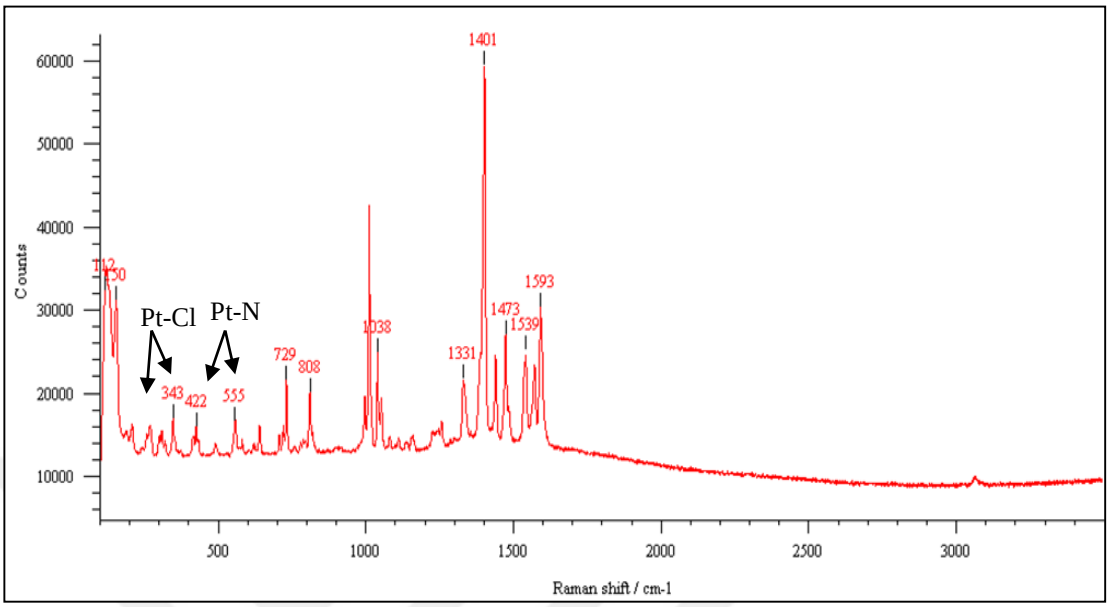

Figure D.3 Raman spectrum of $[Pt(dpq)_2Cl_2]$.

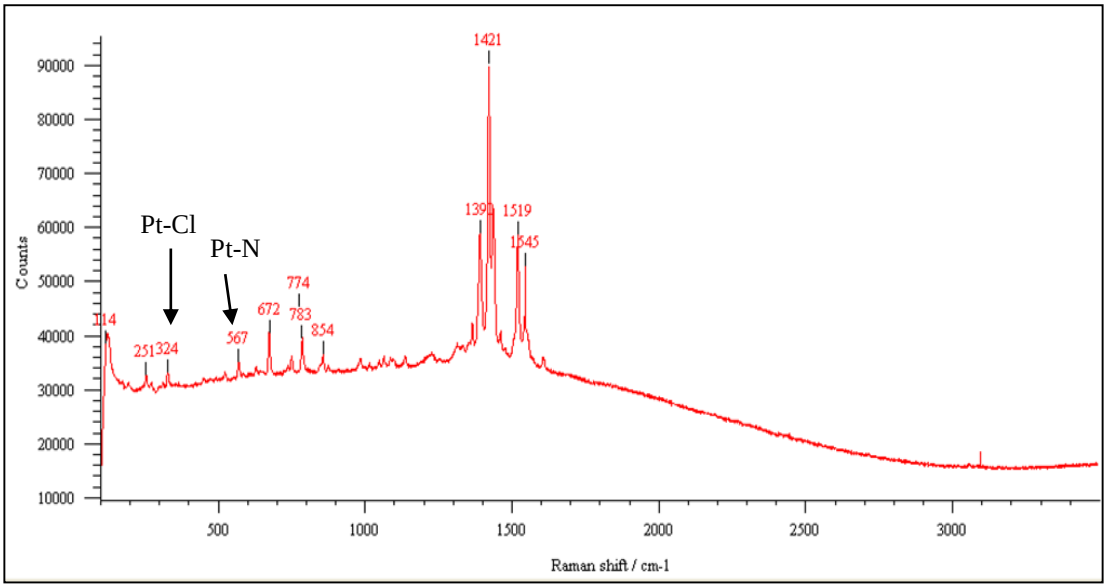

Figure D.4 Raman spectrum of $[Pt(dtq)_2Cl_2]$.

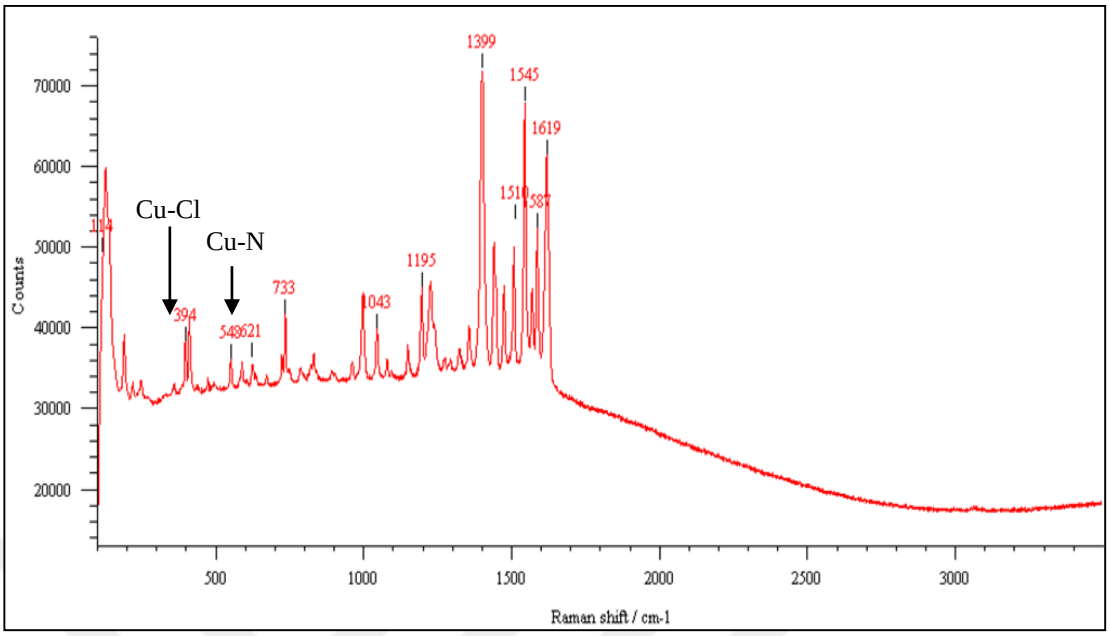

Figure D.5 Raman spectrum of [Cu(tpbq)Cl_2].

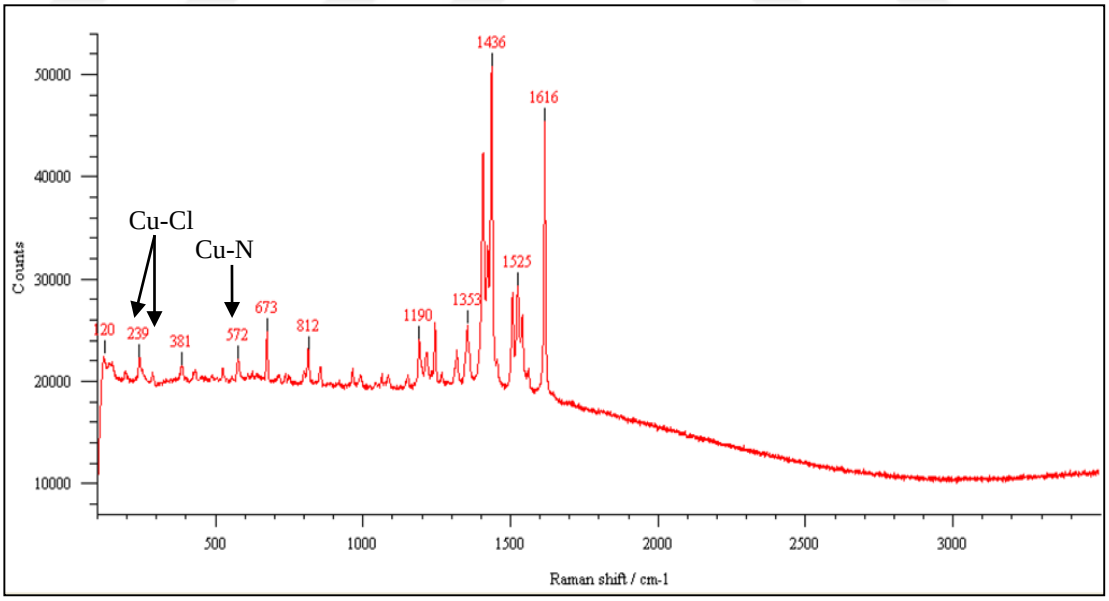

Figure D.6 Raman spectrum of [Cu(ttbq)Cl_2].

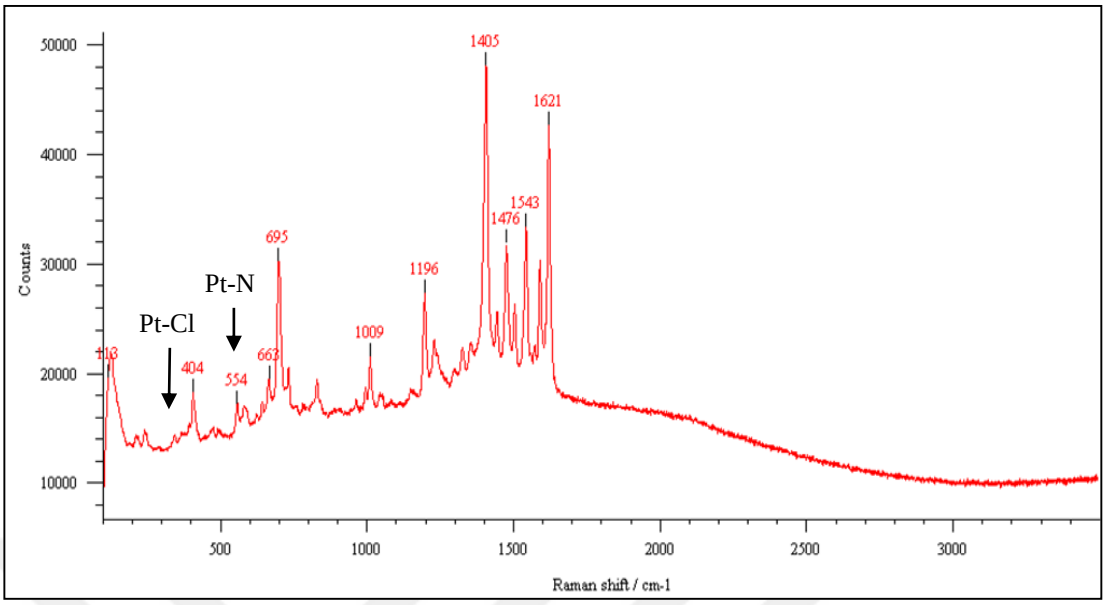

Figure D.7 Raman spectrum of [Pt(tpbq)Cl_2].

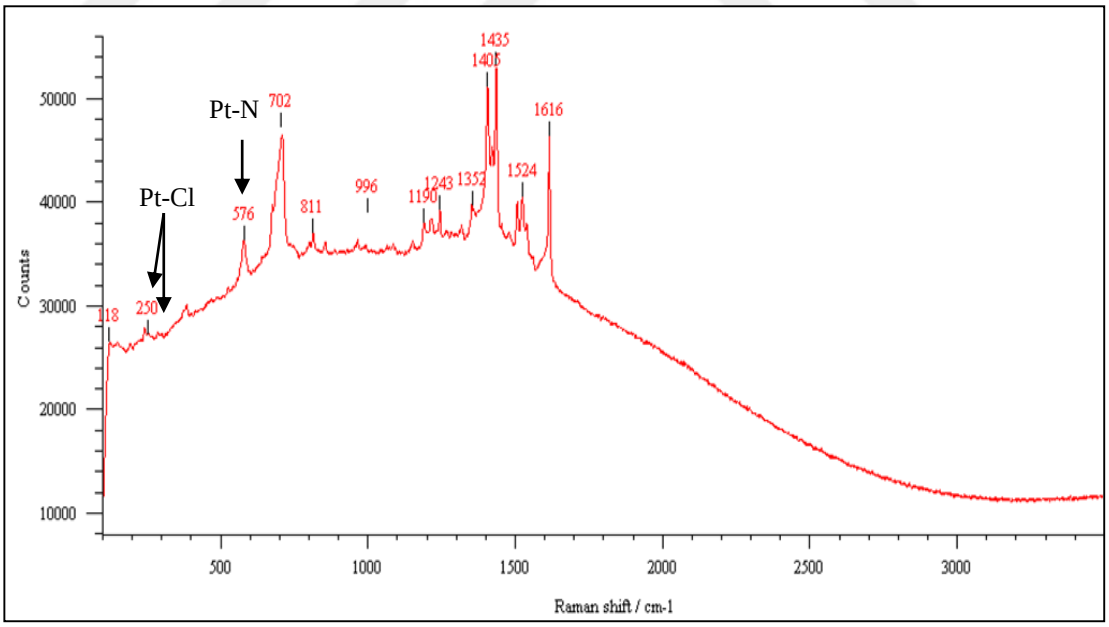

Figure D.8 Raman spectrum of [Pt(ttbq)Cl_2].

APPENDIX E

UV-VIS SPECTRA .AND PLOTS RELATED TO DNA – BINDING ACTIVITY

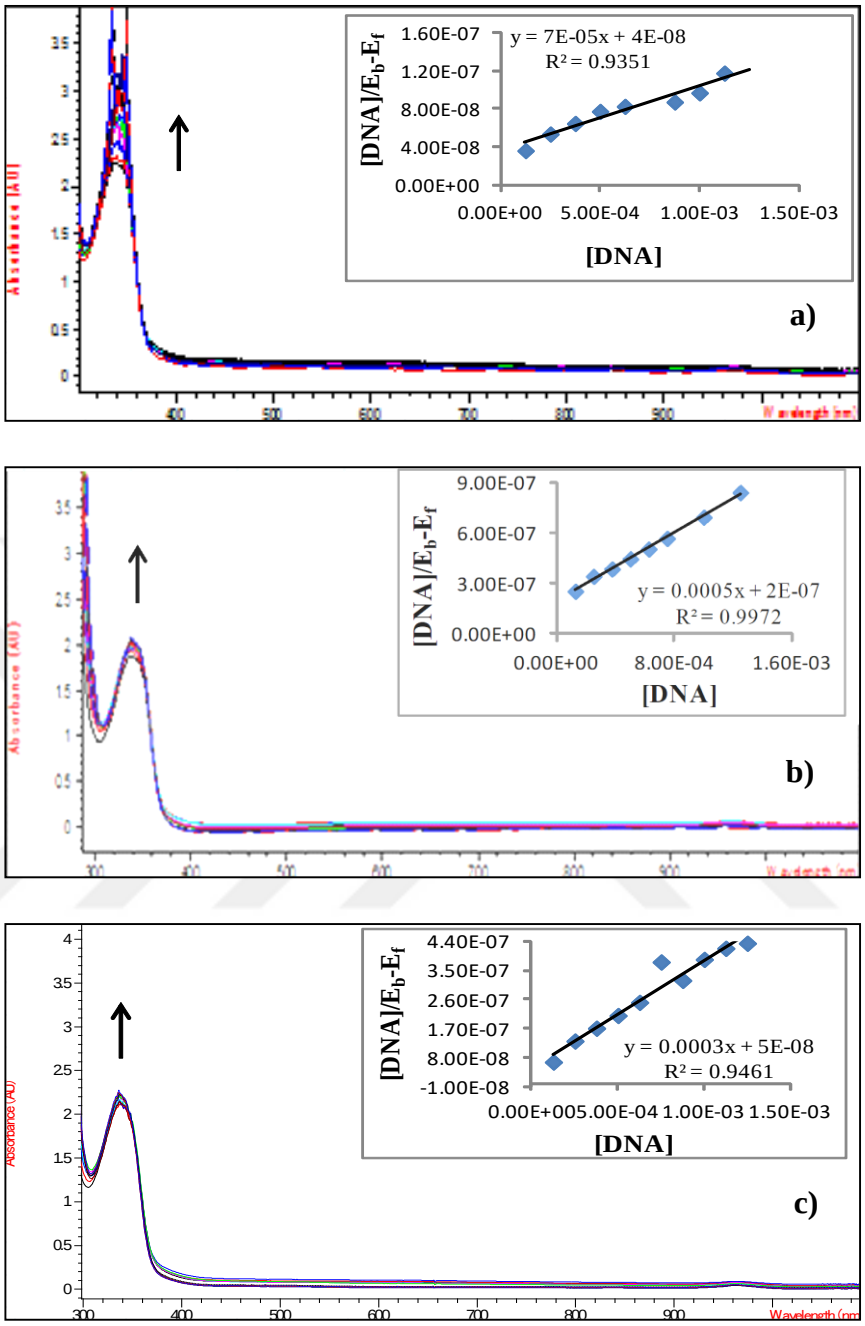

Figure E.1 The change in the electronic absorption spectrum of $[Cu(dpq)_2Cl_2]$ at a) 45 ^oC, b) 57 ^oC and c) 67 ^oC), in Tris-HCl buffer (pH = 7.10) in the absence and in the presence of CT-DNA (R=0-10). Inset: Plot of [DNA]/ $[\varepsilon_a - \varepsilon_f]$ *vs.* [DNA].

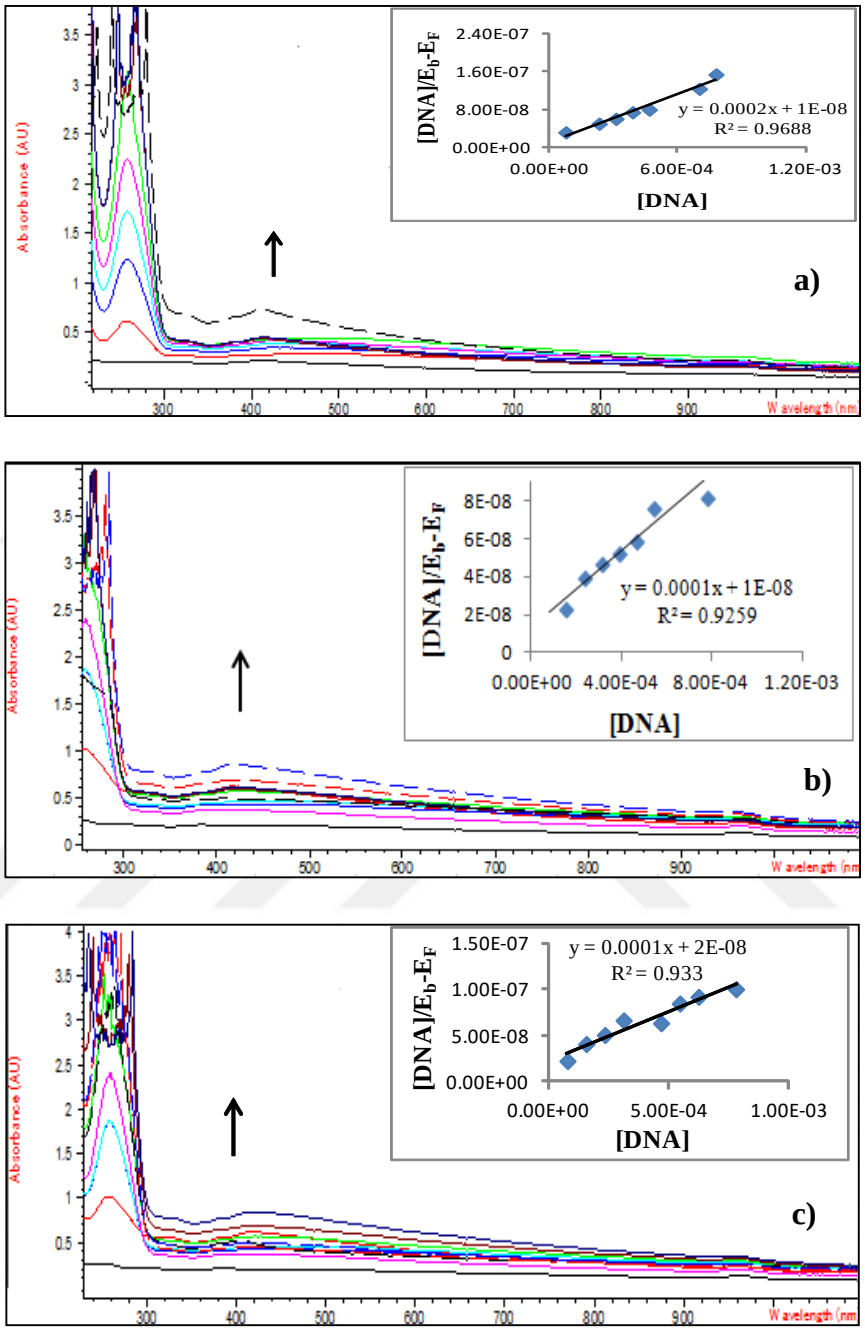

Figure E.2 The change in the electronic absorption spectrum of $[Cu(dtq)_2Cl_2]$ at a) 45 ^oC, b) 57 ^oC and c) 67 ^oC), in Tris-HCl buffer (pH = 7.10) in the absence and in the presence of CT-DNA (R=0-10). Inset: Plot of [DNA]/ $[\varepsilon_a - \varepsilon_f]$ *vs.* [DNA].

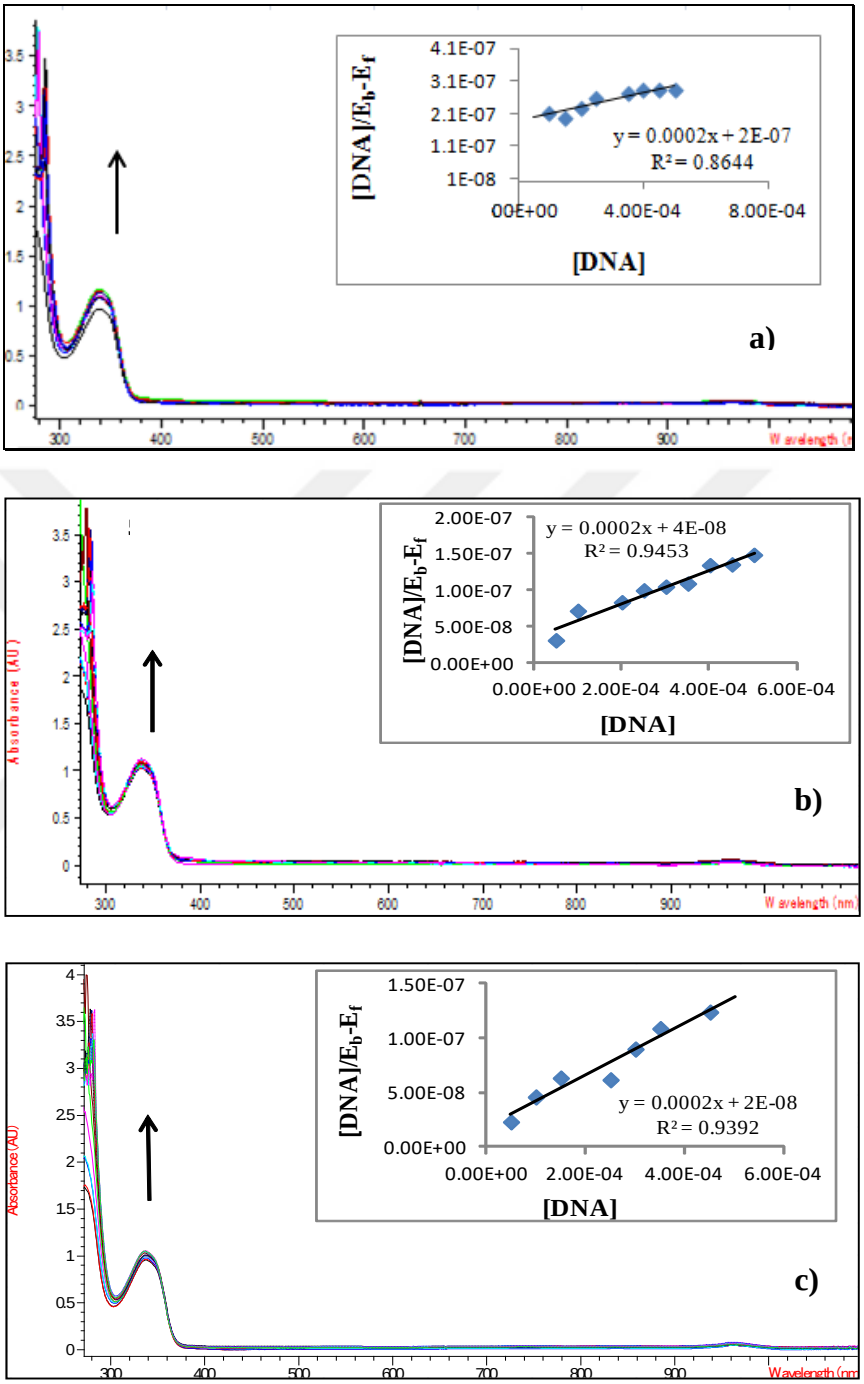

Figure E.3 The change in the electronic absorption spectrum of $[Pt(dpq)_2Cl_2]$ at a) 45 ^oC, b) 57 ^oC and c) 67 ^oC), in Tris-HCl buffer (pH = 7.10) in the absence and in the presence of CT-DNA (R=0-10). Inset: Plot of [DNA]/ $[\varepsilon_a - \varepsilon_f]$ *vs.* [DNA].

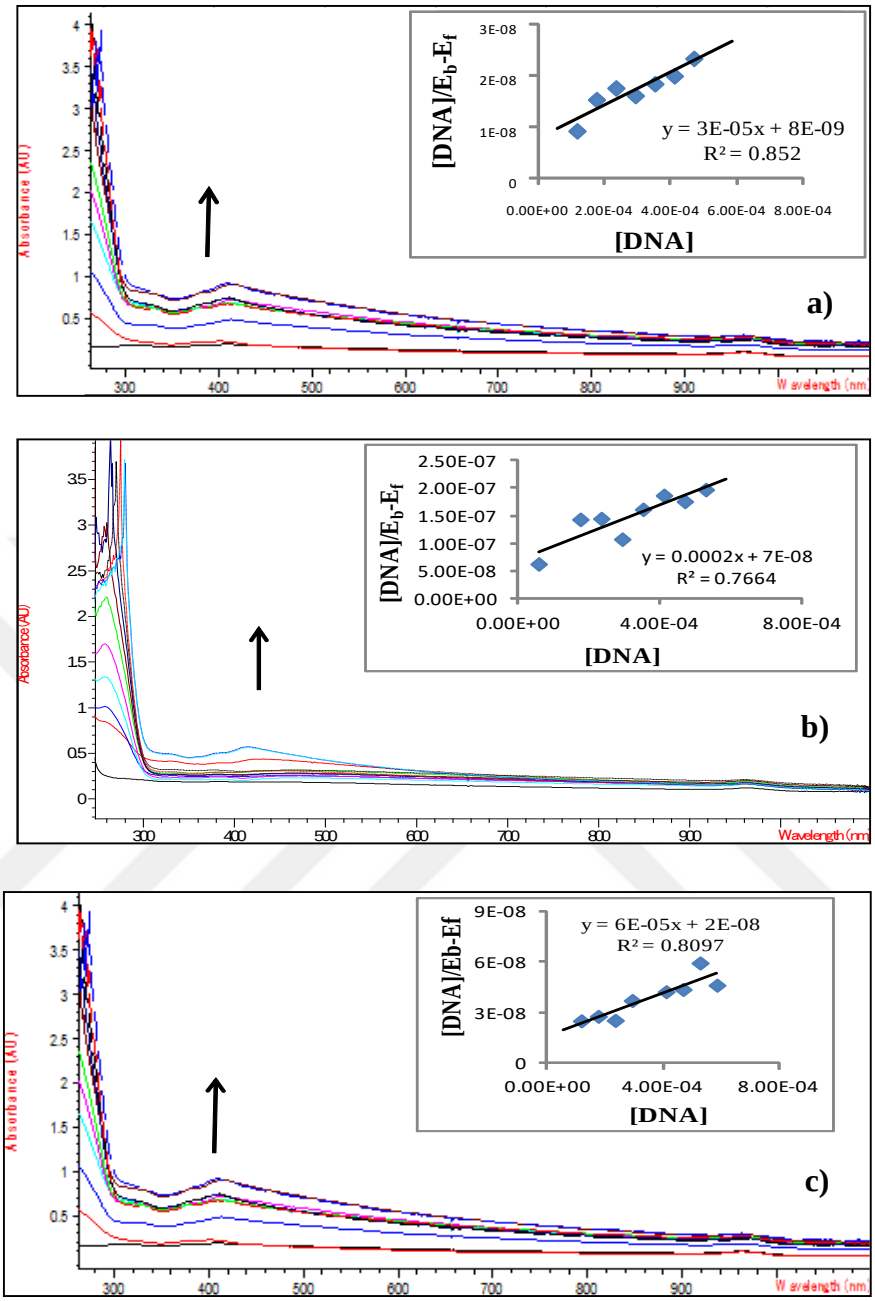

Figure E.4 The change in the electronic absorption spectrum of $[Pt(dtq)_2Cl_2]$ at a) 45 ^oC, b) 57 ^oC and c) 67 ^oC), in Tris-HCl buffer (pH = 7.10) in the absence and in the presence of CT-DNA (R=0-10). Inset: Plot of [DNA]/ $[\varepsilon_a - \varepsilon_f]$ *vs.* [DNA].

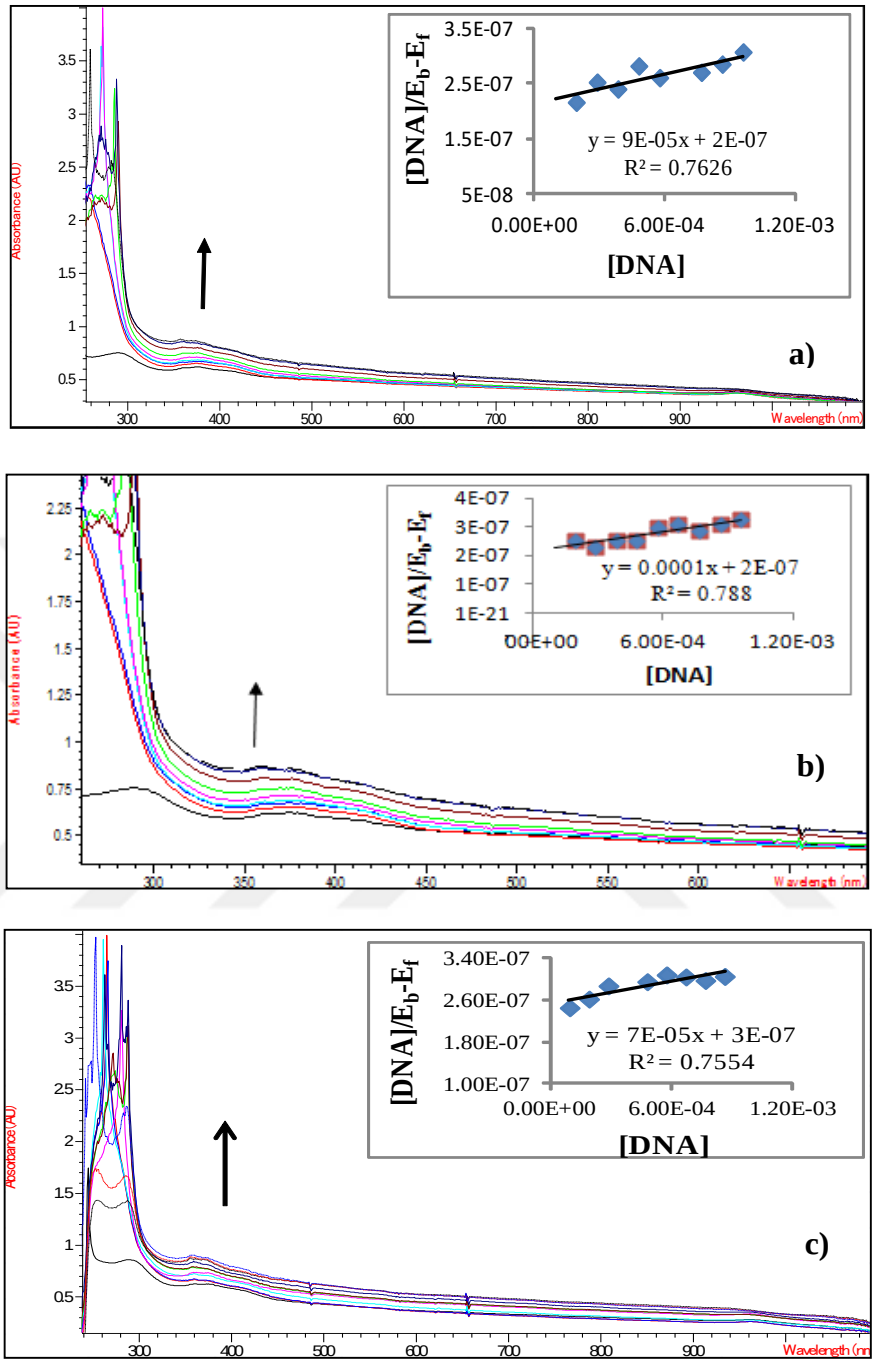

Figure E.5 The change in the electronic absorption spectrum of [Cu(tpbq)Cl_2] at a) 45 ^{o}C, b) 57 ^{o}C and c) 67 ^{o}C), in Tris-HCl buffer (pH = 7.10) in the absence and in the presence of CT-DNA (R=0-10). Inset: Plot of [DNA]/ [$\varepsilon_a - \varepsilon_f$] *vs.* [DNA].

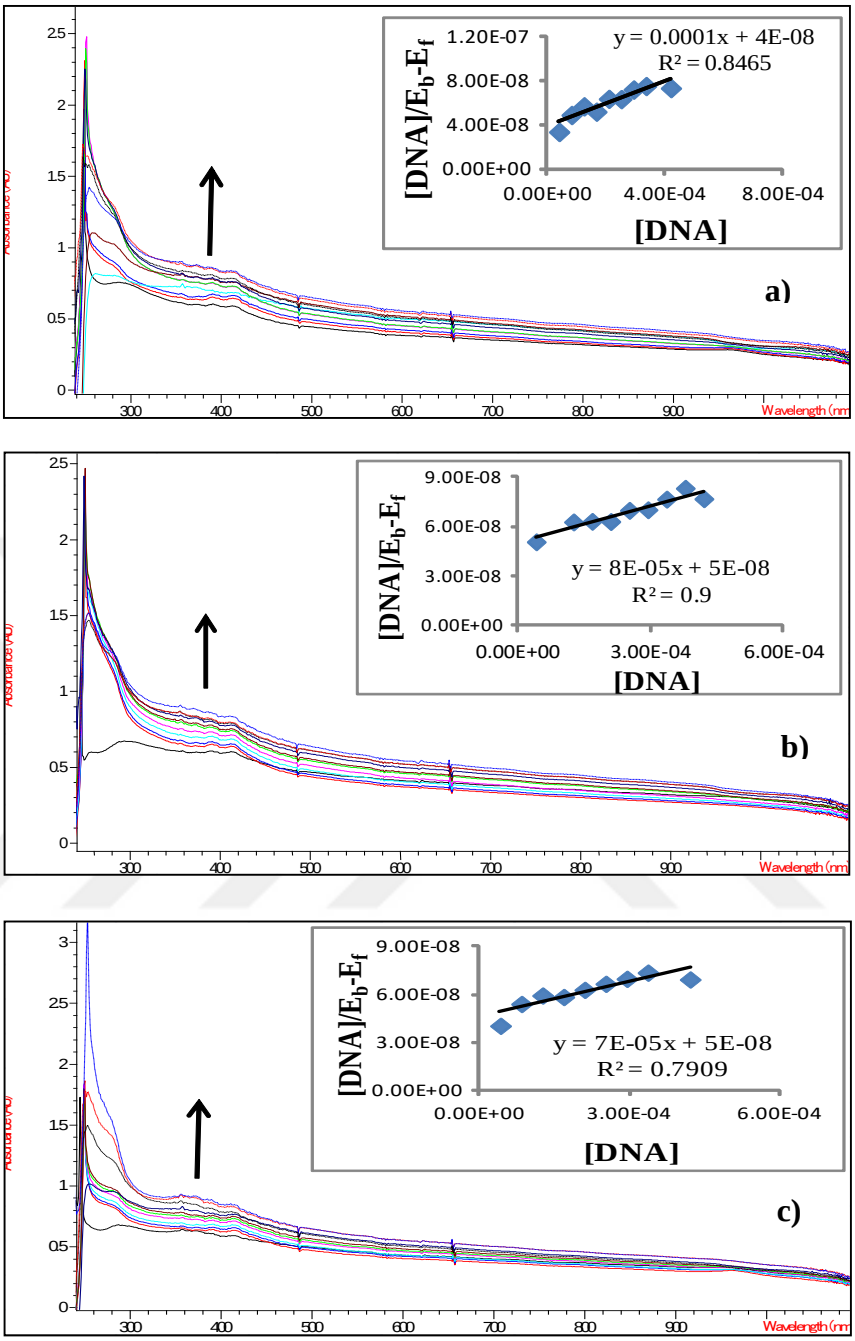

Figure E.6 The change in the electronic absorption spectrum of [Cu(ttbq)Cl_2] at a) 45 ^oC, b) 57 ^oC and c) 67 ^oC), in Tris-HCl buffer (pH = 7.10) in the absence and in the presence of CT-DNA (R=0-10). Inset: Plot of [DNA]/ [$\varepsilon_a - \varepsilon_f$] *vs.* [DNA].

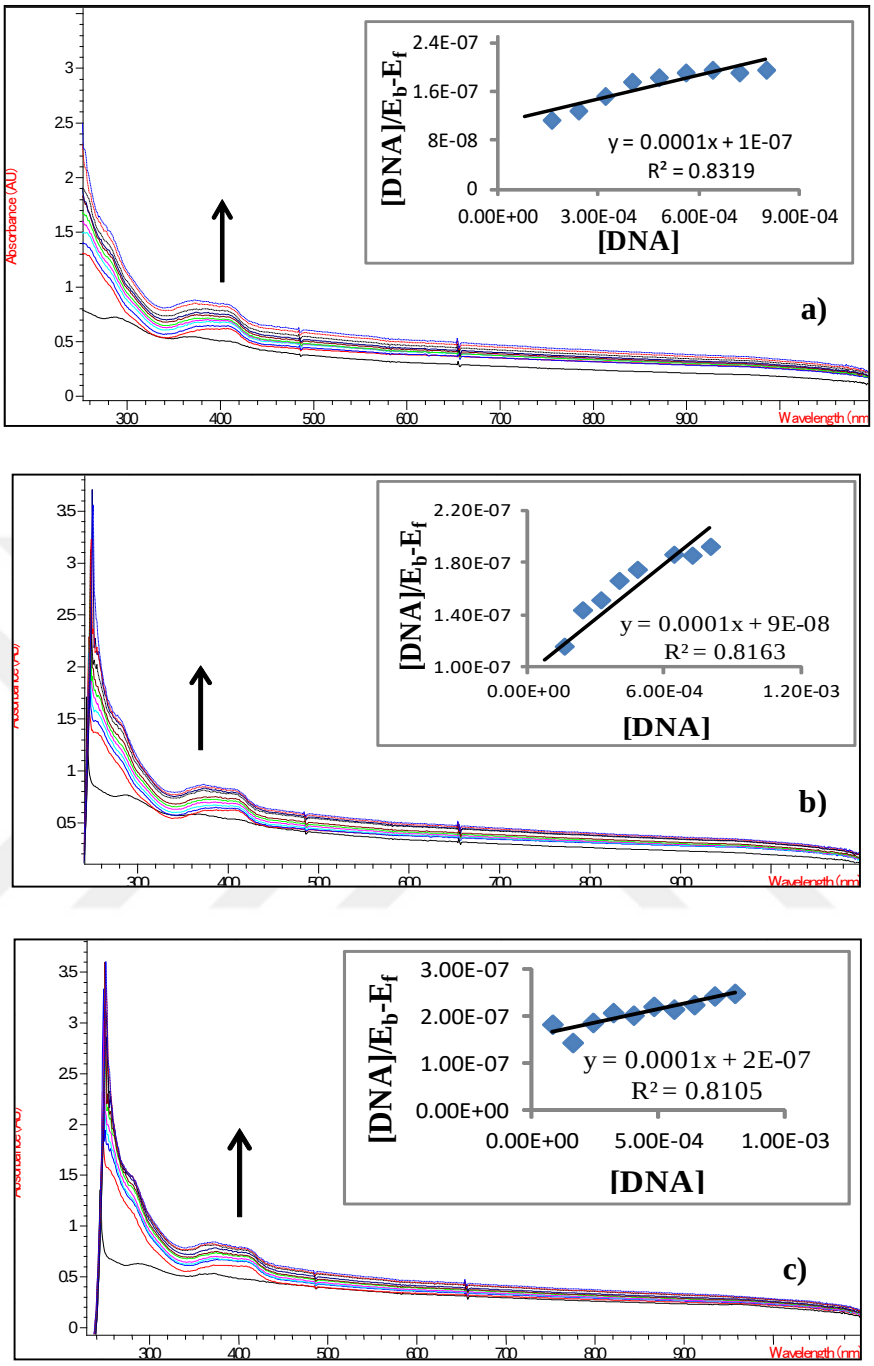

Figure E.7 The change in the electronic absorption spectrum of [Pt(tpbq)Cl_2] at a) 45 ^oC, b) 57 ^oC and c) 67 ^oC), in Tris-HCl buffer (pH = 7.10) in the absence and in the presence of CT-DNA (R=0-10). Inset: Plot of [DNA]/ [$\varepsilon_a - \varepsilon_f$] *vs.* [DNA].

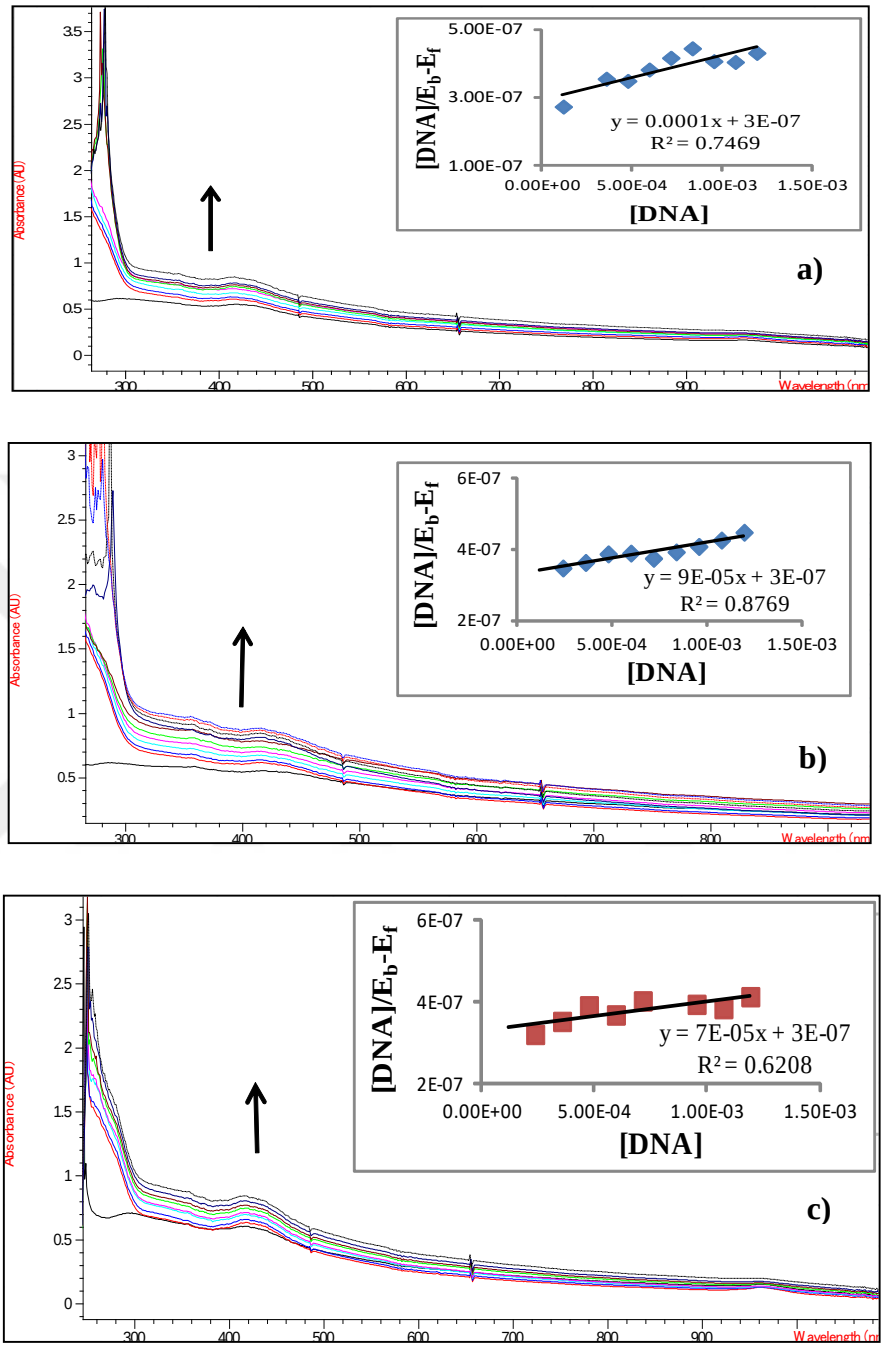

Figure E.8 The change in the electronic absorption spectrum of [Pt(ttbq)Cl_2] at a) 45 ^oC, b) 57 ^oC and c) 67 ^oC), in Tris-HCl buffer (pH = 7.10) in the absence and in the presence of CT-DNA (R=0-10). Inset: Plot of [DNA]/ [$\varepsilon_a - \varepsilon_f$] *vs.* [DNA].

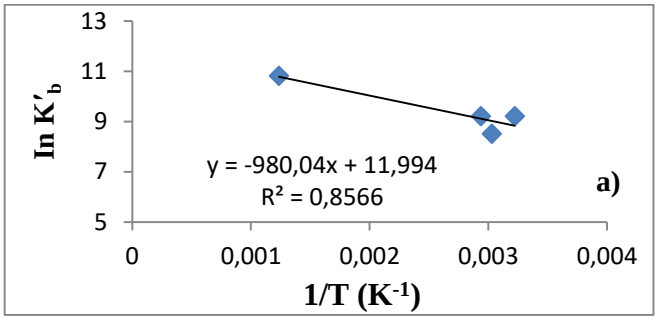

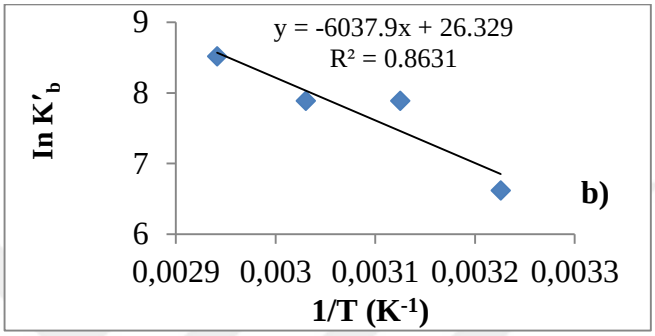

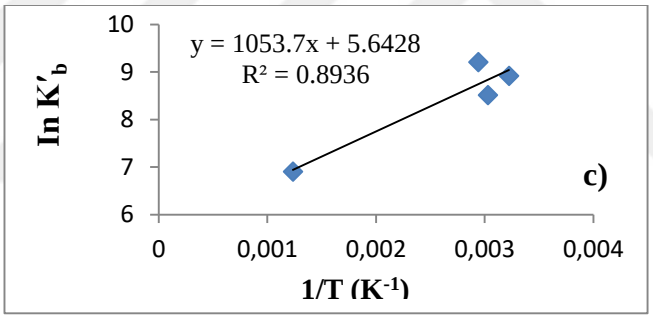

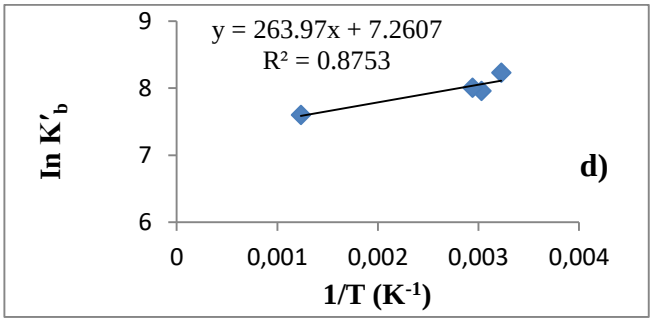

Figure E.9 The linear van't Hoff plot based on ln K'_b versus 1/T for a) $[Cu(dpq)_2Cl_2]$, b) $[Cu(dtq)_2Cl_2]$, c) $[Pt(dpq)_2Cl_2]$, d) $[Pt(dtq)_2Cl_2]$.

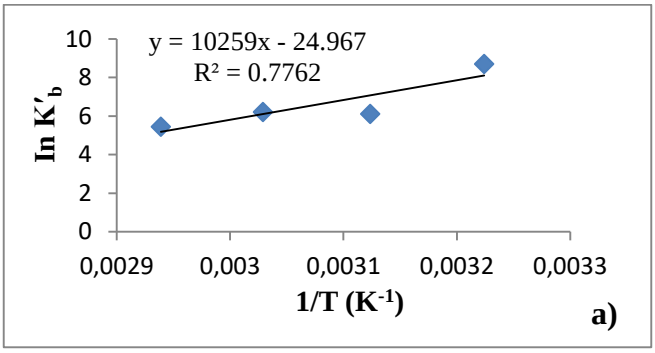

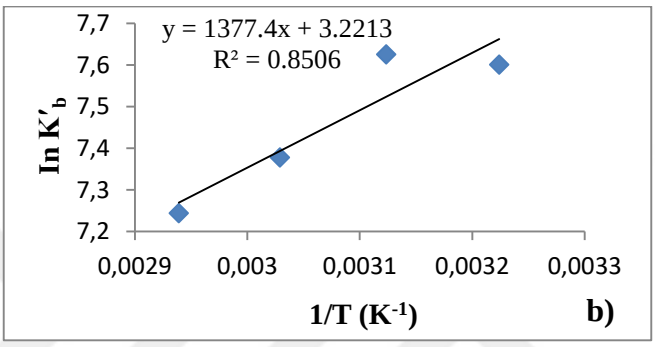

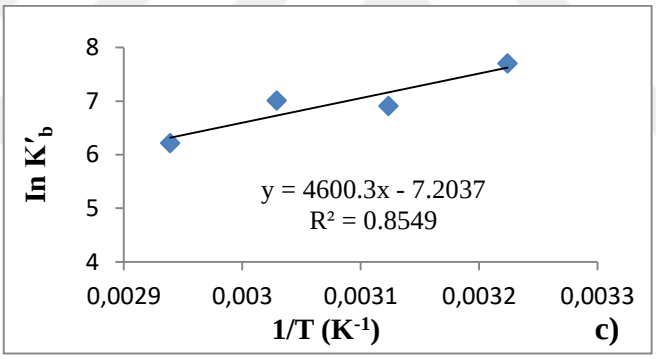

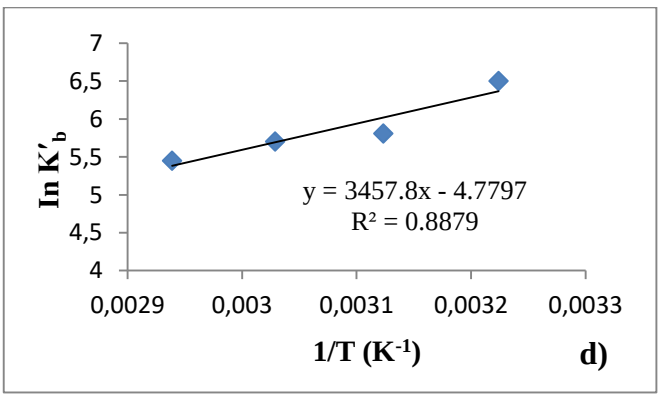

Figure E.10 The linear van't Hoff plot based on ln K′$_b$ versus 1/T for a) [Cu(tpbq)Cl$_2$], b) [Cu(ttbq)Cl$_2$], c) [Pt(tpbq)Cl$_2$], d) [Pt(ttbq)Cl$_2$].

APPENDIX F

UV-VIS SPECTRA .AND PLOTS RELATED TO HSA – BINDING ACTIVITY

.

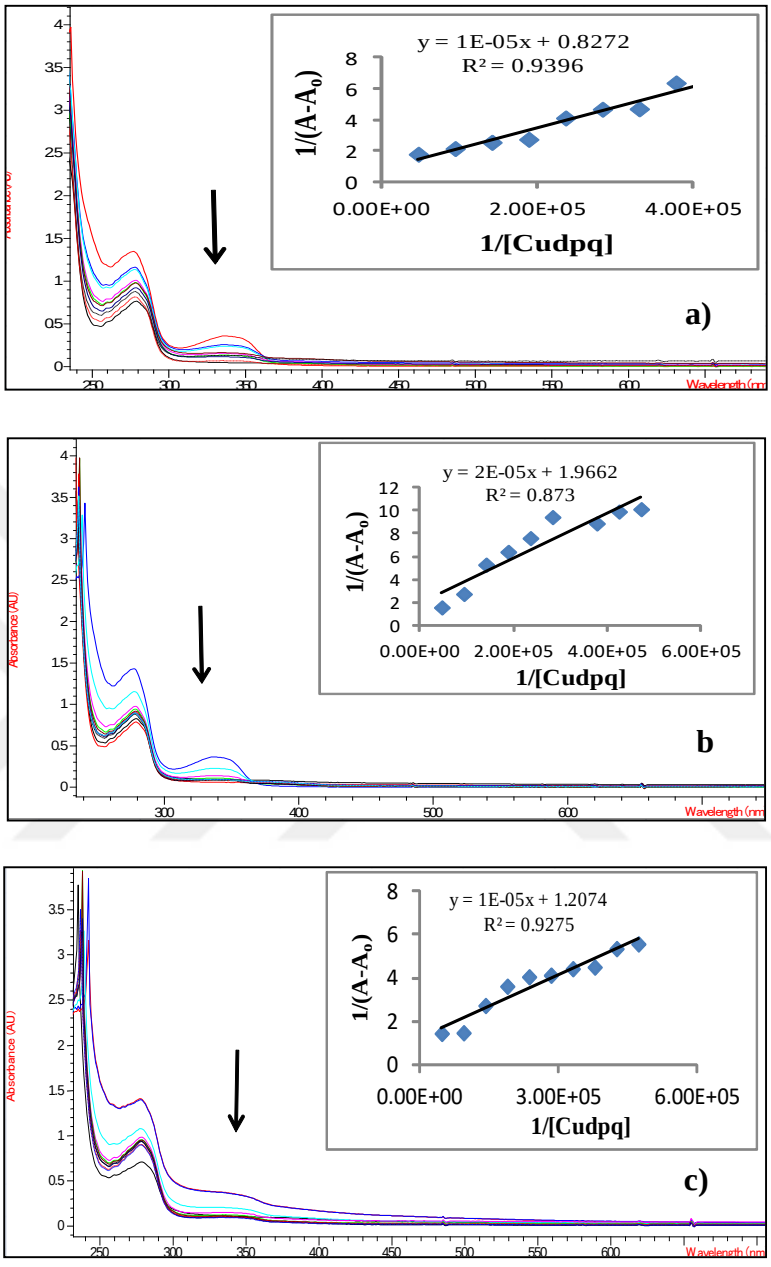

Figure F.1 The change in the electronic absorption spectrum of $[Cu(dpq)_2Cl_2]$ at a) 45 ^oC, b) 57 ^oC and c) 67 ^oC), in Tris-HCl buffer (pH = 7.10) in the absence and in the presence of HSA (R=0-10). Inset: Plot of $1/(A–A_o)$ vs $1/[Cu(dpq)_2Cl_2]$.

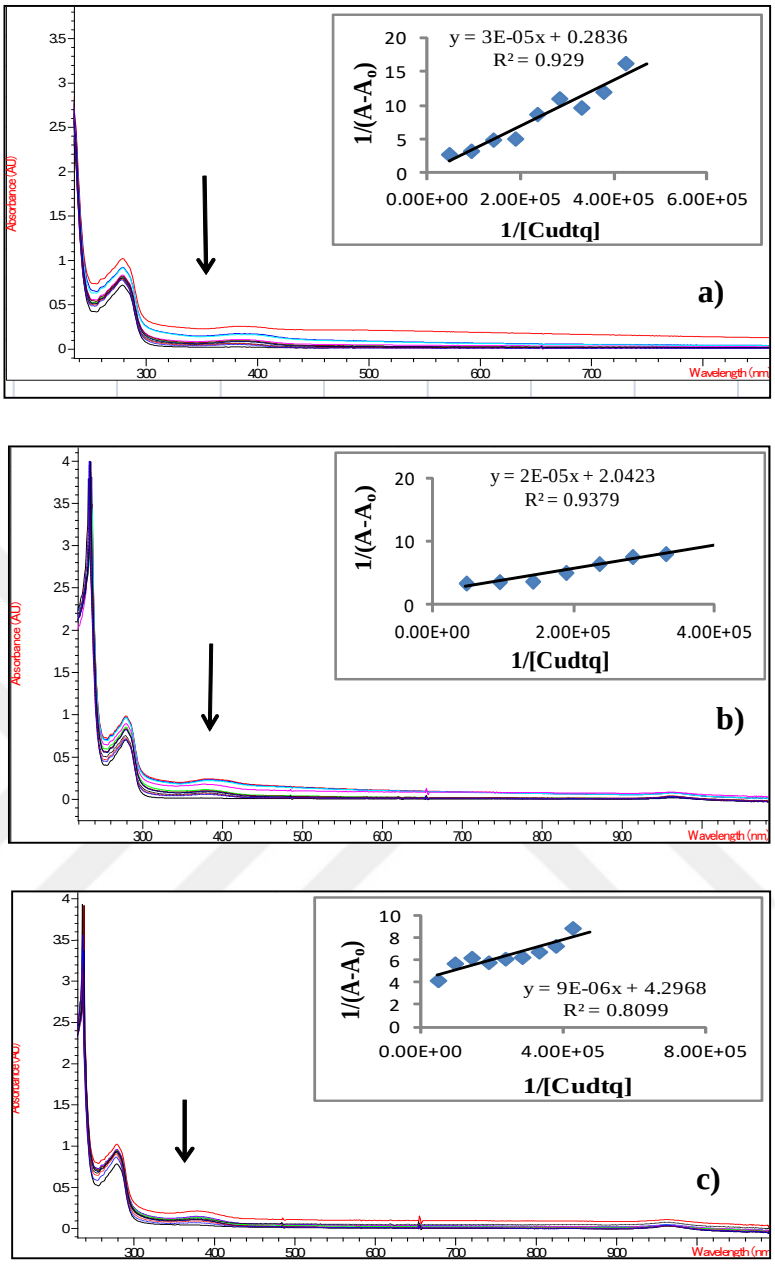

Figure F.2 The change in the electronic absorption spectrum of $[Cu(dtq)_2Cl_2]$ at a) 45 ^oC, b) 57 ^oC and c) 67 ^oC), in Tris-HCl buffer (pH = 7.10) in the absence and in the presence of HSA (R=0-10). Inset: Plot of $1/(A–A_o)$ vs $1/ [Cu(dtq)_2Cl_2]$.

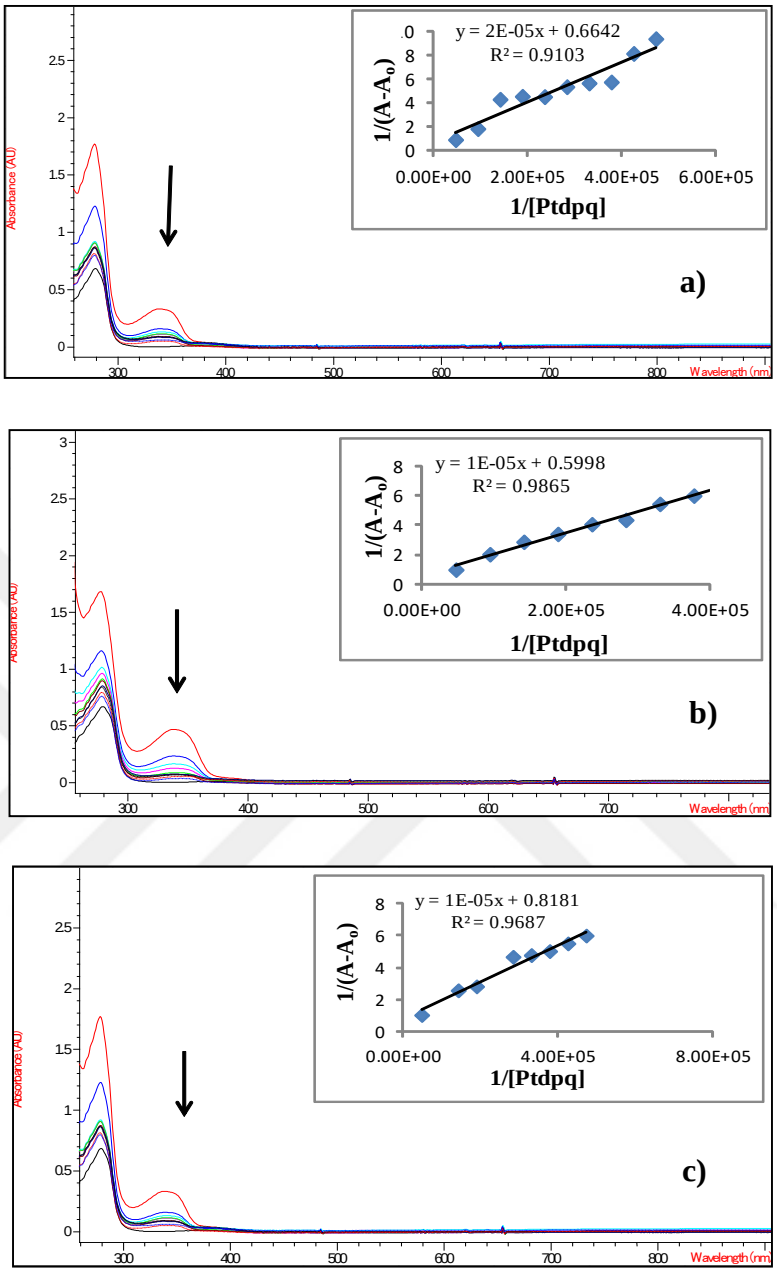

Figure F.3 The change in the electronic absorption spectrum of $[Pt(dpq)_2Cl_2]$ at a) 45 ^oC, b) 57 ^oC and c) 67 ^oC), in Tris-HCl buffer (pH = 7.10) in the absence and in the presence of HSA (R=0-10). Inset: Plot of $1/(A–A_o)$ vs $1/ [Pt(dpq)_2Cl_2]$.

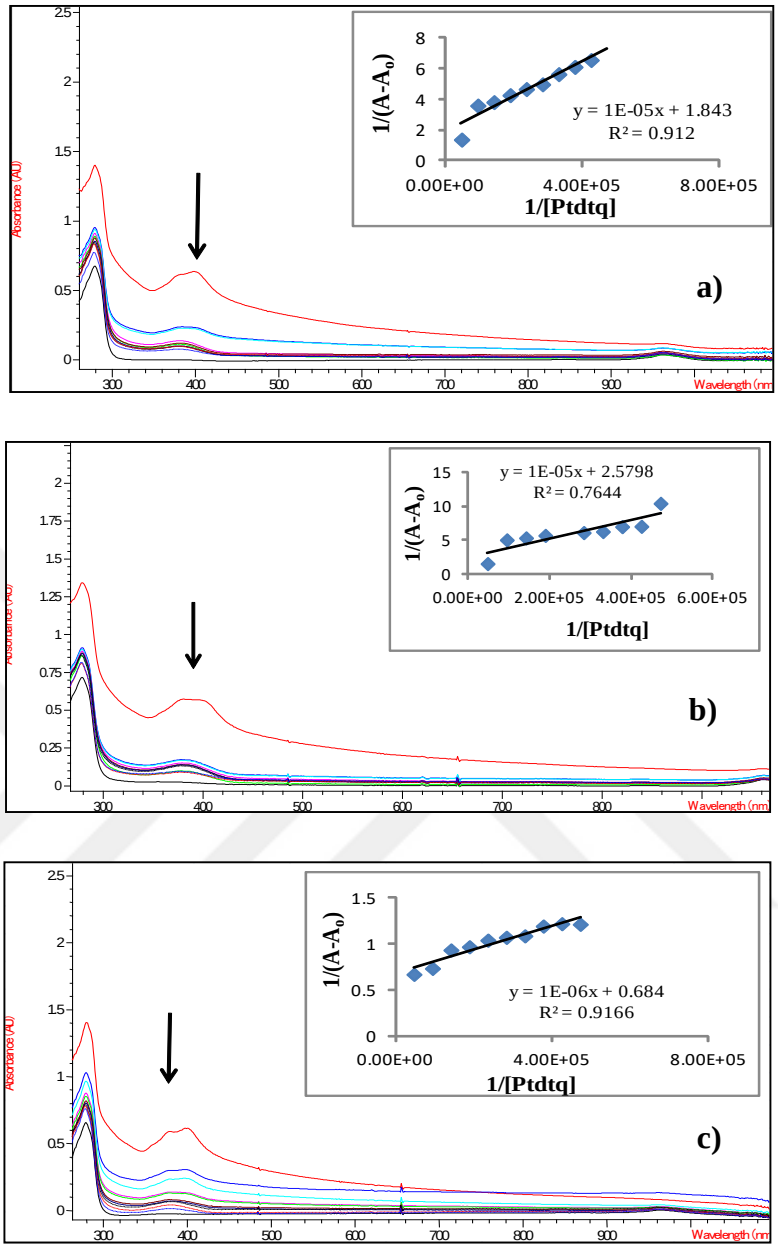

Figure F.4 The change in the electronic absorption spectrum of $[Pt(dtq)_2Cl_2]$ at a) 45 ^oC, b) 57 ^oC and c) 67 ^oC), in Tris-HCl buffer (pH = 7.10) in the absence and in the presence of HSA (R=0-10). Inset: Plot of $1/(A–A_o)$ vs $1/ [Pt(dtq)_2Cl_2]$.

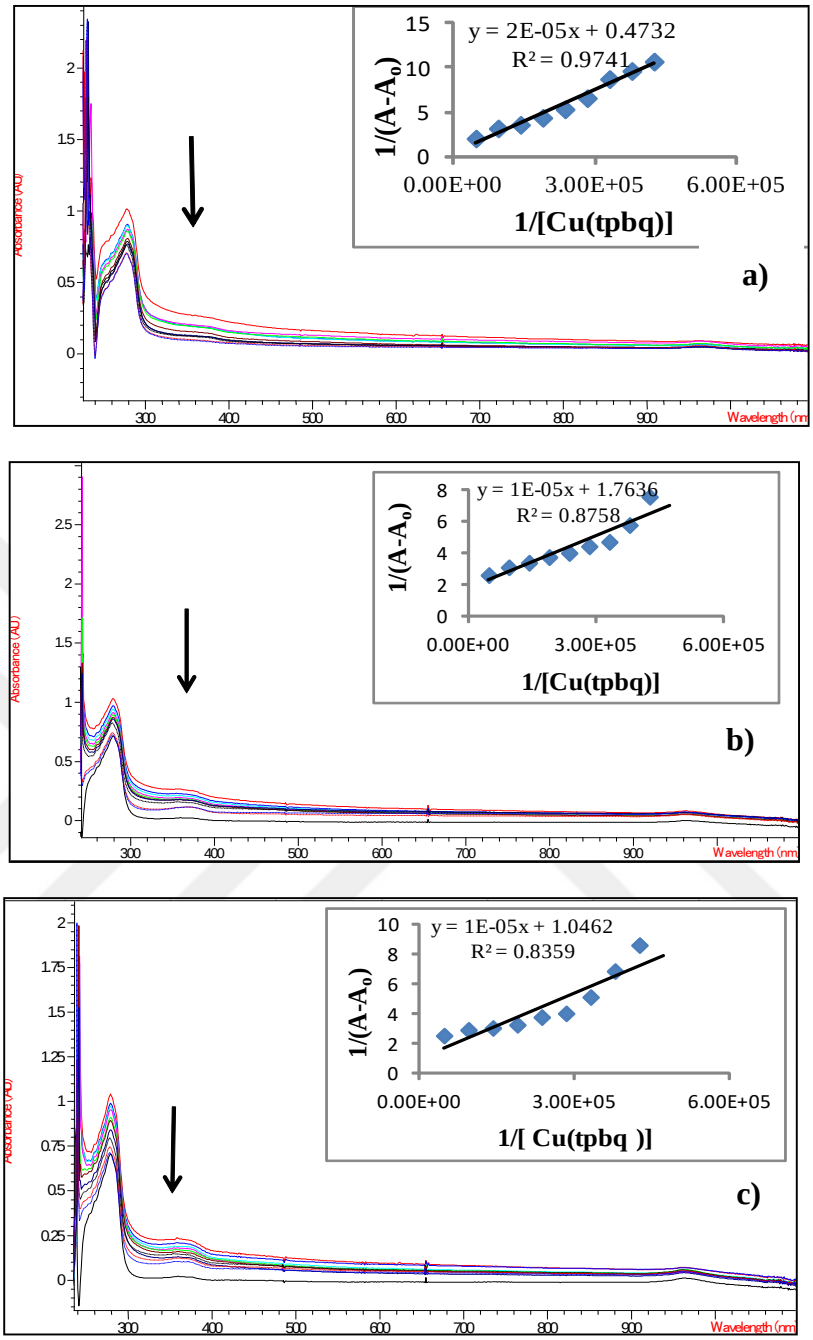

Figure F.5 The change in the electronic absorption spectrum of $[Cu(tpbq)Cl_2]$ at a) 45 ^oC, b) 57 ^oC and c) 67 ^oC), in Tris-HCl buffer (pH = 7.10) in the absence and in the presence of HSA (R=0-10). Inset: Plot of $1/(A–A_o)$ vs $1/ [Cu(tpbq)Cl_2]$.

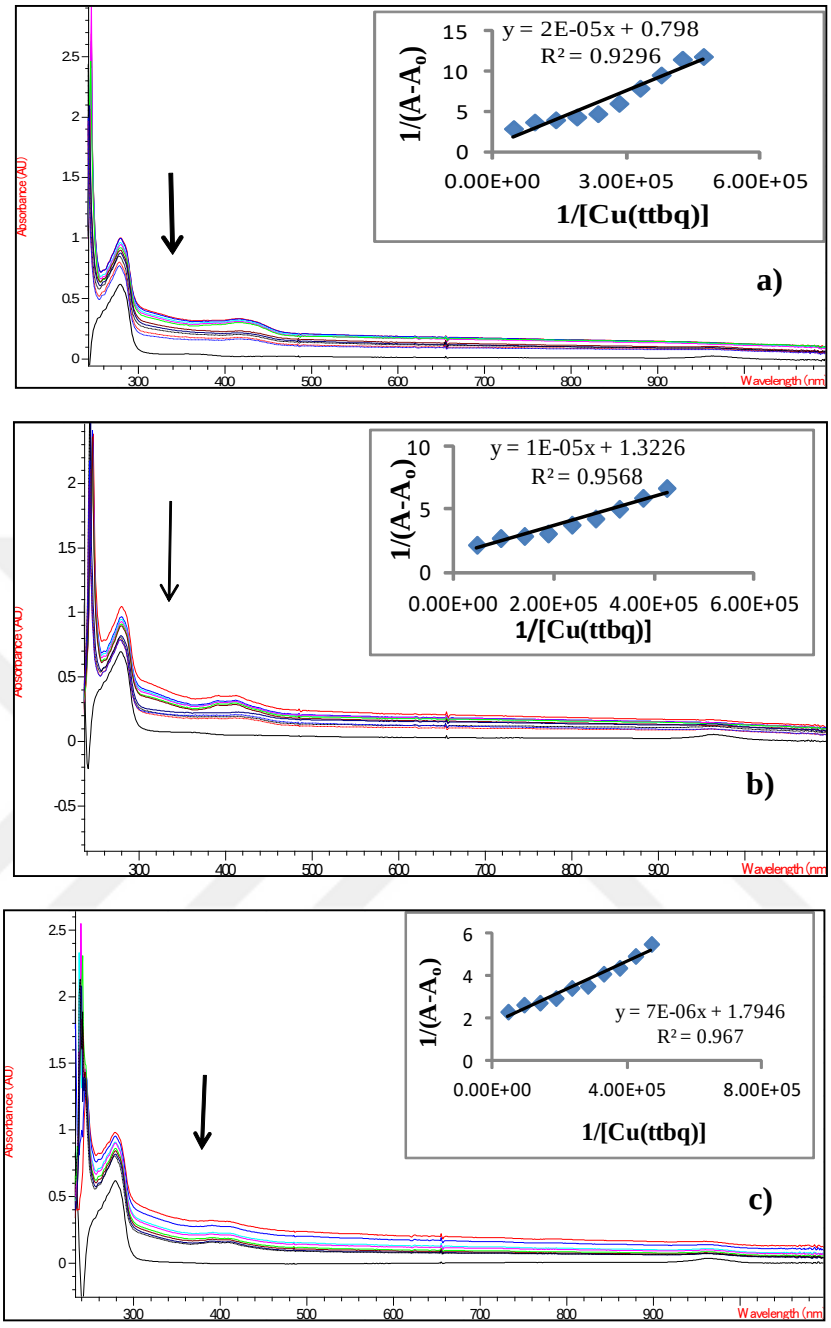

Figure F.6 The change in the electronic absorption spectrum of [Cu(ttbq)Cl_2] at a) 45 ^oC, b) 57 ^oC and c) 67 ^oC), in Tris-HCl buffer (pH = 7.10) in the absence and in the presence of HSA (R=0-10). Inset: Plot of 1/(A–A_o) vs 1/ [Cu(ttbq)Cl_2].

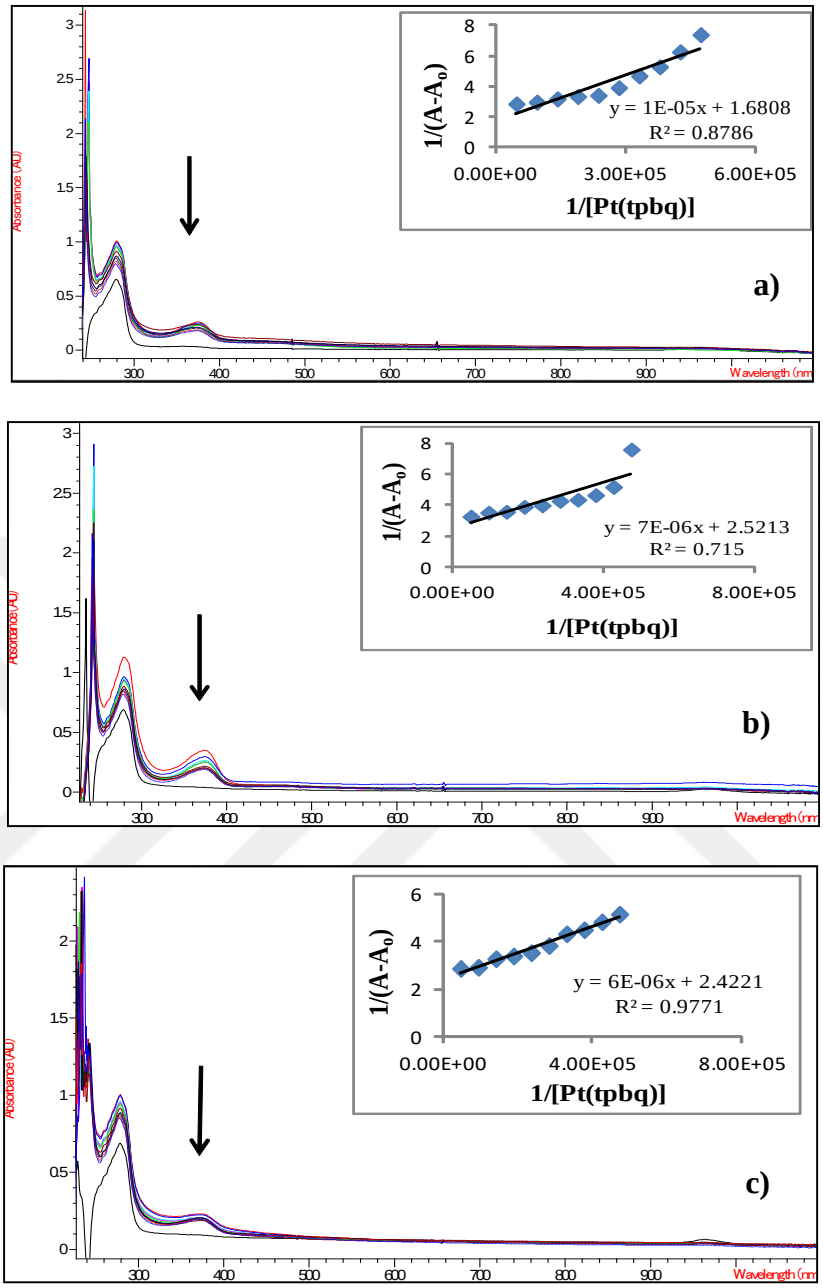

Figure F.7 The change in the electronic absorption spectrum of $[Pt(tpbq)Cl_2]$ complex at a) 45 ^oC, b) 57 ^oC and c) 67 ^oC), in Tris-HCl buffer (pH = 7.10) in the absence and in the presence of HSA (R=0-10). Inset: Plot of $1/(A–A_o)$ vs $1/ [Pt(tpbq)Cl_2]$.

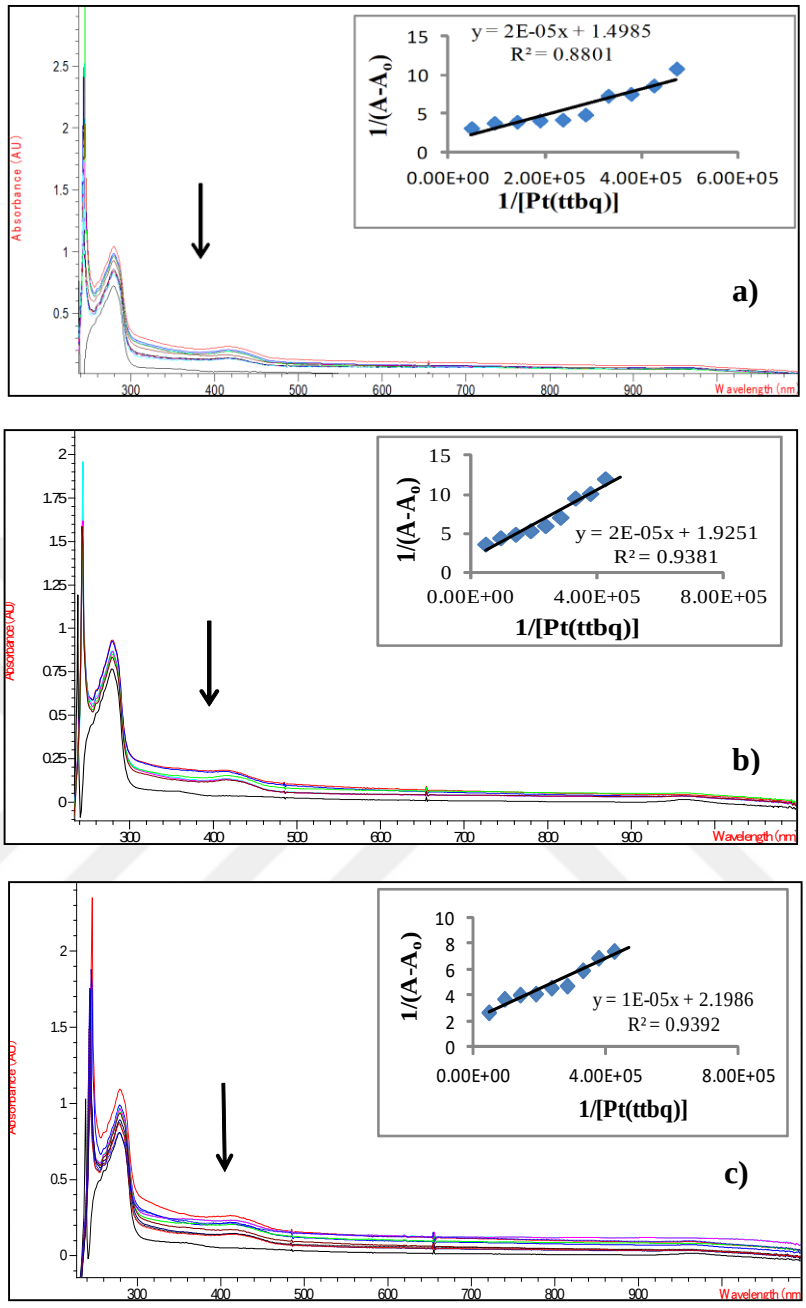

Figure F.8 The change in the electronic absorption spectrum of [Pt(ttbq)Cl_2] at a) 45 ^oC, b) 57 ^oC and c) 67 ^oC), in Tris-HCl buffer (pH = 7.10) in the absence and in the presence of HSA (R=0-10). Inset: Plot of 1/(A–A_o) vs 1/ [Pt(ttbq)Cl_2].

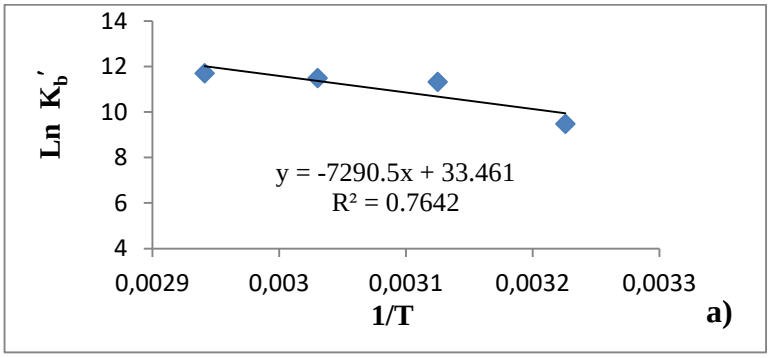

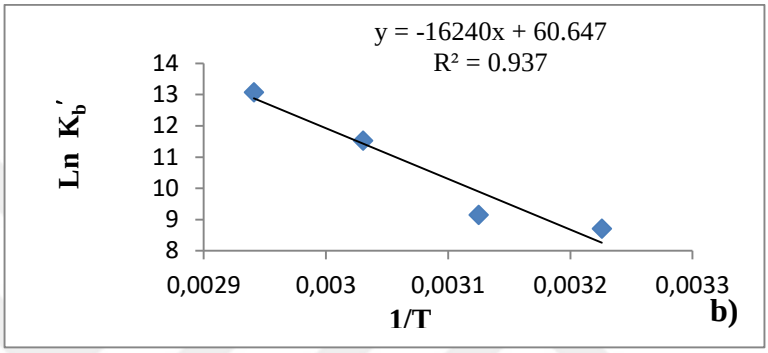

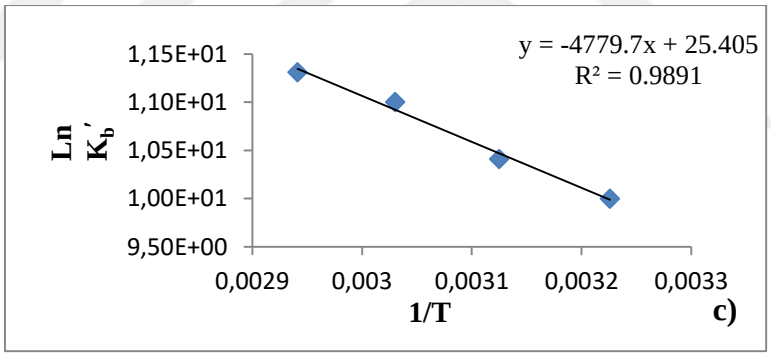

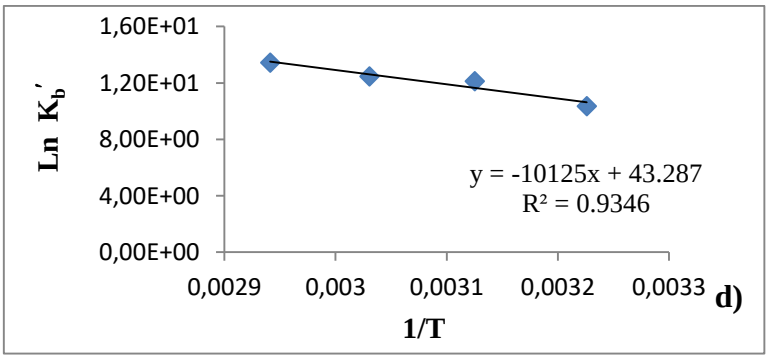

Figure F.9 The linear van't Hoff plot based on ln K′$_b$ versus 1/T for a) [Cu(dpq)$_2$Cl$_2$], b) [Cu(dtq)$_2$Cl$_2$], c) [Pt(dpq)$_2$Cl$_2$], d) [Pt(dtq)$_2$Cl$_2$].

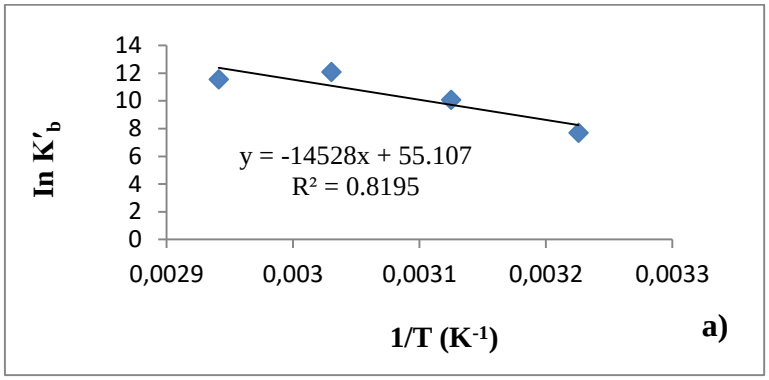

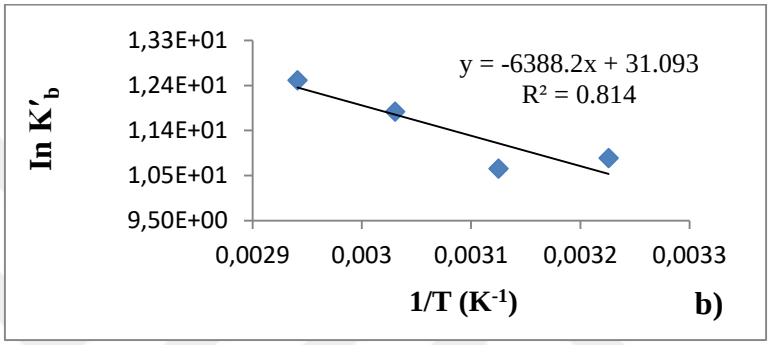

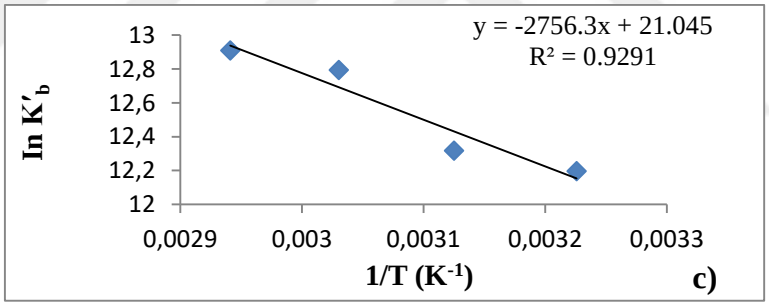

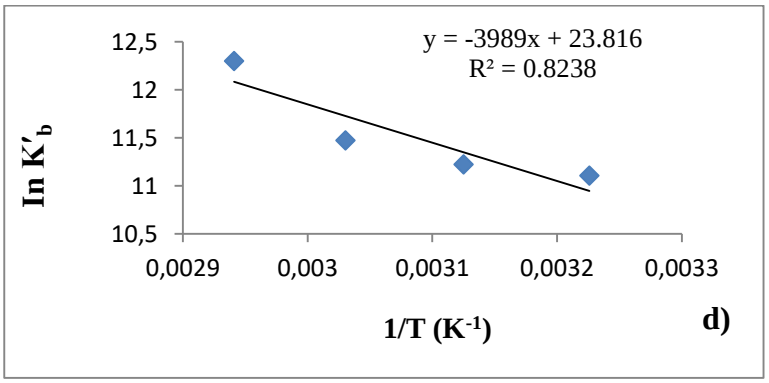

Figure F.10 The linear van't Hoff plot based on ln K'_b versus 1/T for a) [Cu(tpbq)Cl_2], b) [Cu(ttbq)Cl_2], b) [Pt(tpbq)Cl_2], d) [Pt(ttbq)Cl_2].